THE EFFECTS OF LARGE SCALE IONOSPHERIC GRADIENTS ON H.F. DIRECTION FINDING AT HIGH LATITUDES

Thesis submitted to the Faculty of Science,
University of Leicester in candidature for the degree of
Doctor of Philosophy

by

Neil Christopher Rogers

B.Sc.(Dunelm), M.Sc.(Cranfield), AMIEE

Department of Engineering

University of Leicester

January 2000

Abstract

The high latitude ionosphere contains a multitude of large-scale ionospheric density structures. These act as tilted reflecting surfaces, which cause HF (3-30 MHz) radio signals to deviate from the plane of the great circle between the transmitter and receiver. There are also a large number of smaller scale electron density irregularities that scatter the signal out of the plane of the great circle. Consequently, measurements of the bearing of incoming HF signals are often found to be displaced from the great circle bearing of the transmitter, sometimes by as much as 100°.

This thesis is a study of bearing measurements obtained during the period 1993 to 1996 over seven high latitude paths of various lengths and orientation. Characteristics of the bearing deviations are found to be strongly related to geophysical parameters such as geomagnetic activity (A_p) indices and the orientation of the interplanetary magnetic field since these also parameterise the morphology of large scale ionospheric density structures. In addition, the daily times of near-great circle propagation are found to relate strongly to A_p on paths lying in the region of the mid-latitude trough. Relationships are identified between bearing deviations and signal parameters such as the signal strength and the Doppler spread of the signal spectrum.

Ionograms have been recorded on two paths, and exhibit characteristic features that identify modes of propagation associated with reflections from tilted ionospheric layers and scattering from ionospheric irregularities. The associated bearings have been examined to determine the orientation of these tilts and/or the approximate location of scattering centres.

The results of this research may be used as a basis for devising diagnostic tests to determine the level of confidence in the accuracy of bearing measurements made of HF signals at high latitudes.

Acknowledgements

I would like to offer my thanks to Dr. Mike Warrington for supervising this research, and to Prof. Tudor Jones for the opportunity to study with the Radio and Space Plasma Physics Group at Leicester. I would also like to acknowledge and thank all those others who have contributed to the success of the experimental campaign.

Contents

List of symbols and acronyms

a_p	a 3-hourly geomagnetic index
A_p	daily average a_p geomagnetic index
AA	auroral absorption
AGC	automatic gain control (setting)
AMIEE	associate member of the institution of electrical engineers
APE	anomalous propagation event
ASK	amplitude shift keying
B	geomagnetic field
B_x	sun-earth aligned component of IMF
B_y	duskward component of IMF
B_Z	northward component of IMF
c	speed of radiowaves in free space
CCIR	international radio consultative committee
CDAA	circularly-disposed antenna array
CW	continuous wave
χ	*either* complex component of refractive index
	or solar-zenith angle
D	distance between receiver and transmitter
D_{st}	a geomagnetic index (Disturbance storm time)
DAT	digital audio tape
DC	direct current
DF	direction finding
DOA	direction of arrival
ε_0	permittivity of free space
e	charge on electron
E_S	sporadic E
eV	electron volt
EW	east to west
ϕ_O	angle of incidence of ray on base of ionosphere
Φ	ratio of CCIR-predicted F2-peak electron density to that measured in the subauroral trough
f	radio wave frequency
f_B	electron gyrofrequency
f_C	critical frequency
FAI	field-aligned irregularity

FFT	fast Fourier transform
FM	frequency modulation
FMCW	frequency modulated, continuous wave
FSK	*either* frequency shift keying
	or the signal recognition index
GC	*either* great circle
	or gradual commencement (storm)
GCB	great circle bearing
GCP	great circle path
GPS	global positioning system (a satellite navigation system)
h'	virtual height
HF	high frequency (3-30 MHz)
HSSWS	high speed solar wind streams
i	square-root of -1
ICEPAC	ionospheric communications enhanced profile analysis and circuit (prediction program)
IEE	institution of electrical engineers
IMF	interplanetary magnetic field
IONCAP	ionospheric communications analysis and prediction
ITU	international telecommunication union
κ	attenuation coefficient
keV	kiloelectronvolt
K_p	a geomagnetic index
Λ	invariant latitude
Λ_{nb}	northernmost Λ of base of the subauroral trough
Λ_{nt}	northernmost Λ of top of the subauroral trough
Λ_{sb}	southernmost Λ of base of the subauroral trough
Λ_{st}	southernmost Λ of top of the subauroral trough
L	a measure of geomagnetic latitude (e.g. the L=3 shell extends to 3 earth radii at the geomagnetic equator, assuming a dipolar magnetosphere)
LT	local time
LUF	lowest usable frequency
μ	real component of refractive index
MeV	megaelectronvolt
MHz	10^6 Hertz
MOF	maximum observed frequency (on ionograms)
MUF	maximum usable frequency

ν	electron-neutral collision frequency
n	complex refractive index
N	electron density
N_m	maximum electron density (of an ionospheric layer)
NGC	non great circle
OPMUF	operational MUF
PCA	polar cap absorption
PIM	parameterised ionospheric model
r	(as subscript) = value at reflection point
R_X	receiver
RF	radio frequency
SC	sudden commencement (of geomagnetic storm)
SDF	sudden disappearing filaments
si	Doppler spread index
SID	sudden ionospheric disturbance
SIT	systematic ionospheric tilt
SNR	signal-to-noise ratio
SPE	solar proton event
SSN	sunspot number
SWF	short-wave fadeout
t	time
T_X	transmitter
TID	travelling ionospheric disturbance
UHF	ultra high frequency (300-3000 MHz)
UT	universal time (Greenwich Mean Time)
UV	ultra-violet
VHF	very high frequency (30-300 MHz)
VOACAP	Voice of America Coverage Analysis Program
Ψ	phase path

1: Introduction

HF direction finding is the science of determining the direction to a transmitter based upon measurements of the HF radiowaves that it radiates. If the transmitter is within direct line of sight of the receiver, its direction will coincide with the normal to the wavefronts emanating from it.

Modern DF systems employ arrays of antennas to determine the orientation of the wavefronts and hence their direction of arrival (DOA). This is usually performed in one of three ways: -

(i) by measuring the phase of signals induced by the wave in an array of antennas and calculating the wavefront normal using interferometric methods,

(ii) by combining amplitude and phase measurements and applying computerised, superresolution techniques [*Gething*, 1991],

or (iii) by beamforming with hardware scanned beamformers and goniometers.

The DF systems in this study employ the latter method, using delay lines and a goniometric switching system to form a rotating, narrow beam from a relatively large (up to ~150m diameter) circular array of antennas. These wide aperture, HF direction finding systems are capable of determining the angle of arrival with a standard deviation of about 0.1° [e.g. *Gething*, 1991].

When the transmitter is located well beyond the line of sight of the receiver the HF radiowaves propagate by means of one or more reflections from the ionosphere. If the ionosphere is perfectly horizontally stratified (in effect, acting as a horizontal mirror) then the radiation ray path will be confined to the great circle plane (GCP), which passes through the transmitter, the receiver and the centre of the Earth. In these circumstances, the azimuthal angle of arrival (bearing) of the ray coincides with the great circle bearing (GCB) of the transmitter. However, the high latitude ionosphere is characterised by large, horizontal gradients in electron density (in effect, resembling tilted mirrors) which cause the ray to deviate considerably from the great circle direction. Large electron density irregularities are also present at high latitudes and these scatter HF radiation out of the great circle plane. This thesis presents bearing deviations of up to 100° that are regularly observed on propagation paths traversing the high latitude region. The ability to predict when and where such large bearing deviations occur is, therefore, essential for the correct interpretation of HF direction finding measurements.

To investigate this problem, several experimental campaigns were undertaken in which measurements of the bearings of three fixed HF transmitter stations were made on a number of high latitude paths over a period of several years (from 1993-1996). Various signal characteristics were measured including signal strength and Doppler frequency spread, and these observations are related to the bearing measurements. This improves our ability to predict the times of successful signal reception due to propagation either within or displaced from the great circle plane. Oblique ionograms recorded over some of the paths also reveal characteristics that may be correlated to the bearing measurements.

This thesis will introduce the ionospheric physics relevant to high latitude propagation (Chapter 1) and summarise the results of previous studies of off-GCP propagation (Chapter 2).

The experimental arrangement and technical information is covered in Chapter 3, whilst Chapter 4 presents an overview of the measurements, paying particular attention to the times of propagation near the GCP and its variation with changing geophysical conditions.

The results relating to off-GCP propagation are covered in two chapters, with Chapter 5 dealing with paths lying tangential to the auroral oval (roughly East-West aligned) and Chapter 6 dealing with paths crossing the auroral oval and entering the polar cap (aligned approximately North-South).

The final chapter is a summary of the main points of the study, indicating the importance of the findings for HF systems and pointing the way for future research.

1.1: The ionosphere

1.1.1: Background

The ionosphere is the region of partially ionised gas in the Earth's atmosphere that extends in altitude from about 65 km to over 1000 km. This ionisation is produced principally by solar radiation in the extreme-UV, X-ray and Lyman-α bands although other sources of ionisation such as the precipitation of energetic charged particles and cosmic rays also play an important rôle. The level of ionisation at any point in the ionosphere depends on a balance between production processes (due to photoionisation and collisional ionisation) and loss processes (such as ionic recombination and diffusion).

A typical example of the daytime and nighttime profiles of ionisation density as a function of height is presented in Figure 1.1. The chemical composition of the atmosphere and the spectral content of the ionising radiation both vary non-uniformly with altitude such that different physical and photochemical ionisation and recombination processes predominate at different heights. The regions of the ionosphere associated with peaks in the electron concentration are labelled by the letters D to F in order of increasing altitude. In the daytime the F region is split into two regions labelled F1 and F2 and after sunset the D region recombines and disappears completely.

The sun is an inconstant source of ionising radiation that varies in cycles of activity with a period of about 11 years. Figure 1.1 illustrates that when the solar activity is high (at "solar maximum"), the overall level of ionospheric ionisation is correspondingly high. Solar activity may be quantified by measuring either the flux of 10.7 cm solar electromagnetic radiation ($F_{10.7}$) or the number of sunspots apparent on the solar disk. Sunspots are cool (about 4000°C), and comparatively dark regions of the solar photosphere and their abundance is closely correlated with the 10.7 cm flux. One of the most frequently adopted measures of solar activity is the 12-month smoothed sunspot number, R_{12}, which is defined as

$$R_{12} = \frac{0.5 \times (R(k-6) + R(k+6)) + \sum_{i=k-5}^{k+5} R(i)}{12} \qquad \text{Eqn. 1.1}$$

where R(k) is the mean sunspot number (SSN) for the k^{th} month.
SSN is defined as

SSN=10×(number of sunspot groups)+(number of individual sunspots) Eqn. 1.2

Changes in solar zenith angle with local time, latitude and season and the absence of solar radiation at night determine the local time and latitudinal distribution of the ionospheric electron concentration at all altitudes. At high latitudes the distribution of energetic particle precipitation and processes of ionospheric plasma transport are also important, and will be described later in this chapter.

1.1.2: The D region

The D region ionosphere extends from 50-90 km altitude and is a weakly ionised region created by highly penetrating, high-energy radiation. Photoionisation of the D region is strongly correlated to the solar-zenith angle since where this is large the solar radiation follows a longer path in the ionosphere and consequently undergoes greater attenuation. This results in a diurnal variation in the ionisation density, which varies as a function of the cosine of the solar-zenith angle, χ. Typical noon electron densities of the D regions are 10^8-10^9 m^{-3}. At night, the D region ionisation is greatly depleted. The seasonal variation in solar radiation intensity is clearly reflected in the D region ionisation density except in the winter months when a change in the chemical composition of the D region neutral atmosphere results in anomalously large electron densities. Ionisation densities may be temporarily enhanced in the D region as a consequence of enhanced solar activity.

1.1.3: The E region

The E region lies between 90-125 km and peaks at an altitude of about 110 km with a daytime electron density of around 10^{11} m^{-3}. The electron density of this layer at mid-latitudes is principally determined by the solar ionisation rate and is consequently a strong function of the solar-zenith angle with maximum densities occurring near noon and in summer. The density profile of the E region is well approximated by the model of *Chapman* [1931].

Thin layers of often relatively intense ionisation, a few kilometres thick often develop in the E region and these are termed "Sporadic E" (or E_s) layers. At mid-latitudes, these regions may form as a result of high altitude turbulence or wind shears compressing meteoric debris. They can extend over areas a few 100 km across and are generally a daytime, summer phenomenon. Sporadic E often forms a thin, dense layer that is highly reflective to HF radio waves. It may perpetuate for several hours before dissipating and often drifts with velocities of several hundred kilometres per hour, normally in a westerly direction in the Northern Hemisphere [*MacNamara*, 1991].

In the auroral zones, a relatively thick E region called Auroral-E or night-E forms at night (principally before local midnight) and results from the precipitation of energetic (10-30 keV) electrons from the magnetosphere. The critical frequency of the auroral-E layer (at which signals propagated vertically will penetrate) ranges from around 2.5 MHz up to 5 MHz. Thin layers of auroral sporadic E are also commonly observed and are associated with the presence of visual auroral forms [*CCIR*, 1990a]. Auroral-E_S commonly has a critical frequency of 5-6 MHz and has been observed on some high latitude paths for 50% of the time at sunspot minimum [*Cannon*, 1989 and references therein].

Studies have shown that sporadic E is frequently observed under the equatorward and poleward edges of the sub-auroral trough (see Section 1.3.6) and also poleward of the trough, particularly under disturbed geomagnetic conditions [*Rodger and Pinnock*, 1980; *Rodger et al.*, 1983].

1.1.4: The F region

The region of ionosphere lying above about 125 km is termed the F region ionosphere. The region of peak solar ionisation in this region lies between about 150 km and 200 km and gives rise to a peak in electron concentration, which is the F1 layer. As with the E region, the electron density of this layer is strongly dependant on the solar zenith angle, is well approximated by the Chapman model and is seldom observed during the night or during the winter.

The peak electron concentration of the entire F region is labelled F2 and lies above the F1 region at around 250-300 km. This region marks a local minimum in the sum of recombination loss processes (predominantly ion-atom exchange / dissociative processes) which decrease with altitude, and diffusion loss processes which increase with altitude. The electron density of the F2 region is typically 10^{12} m^{-3} in the daytime and 5×10^{10} m^{-3} at night but this is not a simple function of the solar-zenith angle. Indeed, the electron density at noon is over four times higher in January than in June due to a 'Winter Anomaly' in which winter recombination rates decrease due to a lower molecular to atomic composition of the neutral atmosphere. At high latitudes, processes of plasma 'convection' dominate the geographical and local time distribution of electron density in the F region (see Section 1.3.1).

1.2: Solar, geomagnetic and ionospheric disturbances

1.2.1: Solar disturbances

There are three principal types of solar disturbance that modify the Earth-Space environment and result in the disturbance of the magnetosphere and ionosphere. These are solar flares, coronal holes and disappearing filaments.

A solar flare is a large explosion on the surface of the sun caused by a sudden release of energy and plasma stored in contortions of the solar magnetic field. Energetic flares directed towards the Earth will emit a large flux of UV, gamma and X-rays that eventually penetrate through to the day-side D-region of the ionosphere causing photo-ionisation and raising the electron density by a factor of up to ten for a period of several minutes to a few hours.

Some very energetic flares will emit a large flux of energetic protons (E = 1 MeV) which may arrive at the Earth after a few minutes to a few days. This phenomenon is known as a solar proton event (SPE). The protons spiral down the

Earth's magnetic field lines to the polar cap ionosphere where they cause collisional ionisation in the D region.

Some flares may eject a cloud of plasma that arrives 2-4 days later at the Earth. The resulting modification to the chemistry and large-scale movements of the F-region ionosphere is known as an ionospheric storm.

The occurrence of solar flares is closely correlated with solar activity, occurring most frequently at solar maximum.

A coronal hole is a cool, plasma-depleted region of the solar corona in which the magnetic field lines extend radially outwards into interplanetary space to form the Interplanetary Magnetic Field (IMF). Although coronal holes persist in the solar polar regions, the existence of low latitude coronal holes is associated with the declining phase of the solar activity cycle. The solar wind emanating from these regions is unimpeded by the radial magnetic field orientation and so form High Speed Solar Wind Streams (HSSWS) in which the bulk flow velocity rises to about 600 km/s compared with the usual 300 km/s solar wind velocity. As the HSSWS impinge upon the Earth's ionosphere, they generate geomagnetic and ionospheric storms.

A solar filament is a large, cool plasma structure on the solar surface (also observed in profile as prominences on the solar limb). When the magnetic flux tubes confining these structures break free from the solar surface and connect to the IMF, the material they contain is blown away from the sun as part of the solar wind and may arrive at the Earth to generate an ionospheric storm. This is observed as a disappearance of the dark filament over a period of a few hours. Sudden disappearing filaments (SDFs) are associated with high solar activity.

1.2.2: Geomagnetic disturbances

Geomagnetic storms are disturbances in the geomagnetic field resulting from changes in solar wind parameters associated with solar flares, HSSWSs and SDFs. These disturbances may also result from changes in the level of coupling between the IMF and the geomagnetic field.

The intensity of geomagnetic disturbance is quantified by a variety of magnetic indices based on measurements of surface geomagnetic field fluctuations at magnetometer sites around the globe. At mid-latitudes the most appropriate index is the three-hourly Kp index which is determined from 12 stations in geomagnetic latitudes of 48° to 68° in both hemispheres (thus filtering out local and seasonal variations). The Kp index is quasi-logarithmic and ranges from 0 (quiet) to 9 (disturbed) with one-third integer sub-divisions represented by $_o$, $_+$, and $_-$.

An equivalent index known as a_p is obtainable from Kp (see Table 1.1). Since a_p is linearly related to the magnitude of magnetic field fluctuations it may be averaged with meaningful results. The mean of a_p values over each UT day is called the A_p index.

K_p	0_o	0_+	1_-	1_o	1_+	2_-	2_o	2_+	3_-	3_o	3_+	4_-	4_o	4_+
a_p	0	2	3	4	5	6	7	9	12	15	18	22	27	32
K_p	5_-	5_o	5_+	6_-	6_o	6_+	7_-	7_o	7_+	8_-	8_o	8_+	9_-	9_o
a_p	39	48	56	67	80	94	111	132	154	179	207	236	300	400

Table 1.1: Equivalent range a_p for given K_p [from *Davies*, 1990].

At equatorial latitudes the D_{st} geomagnetic index is compiled from magnetometer measurements of the horizontal component of the geomagnetic field.

A geomagnetic storm resulting from a solar flare is characterised by a sequence of events starting with a Sudden Commencement (SC) in which the field strength (or D_{st}) is suddenly enhanced as the shock in the solar wind collides with the magnetosphere, compressing the geomagnetic field lines. An example of a sudden commencement storm is presented in Figure 1.11a. A short Initial Phase of positive D_{st} associated with the initial shock collision is followed by a Main Phase in which D_{st} decreases as magnetotail field lines undergo accelerated reconnection and convection, accelerating energetic (10-100 keV) particles into the near-earth space environment and enhancing the ring current of the magnetosphere (see Figure 1.2). The maximum size of this large (~100 nT) decrease in D_{st} is a good indicator of the overall magnitude of the storm. During the following Recovery Phase the geomagnetic field strength returns to pre-storm values over a period of several days as the ring current plasma precipitates into the ionosphere.

A geomagnetic storm resulting from a HSSWS usually starts much more gradually than flare induced storms as the HSSWS sweeps slowly over the Earth's magnetosphere. These storms will be less intense and last longer than flare induced storms. They will also recur on a time scale of approximately one solar revolution period (approximately 27 days). An example of a gradual commencement (GC) storm is presented in Figure 1.11b.

The consequences of geomagnetic storms in the ionosphere are manifold. There is great variation between individual storms and the ionospheric effects do not always manifest themselves.

1.2.3: Ionospheric disturbances

Ionospheric storms are the ionospheric manifestation of solar and geophysical disturbances. At geomagnetic latitudes greater than about 45°, an ionospheric storm typically begins with a short (1-2 hour) initial phase in which the F region density is enhanced by over 100% in the evening sector. This stage is coincident with the initial phase of the geomagnetic storm. During the ensuing main phase of the geomagnetic storm the F region electron density is reduced to 50-75% of pre-storm values and the virtual height of the F2 layer rises. These effects may persist for several days. In the recovery phase of a geomagnetic storm, the density of the D region is enhanced at sub-auroral latitudes (~45-62° magnetic) due to the precipitation of energetic electrons trapped in the magnetospheric Van Allen radiation belts. This 'post-storm effect' leads to increased HF absorption levels after a geomagnetic storm).

1.3: The high latitude ionosphere

1.3.1: Ionospheric and magnetospheric convection

At low latitudes the magnetic field lines (or flux tubes) of the magnetosphere (an extended region of space around the Earth that is dominated by the geomagnetic field) are closed and quasi-dipolar. The magnetic confinement of plasma by these flux tubes gives rise to a toroidal region of high density plasma around the Earth known as the plasmasphere whose boundary is known as the plasmapause. This region co-rotates with the Earth and tends to shield the low to mid-latitude ionosphere from the precipitation of high-energy ions and electrons from the solar wind and outer magnetosphere. Figure 1.2 provides the nomenclature of the magnetosphere.

At higher latitudes, however, the magnetic flux tubes connect to the outer regions of the magnetosphere and to the interplanetary magnetic field (IMF). The outer magnetosphere is dominated by a convection flow in which the magnetic flux tubes in the magnetosphere sweep sunwards in the equatorial plane over the Earth and return anti-sunwards at greater distances (see Figures 1.3 and 1.4). These flux tubes "fold over" and connect to the high latitude ionosphere such that the subsequent convection in the ionosphere is anti-sunwards over the poles, returning sunwards at lower latitudes (see Figure 1.5).

When the IMF has a southward directed component (i.e. a "negative B_z component") this convection process is strongly driven by a process of reconnection of the magnetic flux tubes in the tail region of the magnetosphere to the IMF with return flow driven by viscous interaction with the solar wind. This produces a large, two-cell convection pattern as illustrated in Figure 1.5. When B_z is positive (a northward IMF) however, the convection flows are weaker and hence the convection dominated region of the ionosphere contracts to higher latitudes and becomes convoluted with highly disordered flows.

1.3.2: The auroral zones

The most important features of the high-latitude ionosphere are the auroral zones. These are annular regions centred about the north and south geomagnetic poles where charged particles from the sun and those accelerated back from the outer magnetosphere spiral along magnetic flux tubes and penetrate to predominantly E-region altitudes before generating secondary (collisional) ionisation. The auroral ionosphere is highly irregular, varying strongly in both time and space dimensions. Auroral substorms lasting typically one hour cause transient enhancements of the HF absorbing D region and sporadic E layers. In addition, irregularities in the E and F regions may lead to scattering of signals (see Section 2).

The extent of the auroral zones may be demarcated by the high occurrence of discrete, visual auroral forms. The auroral zone widens and extends equatorwards during periods of increased geomagnetic activity. Mathematical expressions relating the location of the auroral zone boundaries to the auroral, geomagnetic activity index, Q, have been published by *Holzworth and Meng* [1975], based on observations by *Feldstein* [1963].

1.3.3: The polar cap

The polar cap ionosphere is defined as the region of ionosphere that lies poleward of the auroral oval. During the summer the polar cap ionosphere is under constant solar illumination and is a relatively undisturbed region for HF propagation purposes. During the winter however, the polar cap ionosphere receives no solar illumination and penetration frequencies fall to around 2-3 MHz, with a minimum around local midnight. The plasma forming the winter, F region, polar cap ionosphere is mainly transported from lower latitudes by means of convection flows.

Low energy particle precipitation also contributes to the ionisation, particularly during periods of positive B_z.

1.3.4: Polar patches and auroral blobs

Large, horizontal electron density gradients in the high latitude F-region ionosphere can be produced by drifting localised regions of enhanced plasma density known as "auroral blobs" [*Vickrey et al.*, 1980] or "polar patches" [*Weber et al.*, 1984] depending on their location. Polar patches are ~200-1000 km in diameter and have peak electron densities of up to 10 times that of the background density of $\sim 10^{11}$ el. m^{-3}. After forming in the noon sector, they drift in an anti-sunward direction at velocities ranging from 300 to 1000 ms^{-1} (consistent with negative B_z convection flow velocities) and therefore may transit the polar cap region in an hour or less. This compares to the lifetimes of ions in the dark F-region polar cap of several hours and patches have been observed to persist long enough to exit the polar cap region in the midnight sector [e.g. *Weber et al.*, 1986].

Blobs in the auroral region have been categorised into three forms, namely, sub-auroral blobs, auroral boundary blobs and auroral blobs. Boundary blobs are persistent, E-W elongated, field-aligned electron density enhancements on the equatorward edge of the auroral zone. They have been observed drifting in the return flow from the midnight sector of the convection region along the equatorward edge of the auroral oval near the evening trough [*Vickrey et al.*, 1980; *Rino et al.*, 1983; *Weber et al.*, 1985; *Robinson et al.*, 1985]. They may therefore represent polar patches on their return journey in the convection flow [*Carlson*, 1994].

Sub-auroral blobs are located near the equatorward side of the trough region and are thought to be the 'fossil' remains of auroral ionisation after the auroral zone retreats polewards following a sub-storm. Auroral blobs are a more transient feature of the auroral zone and probably result from bursts of energetic particle precipitation from the magnetosphere.

Polar patches are observed most frequently in winter and at sunspot maximum [see e.g. *Buchau et al.*, 1985] although they have also been observed in summer and at sunspot minimum [according to *Rodger et al.*, 1994]. Patches are only ever observed when the northward component (B_Z) of the IMF is negative. Initial observations suggested they were only observable when Kp $\geq$ 4 [e.g. *Carlson et al.*, 1984; *Weber et al.*, 1984] but further observations suggest their existence over a large range of geomagnetic conditions [*Buchau et al.*, 1985; *Stepanov et al.*, 1993].

Normally polar patches are observed in trains with each patch following the last after a period of about ten minutes. Since the geomagnetic and geographic poles are offset by about 11° in the northern hemisphere, the equatorward midday extent of the convection flow region will have a longitudinal dependence. This leads to a UT dependence of the envelope of the peak patch density observed in the polar cap, with the most pronounced patches occurring around 1700 UT and the smallest density perturbations occurring around 0500 UT [*Carlson*, 1994 and references therein].

The time evolution of a polar patch leads to a steepening of the trailing edge and it has been observed that the leading edges have considerably weaker horizontal electron density gradients than the trailing edges [*Weber et al.* 1984]. Polar patches are highly structured at scale sizes of 0.1-10 km and these irregularities cause scintillation on high-latitude, trans-ionospheric UHF radio transmissions. Stronger scintillation (which indicates a greater level of structure) is usually observed at the trailing edge of the patches.

1.3.5: Auroral arcs

Electron density enhancements of 2-3 times the ambient density are frequently observed in the F-region, polar cap ionosphere and are termed auroral arcs. These structures are generally aligned in the direction of the sun-earth line and have dimensions of 10-100 km dusk-dawn width [*Ismail et al.*, 1977, *Carlson et al.*, 1988, *Weber et al.*, 1989] and from 1000 km to trans-polar in length. Trans-polar arcs are often termed "Theta aurorae" due to their similarity to the Greek letter θ when viewed in satellite images that include the auroral oval [*Frank et al.*, 1986]. In contrast to the polar patches, the sun-aligned arcs form during periods of low geomagnetic activity and northward IMF and coincide with regions of soft (100s of eV average energy) particle precipitation that demarcate the boundaries of velocity shear in the weakly ordered plasma flows of the polar cap.

Auroral arcs are roughly twice as common in the morning magnetic local time (MLT) sector as in the evening sector [*Lassen and Danielson*, 1978, *Ismail et al.*, 1977, *Gussenhoven*, 1982, *Rairden and Mende*, 1989] with relatively few occurring near the noon-midnight plane. Some studies have found a greater abundance of morning (*evening*) arcs for conditions of negative (*positive*) B_y in the northern hemisphere (with the correlation reversed in the southern hemisphere) [e.g. *Ismail and Meng*, 1982, *Gussenhoven*, 1982] although other authors have found no such correlation [e.g. *Rairden and Mende*, 1989]. The arcs have been observed drifting across the polar cap with speeds of up to 300 m/s either in a duskward or dawnward direction [*Weber et al.*, 1989], whilst plasma flows in the noon-midnight direction along the length of the arcs at up to 1000 m/s. Duskward drift of the arcs is the most commonly observed drift direction [*Buchau et al.*, 1983] and there is some evidence that the arcs drift in the direction of the dawn-dusk component of the IMF

(B_y), with a dawnward (*duskward*) motion prevalent for positive (*negative*) B_y [e.g. *Rairden and Mende,* 1989].

1.3.6: The sub-auroral trough

The sub-auroral trough (also known as the mid-latitude trough or main ionospheric trough) is a region a few degrees wide on the equatorwards edge of the auroral oval in which the electron densities drop by a factor of 4-16 or more and the altitude of the peak rises by 100 km or more.

The trough is a depletion in the ionisation density of the ionosphere where the main ionic constituent is O^+ (<600 km) and is mainly a night-time phenomenon, stretching in a band from the evening sector to the morning sector between the invariant latitudes of 55° and 75° (L=3-15) [*Moffett and Quegan,* 1983]. Troughs of sub-auroral type have also been observed in the noon sector [e.g. *Whalen*, 1989, 1994] and are thought to result from the convection of ionisation depleted plasma from the nighttime hemisphere.

The trough lies at high latitudes at dawn and dusk and moves to mid-latitudes during the night [*Muldrew,* 1983]. The mechanism by which the trough is formed is still a topic for scientific debate.

The poleward edge of the trough lies just equatorward of the boundary of diffuse auroral precipitation and is usually steeper than the equatorward edge, which is probably an extension of the mid-latitude ionosphere. The poleward edge exhibits much more Spread-F on ionograms (see Section 1.4) than the trough minimum or equatorward walls [e.g. *Rodger and Pinnock*, 1980], and *Bates et al.* [1973] suggest that this boundary is formed by particle precipitation into the auroral oval followed by diffusion up field lines from the E-layer to the F2-layer by the effects of auroral heating thus forming a field-aligned "cliff" of ionisation.

The trough is most regularly observed during winter and equinoctial periods whereas in summer it may only be observed rarely and near local midnight [*Moffett and Quegan* 1983]. Analysis of Alouette I and II satellite data by *Feinblum and Horan* [1973] shows that during the autumn and winter nighttime the trough is "very pronounced" whereas in summer the trough is not so clearly defined. These authors also describe how the trough develops from a high latitude, shallow, narrow V-shaped feature at dusk to a deeper, wide, bucket-shaped (or cattle-trough shaped) feature moving to lower latitudes during the night followed by a narrowing and gradual in-filling of the trough as it moves back to higher latitudes at dawn (see Figure 1.6).

The trough locations and dimensions vary with the level of geomagnetic activity. The trough occurs at lower latitudes and forms at earlier local times during periods of increased geomagnetic activity. It has also been noted that the equatorward wall of the trough is steeper during periods of higher geomagnetic activity [*Karpachev*, 1992].

Many authors have attempted to provide empirical relationships between the observed invariant latitude of the trough minimum (Λ_{Trough}) the solar local time relative to midnight, t, and the magnetic activity index K_p, the most widely quoted of these being

$\Lambda_{Trough} = 62.7° - 1.4\ K_p - 0.7t \quad (-5hr < t < 5hr)$ Eqn. 1.3

[*Rycroft and Burnell*, 1970]

and

$\Lambda_{Trough} = 65.2° - 2.1\ K_p - 0.5t \quad (-4hr < t < 7hr)$ Eqn. 1.4

[*Kohnlein and Raitt*, 1977]

Halcrow and Nisbet [1977] published an empirical relationship between the geomagnetic latitude of the trough walls and local time for varying K_p values based on data from the Alouette I and II top-side sounder data. This model, reproduced in Figure 1.7, is intended as a correction to the CCIR (now ITU) global maps of ionospheric electron density. These equations, which also give the local times of trough formation and in-filling, are listed in Appendix A. They have been incorporated into a computer program and an example of the output for a particular day and K_p is shown in Figure 1.8.

Feinblum and Horan [1973] suggest the trough is a result of a plasma instability related to the evening sector bulge in the plasmasphere which explains their observations that if the trough has not formed by a certain time in the evening it will not form at all. For this reason troughs calculated to form after 2030 LT from the Halcrow and Nisbet equations are not expected to form at all.

1.4: HF radiowave propagation

Radio waves of an appropriate frequency launched from a ground-based transmitter may be effectively reflected back to the ground by the ionosphere. This occurs by a process of progressive refraction of the ray as it passes through the ionised plasma. The nature of this refraction is such that the ionosphere may also reflect electromagnetic waves that are directed vertically upwards, in which case the group velocity of the wave is simply retarded and then reversed in direction such that the ray returns to the ground.

1.4.1: Ionospheric reflection

The refractive index, n, for plane waves in an electrically neutral, homogeneous, cold ionospheric plasma is described by the Appleton formula [*Ratcliffe*, 1959] (Equation 1.5).

$$n^2 = (\mu - i\chi)^2 = 1 - \frac{X}{1 - iZ - \frac{Y_T^{\,2}}{2(1 - X - iZ)} \pm \sqrt{\frac{Y_T^{\,4}}{4(1 - X - iZ)^2} + Y_L^{\,2}}}$$

Eqn 1.5

where $X = Ne^2/\varepsilon_0 m\omega^2$

N = electron density

e = charge on electron

ε_0 = permittivity of free space

m = mass of electron

ω = radio wave angular frequency

$Y_T = eB_T/m\omega$

B_T = transverse component of geomagnetic field (normal to wavefront normal (i.e. in the plane of the wavefront)),

$Y_L = eB_L/m\omega$

B_L = longitudinal component of geomagnetic field (parallel to wavefront normal),

$Z = \nu/\omega$

ν = electron-neutral collision frequency

If we consider an example for which collisions are negligible ($Z \approx 0$) (e.g. in the E and F regions) and the magnetic field term is negligible ($Y << 1$), Equation 1.5 reduces to

$$\mu^2 = 1 - X = 1 - \left(\frac{f_N}{f}\right)^2$$

Eqn 1.6

where $f_N = \dfrac{1}{2\pi}\sqrt{\dfrac{Ne^2}{\varepsilon_0 . m}}$, the 'plasma frequency' (Hz) Eqn 1.7

f = radio wave frequency (Hz)

Equations 1.6 and 1.7 suggest that as the ray passes through denser plasma the refractive index decreases.

Snell's law of refraction may be written as follows

$$\mu \sin \varphi = \mu_0 \sin \varphi_0 \qquad \text{Eqn 1.8}$$

where φ = angle between wave normal and the perpendicular to planar isoionic contours.

As the ray enters the ionosphere, μ_o = 1 and φ_o is the angle of incidence. At the reflection point the ray is horizontal, ($\varphi_r = \pi/2$) and so from Equation 1.8,

$$\mu_r = \sin \varphi_0 \qquad \text{Eqn 1.9}$$

A ray launched into a horizontally stratified ('flat') ionosphere at vertical incidence, (φ_0 = 0), will therefore reach a reflection point where $\mu = \mu_r = 0$. From Equation 1.6, we see that this occurs when the plasma frequency, f_N, equals the wave frequency, f.

For vertical incidence reflection to occur, therefore, the ionosphere must have a maximum (or 'critical') plasma frequency greater than or equal to the wave frequency. Evaluating Equation 1.7 we find the critical frequency is related to the maximum electron density, N_m by the following equation

$$f_c(MHz) = 8.98 \times 10^{-6} \sqrt{N_m (m^{-3})} \qquad \text{Eqn. 1.10}$$

For oblique incidence propagation $\varphi_0 > 0$ and using Equations 1.6 and 1.10, Equation 1.9 can be expressed as

$$\mu_r = \sqrt{1 - \left(\frac{f_c}{f}\right)^2} = \sin \varphi_0 \qquad \text{Eqn 1.11}$$

Rearranging the right-hand equality of Eqn 1.11, Martyn's secant law is obtained, which is written

$$f = f_c \sec \varphi_0 \qquad \text{Eqn 1.12}$$

The secant law provides a useful approximation of the maximum usable frequency (MUF) on an oblique path where the critical (vertical) frequency is known near the path midpoint. For example, if a transmitter and receiver are separated by a ground range, D, a vertical incidence ionosonde near the midpoint of the path may be used to measure the critical frequency, f_c, and the virtual height of reflection, h'. Assuming single hop propagation over a flat earth, the MUF on the oblique path is given approximately by

$$MUF = f_c \sec\varphi_0 = f_c\sqrt{1+\left(\frac{D}{2h'}\right)^2} \qquad \text{Eqn 1.13}$$

The ratio of basic MUF to f_C is called the MUF factor or obliquity factor.

In the presence of a magnetic field (when collisions are still negligible), Equation 1.5 may be written,

$$\mu^2 = 1 - \frac{2X(1-X)}{2(1-X)-Y_T{}^2 \pm \sqrt{Y_T{}^4 + 4(1-X)^2 Y_L{}^2}} \qquad \text{Eqn 1.14}$$

The positive solution in Equation 1.14 describes the single 'ordinary' ray (o-ray) and the negative solution describes two 'extraordinary' rays (x-rays). The conditions for vertical incidence reflection are found by substituting $\mu = 0$ in Equation 1.14. Solutions are

	$X_r = 1$	for the ordinary ray	Eqn. 1.15
	$X_r = 1 - Y$	when Y<1, for the first extraordinary ray,	Eqn. 1.16
and	$X_r = 1 + Y$	when Y>1, for the second extraordinary ray,	Eqn. 1.17

On ionograms, (described in Section 1.5), Equation 1.15 describes the 'o-trace' and Equation 1.16 describes the 'x-trace'. For frequencies well above the electron gyrofrequency, $\omega_B=eB/m$, it is straightforward to show that at vertical incidence the critical frequency of the x-trace exceeds that of the o-trace by half the electron gyrofrequency (~ 1.4 MHz in the UK). Where propagation is parallel to the magnetic field (e.g. near-vertical propagation at high latitudes) it is possible for the o-ray to excite the extra-ordinary wave described by Equation 1.17 and this composite wave is observed as a third, 'z-trace' on ionograms.

1.4.2: Propagation modes

HF rays launched from a transmitter may often follow more than one path through the ionosphere to the receiver. A few examples of various propagation modes are presented in Figure 1.10. The various ionospheric 'modes' of propagation are described by a simple nomenclature. For example, a single hop path reflected from the E layer is called a 1E mode. Two reflections from the F region with an intermediate ground reflection is termed a 2F or F-F mode, where the '-' signifies a ground reflection. Similarly, an E hop followed by an F2 hop is called an E-F2 mode. Where there is no ground reflection the '-' sign is omitted, so for example, the FE_sF mode is an M-shaped path where a sporadic-E layer reflects rays back upwards between F region reflections, and an FF mode is a chordal hop or 'whispering gallery' mode.

Scatter modes (described in Chapter 2) are designated by a '/' following either the ionospheric region letter (for ionospheric scatter) or the '-' sign (for ground or sea scatter).

On oblique paths, a high elevation angle 'Pederson' ray path to the receiver co-exists with a low angle ray. The subscript (o), (x) or (z), as described in Section 1.4.1 may indicate the polarity of the wave.

The importance of each mode depends on the ground range, operating frequency and the types of ionospheric layers present. The modes on a particular path may be predicted from standard prediction computer programs such as REC533 [*CCIR*, 1992] or distinguished from ionograms recorded over the path.

Often the azimuthal deviation may differ between the various modes of propagation by a small amount.

1.4.3: Absorption

The Lowest Usable Frequency (LUF) that ionospheric propagation can usefully support is dependent on a number of factors including the transmitter power, the required SNR for acceptable system operation, the path loss and the level of ionospheric absorption. Ionospheric absorption occurs when free electrons, induced into motion by the HF electromagnetic fields, pass their energy to the neutral atmosphere through collisional heating.

When the magnetic field is negligible, (Y << 1) Equation 1.5 becomes

$$n^2 = (\mu - i\chi)^2 = 1 - \frac{X}{1 - iZ} \qquad \text{Eqn 1.18}$$

The coefficient of absorption is given by imaginary part of the complex propagation function, as follows

$$\begin{aligned}\kappa &= -\frac{\omega}{c}\chi \\ &= -\frac{\omega}{c}\left(\frac{-XZ}{2\mu\left(1+Z^2\right)}\right) \\ &= \frac{e^2}{2\varepsilon_0 mc}\cdot\frac{N\nu}{\mu\left(\omega^2+\nu^2\right)}\end{aligned}$$

Eqn. 1.19

The absorption loss is then found by integrating κ along the ray path.

From Equation 1.19 it is evident that strong absorption occurs near the apogee of a ray trajectory where $\mu \to 0$. This mechanism is called deviative absorption and is associated with group retardation.

In the lower parts of the ionosphere where the ray is little affected by refraction the absorption is termed 'non-deviative'. Non-deviative absorption occurs most strongly in the D region where $N\nu$ is a maximum. At HF and higher frequencies, $\omega^2 >> \nu^2$ above about 90 km altitude, so (from Equation 1.19) the absorption is inversely proportional to the square of the wave frequency.

Since the density of the D region is strongly related to the solar-zenith angle, the level of absorption usually peaks soon after local noon and is very low during the night.

Enhanced solar activity and associated geomagnetic activity may also lead to periods of enhanced absorption of HF signals. These absorption events are known as sudden ionospheric disturbances (SID) (which cause short-wave fadeouts (SWF)), polar cap absorption (PCA) events and auroral absorption (AA) events.

1.4.3.1: Sudden Ionospheric Disturbances and Short-wave Fadeout

A sudden ionospheric disturbance (SID) occurs as a result of the arrival of a burst of solar EM radiation (UV, gamma and X-rays). The dayside D region is rapidly ionised and HF radio signals traversing the region are rapidly attenuated over a period of up to one minute. The loss of HF signal strength, particularly at the lower end of the HF spectrum is called a short-wave fadeout and may last from a few minutes to several hours.

1.4.3.2: Auroral absorption

Precipitating magnetospheric electrons are responsible for enhancing the D-region ionosphere during substorms and this leads to increased levels of auroral absorption (AA). AA is generally observed in a region just equatorwards of the visible aurora. Direct or "splash" precipitation from the magnetotail in the midnight sector results in the formation of small regions of short-lived intense absorption in the midnight sector. A more continuous "drizzle" precipitation is also observed, peaking in the morning sector, and this results from energetic electrons precipitating from the magnetospheric ring current following a period of eastward drift. Typical auroral absorption values range from 0.5 dB to 3 dB on 30 MHz trans-ionospheric signals measured with a riometer [e.g. *Hartz et al.*, 1963].

1.4.3.3: Polar cap absorption

Polar Cap absorption (PCA) occurs polewards of the auroral zones (>65° latitude) and is caused by the ionisation of precipitating energetic protons that spiral down geomagnetic field lines into the polar ionosphere. These protons originate from solar flare ejecta (in a Solar Proton Event, SPE) and arrive at the Earth a few hours after the electromagnetic radiation burst. Geomagnetic activity (which results from the more slowing propagating shock in the solar wind) is therefore normally absent during the first 24 hours of the PCA, after which time a sudden commencement of a magnetic storm may occur. PCAs last from a few hours to several days and occur with frequency of approximately one per year at solar minimum, rising to about 15 per year at solar maximum. The level of absorption is typically 170 dB for 10 MHz, F-region mode propagation though this decreases during the night due to the recombination of O_2 molecules [*Davies*, 1990]. Absorption commences at high latitudes and spreads to lower latitudes during the course of the event.

1.4.4: Doppler frequency shift and spread

HF radio signals propagating via the ionosphere are often subjected to changes in the peak frequency and a broadening of the signal spectrum. This phenomenon is a result of the well-known Doppler effect.

The frequency of a signal measured at a receiver differs from that transmitted by an amount given by

$$\Delta f = -\frac{f}{c}\frac{d\Psi}{dt}$$ Eqn. 1.20

where f = wave frequency
c = speed of light
and Ψ = phase path

For example, at sunset, the height of the reflecting layer rises and the group path length of the ray steadily increases. There is consequently a steady increase in phase and the received signal is 'Doppler shifted' down to a frequency of f+Δf where Δf is negative. Doppler shifts may also depend on changes in the electron density (and refractive index) along the path.

At high latitudes, the ionosphere often contains irregularities and ripples such that the received signal is comprised of many rays, each being subject to a range of Doppler shifts. A narrow band transmission may therefore be received with a large 'Doppler spread' of the frequency. At high latitudes the ionosphere is subject to fast horizontal flows (up to 1 km/s) and large Doppler shifts and spreads are often observed (typically in the range 5-10 Hz).

1.5: Ionospheric sounding

One of the most effective means of determining the distribution of electron density in the ionosphere is to generate an ionogram using an ionospheric sounder called an ionosonde. An ionogram is a record of the group delay (the time between the launch of a wave packet from the transmitter and its reception at the receiver) plotted against the frequency of the radiowaves. If the transmitter and receiver are co-located, the system may generate "vertical incidence" ionograms, whereas if a considerable distance separates the transmitter and receiver an "oblique ionogram" is produced. Co-located transmitters and receivers may also be used to generate "backscatter ionograms", where the signals are launched at low elevation angles, reflected obliquely from the ionosphere and backscattered from irregularities (on the ground or in the ionosphere) before returning on a similar path to the receiver.

The successful interpretation of ionograms requires considerable expertise and experience, especially for ionograms recorded at high latitudes where the ionosphere is highly structured and complex modes are supported. Detailed introductory texts on the subject of ionogram interpretation and scaling are available [*Wakai et al.*, 1986; *URSI*, 1972] and special guidance in the interpretation and scaling of high latitude ionograms is provided by *Piggott* [1975].

Ionograms are used to determine the density, thickness and height of the individual layers of the ionosphere, but can also provide important information about the effects of the ionosphere on HF waveforms. For example, under disturbed ionospheric conditions, an HF pulse of radiation reflected from the F2 region may return with a considerable spread in time delay. The resulting trace on an ionogram is known as range spread F. At high latitudes, Doppler spreading is more commonly observed, particularly at frequencies close to the critical frequency at which the ray penetrates the ionosphere.

A description of an ionosonde will be given in Chapter 3 and several examples of ionograms are presented in Chapters 5 and 6.

2: Previous DF studies of off-GCP propagation

Observations of HF radiowaves propagating over paths that deviate from the great circle have been reported since the 1930s and a number of mechanisms have been postulated to explain these effects. Scattering from irregularities in the ionosphere and on the ground may cause the deviation of the ray, and the effects of ionospheric tilts are also important at high latitudes. These mechanisms are described in this chapter.

2.1: Scatter propagation

2.1.1: Ground sidescatter

Many researchers have shown the mechanism of ground (or sea) sidescatter to be important in explaining observations of off-GCP propagation. This propagation mechanism describes a multiple hop mode in which the ray is launched to the side of the GCP and a subsequent ground reflection scatters a component of the signal back towards the receiver. Scattered signals typically have signal strengths between 25 dB and 40 dB below that of the GCP signal and are characterised by rapid (>1 Hz) fading [*CCIR*, 1990b and references therein]. Ground sidescatter normally occurs when F region propagation conditions are favourable (during the daytime).

Miya *et al.* [1957] have described bearing deviations of up to 110° that occurred only during periods for which the MUF on the great circle path was exceeded, attributing the phenomena to "continental forward scatter". On high latitude E-W paths ground sidescatter modes of propagation have been observed where the GCP mode MUF is exceeded but the F region ionisation to the south remains sufficient to support propagation. The strongest signals received are those which reflect at points close to the skip distance (the minimum ground range supported for a single hop mode) where there is a convergence of the high and low angle rays which focuses the radiation from the transmitter. Focusing factors of 6 dB to 9 dB have been observed at the skip distance [p.196, *Rohan*, 1991]. Signals propagating by this mode of propagation were reported by *Jenkins et al.* [1979] as a "weak but persistent" feature associated with bearing deviations of over 90° to the south of a 2000 km, W-E, sub-auroral path. The mode has also been observed on BBC transmissions at VHF received in North America by *Hagg and Rolfe* [1963].

2.1.2: Ionospheric backscatter

An alternative scattering mechanism that results in non-GCP propagation involves scatter directly from irregularities in the ionosphere - a process requiring only a single hop. Electron density irregularities in the auroral ionosphere are known to backscatter signals at frequencies in the HF and VHF bands. These echoes are known as problematic "auroral clutter" in over-the-horizon radar systems.

The electron density irregularities are located mainly in the auroral F region, principally on the night side of the Earth, and result from plasma instabilities induced by the strong electric fields in this region. Since the conductivity of the plasma is greatest in the direction of the geomagnetic field, diffusion processes cause plasma precipitated into the auroral E region to become rapidly aligned to the field, extending upwards into the F region ionosphere as rods or sheet-like structures. The planar alignment of the scattering centres causes the phases of the scattered radiation components to constructively interfere where the ray is perpendicular to the field, leading to a strong, coherent back-scattered signal. Scattering from both E and F region irregularities has consequently been found to be aspect angle sensitive with the greatest reflectivity occurring where the ray is perpendicular to the field. For example, *Bates and Albee* [1970] reported a drop of about 5 dB per degree of off-perpendicularity in their analysis of F-region backscatter echoes in the 6-15 MHz-frequency range. At high latitudes, where the field is nearly vertical, the perpendicularity condition is satisfied for a large portion of the transmitted radiation beam on meridional paths at HF frequencies since the rays are refractively deviated towards the horizontal by the F region ionosphere. Consequently, strong coherent backscatter echoes are frequently observed on high latitude, HF paths.

The scattering cross-section of FAIs varies exponentially with frequency and *Chestnut* [1972] found that the strength of scattered signal falls off by 33 dB/GHz in the VHF/UHF bands.

Field aligned irregularities are usually in motion and the scattered signals are therefore subject to Doppler spectral spreading. The FAIs introduce multiple path trajectories with a range of propagation time delays and this leads to delay spreading ("delay spread-F") on ionograms typically of 1-2ms (*c.f.* ~0.1-0.2ms for normal GCP modes [*Davies*, 1990]).

2.1.3: Ionospheric sidescatter

The term 'sidescatter' describes mechanisms that scatter radiation out of the great-circle plane but do not necessarily return a large part of the energy back to the transmitter. Ionospheric sidescatter has been reported by *Bates et al.* [1966] who determined that the scattering region lay close to the auroral zones. Measurements of the group delay of the signals decreased with increasing geomagnetic activity as the auroral zone expanded towards the GCP. The ionospheric sidescatter (and backscatter) mode is most frequently observed at night at auroral latitudes since the ionospheric electron density perturbations are strongest in the night hemisphere. Figure 2.1 illustrates the sidescatter mechanism.

2.1.4: Ionogram signatures of scatter propagation

Scatter modes of propagation may often be identified from information contained in ionograms. *Choi et al.* [1992] have presented backscatter ionograms from an experimental HF backscatter radar system (the Verona-Ava Linear Array Radar - VALAR) that clearly displays three scatter modes of propagation. Figure 2.2a (reproduced from *Choi et al.* [1992]) presents a typical ground backscatter trace, characterised by a delay-spread signal with a well defined leading edge which slants upwards from the 2-hop vertical trace. The leading edge corresponds to signals reflected at the skip distance, the range of which increases with frequency.

Figure 2.2b presents two forms of ionospheric backscatter. The first of these is called 'Slant-F' and is characterised by a delay-spread signal with a well-defined leading edge which slants upwards from the 1-hop vertical trace. *Choi et al.* [1992] identified these slant-F echoes as originating the sub-auroral F-region ionosphere and observed only small Doppler shifts and very small (a few Hz) Doppler spreads on these signals.

The second form of scatter propagation in Figure 2.2b is the auroral backscatter mode that has been associated with echoes from field-aligned irregularities in the auroral F region. The traces are characterised by horizontal 'bars' that may be observed at both long and short slant ranges. The short slant range trace corresponds to a low angle ray path and the long slant range trace corresponds to a high angle (Pederson) ray path [*Montbriand,* 1988]. *Choi et al.* [1992] measured Doppler shifts and spreads on the low ray echoes as being confined to a 25 Hz bandwidth, whilst the high ray echoes often exceeded the 25 Hz resolution of their equipment.

2.1.5: Sporadic E

When an ionogram indicates that an HF signal is propagating via an E_s mode at mid-latitudes, the bearing errors are often small since the E_s layer is typically a thin, untilted and highly reflective layer, acting effectively as a perfect plane mirror.

For example, *Minullin* [1986] observed mean bearing deviations of less than 5° and mean square deviations of less than 9° for E_s propagation at 9-15 MHz on five mid-latitude paths, based upon bearings taken in 5min intervals over a 24hour period. Even the appearance of additional modes (e.g. E and F2), which sometimes occurs as a result of the semi-transparency of the E_s layer, had an insignificant effect on the statistical distribution of the bearings.

However, at high latitudes, the E_s type traces on ionograms are more likely to be due to reflections from field-aligned structures, which may be significantly tilted and displaced from the great circle plane. Scattering of HF signals from these structures has been observed at frequencies as high as 80 MHz [*Rohan*, 1991].

2.1.6: Sun-aligned (auroral) arcs

The auroral zone is not the only region to exhibit strong field-aligned irregularity structures. Other important regions include the equatorial F region and the polar cap. A study by *Buchau et al.* [1983] demonstrated that sun-aligned, auroral arcs (described in Chapter 1) could yield F-region ionosonde returns in excess of 10 MHz. Thus it is plausible that drifting auroral arcs could be detrimental to the accuracy of HF direction finding at high latitudes during low geomagnetic activity and positive B_z.

2.2: Specular reflections from a tilted ionosphere.

A number of researchers have ascribed their observations of off-GCP propagation to specular reflections from an ionosphere containing horizontal electron density gradients directed normal to the GCP. If the ionosphere is represented by a plane mirror tilted at an angle β to the horizontal (but remaining parallel to the GCP) and at an altitude, h', then the deviation in bearing at a DF receiver site is given by,

$$\phi = \arctan\{ (2h'/D) \tan \beta \} \qquad \text{Eqn. 2.1}$$

where D = hop length.

For small tilts (and/or long paths (D>>h')), the bearing deviation, $\phi \approx 2h'\beta/D$.

If horizontal gradients also exist in the GCP direction such that the proximity of the reflection point closest to the DF is increased, then these will tend to amplify the bearing deviation observed (effectively reducing the value of D in the above).

Clearly, this 'plane mirror' approach is not suitable where the ray undergoes significant deviative refraction in a structured ionosphere. Perhaps the most reliable method for accurately determining the ray trajectory through a known vertical profile of electron density is to perform step-wise, numerical integrations of the Haselgrove ray equations [*Haselgrove*, 1954]. However, this numerical method of ray tracing requires a large number of calculations and intensive use of computer resources.

Davies and Rush [1985] published a useful summary of the typical maximum gradients observed in the critical frequency of the F2 region (foF2) associated with a range of common ionospheric phenomena. These values are reproduced in Table 2.1 and provide a good indication of the relative importance of the various ionospheric features to direction finding systems. It should be noted, however, that a measure of the effective tilt of the ionosphere must also take into account variations in the height of the maximum (hmF2) and changes in the parabolic semi-thickness of the layer (ymF2).

Ionospheric Phenomenon	Principal Direction	Horizontal gradient in $(f_oF2)^2$ (10^{-3} MHz^2 km^{-1})
Sub-auroral Trough	N-S	100
Sunrise terminator	(E-W)	60
Latitudinal gradient	N-S	40
Travelling Ionospheric Disturbance (TID)		40
Geomagnetic Storm	E-W	30
Sunset terminator	(E-W)	30
Equatorial Anomaly	N-S	>15
Sudden Ionospheric Disturbance (SID)	(E-W)	1 - 5

Table 2.1: Summary of maximum horizontal gradients in $(foF2)^2$ [after *Davies and Rush*, 1985].

Helms and Thompson [1973] have used a modification of the *Jones and Stephenson* [1975] computer program to perform ray-tracing analysis of a simple model of the sub-auroral trough. They modelled the trough as a Gaussian, latitudinal perturbation in electron density and the ray tracing was performed with the simplifying assumptions of zero magnetic field and zero electron-neutral collision frequency. They concluded that the greatest deviation of ray paths occurred for rays which reached apogee near the trough centre and off-GCP deflection was greatest for paths orientated parallel to the trough. Wide, shallow troughs were found to have little deviative effect whereas narrow, deep troughs were found to have a large effect. They showed also that when a deep trough lies directly over the path it may appear as a 'hole' to rays which exceed the critical frequency of the trough centre, and a nearby trough can support propagation along more than one ray path (from both walls of the trough).

A similar ray tracing study was performed by *Yevlashina et al.* [1986] for 1000 km, meridional paths through a model trough at frequencies ranging from 3-5 MHz. This study confirmed that the trough could act as a 'hole' to incident HF radiation in a narrow range of elevation angles. These authors also found that rays on a S-N path were often reflected backwards by the poleward wall of the trough arriving at the receiver with a bearing error of 180°. A similar phenomenon was predicted to occur (though slightly less often) on N-S paths with reflections from the equatorward wall of the trough.

Experimental observations of specular reflections from the poleward trough wall were recorded on oblique ionograms taken on a 2000 km E-W path by *Jenkins et al.* [1979]. These 'trough edge' modes were recorded at 5.6 MHz and not observed at frequencies at or above 9.0 MHz. They persisted for about an hour after the GCP F-mode had ceased and had an MUF of 0.5-1.0 MHz above the GCP, F-mode MUF. The trough edge mode exhibited a relatively strong and constant signal strength and low Doppler shift and spread.

Very high latitude direction finding studies have been performed in the KESTREL experiment [*Jenkins*, 1992] over a few days in November 1990. An Andrews Corporation interferometric DF system at Alert, NWT, Canada measured the angle of arrival (bearing and elevation angles) of signals propagated from Halifax, Nova Scotia and Thule, Greenland. Analysis of measurements from KESTREL demonstrated the large scale of the ionospherically induced bearing errors at high latitudes with bearing distributions on the Thule path spread typically 30-40° at half-maximum. An interesting feature of the bearing measurements was the repeated steady swings of the bearings (within 90° of the GCB) with periods of 10-20 minutes, persisting over periods of several hours. The directional sense of the swings (high-low or low-high bearing) were dependent on the time of day and found to be consistent with the motion of scattering regions within polar patches drifting in the two-cell convection flow of the F region polar cap ionosphere [*Jones and Warrington*, 1992; *Jenkins*, 1992; *Warrington et al.*, 1997].

2.2.1: Travelling ionospheric disturbances (TIDs)

Joule heating of the neutral atmosphere in the night-side auroral zones caused by particle precipitation leads to heating of the neutral atmosphere. The pulse-like nature of this precipitation stimulates the production of acoustic gravity waves, which propagate to lower latitudes. These waves are observed as large scale, travelling ionospheric disturbances (TIDs) in the mid-latitude, F-region ionosphere [*Georges*, 1967].

TIDs vary in size from 100m to 100 km in scale and may propagate with horizontal velocities of a few m/s to 1000m/s. Medium to very large scale TIDs (10^2-10^3 km size) are thought to cause the largest bearing errors on DF systems [*Jones and Reynolds*, 1975], the latter causing typical deviations of about 5° [*Tedd et al.*, 1984], usually occurring at night and undergoing 2-3 cycles with a period of 30-60 minutes. *Georges* [1967] has shown that very large scale TIDs show a strong correlation with periods of geomagnetic activity (Kp>5).

This thesis is generally concerned with bearing deviations larger than 5° and so will not consider TIDs in any detail.

2.2.2: Systematic ionospheric tilts and diurnal changes in bearing

The effects on bearing of sunrise and sunset gradients have been observed on a north-south path from Clyde River (70°N) to Boston, USA (42°N) by *Jones et al.* [1992]. A systematic, diurnal pattern emerges in the bearing data with positive bearing deviations of a few degrees occurring at sunrise and a smaller, negative bearing deviation at sunset. The difference in magnitude of the bearing changes reflects the smaller longitudinal, ionospheric gradients at sunset than at sunrise. The magnitude of the bearing deviation tended to zero towards local noon since the longitudinal ionospheric gradients are small at this time. Bearing deviations were small in the summer months and this was attributed to the small longitudinal gradients in foF2 at that time of year.

An extensive study of bearing offsets due to systematic ionospheric tilts (SITs) has been performed on a number of single-hop, mid-latitude paths by *Tedd et al.* [1985]. Typical bearing deviations of 2-3° are observed on both W-E and S-N paths, the former being attributed to latitudinal density gradients. In general, the daytime bearings followed a repetitive, predictable pattern from day to day, but the magnitude of bearing deviations at sunrise and during the night varied greatly from day to day. This night-time variability was attributed (a) to a greater sensitivity of the night-time ionosphere to plasma transport processes associated with varying geomagnetic conditions and (b) to the fact that the night-time MUF was closer to the radiowave frequency such that small variations in horizontal electron density gradients would lead to large changes in the effective ionospheric tilt [*Titheridge*, 1958] and produce correspondingly large variations in the bearing.

Most of the above off-GCP propagation measurements were based on limited periods of observation. A co-ordinated set of experimental campaigns was therefore conducted to determine the statistical occurrence, severity and identifying characteristics of each off-GCP propagation mechanism. These experiments would provide bearing measurements with unprecedentedly high time resolution such that rapid fluctuations in the bearing could be resolved. The configuration of the experimental campaign is described in the next chapter.

3: Experimental arrangement

In order to investigate the many and varied causes of off-GCP propagation discussed in Chapter 2, measurements of bearings have been made on several high latitude paths for a range of HF frequencies. The measurements were made continuously over three years such that the statistical occurrence of the off-GCP propagation mechanisms could be determined. In addition to bearing measurements, the spectral properties of the incoming signals were analysed to determine characteristics that could be associated with the off-GCP bearings. Supporting measurements from ionograms and geophysical data from a number of sources were also used to help define and understand the causes of the deviations in the bearing of signals.

3.1: Transmitters, receivers and propagation paths

The locations of the transmitters and receivers and the GCPs over which measurements were taken during the experimental campaign are illustrated in Figure 3.1. Included in this figure is a model representation of the approximate location of the visible auroral oval [*Holzworth and Meng,* 1975]. These locations are also listed in Table B1 of Appendix B together with the locations of the GCP midpoints. Corrected geomagnetic latitude and local times are also provided for reference. The GC bearings of the transmitters at each receiver site are presented in Table B2 and the lengths of the GCPs are presented in Table B3.

The transmitter at Halifax (call sign CFH) is a commercial, maritime transmitter that has modulated its transmissions by FSK since November 1993. The other two transmitters at Wainwright (CZB) and Iqaluit (CZD) employ CW ASK modulation and have been installed and operated by personnel associated with the present campaign. Each transmitter broadcasts on three frequency bands that are widely spaced across the HF band. These frequencies are presented in Table B4.

3.2: Direction finding systems

The receiver sites each employed an automated system consisting of a circularly disposed antenna array (CDAA) connected to a wide aperture, goniometric, DF system. The CDAA at each site was a dual-band, Plessey PUSHER system consisting of two concentric, circular arrays of 24 elements. The larger, low band array had a radius of 75m and operated at frequencies of 3-10 MHz and the smaller, high band array had a radius of 25m and operated at frequencies of 10-30 MHz. At Leitrim and Alert, both arrays consisted of single element, vertical monopoles whereas at Cheltenham the low band array consisted of doublet antennas that improved the azimuthal beam pattern.

A 1.0 MHz test signal was injected into the receivers every hour to calibrate the receiver delays. This was recorded as a bearing offset, which was then used for calibrating the subsequent bearing measurements.

Each DF system monitored each of three transmitter frequencies for 30 seconds at a time on a 90-second cycle. The data were recorded automatically by computer and logged onto DAT tapes, which were then posted to Leicester for analysis.

3.3: Signal monitoring systems

At each site, a single element of the PUSHER array was connected to a separate receiver that was used to determine the signal spectrum. For each 30s period, this receiver system recorded the time, signal phasor (real and imaginary components), AGC setting, and the tuned frequency. Calibration signals were sent to this receiver once every 12 hours.

3.4: Initial data processing

3.4.1: DF data processing

For each 30 second recording period, a large number of goniometer beam patterns ('composite scans') were obtained, examples of which may be observed in Figure 3.2 (lower panels). Snap bearings were calculated and recorded from each composite scan using the technique described by *Warrington and Jones*, [1992].

Composite bearings were determined as weighted averages of the snap bearings for each 30s period. Further details of the bearing determination procedure are provided in Appendix C.

3.4.2: Signal spectrum data processing

Calibration of the signal monitoring receiver was performed at 0000 UT and 1200 UT each day. A calibration curve was obtained for each transmission frequency and for each setting of AGC, which related amplitude (i.e. the magnitude of the signal phasor) to the signal strength in dB above 1μV. Where possible, a linear 'best-fit' relation was automatically determined for the linear portion of each calibration curve. The maximum signal amplitude in subsequent 30 second observing periods in the following 12 hours were calibrated by means of these linear relations and the resulting value of signal strength recorded (in dBμV). Where the modulation type was ASK (i.e. Iqaluit and Wainwright transmitters) the call sign of the transmitter (modulated in Morse code) could often be observed in plots of the signal phasor amplitude, providing confidence in the origin of the signals.

A Fast Fourier Transform (FFT) was performed on each 30-second period of signal amplitude values (which were sampled at 40 ms intervals). The resulting 50 Hz wide signal spectrum shows a signal frequency peak with modulation sidebands (at times when the transmissions were being modulated) above a background of noise (see Figure 3.2 (upper panels)). Note that a +10 Hz offset has been applied to the received signals to prevent confusion between DC offsets in the receiver and the signal itself, as would have been the case with a zero offset. A signal recognition confidence factor was then assigned a value of 2 where no peak was observed in the appropriate frequency bracket, 1 for a peak with no modulation sidebands and 0 where both a peak and sidebands were observed. As an example, the spectra in the upper panels of Figure 3.2 were assigned confidence factor values of 1 (indicating peak correctly placed, but no sidebands observed).

To provide a measure of the spectral width of the signal peak a Doppler spread index was determined from the signal spectrum using a method that makes no assumptions about the profile of the spectrum. The noise background was first calculated by finding the "area" under the quarter of the normalised FFT spectrum lying between -25.0 Hz to -12.5 Hz and multiplying this value by four (see Figure 3.3). This is then subtracted from the total "area" under the normalised FFT. The result is multiplied by a factor of 20 such that a normalised triangular spectrum of width 10 Hz at its base would return a spread index of 100 Hz.

The signal to noise ratio (SNR) was computed as the ratio of the peak signal strength to the average level of the noise background (as defined above) (see *Warrington et al.*, [1991]).

3.5: Oblique incidence, ionospheric sounding

The oblique ionosonde used in this study was a Frequency Modulated, Continuous Wave (FMCW) (or "chirp") sounder [*Barry and Fenwick*, 1975]. Oblique ionograms were recorded at 30-minute intervals over the Halifax-Leitrim and Iqaluit-Alert paths using BR Communications RCS-5 chirp sounders in which the CW signal ramped from 2 MHz to 30 MHz at 100 kHz/s over a 280s period. The receiver determined the frequency difference between the received signal and a (time-locked) duplicate of the transmitted signal by mixing the two signals to produce a heterodyned, baseband frequency output. The group path delay ('time-of-flight') was then calculated from the baseband frequency divided by the ramp rate. A baseband signal bandwidth of 500 Hz limited the range of group delay values to 5ms. Spectral analysis was performed on the baseband signal with a 2.5 Hz resolution (corresponding to a 0.025ms group delay resolution) at 1.0s intervals (corresponding to a frequency resolution of 0.1 MHz).

The transmitter and receiver in an oblique sounder should ideally be synchronised to sub-millisecond accuracy - a process usually achieved using the timing information from GPS (Global Positioning System) navigation satellite receivers. In this study, however, GPS information was unavailable and synchronisation was performed by means of the systems' internal clock signals. The BR receivers were designed to slip the time reference to position the first arrival mode at around 1ms on the ionogram display. This means that the zero of group path delay on the ionogram traces may 'wander' slightly between successive ionograms, although the relative delay between individual traces is unaffected.

4: A general overview of the measurements

The times of propagation and signal characteristics (signal strength, Doppler spread etc.) and their variation with season, time of day, solar activity and geomagnetic activity for each path and transmission frequency are described within this chapter. Parameterised models of large scale ionospheric density structures and absorption regions will be introduced and compared with the measurements and times of propagation will be compared with those predicted by a standard CCIR prediction model. Descriptions of large scale bearing deviations observed in the data are deferred to chapters 5 and 6.

The experimental campaign took place during the period April 1993 to April 1996 although most of the receiver sites were not operational until November 1993. In Figure 4.1 a bar chart indicates the dates for which post-processed bearing measurements are available for each of the paths. The quality of the data varied considerably throughout the campaign, possibly due to changes in the transmitter power or receiver configurations and/or abrupt changes in the level of noise or interference at the DF receiver sites. Information about such matters was unobtainable from the operators of the equipment.

4.1: The prevailing geophysical conditions during the experimental campaign

4.1.1: Solar activity and geomagnetic storms

Reference to Figure 4.2 indicates that the experimental measurements were taken during the declining phase of solar cycle 22. In Section 1.2 it was noted that many geomagnetic storms during this period would be expected to be of the gradual commencement, long duration, recurrent variety since this is a period of declining solar flare activity and recurrent High Speed Solar Wind Streams (HSSWS). In Figure 4.3 the geomagnetic activity index, D_{st}, is plotted in 27-day format for the whole of 1994 (solar rotation numbers 2191 to 2204). Examples of recurrent storms are observed on 5th February, 6th March, 2nd April, 1st and 28th May and 26th June and on the 25th September, 23rd October, *etc.*. Notable non-recurrent storms occur on 21st February and 17th April.

The A_p values and sunspot numbers for 1994 are provided for later reference in Figures 4.4 and 4.5.

4.1.2: Models of auroral oval location and auroral D-region absorption

The paths of the campaign are plotted (in corrected geomagnetic co-ordinates) in Figures 4.6 and 4.7 for a Kp of 1 and 4 respectively. The shaded oval region representing the extent of the visual aurora is determined by the model of *Holzworth and Meng* [1975], which is a parameterised, mathematical representation of the observations of *Feldstein* [1963]. The contours represent the percentage of the days, Q1, on which the absorption measured by a riometer at 30 MHz exceeds 1 dB as calculated using the empirical model of *Foppiano and Bradley* [1983]. An average of the seasonal variations is shown. This model was based on observations in the years 1959-1961 - a period with SSN ~100. *Hargreaves et al.* [1987] subsequently observed that the SSN parameterisation of the model lead to predictions of Q1 that were too large during periods of low solar activity. The SSN parameter was therefore fixed at a value of 100 in this study.

The model of *Foppiano and Bradley* [1983] has been adapted to calculate the diurnal variation of Q1 for each path by finding the probability sum of Q1 for each position at which the path traverses the D region. The results of this modelling are presented in Figure 4.8 for one-hop paths and in Figure 4.9 for two-hop paths. These results will be referred to in the following sections in conjunction with the analysis of experimental measurements.

4.2: Times of propagation near the great circle path

Examined in this section are the times of day during which propagation occurred on paths close to the GCP. These results will be presented alongside the times of propagation predicted from the MUF and LUF curves produced by a computer program which incorporates the semi-empirical HF propagation prediction method currently recommended by the ITU [*CCIR*, 1992].

The times of propagation were recorded for all the bearing data available from 1994 on all the paths and all transmitted frequencies. Propagation commencement and cessation times were based upon threshold values of the number of composite bearing returns within a sliding window on the bearing-UT plane (see Figure 4.10). A propagation commencement time was recorded when the number of composite bearing returns within ±10° of the GCB rose above a value of 10 in the preceding 60 minute period. A propagation cessation time was recorded when the number of composite bearing returns within ±10° of the GCB fell below a value of 3 in the subsequent 60 minute period (this threshold value was smaller to prevent large files being created where the "bearing density" hovered around the threshold value). The threshold values used in this method were chosen to reflect a reasonable fit to the times of commencement and cessation as judged "by eye" from the bearing data. It should be noted that breaks in propagation, which lasted for less than one hour were not detected by this method.

This method of determining times of propagation was chosen in preference to that of analysing signal strength measurements since the latter contained a large number of gaps and omissions that would have led to fewer and more spurious results. The three receivers tuned to the Iqaluit transmitter frequencies consistently failed to provide sensible values of signal strength, perhaps because of the relatively low power of this transmitter. The goniometric DF systems appeared to return consistent composite bearings at signal strength levels below that which could be properly detected and calibrated by the signal monitoring receivers. The method chosen also excluded off-GCP propagation, thus excluding most of the co-channel interferer signals and so providing results that were more suitable for comparison with the HF propagation predictions which assume that propagation lies along the GCP.

4.2.1: HF propagation prediction model results

Predictions from HF ionospheric propagation prediction computer programs were used to as an aid to understanding the observed times of propagation near the GCP. Three computer models were used, namely ICEPAC [*NTIA/ITS,* 2000], VOACAP [*NTIA/ITS,* 2000] and REC533 [*CCIR*, 1992], each using, as far as possible, the same input parameters. ICEPAC and VOACAP are independent developments of the Ionospheric Communications Analysis and Predictions (IONCAP) program from the US National Telecommunications and Information Administration (NTIA) [*Teters et al.*, 1983]. VOACAP was developed for the Voice of America (VOA), and ICEPAC (Ionospheric Communications Enhanced Profile Analysis and Circuit prediction) incorporates the Ionospheric Conductivity and Electron Density (ICED) high latitude model of *Tascione et al.* [1987].

The models were run and predictions of MUF and LUF levels were recorded for each UT hour for each month of the year. The ICEPAC program was run at two levels of geomagnetic activity, whilst the other two models are not parameterised by geomagnetic activity indices. The times of propagation commencement and cessation at the transmitter frequency were then determined from the MUF and LUF values by linear interpolation.

Precise information regarding the transmitter power, frequency response and directivity of the transmit antennas and receiver gain and noise levels were not easily obtainable. Therefore, in this study, only an indication of the LUF is given, based upon system parameters of a typical HF world service broadcasting system. Errors in these estimates will affect the predictions of LUF but do not affect the predictions of MUF, which are determined entirely by ionospheric rather than system parameters.

A full list of the parameters used as input to the prediction models are listed in Table 4.1:-

Minimum elevation angle	3°
Transmitter power	500kW
Tx design	Constant 17 dB transmit antenna design used by VOA. Design frequency = operating frequency.
Rx design	Non-directional SW whip antenna.
Rx bandwidth	1 Hz
Noise level	-145 dBW (in a 1 Hz bandwidth at 3 MHz)
Required SNR	73 dB in 1 Hz Rx bandwidth on at least 90% of days.
Ionospheric model	URSI 1988 (Australian) coefficients

Table 4.1: Parameters used in the propagation model predictions.

In addition the appropriate 12 month running mean SSN (R_{12}) for each month was used. The URSI 1988 parameterised database of scaled ionogram characteristics were used in preference to the original CCIR database since it is derived from measurements that included data taken over the oceans (a deficiency in the CCIR data).

This work is not intended as a test of the models (which, incidentally, varied greatly in their predictions) so for brevity only the results from program REC533 [*CCIR*, 1992] will be presented since it produced by far the best correlation with the observations in the majority of cases.

4.2.2: Times of propagation on the Halifax - Cheltenham path.

The results of this analysis are given in Figure 4.11 for each of the three frequencies of the Halifax transmitter. The vertical lines in this figure represent the times during which propagation occurred. The times at which the solar zenith angle reached 90° at the path mid-point are also given (solid curved line) and this is broken to indicate where bearing data was unavailable. It should be noted that missing DF data is indistinguishable from times of no propagation in this analysis and this is most evident in the first hour of the UT day where a data logging error led to data being lost on a number of days.

Shaded blocks represent the times of propagation as predicted by the REC533 model. A solid horizontal line at the edge of a block indicates the time that the MUF is at the operating frequency whilst the lack of a solid edge at the edge of a block indicates when the LUF is at the operating frequency.

At 5.097 MHz a high correlation is observed between times of propagation and sunrise/sunset times. A solar zenith angle (χ) dependence of times of propagation is to be expected since D-region, non-deviative absorption varies approximately with $\cos(\chi)$. The LUF predictions of REC533 agree with the propagation time observations at 5.097 MHz to within about 2 hours. At 10.945 MHz the REC533 model predicts a loss of propagation due to D region absorption around midday that is not reflected in the observations, though the inaccuracy of the system gain and noise parameters prevents any conclusion being drawn from this.

At 10.945 MHz and 15.920 MHz propagation generally commences soon after sunrise but continues well beyond sunset due to the slow recombination time of the F region plasma (compared with the rapid photo-ionisation at sunrise). Day-to-day variations in propagation times are larger at these frequencies and indicate a greater sensitivity to changes in geomagnetic activity.

The REC533 model is a poor predictor of the MUF during the summer months at 15.920 MHz.

To assess the overall influence of geomagnetic activity, the times of propagation are re-plotted in Figure 4.12 against the A_p value for each day. Where two or more days shared the same A_p value, the lines are spaced by up to 0.5 A_p units either side of the true value to prevent overlaps on the plots. The measurements were divided into four seasonal date ranges to minimise the seasonal variance in each plot. To be concise, only the spring measurements (dates 4/2/94 - 5/5/94) are presented in this thesis.

At 5.097 MHz the variation in times of propagation with A_p is minimal, regardless of season. At 10.945 MHz and 15.920 MHz a strong A_p dependence is evident. The times of propagation commencement vary by less than 2 hours with later propagation commencement at high A_p, but the times of propagation cessation at A_p=40 is about 4 hours earlier than at A_p=0 during summer and up to 6 hours earlier in spring. The importance of including a geomagnetic activity index in propagation prediction models is clearly demonstrated in these examples.

The Halifax-Cheltenham path runs along the line of the F-region sub-auroral trough. The trough model of *Halcrow and Nisbet* [1977] is shown in Figure 4.13 for three levels of geomagnetic activity. The model indicates that the trough forms at earlier times in the evening for higher levels of geomagnetic activity. In Figure 4.14 the composite bearings measured within ±10° of the GCB are plotted for the 15.920 MHz signal for each day of December 1993. The stepped, solid lines running down the page represent predictions of the times of formation and dissipation of the trough at the location of the first of the two-hop reflection points for this path. Averages of the three-hourly Kp values from 1500-2100 UT were used as a parameter in the Halcrow-Nisbet model and are plotted on the right hand side. This UT range was chosen to reflect the current and recent geomagnetic conditions at the times of trough formation. The close correlation between the predictions of trough formation and the end of propagation for each day is clearly evident. A similar behaviour is observed in the propagation times of the 10.945 MHz signals. However at 5.097 MHz the signals propagate during the nighttime only, indicating that this frequency is well below the MUF even in the presence of the trough.

4.2.3: Times of propagation on the Halifax - Leitrim path

The times of propagation on the Halifax-Leitrim path are shown in Figure 4.15 for all the data available for 1994. The only occurrences of 15.920 MHz signals being observed in the DF measurements in the period February to April 1994 were brief (<1hour) periods on the 8th March, 3rd April and 17th April. These were all days that followed the onset of a geomagnetic storm and this suggests that the propagation was due to the positive F region storm effect in which foF2 levels are temporarily enhanced, briefly raising the MUF above 15.920 MHz.

At 5.097 MHz propagation loss in the noon sector (around 1639 UT) is probably due to solar controlled D-region photoionisation and subsequent non-deviative absorption. The REC533 model predicts the 5.097 MHz signal to be above the MUF in the spring months for several hours following local midnight (roughly 0500-0900 UT). The resulting loss of propagation at this time of day is often observed in the data at these times (for example, day numbers 55-66 and 109-123). However, this is not a general propagation condition and propagation loss is just as frequently observed for several hours in the pre-local-midnight sector with normal, great circle propagation resuming after midnight (for example, day numbers 93-106 and 149-151). At the same time the propagation cessation time on the 10.945 MHz signal is observed about 4 hours earlier.

When the times of propagation are re-plotted as a function of A_p (Figure 4.16) it becomes clear that pre-midnight propagation loss at 5.097 MHz and the loss of propagation in the late afternoon at 10.945 MHz are conditions associated with high geomagnetic activity (A_p>20). The latter effect is most likely due to the extension of the sub-auroral trough to earlier local times, reducing the MUF in the late afternoon. An analysis of the effects of individual storms will be presented in Chapter 5 together with a discussion of the large off-GCP signals observed at 5.097 MHz at times when the GCP MUF is exceeded.

4.2.4: Times of propagation on the Iqaluit-Leitrim path

Figure 4.17 presents the times of propagation on the single-hop, trans-auroral path from Iqaluit to Leitrim for each day of 1994. No propagation was observed at all on the 20.3 MHz signal, suggesting that this frequency exceeded the MUF at all times. However at the lower two frequencies the times of propagation are reasonably consistent with the REC533 predictions although there is a periodical loss of signal associated with the recurrent geomagnetic storms. Figure 4.18 indicates that as A_p rises the 5.832 MHz transmission is attenuated in the period 0400-1000 UT and propagation at 9.292 MHz becomes restricted to the 1900-0000 UT period. At $A_p > 35$, 5.832 MHz signals only propagate in the 2300-0100 UT period and 10.195 MHz signals propagate from 1900-2200 UT only.

Reference to Figure 4.8 indicates that increases in geomagnetic activity lead to large changes in the D region absorption in the period 0500-1700 UT with the greatest differential occurring at 1230 UT. These periods are broadly consistent with the observed breaks in propagation although the persistence of a short (~2 hour) propagation period just after sunrise (around 1130 UT) remains unexplained.

4.2.5: Times of propagation on the Iqaluit-Alert path

Propagation on the single-hop, polar cap path from Iqaluit to Alert is generally observed for 24 hours a day at the two lower frequencies of 5.832 MHz and 9.292 MHz although in the winter nighttime the bearings measured become well removed from the true bearing. This accounts for the gaps in the near-GCB times of propagation presented in Figure 4.19. At 20.3 MHz bearings near the GCB have only been rarely observed, indicating that this frequency is usually well above the MUF. There are no discernible changes in the times of propagation with A_p at any frequency (see Figure 4.20).

4.2.6: Times of propagation on the Halifax-Alert path

The times of propagation on this two-hop, trans-auroral path, which enters the polar cap, are presented in Figure 4.21 against day number and in Figure 4.22 against A_p. At 5.097 MHz the effect of daytime D region absorption is evident and in the winter months gaps in the times of propagation result from off-GCP propagation (see Chapter 5). At the two higher frequencies, there is a trend towards earlier propagation cessation times at higher A_p values.

4.2.7: Times of propagation on the Iqaluit-Cheltenham path

The times of propagation on the two-hop, trans-auroral path from Iqaluit-Cheltenham are plotted as a function of day number in Figure 4.23 and as a function of A_p in Figure 4.24. At 5.832 MHz and 9.292 MHz the effects of daytime, D-region absorption around local noon (1357 UT at the midpoint) cause breaks in the propagation. Reference to Figure 4.9 indicates that auroral D region is enhanced in the 0700-1000 UT period with increasing geomagnetic activity with the peak absorption region expanding to earlier local times. This is the probable cause of a loss of propagation in the 0700-1000 period observed at the two lower frequencies for $A_p > 20$. The times of propagation cessation on the 9.292 MHz transmission move up to 4 hours earlier at high A_p and since the 5.832 MHz signal is unaffected at the local times concerned this is most probably a result of a reduction in MUF associated with ionospheric storms.

4.2.8: Times of propagation on the Wainwright - Leitrim path

Times of propagation on the two-hop, sub-auroral path from Wainwright - Leitrim are presented in Figures 4.25 and 4.26 against day number and A_p respectively. In general, the 20.9 MHz signal constantly exceeds the MUF for this path. At the two lower frequencies propagation periods are limited by daytime D region absorption and the 10.195 signal exceeds the MUF at night. However, this path is strongly sensitive to changes in geomagnetic activity and signals were only observed at low levels of A_p. Figure 4.9 illustrates that strong auroral absorption is likely to occur at high A_p between about 0400 UT and 2000 UT and this is likely to have caused the observed confinement of propagation periods to 2300-0300 UT at high A_p.

4.3: Average diurnal variations in signal strength and Doppler spread index

4.3.1: Halifax - Cheltenham

The average signal strengths of transmissions from Halifax to Cheltenham are presented in Figure 4.27 for each UT hour and month in the period 12/93 to 11/94. Prior to averaging the data was divided into geomagnetically quiet (A_p<15) and active (A_p≥15) periods. Each curve is offset by +50 dB and the error bars represent ±1 standard deviation of each hourly average value.

The 5.097 MHz signal strengths are controlled mainly by the level of daytime D region absorption. However a small reduction in signal strength occurs during periods of geomagnetic activity around 0000 UT. This is associated with a loss of GCP propagation and the development of off-GCP propagation associated with the passing of the sub-auroral trough across the path (see Chapter 5).

At 10.945 MHz and 15.920 MHz, the signal strength is largely controlled by the MUF. There is a reduction in the average signal strength at the end of propagation when A_p is high. This is a result of the sub-auroral trough extending into earlier local times, causing the propagation path to close earlier. At 10.945 MHz there is also evidence for a local signal strength minimum in the curves centred about the local noon at the midpoint (1430 UT) due to zenith angle dependant D region absorption.

4.3.2: Halifax - Leitrim

The 5.097 MHz signal strength plots (Figure 4.28) have a primary minimum around 1630 UT which is close to the time of local noon at the path mid-point (1639 UT) and is due to the zenith angle dependence of D-region electron density and non-deviative absorption. There is, however, a secondary minimum in the signal strength in the ~0400-1000 UT period. This period corresponds to the times at which the MUF lies close to the wave frequency. In Chapter 5 it will be shown that since the GCP does not support propagation at these times, alternative, off-GCP paths become dominant and this often involves attenuation due to scattering of the signal or greater free space path loss. The corresponding plots of Doppler spread index averages (Figure 4.29) exhibit broad maxima in the same UT period, and this is indicative of propagation by means of rapidly moving, reflecting and/or scattering electron density structures.

5: Large scale bearing deviations on sub-auroral paths

The bearings and signal parameters for three paths that run W-E or E-W in the region just equatorwards of the auroral oval are examined in this chapter. The ionosphere over these paths is dominated by north-south ionospheric gradients related to the sub-auroral trough and the equatorward wall of the auroral oval particularly at night and at times of geomagnetic activity.

5.1: The Halifax to Cheltenham path

The Halifax - Cheltenham path lies just equatorwards of the auroral oval in the region of the sub-auroral trough. The path is presented in Figure 5.1 together with a modelled location of the auroral oval [*Holzworth and Meng*, 1975]. Figure 5.2 illustrates the composite bearings returned for this path for 25 December 1993 on each of the three transmitted frequencies. This plot represents a day when few bearing deviations from the true bearing of 285° were observed. The two higher frequencies propagate during the day and the reception period is determined by the MUF, whereas the lower frequency propagates only at night since it encounters strong D-region non-deviative absorption during the day but remains well below the MUF at night.

Figure 5.2 also provides an example of co-channel interference observed on the 5.097 MHz signals as an intermittent signal at 318°, 11-19 UT. The signal recognition procedures defined in Chapter 3 can go some way to identifying the bearing associated with the true signal when the bearing is 'single-valued' but cannot discriminate between signals arriving at two different bearings simultaneously. Some co-channel interferers are identifiable by their bearing stability relative to the 'true' signals. This occurs when the interferer is local and propagating via the ground wave, whilst the true signal is in sky wave mode and subject to ionospheric deviation.

The standard deviation and variability of the bearings is generally lower for higher frequencies. This may partly be due to the wider effective aperture of the array at higher frequencies. At the lowest frequency (5.097 MHz) the variability may be attributed to the increased "roughness" of the ionosphere at night [*MacNamara*, 1991 p.190]. The VOACAP commercial computer model predictions often predict a 3F2 mode at dawn/dusk for the lower frequency signal compared to a 2F2 mode during the night and this may also contribute to the increased variance of bearings on the low frequency signal since each ionospheric reflection introduces a further azimuthal deviation where horizontal, cross-path ionospheric gradients are present.

5.1.1: Large bearing swings on the 5.097 MHz signal

The 5.097 MHz bearings for the months of February and March 1994 are presented in Figure 5.3 and 5.4 respectively. The daily A_p values are represented in these figures by the shaded bars.

Significant bearing deviations are observed, the largest of which are observed during periods of high geomagnetic activity ($A_p >= 15$). From the start of propagation in the evening the bearings fall by up to 25° below the true bearing over several hours. Bearings are acquired at around 0000 UT from about 25° north of the true bearing and decline steadily over the next few hours until the true bearing is regained just prior to the cessation of propagation in the morning. An example of the effect for the geomagnetically active period February 6-10 1994 is presented in Figure 5.5 together with the Doppler spread index variations, which increase substantially when large bearing deviations are observed.

These features in the bearings are thought to be due to the reflections from the walls of the sub-auroral trough since at high A_p levels the north wall is expected to lie closer to the GCP 2-hop reflection points during the night (permitting northward deviations) and the southward wall of the trough is much steeper (permitting southward deviations) during periods of geomagnetic activity.

On days when the A_p was particularly high, the signals were observed arriving simultaneously from both north and south of the GCP bearing in the hours around 0000 UT with little or no propagation observed at the GCP bearing. This suggests that reflections are supported from the north and south walls of the trough at this time but penetrate the ionosphere where the rays enter the density depleted trough minimum as it passes over the GCP. On days of moderate A_p or during the summer months a progressive transition was more commonly observed with the bearing swinging from south to north through the great circle bearing. Under the latter conditions the trough minimum would be less pronounced and the reflection point would shift from the equatorward wall to the trough minimum and thence to the poleward wall in a continuous, positive change in bearing as the trough passed over the GCP.

The occurrence of this feature is plotted against Kp in Figure 5.6. A clear, positive correlation with geomagnetic activity is observed. Figure 5.7 illustrates the seasonal variation in the occurrence of this feature. During the winter and equinoctial months (October to March) the number of days on which the characteristic bearing changes are observed (light bars) is closely correlated with the number of geomagnetically active (A_p>15) days in that month (dark bars). In the summer months, however, there is a disproportionately low occurrence of the characteristic bearing changes. This is consistent with the well documented absence of trough related ionospheric gradients normal to the GCP during the summer months. There is some evidence for a secondary minimum in the occurrence frequency of large scale bearing swings around the 1994 winter solstice, though this may not be statistically significant.

The times (UT) at which the bearings (related to this characteristic bearing feature) were suddenly acquired from north of the GCP are plotted against A_p in Figure 5.8 for all such features observed in 1994. Data points are represented by the month number (1=January, 2=February, etc.). The distribution exhibits a clear tendency for the bearings to appear from the north earlier in the night at higher A_p levels. The regression line (least squares fit) plotted on the graph has a 0000 UT intercept of A_p=33.0 and a gradient of -2.4 A_p/hour. This trend can be explained by considering the change in location of the trough with local time and with increases in geomagnetic activity. The trough descends to lower geomagnetic latitudes in the hours leading towards local midnight and propagation is supported from the poleward wall only when it comes into close proximity with the GCP. Since the poleward wall of the trough lies further equatorwards at higher A_p levels, it will pass close to the GCP and support non-GCP at earlier local times.

Large (15° peak to peak) oscillations in the bearing with periods of 1-2 hours are often superimposed upon these diurnal trends and these are possibly due to large scale irregularities such as convecting auroral blobs on the north wall of the trough.

Large scale bearing deviations to the north of the GCP are also frequently observed in the final 1-2 hours of propagation at this frequency on a number of days in winter. Similar 'tails' from the north have also been observed prior to the commencement of GCP propagation (though this is less common). Examples of this may be observed in Figure 5.9 for days 2,3,8,18,19,23 and 31/12/93. These phenomena may result from reflections from the northward trough wall, which would be expected to recede away from the GCP in the hours before sunrise. In winter the solar produced, winter anomaly enhanced, D region would spread across the GCP from the equatorward side such that just before sunrise a reflection from the poleward trough wall would not be greatly attenuated by D region absorption and thus form the strongest signal detected by the direction finder.

5.1.2: Large bearing deviations at 10.945 MHz and 15.920 MHz on the Halifax-Cheltenham path

The bearings recorded on the 10.945 MHz and 15.920 MHz signals for the month of March 1994 are presented in Figures 5.10 and 5.11 respectively. In general the qualitative features of the bearing deviations on the 15.920 MHz measurements are very similar to those at 10.945 MHz, differing only in magnitude or frequency of occurrence. These features are discussed below.

5.1.2.1: Tails in bearing at the beginning and end of propagation

A feature commonly observed throughout the year on the two higher frequency signals is the tailing-off of bearings to the south of the true bearing during the final hour of propagation (in the evening) and similar tails leading up to the true bearing during the initial hour of propagation (in the morning). A 'bearing tail' is defined as a progressive change in the bearing with time, (the term does not relate to the density of bearing points or to signal strength variations). These bearing tails, which can have magnitudes of over 50°, occur on roughly 50% of days. Bearing tails have also been observed north of the GCP though these account for only 10% of the total occurrence.

Good examples of bearing tails are presented in Figure 5.12 for the 15.920 MHz signals of 19th, 20th and 21st March 1994. The panels in each column are (from top) bearing, Doppler spread index, SNR, signal strength and the signal recognition index. The recognition index values remain at 1 during the times of the bearing tails, providing confidence that the tail signals do originate from the Halifax transmitter. The Doppler spread index generally rises from values of around 5 Hz during near-GCP propagation, to around 10 Hz at times of bearing tails. SNR measurements fall from 40 dB to roughly 30 dB during the tail events. Unfortunately, few absolute signal strength measurements were obtainable during the tail periods, presumably due to the failure of the automatic calibration and scaling procedures in processing these very weak signals. It is interesting to observe, however, that during the final hour of propagation on the 19th and 20th March (upper panels of Figure 5.12) the signal strength rises by around 10 dB towards the end of GCP propagation before a rapid fall as the bearings also fall away. The rise is almost certainly due to skip distance focusing - a convergence of the high angle (Pederson) and low angle rays. The fact that the bearings tail off after this rise suggests a mode of propagation at frequencies above the "basic MUF" (also the "junction frequency" (JF) on ionograms). Such modes are often observed as a frequency spread F trace that is called a "nose extension" on ionograms. Examples of these are presented and discussed in the next section for similar bearing tails on the Halifax-Leitrim path.

The percentage frequencies of occurrence of the bearing tails observed below the GCB are represented by the four histograms in Figure 5.13 for three ranges of the maximum bearing deviation magnitude. The charts represent bearing tails observed in the period April 1993 to November 1994 and are divided according to frequency, month of the year, and whether the tail occurred at the beginning or the end of propagation (which at these frequencies occurs in the morning and evening, respectively). The tails are generally larger and more frequently observed at the end of propagation than at the beginning and at the lower frequency of 10.945 MHz rather than at 15.92 MHz. A broad minimum in occurrence is observed in the summer months with a possible secondary minimum about the winter solstice.

Conventional models of the ionosphere (e.g. IRI, PIM, etc.) all display a significant cross-path, electron density gradient (increasing in the equatorwards direction) at sunrise and sunset at the latitude of this path. This information alone is sufficient to explain the predominance of equatorward bearing deviations at times when the signal frequency fractionally exceeds the MUF on the GCP. The combination of larger MUFs and a favourable ionospheric tilt on the equatorward side leads to the observed bearing deviation.

Figure 5.14 is a schematic diagram to illustrate how ionospheric tilts associated with the solar terminator might explain how the observed bearing deviations are larger at sunset than at sunrise despite the steeper ionospheric gradient associated with the solar terminator at sunrise. This path requires two ionospheric reflections and thus the ionospheric tilts associated with the solar terminator must lie closer to the reflection point farthest from the receiver at sunrise whereas at sunset it would lie closer to the reflection point nearest the receiver. Thus, if the maximum equatorward deviation of the ray path were similar at sunrise and sunset, the bearing deviation at the receiver end would far exceed that observed at sunrise.

The fact that the bearing tails are larger and more prevalent at 10.945 MHz than at 15.920 MHz indicates that the isoionic contour surface reflecting the lower frequency signal moves more slowly away from the GCP at sunset (for example) and remains appropriately oriented for a longer period.

The occurrence statistics of the equatorward tails are given as a function of Kp ranges in Figure 5.15. This figure indicates a slight increase in the frequency and magnitude of southerly deviations at large Kp at the end of propagation. Such a change might reflect the increase in the steepness of the equatorward trough wall, which would extend across the path in the evening and enhance the ionospheric gradients associated with the sunset terminator.

On a small number of days, the 10.945 MHz or 15.920 MHz signals may exhibit a short, 1.5-2.0 hour period of GCP propagation prior to the normal commencement of propagation, often with a tail. There is usually a short break in propagation between the two modes. Occasionally both commencements are preceded by the equatorward tails in bearing. A similar effect may be observed at the end of propagation.

An example of this type of propagation is presented in Figure 5.16. (Note that the signal recognition index (marked "FSK") in this figure refers to the procedure explained in section 3.4.2 in which the signal spectrum is analysed to determine whether peak and sidebands are present at the correct frequency offsets.) Further examples of this extra mode of propagation are observed on the 10.945 MHz signals on 27th December 93, and on the 15.920 MHz signals on 14th January 1994, 25th, 26th, 28th and 30th March 1994 and 5th, 9th and 15th November 1994.

Without the aid of ionograms, it is impossible to be certain as to the cause of this extra mode of propagation. A 1F mode would be possible when the virtual height of reflection was greater than

$$h' = R_E \cdot \left(\sec\left(\frac{D}{2R_E} \right) - 1 \right) \qquad \text{Eqn. 5.1}$$

$$= 417 \text{ km}$$

(taking R_E =6370 km, and the path length, D = 4491 km).

It may be that only the high angle 1F ray is able to propagate at these times. Alternative candidates are the F-E mode at sunrise or the E-F mode at sunset.

5.1.2.2: Anomalous, night-time propagation at bearings north of the GCP

There are many examples in the data where propagation occurs at a bearing >10° greater than the true bearing at times when GCP propagation does not occur and is not expected from propagation prediction models. The phenomenon occurs during the night for the two higher frequencies (10.945 MHz and 15.920 MHz) at times when the predicted MUF is exceeded. Figure 5.17 presents receiver data from three out of five days on which the anomalous propagation events (APEs) were of sufficient signal strength to provide measurements of spread index, SNR and signal strength. In all cases the signal strength is much reduced during the APE although

SNRs are similar to the daytime values. The Doppler spread index on these three days is seen to rise to extraordinarily large values (up to about 90 Hz) during the APE - especially at times where the bearing suddenly moves to the north (to higher bearings). This would be as expected for propagation involving scatter from FAIs which rapidly fluctuate in position. The signal strength of the anomalous nighttime propagation generally appears to be negatively correlated with the magnitude of the bearing deviation. A sudden contraction of the irregularity zone to higher latitudes (or disappearance of irregularities at lower latitudes) would increase both the free space path loss and the required angle of scatter, thus reducing the strength of the scattered signal at the receiver. The signal spectra for these nighttime propagated transmissions show a well-defined signal peak within about ±2 Hz of the frequency observed during normal daytime propagation suggesting that the signals are indeed transmitted from the CFH transmitter in Halifax.

This phenomenon is usually associated with a sudden onset of geomagnetic activity. For example, of the twelve anomalous propagation events (APE) in the 26/11/93-31/3/94 period, seven (58%) occurred within 24 hours of a rise from $Kp < 2$ to $Kp > 4$ and four of the remaining five were recurrences of an event that occurred the previous night (i.e. they occurred on the second night of a geomagnetic storm). Eight (67%) of the APEs were associated with the onset times of principal magnetic storms in this period although there are storms where events are not evident and a few APEs occur where there are no obvious storm onsets. D_{st} values for December 1993 indicate that all four events in that month coincided with the four large (< -40nT) drops in D_{st} for that month.

In Figure 5.18, the times of occurrence are plotted as red bars on a plot of a_p index for twelve months. (The length of these bars indicates the a_p level during the APE events). Many (but not all) of the occurrences are concurrent with sharp increases in the a_p index.

During the main phase of geomagnetic storms the trough moves equatorwards in conjunction with the equatorward boundary of energetic particle precipitation in the auroral zone. This brings this tilted region close to the GCP, so increasing the likelihood of reflections from ionospheric locations to the north of the GCP. In addition, enhanced energetic particle precipitation in the first 24-48 hours of a storm leads to the formation of field-aligned electron density structures on the poleward trough wall from which HF signals may be forward scattered. The times (UT) of anomalous propagation show a hint of a seasonal dependence - shifting to later hours in the spring.

For the 10.945 MHz frequency - where such anomalous propagation is most common - the times of anomalous propagation north of the true bearing (observed from 5° to 55° above the GCB) has been measured during the period 26/11/93 to 31/3/94 (a continuous dataset). These measurements are presented in Figure 5.19 together with the associated Kp values (averaged from 1200 to 1200 UT). At higher Kp the propagation start and end times are observed to occur at earlier times. The earlier APE start times at high Kp may be a consequence of the more equatorward location of the auroral oval that is subsequently encountered at earlier local times in the evening.

Further analyses of examples of APEs on the Halifax-Cheltenham path for the period up to 31/12/94 have shown at least two occasions where the off-GCP propagation is observed during the daytime in association with large drops in D_{st}.

5.1.2.3: Anomalous night-time propagation to the south of the path at 10.945 MHz

Presented in Figure 5.20 are three examples for which 10.945 MHz signals arrive at bearings of up to 50° to the south of the GCP during night-time periods for which this frequency is predicted to lie well above the MUF on the GCP (as determined from propagation prediction models such as REC533). Doppler spread index values tend to rise only slightly (up to 5 Hz) or not at all during these events whilst signal strengths are 40-50 dB below the daytime values.

The bearing changes are often continuous and smoothly varying and form a predictable U-shaped curve joining the daytime propagation bearings that are close to the GCB. This U-shaped curve varies little between the days of occurrence (see Figure 5.21) and often occurs over periods of several days. Of 450 days between 1/12/93 and 30/4/95 for which measurements are available, this type of propagation was identifiable on 26% of the days. On these days, geomagnetic activity was markedly low, with a mean A_p value of 11.6 and a standard deviation of 7.6.

The fact that there are often no large increases in Doppler spread index during these night-time propagation events suggest that the ray is not scattered from ionospheric irregularities but may be reflected from North-South (path normal) gradients in the ionosphere that persist throughout the night. The magnitude of the deviation is seen to peak around the times where the signal frequency would be expected to be closest to the MUF. In these conditions the horizontal electron density gradients cause the largest effective tilts in the ionosphere [*Titheridge*, 1958] and thus the largest lateral deviation in bearing. At periods of low A_p, the poleward trough wall lies well to the north of the GCP and would play no active rôle in supporting propagation. However, propagation may be supported at night due to reflections off the equatorward wall of the trough.

Warrington et al. [1999] recently investigated an alternative mode of propagation for these signals, which involves forward scatter from a rough sea surface. Numerical ray tracing was performed through a two-layer Chapman model of the ionosphere with layer parameters based upon the International Reference Ionosphere (IRI) model [*Bilitza*, 1990]. A latitudinal electron density gradient was applied to the model, together with a model of the sub-auroral trough based upon the equations of *Halcrow and Nisbet* [1977]. These ray-tracing studies demonstrated how the formation of the trough prevented rays from the first hop to land on the GCP, but these rays could propagate to regions to the south of the GCP. Further ray tracing was performed for the second hop starting from the extreme positions of the regions of high power density at the sea reflection. The bearings of those signals returning to the Cheltenham receiver were determined and compared very well with those measured experimentally. Further ray-tracing studies are in progress and will assess the correspondence between the observed bearings and the changes in the position of the trough with changes in geomagnetic activity.

A summary of the distribution of 10.945 MHz signal bearings from Halifax to Cheltenham and their variation with A_p is presented in Figure 5.22 for spring 1994 (4/2/94-5/5/94). Each frame represents the number of composite bearings returned within 10°×30minute bins on the bearing-UT plane and the values are normalised for each 30minute UT bin. The total number of data points used in each 30min UT bin is represented in the underlying histograms. Equatorward, U-shaped bearing deviations occur at night at low A_p (<20), and as A_p rises propagation cessation occurs at earlier local times due to the expansion of the trough into the evening/late afternoon sector. At high A_p (>50) propagation to the north of GCP occurs during the night and large tails are observed at the end of propagation.

5.2: The Halifax-Leitrim path

The 911 km path from Halifax to Leitrim is the shortest path of the experimental campaign and exhibits the largest systematic bearing deviations of all paths except those entering the polar cap ionosphere. This is unsurprising when one considers the large, horizontal ionospheric gradients at this latitude associated with the sub-auroral trough and the proximity of reflective structures in the auroral zone, which lies to the north.

Examples of the composite bearings for the 5.097 MHz and 10.945 MHz signals are presented together with the daily A_p index in Figures 5.23 and 5.24

respectively for each day in March 1994. Note that there are data missing on the 1st March and from 1900 UT on the 28th to 1700 UT on the 29th. Bearings measured at the frequency of 10.945 MHz were far less disturbed than the 5.097 MHz bearings. From February to March there were only one or two large (>10°) swings in the bearing per month and these occurred during the first and (more usually) the last hours of propagation (see for example the night of March 26th/27th). At 5.097 MHz however, very large bearing deviations of up to ±100° are evidently a common feature.

Of 164 days between 17/2/94 and 24/11/94 for which measurements were made, large, off great circle bearings were observed at 5.097 MHz on about 70% of days. At the beginning of propagation, the bearings generally commenced from the north of the true bearing (89% of days) whereas at the end of propagation the 'tail-off' in bearing was predominantly towards the south of the true bearing (62% of days). In Figure 5.25 the percentage frequency of occurrence of these bearing tails at the beginning and end of normal propagation are plotted against ranges of A_p for all days in the period 17/2/94-24/11/94 for which data were available. The data are divided according to whether the bearing tail increases or decreases in bearing. The predominance of tails that increase in bearing is evident in these graphs, as is the increase in occurrence for greater values of geomagnetic activity.

The fact that both positive and negative bearing deviations are observed indicates that propagation is supported from both the equatorward and poleward walls of the sub-auroral trough. As the MUF approaches the signal frequency, the ray-path remains in the ionosphere for an increasing length of time and is therefore subjected to progressively larger bearing deviations until the ray penetrates. The trough is deeper and has steeper walls during geomagnetically active periods such that off-GCP modes of propagation are far more likely to occur at these times.

A 1F mode of propagation was predicted from commercial prediction models (VOACAP and REC533) and 1F and $1E_s$ propagation were the most frequently observed modes on the oblique incidence ionograms recorded over this path in February to April 1994. Modelling of the propagation conditions for March 1994 using the REC533 prediction software yielded the MUF and operational MUF (OPMUF) curves in Figure 5.26. The program calculates Operational MUF as the basic MUF multiplied by a correction factor (>1) to allow for propagation mechanisms at frequencies above the basic MUF. At 5.097 MHz the MUF is exceeded during the period 0500-1000 UT although the OPMUF is never exceeded.

Figure 5.27 provides an enlarged view of the bearing deviations for a geomagnetically quiet period from March 24th to 26th. Note the slight increase in the spread of the bearings from about 0000 UT onwards - a period during which propagation is supported by the rougher, nighttime ionosphere. GCP propagation is completely lost at times where the model MUF is less than the operational frequency, but signal reception is maintained at bearings displaced from the GCP by up to 100° either side of the GCB.

During periods of high geomagnetic activity (Figure 5.28) the times at which the great-circle propagation path closes and opens are several hours earlier than those predicted from model MUF predictions. As before, these coincide with large bearing deviations of up to 100°. This behaviour may result from the extension of the trough into earlier local time sectors at high A_p.

When several months of data are analysed, a good correlation emerges between the periods of large bearing errors and the level of geomagnetic activity (A_p). In Figure 5.29 the dependence of the start time of the large bearing errors is presented as a function of the A_p index for March 1994. Periods of large bearing error (> ±50°) are plotted alongside A_p values in Figure 5.30 for days in the period 20/2/94-20/6/94. Relationships of this nature can provide a useful guide for the HF communications or DF operator and could be incorporated into prediction and planning tools.

5.2.1: Inverted-U bearing structures

A class of bearing deviation feature that are distinct from the 'tails' discussed above is evident on a large number of days on the 5.097 MHz signal. These are characterised by the sudden acquisition of a signal well to the north of the GCB as the GCP propagation ceases. Sometimes these bearings approach the GCB over a period of about two hours, reaching minimum deviation close to local midnight (0430 UT) and then receding away to the north, ceasing entirely as GCP propagation resumes. Examples of this type of bearing structure are observed on 2nd, 5th, 21st and 23rd March (see Figure 5.23). The magnitude of the bearing offset generally diminishes with increasing levels of geomagnetic activity. This trend may be observed in Figure 5.31, which represents the normalised distribution of composite bearings on the bearing-UT plane for all days in 1994. The distributions are normalised within each 5°-bearing bin and the results binned into A_p ranges. For A_p levels up to A_p=30, the inverted-U structure is very clear, peaking at about 5-6 UT (0030-0130 LT). There is also a clear trend towards smaller, negative bearing deviations at higher geomagnetic activity levels. At A_p levels above 30, the inverted-U structure is less clear, and tails in the bearing are the most prevalent features, with tails to higher bearings occurring before local midnight, and tails from lower bearings after local midnight. The general trend for bearing deviations to occur at earlier local times is also apparent at the higher A_p levels.

These characteristic features are all consistent with the suggestion that these bearings result from reflections near the equatorward wall of the auroral oval (or equivalently the poleward wall of the trough). The auroral zone moves closer to the GCP at higher levels of A_p such that bearing offsets to the north of the GCP would diminish with increasing A_p levels. In addition, the equatorward auroral boundary is shaped in local time such that it lies closer to the GCP near local midnight, thus explaining the inverted U shape often present in these bearing structures.

To provide a reference for comparison, Figure 5.32 presents the 5.097 MHz signal characteristics alongside bearing measurements for the 20th March 94, a day during which few bearing deviations occurred and geomagnetic activity was low to moderate. The Doppler spread index is constant and generally below 10 Hz, the signal strength at the receiver varies smoothly from 55 dBµV at local midnight to about 15 dBµV at local midday and signal recognition procedures (FSK) identify correctly placed spectral peaks and modulation sidebands throughout the day.

In Figure 5.33 the same characteristics are presented for the following day (21/3/94) on which an inverted-U bearing structure was observed between 0430 and 1030 UT. The Doppler spread index of the signal exhibits a close correlation to the bearing offset during this period, extending up to 60 Hz. The signal strengths are about 20 dB below normal levels and exhibit a negative correlation to the magnitude of the bearing offset.

In Figure 5.34 the bearings and signal characteristics are presented for the 27th February 1994. The measurements on this day exhibit reflections from both poleward and equatorward walls of the sub-auroral trough. For a few hours around local midday (1630 UT) the signal strength is a minimum, the signal recognition procedures fail to identify the signal and the composite bearings returned by the DF become spread in bearing and sparsely distributed. This noontime loss of signal, observed on some but not all days at this time of year (82% of days in February, 17% of days in March) is most likely due to non-deviative absorption of the ray as it traverses the solar UV enhanced D region of the ionosphere.

The signal strength starts to fall from about 0350 UT. 30 minutes later at 0420 UT, the bearings begin to move away from the GCB to higher values, indicating reflections from equatorward side of the path. The bearing offset increases to +30° over a period of one hour, during which the signal falls 40 dB and the Doppler spread index rises by only 15 Hz (typically bearing tails do not exceed 30 Hz in Doppler spread). At this point the direction finder begins to lock-on to a weak signal arriving from 65° below the GCB (i.e. from the Northeast). The Doppler spread index of this type of signal is very large (typically 40-70 Hz). The signals are observed from both north and south of the GCB throughout the night.

The observations suggest that the weak, spectrally diffuse reflections from the North arise from physical processes that are distinct from those producing the less attenuated bearing tail signals which are subject to more moderate spectral spreads. The former may arise from scattered signals from field-aligned irregularities in the poleward trough wall, which are rapidly fluctuating on temporal and spatial scales. The latter are more probably due to specular reflections from the walls of the trough. In both cases an increase in the bearing offset is generally associated with an increase in spectral spread and a reduction in signal strength.

5.2.2: Oblique ionograms over the Halifax - Leitrim path.

Oblique ionograms were obtained over the Halifax-Leitrim path from 22nd February to 15th April 1994. The receiver at Leitrim recorded ionograms at 30 minute intervals over the frequency range 2-30 MHz from a BR Communications RCS-5 chirp sounder in Halifax. Sequences of these ionograms are presented to help identify the cause of the large bearing offsets described above. For clarity, only frequencies in the range 2-16 MHz are presented here and the operating frequencies of the Halifax transmitter are marked as black vertical lines. Since there was no facility available for accurate clock synchronisation between transmitter and receiver sites, the absolute time-of-flight could not be measured and only the relative delay between modes could be recorded on each ionogram. A zero 'relative delay' therefore represents a non-fixed range of absolute group path delays. For reasons of clarity, the colour scale represents the signal amplitude measured relative to the strongest signal at each frequency.

5.2.2.1: Ionogram nose extensions and bearing tails.

27th February 1994

The 5.097 MHz bearings of Figure 5.34 remain close to the GCB until about 0420 UT and the signal remains strong and exhibits little Doppler spread. The ionogram for 0335 UT presented in Figure 5.35 indicates that propagation at this time is via a strong, single-moded, 1F mode. Note that 2F and 1E modes are evident at lower frequencies and there is no division of the F-layer trace into F1 and F2. From 0435 UT to 0505 UT the bearings exhibit a positive deviation from the GCB, a small rise in the Doppler spread index (from 5 to 20 Hz) and a drop in signal strength by up to 40 dB. The associated ionograms exhibit a diffuse, upward slanting, spread-F feature at the 5.097 MHz propagation frequency that extends up to 1 MHz above the 1F(x) junction frequency. This feature is called a "nose extension".

Nose-extensions are commonly observed on high latitude, oblique incidence ionograms and are indicative of reflections from a tilted ionosphere. To visualise this phenomenon, one may consider the case where the reflection height (hmF2) remains roughly constant but critical frequencies increase away from the path midpoint in a direction normal to the GCP plane (see schematic in Figure 5.36). As the operating frequency approaches the MUF for the GCP (i.e. the junction frequency), the high and low angle rays converge. At frequencies higher than the junction frequency, the rays will penetrate in the GCP plane and may only be reflected at the higher critical frequency contours to the side of the path. Thus the path length (group path delay on the ionograms) increases steadily above the junction frequency.

It is highly probable that nose-extensions result from the same physical processes that lead to slant-F on backscatter ionograms (see Figure 2.2b). Both are characterised by relatively low Doppler spreading of the signal spectrum.

5.2.2.2: Auroral backscatter and large, northward displacements in the bearing

During the period 0520 to 0620 UT signals are also observed at bearings 65° north of the GCB and indicate a reflection from a point well to the north of the GCP. At these times, the ionograms indicate that 5.097 MHz signals also reflect from a diffuse, horizontal band about 3.5ms above the minimum of the 1F trace, just visible at the top of the ionogram. The associated Doppler spread increases up to 30 Hz. The period 0800 to 1020 UT returned bearings deviated to the north only (by up to 90°) and showed Doppler spread indices of 40 to 70 Hz. The ionograms show that at this time the MOF of the nose-extension mode is exceeded and propagation is solely by means of the 3ms delayed horizontal band. At around 1030 UT the MOF of the nose extension exceeds 5.097 MHz and propagation is again observed from bearings up to 20° south of the GCB with Doppler spread indices returning to less than 25 Hz. At 1105 the bearings return close to the GCB, the Doppler spread index falls to below 10 Hz and the signal strength recovers, increasing by 30 dB. The ionograms show that the daytime 1F mode of propagation has returned.

The delayed, horizontal, diffuse band associated with the large Doppler spreads and displacement of bearings to the North exhibit distinct similarities to the auroral backscatter echoes discussed in Chapter 2 (see Figure 2.2). One could therefore postulate that they are caused by the same physical mechanisms (i.e. reflection from field-aligned irregularities in the auroral F region). The fact that only a single band is observed may be due simply to the limited delay dimensions of the ionogram window.

2nd March 1994

A clearer example of the horizontal 'spur' was observed on the ionograms recorded for 2nd March 1994. Figure 5.37 shows that the GCB propagation was lost for a period of a few hours during the night during which propagation continued at bearings well to the north of the GCP. The ionograms for these times clearly indicate the 3ms delayed, horizontal trace associated with this type of off-GCP propagation (see Figure 5.38). From 0405 UT, the 5.097 MHz bearings are close to the GCB (at 89°) and a strong 1F mode of propagation is observed in the ionograms with the MOF of the F region trace well above the 5.097 MHz operating frequency. The MOF steadily diminishes towards 5.097 MHz over the next few hours until 0705 UT. As this happens the delay of the ionogram at 5.097 MHz increases relative to the minimum of the F layer trace and the bearings steadily increase at this frequency (indicating a progressive swing to the south of the GCP). The junction frequency (JF) in the F layer trace is often difficult to ascertain in these ionograms due to the relative weakness of the high angle ray. However the trace generally appears to curve sharply upwards and spread in time towards the MOF and is often split into two traces due to magneto-ionic splitting of the ray into its o and x components (see for example, the ionogram of 0635 UT at 5.3 MHz and 5.9 MHz).

Between 0735 UT and 1035 UT the F region MOF drops below 5.097 MHz and the strongest ionogram trace is the roughly horizontal (though slightly upwards slanting), highly spread trace roughly 2.75 ms above the minimum of the F-region trace. This trace is delay spread by over 0.5ms and may support frequencies up to about 10 MHz. The bearings at this frequency show a sudden shift to between 0° and 15° (i.e. signals arriving from the North) and near–GCP bearings cease. At 1035 UT, the bearings return close to the GCB and the MOF of the 1F trace again exceeds the operating frequency.

5.2.2.3 Nose extensions and bearing tails at 10.945 MHz

A clearer example of the association between bearing tails and nose extensions on ionograms was observed on the 26th/27th March 1994. This followed an extended period of low geomagnetic activity. The bearings at 5.097 MHz and 10.945 MHz are presented in Figure 5.39 and the higher frequency bearings exhibit a relatively rare bearing tail. The associated ionograms in Figure 5.40 indicate that at 2235 UT the junction frequency of the 1F trace is just coincident with the operating frequency at 10.945 MHz. Propagation is still supported above this frequency by a 'nose extension' extending to about 11.7 MHz. In the following hours (to 0135 UT) the junction frequency steadily declines to about 9.5 MHz whilst the nose extension remains in place, extending out to about 12 MHz. The relative delay of the nose extension trace above the minimum of the 1F trace also increases. Meanwhile, the bearings at 10.945 MHz steadily decrease up to 30° (poleward of the GCP).

A similar effect is observed at 5.097 MHz on the ionograms and bearings in the 0700 to 1000 UT period of 27 March 94 though the bearing deviation is much larger (up to -110°). The same nose-extension feature may be observed in all the intervening ionograms, the only change being a steady drop in the associated frequencies. It is interesting to note the development of the ionograms from an upward slanting spread F trace at 0735 UT to a distinct horizontal 'spur' at 0805 UT which then proceeds to increase in relative delay above the minimum of the F layer trace over the next two hours as the bearing deviation increases.

5.2.2.4: Approximate location of the reflection regions

An approximation of the location of the reflection region in the ionosphere may be obtained by combining the information from bearing measurements with the group path delay measurements from ionograms. The location is found by simultaneously solving the equations of the absolute group path delay ellipsoid, the great circle plane corresponding to the bearing and the sphere corresponding to an assumed virtual height of 300 km (assuming low angle ray reflections from F-region altitudes). The absolute group path delay was estimated from the relative delay on ionograms by assuming a virtual height for the E (or E_s) layer of 120 km, or where the E trace was not evident the minimum group delay of the F layer trace was assumed to be due to GCP reflections at a virtual height of 300 km. The geometry is detailed in Appendix D.

Some results of this analysis are presented in Figure 5.41 in corrected geomagnetic latitude and local time co-ordinates for the 2nd March 1994. The position of the auroral oval as determined by the *Holzworth and Meng* [1975] model corresponding to the average Kp level for this day is also shown. The co-ordinates of the reflection regions are represented with a + and labelled with the time of observation in UT (note that solutions to the geometry are not always unique). The dashed line indicates the latitude of the mid-point of the great circle path. From 0835 to 1005 UT (the period of large bearing deviations to the north) the approximate reflection regions lie up to 10° north of the mid-point, a few degrees south of the predicted equatorward boundary of the morning-side auroral oval. The latitude of the reflection region decreases by a few degrees throughout the event.

Results presented for the 11th March in Figure 5.42 show the proximity of the reflection region to the evening-side, equatorward auroral boundary at ~0100 UT and the morningside boundary where the bearings return to the reflection from the north at 0705 UT.

5.2.3: Systematic ionospheric tilts and diurnal changes in bearing at 6.43 MHz

One of the most noticeable features on the Halifax-Leitrim path is the moderate (±4°) diurnal change in bearing. This effect was most significant on the lowest frequency signal during April and May 1993 (which at this time was 6.43 MHz). The effect is not so pronounced on higher frequencies or during the other months studied (after Nov. 1993) when the lowest frequency was 5.097 MHz. An example of the effect for the month of April 1993 can be seen in Figure 5.43.

As discussed in Chapter 2, similar effects have been analysed on a similar EW path at a similar frequency by [*Tedd et al.*, 1985], the authors having associated the effect with Systematic Ionospheric Tilts (SITs). These are the ever present latitudinal and local time gradients observed in global maps of foF2 and hmF2.

5.3: The Wainwright-Leitrim path

The propagation path from Wainwright to Leitrim is similar to the path from Halifax to Cheltenham in that it is a long W-E path lying just equatorwards of the region of visual aurorae. However, the shorter path length of 2633 km will support single-hop, F mode propagation and the lower transmitter power at Wainwright results in greater susceptibility to the effects of D-region absorption (as discussed in Chapter 4). Reliable bearing measurements have been obtained for the period 26/11/93 to 31/5/94, though there are several gaps in the data.

At the highest frequency of 20.9 MHz, an analysis of the frequency at which bearings were obtained near the expected GCB of 301° shows that propagation was supported for only a few days in May 1994. There are no large-scale deviations in the bearings at this frequency.

The largest bearing deviations on this path were observed at the lowest transmitter frequency of 6.905 MHz. Examples of these bearings for May 1994 are presented in Figure 5.44. The magnitude of these deviations typically ranged up to 25° in any particular day and this value remained relatively constant over the entire observation period (November -May). The lack of seasonal variation, together with the fact that the vast majority of the deviations were at bearings to the north of the GCP suggests that the deviations are caused by ever-present ionospheric features in the auroral zone and not so much due to changes in the F-region gradients associated with the sub-auroral trough that would be expected to diminish from winter to summer. Examples of such ionospheric features include reflections from patches of auroral E and reflections from F-region auroral boundary blobs, auroral blobs and sub-auroral blobs.

The 6.905 MHz bearings show a number of recurrent, characteristic features. During geomagnetically quiet periods (A_p<10) the bearings remain relatively steady for the first 8 hours of propagation before turning 20° northwards (to higher bearings) for a couple of hours and then returning to the true bearing. Examples of this behaviour may be observed on 20th - 23rd May 1994 in Figure 5.44. The times of the peaks in bearing for this period increase from 0800 to 1000 UT (~0200 to 0400 LT).
The associated variation in signal strength and Doppler spread index is presented in Figure 5.45 for three of the best examples of this feature. The signal strength typically falls by just 10 dB during the bearing deviation and Doppler spread index can rise from ~15 Hz to ~40 Hz. The REC533 HF frequency planning computer program predicts that the MUF on this path lies close to the transmission frequency of 6.905 MHz during the period 0830-1100 UT at this time of year. The transient deviation of the bearing to the north might therefore result from a loss of sufficient ionisation on the GCP and a deviation towards higher levels of ionisation associated with the equatorward edge of the auroral zone.

During periods of moderate geomagnetic activity (A_p ~ 10-30) the bearings exhibit several peaks, generally to higher (more northerly) bearings and with greater bearing point density and coherence observed on the decreasing bearing swings. Examples of this behaviour may be observed in Figure 5.44 for 15-19 May. During high geomagnetic activity (A_p >30) the 6.905 MHz signal is highly attenuated due to storm related, sub-auroral D-region enhancement (see Chapter 4). Often the only bearings returned under these conditions are due to a single, very large bearing swing with a duration of approximately 3 hours, between 0000 UT and 0400 UT (~1800-2200 LT), and invariably from north to west, ranging from +40° to -20° relative to the GCB. Examples of such bearings are observed in Figure 5.44 on the 9th, 10th 14th May as the sole bearing structure, whilst bearing swings of a similar nature form the dominant feature on other days (e.g. 17th-19th May).

A statistical analysis of the swings in the 6.905 MHz bearing measurements was performed by recording the bearing and time of the beginning and end of each distinct swing (as judged by eye from the measurements). The times of commencement of each swing were divided into hourly bins and were sorted according to the direction of bearing swing (positive or negative going) and according to the sign of IMF B_z component and the 3-hourly a_p value. The results are presented in Figure 5.46. The negative going swings (black bars) greatly outnumber the positive going swings (grey bars), and this ratio increases where a_p is high and B_z is negative. The time of maximum occurrence of the negative going swings is also seen to move to earlier local times (from about 2300 LT to 2000LT) for high a_p and negative B_z.

The bearings of the 10.195 MHz signal are plotted for May 1994 in Figure 5.47. The only significant, large scale bearing deviation at this frequency is a ±20° swing in the bearing from above GCB to below the GCB at the end of evening propagation (~0000-0400 UT) and these are usually in good time synchrony with a similar swing in the 6.905 MHz bearings. The bearing rises by 10-20°, returns to the true bearing and then falls steadily to up to ~20° below the true bearing (see for example 14th, 15th, 25th May in Figure 5.47). The statistics of bearing swing occurrence at 10.195 MHz is presented in Figure 5.48 in the same format as Figure 5.46. The overall number of swings observed at this frequency is much reduced and they are predominantly decreasing in bearing. The peak occurrence correlates well with the peak in the distributions for the 6.905 MHz swings and moves from about 2130LT to 1930LT during conditions of high A_p and negative B_z.

The predominance of negative-going bearing swings and their local time distribution may be explained by the presence and motion of auroral blobs near the equatorward boundary of the auroral oval. In the pre-midnight sector these blobs convect in the sunward return flow of ionospheric plasma from the midnight sector in a westerly direction. If the reflection point of the path coincides approximately with the blob location then a bearing swing would commence at high (northerly) bearings when the blob was close to but slightly polewards of the receiver. The bearing would then descend towards the great circle bearing as the blob moved along the propagation path towards the transmitter in the sunward return flow of the convecting F-region ionosphere. A bearing deviation swinging from positive to negative implies that the reflection region (blob) crosses the GCP.

At greater levels of geomagnetic activity the equatorward boundary of the auroral zone expands equatorwards towards the path and the auroral blobs are encountered at an earlier local time. This might explain the earlier peak in the occurrence of bearing swings at higher A_p levels. The convection flow velocity also increases at high A_p, leading to a greater number and speed of auroral blobs arising in and spreading away from the midnight auroral region. This would lead to a larger number of blobs crossing the GCP and hence the multiple swings observed in the bearings. The lack of observations of bearing swings (or indeed any coherent bearings) in the local midnight and morning sectors is probably a result of strong auroral absorption in these local time sectors.

5.4: Summary of large bearing deviations on sub-auroral paths.

Paths lying equatorwards of, and tangential to the auroral zone frequently support off-GCP propagation associated with either the cross-path gradients of the sub-auroral trough or scatter from field-aligned irregularities near the poleward trough wall (equatorward auroral boundary).

The trough is a nighttime feature and so tends to support propagation only at the lowest frequencies. Reflections from both poleward and equatorward walls of the trough have been observed on both a one-hop and a two-hop path during the winter and equinoctial months at periods of high geomagnetic activity (A_p >15) when the gradients of the trough are large. The signals at these times exhibit moderate spectral spread with the Doppler spread index rising by up to about 20 Hz. The bearings usually tail away from the true bearing to the south of the path reflecting from the equatorward trough wall as GCP propagation ceases to be supported. As the poleward trough wall approaches the path, the signals start to arrive from a direction polewards of the GCB and this bearing deviation diminishes over a few hours towards the GCB. Ionograms obtained on the one-hop path (Halifax-Leitrim) show that when this type of bearing error occurs, spread-F, 'nose-extension' traces are observed, increasing in group delay as the frequency rises above the conventional 1F mode, junction frequency.

Deflections towards the equatorward side of the GCP have been observed on 10.945 MHz signals on the 2-hop path from Halifax-Cheltenham on successive nights when geomagnetic activity levels were low. These are not observed during geomagnetically active periods due to the depletion in foF2 values associated with ionospheric storms and the equatorward spread of the trough. Recent ray tracing studies by *Warrington et al.* [1999] have demonstrated that the magnitudes of these deflections are consistent with a seascatter mode of propagation.

A second type of off-GCP propagation path to the north of the GCP has been observed in bearings from both 1-hop and 2-hop paths, during periods for which the MUF on the great circle path is predicted to be exceeded. The bearings typically switch suddenly to and from these northerly bearings rather than tailing away from or towards the GCB and the signal exhibits a very large spectral spread (60-90 Hz spread index) and very low signal strengths. This type of propagation occurs on the 2-hop (Halifax-Cheltenham) path only in the 48-hour period following the onset of a geomagnetic storm and has been observed during the daytime for short periods. These signals are probably due to scatter mode propagation from field-aligned irregularities on or near the equatorward wall of the auroral oval. On the 1-hop (Halifax-Leitrim) path the poleward bearing deviations have been observed to diminish and then recede away from the true bearing during the event. A statistical study has also indicated a tendency for the bearings of this mode to lie closer to the GCB at times of higher A_p, consistent with the increased proximity of the auroral oval at these times. The ionograms for the 1-hop path for these events show a diffuse, horizontal band (or 'spur') extending typically 4 MHz above the 1F junction frequency and delayed by typically 3ms from the 1F mode. Estimates of the approximate location of the reflection region made by combining the measurements of delay with bearing measurements place the reflection region 2-4° equatorwards of the predicted location of the equatorward boundary of the auroral zone.

Swings and peaks in bearing have been observed at moderate to high activity levels at the lowest frequencies on the Wainwright - Leitrim path and also on the Halifax-Cheltenham path (superimposed on northward diurnal bearing shifts). A statistical analysis of these swings on the former path suggests these may be due to the westward motion of auroral boundary blobs convecting away from the midnight auroral zone.

6: Large bearing errors on trans-auroral and polar cap paths

This chapter examines the large scale bearing deviations observed on propagation paths that either cross the auroral oval or are contained within the polar cap ionosphere. The ionosphere in these very high latitude regions is characterised by large scale, localised plasma structures that drift in the F-region convection flows. Consequently, large, rapid and often periodic fluctuations in the bearings are often observed.

The paths under consideration run from Iqaluit to Alert, Iqaluit to Leitrim and Halifax to Alert. Ionograms have been recorded for the Iqaluit-Alert path only, and so particular emphasis has been placed on the analysis of these data.

6.1: The Iqaluit-Alert path

The 2095 km path from Iqaluit to Alert is situated such that at ionospheric altitudes the ray path lies entirely within the polar cap. Propagation on this path is normally observed for 24 hours a day at the two lower frequencies of 5.832 MHz and 9.292 MHz although in the winter months the bearings measured become well removed from the true bearing in the hours around local midnight and bearing errors greater than 50° are commonplace. At the higher operating frequency of 20.3 MHz, bearings near the GCB have only been observed for short time periods (a few hours) on only 14 days of the campaign. This indicates that this frequency is usually well above the MUF.

The signal characteristics obtained from receiver measurements were of poor quality and no reliable values of signal strength, spread index or signal recognition could be obtained. This may have resulted from a problem with the site antenna distribution system.

Bearing data was of good quality between 25/1/94 and 1/6/94, but from 2/6/94, the bearing measurements were suddenly and considerably degraded - probably due to a system fault.

With respect to the above, it should be noted that the data from the more remote sites always took several months for delivery to Leicester. The inaccessibility of the sites led to difficulties in rectifying problems that did occur.

6.1.1: The effects of season, frequency and geomagnetic activity on the overall distribution of bearings

The occurrence of 5.832 MHz and 9.292 MHz signal bearings at high A_p (>=25) and low A_p (<10) are presented as histograms in Figure 6.1 for days in January and February, 1994 and in Figure 6.2 for days in April and May, 1994. The threshold A_p values were chosen to ensure a minimal difference between the number of days in each sample. The occurrence values for each 0.1° bearing bin have been normalised to the maximum occurrence value, which is stated at the top right of each graph together with the bearing at which this occurs.

The widths of the peaks at half maximum for both time periods are much smaller at 9.292 MHz than at 5.832 MHz (~4° and ~11° respectively).

The main seasonal difference lies in the spread of the base of the peak in the distribution. During January and February the distribution is skewed, with a large number of bearing measurements exceeding the true (great circle) bearing. This is not the case in April and May.

The daily standard deviations of the bearings within ±100° of the GCB are plotted for the time period 25/1/94 - 1/6/94 for 5.832 MHz and 9.292 MHz in Figures 6.3a and 6.3b respectively. These figures clearly demonstrate a steady decline in the statistical spread of bearings as the season changes from winter to summer. This reflects the seasonal change in the period of each day during which the propagation path passes through a sunlit ionosphere. Reference to the corresponding A_p values in Figure 6.3c indicates that the spread of the bearings peaks following the onset of geomagnetic storms. This is particularly clear in the 9.292 MHz bearings.

The correlation between the standard deviation and A_p is presented in Figures 6.4 and 6.5 for 5.832 and 9.292 MHz respectively. The measurements have been divided according to month to minimise the seasonal (or 'day length') contribution to the standard deviation. A sharp minimum is sometimes evident in the standard deviations at an A_p of 10, with standard deviations increasing both above and below this level. This is particularly clear in the 9.232 MHz signals of March and April in Figure 6.5. The spread in bearings at very low A_p may be due to the increase in the presence of sun-aligned auroral arcs and an overall reduction in the MUFs (since transmissions close to the MUF undergo greater bearing deviation). The reduction in MUF at low A_p results from a reduction in the convection of solar ionised plasma from the dayside into the polar cap. At high A_p the presence of polar patches increases and so there is an increase in the amount of off-GCP propagation associated with reflections from these patches.

6.1.2: Systematic, diurnal changes in bearing at 5.832 MHz

At 5.832 MHz there are large diurnal trends in the bearing that may be associated with diurnal changes in the tilts in the F region. These trends form the dominant, large scale bearing structures during the summer and during geomagnetically quiet periods when bearing deviations with shorter time scales are small. To illustrate these trends, Figure 6.6 presents a large-scale view of the bearings together with A_p values for each day in April 1994. The median or trend line of the bearings typically varies by ±5° over the course of each day. Comparison of geomagnetically active and quiet periods reveals that the peak positive smoothed bearing error occurs a few hours before midnight UT during high A_p (e.g. 4-14th April) and a few hours after midnight UT during low A_p (e.g. 20-30th April). The minima in the smoothed bearings also occur at earlier times at high A_p than at low A_p.

Figure 6.7 presents the mean and standard deviation values of the bearings for each UT hour in April and May 1994 for different ranges of daily A_p. A solid line represents the mean, and vertical bars represent ±1 standard deviation. The dashed line represents the overall mean bearing for each UT hour for *all* A_p values. This figure clearly illustrates the changes in the diurnal trend in bearing deviations with changes in A_p. For low A_p (0-10) the bearings peak at 0230 UT and are a minimum at 1430 UT, whereas at high A_p (>50) the maximum is at 2230 UT and the minimum has shifted to 0900 UT.

These diurnal changes in the bearing probably result from diurnal changes in the cross-path ionospheric gradients. The UT variations of foF2 and its gradients normal to the GCP at the path midpoint were calculated using the Utah State University (USU) high latitude model contained within the Parameterised Ionospheric Model (PIM) [*Daniell et al.*, 1995], but the results remained inconclusive.

6.1.3: Very large scale bearing movements

Figures 6.8 and 6.9 present the bearings obtained in the month of March 94 at frequencies of 5.832 MHz and 9.292 MHz respectively. In general, the number and size of bearing structures increases with the level of geomagnetic activity. Note that the sparsity of bearing points on the 7th and 8th on both frequencies indicates a low SNR due to polar cap absorption (PCA) associated with the onset of a geomagnetic storm on the 7th.

The large scale bearing structures in the 9.292 MHz measurements may be categorised into two classes (see Figure 6.10):-

Feature A consists of large (±50°), rapid bearing swings that usually occur in trains with a frequency of about 2-3 per hour. A good example of these swings is during the nighttime period of the 21st March 94 (see Figure 6.9). Similar swings were observed by *Jones and Warrington* [1992] in 1990 on a forerunner to the present campaign and were then attributed to the convection of polar patches over the propagation path.

Feature B consists of steady drifts of the bearing over several hours to higher (westerly) bearings at the end of propagation before local midnight and a return from lower (easterly) bearings after local midnight. A good example of this category is evident on the 3rd March 94 (see Figure 6.9). This categorisation is only intended as a rough guide and the two types of feature are often observed superimposed on each other. In a study of the period 1/2/94 to 30/4/94, feature A was clearly recognised on 18% of days, feature B on 43% of days and no significant features were observed on 20% of days. The average daily mean A_p for both feature A and feature B was 31 compared with a mean A_p of 12 on days with no significant features.

Figures 6.11 and 6.12 provide some statistics relating to the diurnal variation of the parameters of all prominent bearing structures observed in the 5.832 MHz and 9.292 MHz bearings (respectively) for the period 25/1/94 - 30/4/94. These were recorded using the same computer interactive procedure as was used for recording the bearing tails in the Halifax-Cheltenham bearings (see Section 5.1). It should be noted that in these figures the mean size and duration may be artificially high since only bearing structures above a minimum time resolution or bearing 'noise' threshold could be included in the averages. The results indicate a broad maximum in the occurrence of large scale bearing deviations around 0500 UT (near local midnight). There is a peak in the mean size and duration of 9.292 MHz bearing swings around 1200 UT. This is the period when propagation generally ceases at higher bearings and resumes at lower bearings (a good example of this is on 20 March (see Figure 6.9)). Perhaps the most important result however, is the diurnal change in the mean rate of bearing swing, which is positive from local midnight to local noon and negative from local noon to local midnight. This is investigated further below.

Figure 6.13 presents an example of a period in February 1994 in which geomagnetic activity levels varied from very active storm conditions to very quiet conditions. The northward component of the interplanetary magnetic field (B_z) is also presented for this period. The signal strength (indicated by the performance of the goniometer in the bearing measurements) is greatly reduced in the daylight hours of the 21st, and to a lesser extent on the 22nd, due to polar cap absorption. More interestingly, however, there is a marked change in the local time distribution and direction (increasing or decreasing) of the bearing swings between the high A_p /

negative B_z period (0900 UT, 21/02/94 – 0600 UT, 22/02/94) and the subsequent low A_p / positive B_z period (1500 UT, 22/02/94 onwards). In the former period the bearing structures are almost exclusively decreasing (W-S-E) and confined to the hours before local midnight, whereas in the latter period the bearings are increasing (E-S-W) and confined to the hours after local midnight.

The two principal, dynamic, large-scale, electron density structures in the polar cap ionosphere are polar patches and auroral arcs. The former are only observed during periods of high A_p and negative B_z whereas the latter are only prevalent during periods of low A_p and positive B_z. The bearing swings of 21-22 February 1994 are therefore most probably due to the passage of polar patches over the path whereas on the 23-24 February 1994 the bearing swings are probably associated with polar cap arcs.

Histograms of the frequency of occurrence of 9.292 MHz bearing swings in each LT hour for swings increasing in bearing (E-S-W) and decreasing in bearing (W-S-E) are presented in Figure 6.14. The data have been sub-divided according to the hourly mean IMF B_z and 3-hourly a_p values at the start of each swing. It should be noted that IMF B_z measurements were available for only 42% of the 95day observation period (*c.f.* 100% for a_p values) such that the number of observation in the upper panels of Figure 6.14 are small. In all of these graphs, the peak in the frequency of decreasing bearing swings occurs before local midnight and increasing bearing swings exhibit a broad peak in the post midnight hours. Since the path is aligned very closely to a local time meridian with a reflection point close to the geomagnetic pole, this distribution of increasing/decreasing swings suggests that the ionospheric reflection point moves in an anti-sunward direction across the path (Figure 6.15). This is what would be expected during conditions of negative B_z and the reflection point may lie on polar patches that drift in the convection flow over the path. However, during periods of low A_p and positive B_z, polar patches are only rarely directly observed and one might not expect to observe the rapid bearing swings associated with them during these times. It is clear from the diagrams however, that although the number of decreasing bearing swings is much reduced during these periods, the frequency of increasing bearing swings remains relatively unchanged. Increasing bearing swings are quite adequately explained by the motion of polar patches in geomagnetically active periods but an alternative explanation is required to explain the presence of these swings during geomagnetically quiet times.

One such explanation is the motion of sun-aligned arcs across the path (see Figure 6.16). Sun-aligned arcs are twice as common on the morning side of the polar cap as on the evening side and this may account in part for the peak in the occurrence of increasing bearing swings in the post-midnight hours. A positive bearing swing would occur on the nightside as the arc drifted from the dawn side to the dusk side of the polar cap.

Histograms of the time intervals between each bearing swing and its precursor are presented for both high (>=20) and low (<20) a_p values in Figures 6.17 a) and b), respectively. The top panels of each figure represent all bearing swings (regardless of direction), middle panels represent time intervals between only the declining bearing swings and lower panels represent time intervals between increasing bearing swings only. All the graphs show a broad peak in the interval between swings at about 40 minutes. According to previous studies, the measurements at high a_p should represent the effects of polar patches whereas low a_p measurements should reflect the characteristics of auroral arcs. It is therefore somewhat surprising that there is little difference in the distributions of the reoccurrence times with a_p.

The influence of B_y (the dawn-to-dusk directed component of the IMF) on the distribution of bearing swings is presented in Figure 6.18. For B_z<0 the number of decreasing bearing swings in the pre-midnight sector is greatly reduced when B_y>0. The high latitude convection pattern for the different signs of B_z and B_y are illustrated in Figure 6.19. With B_z<0 and B_y>0 the convection flow is skewed towards the evening sector and polar patches emanating from the noon sector will drift towards the evening side. This reduces the likelihood of the patches crossing the path in the pre-midnight sector and would account for the lack of bearing swings observed.

A B_y dependence is also observed in the positive B_z data, which might be explained by the difference in the flow patterns at the mid-point latitude. Where $B_y > 0$ the flow is predominantly westward throughout the night and would lead to increasing bearing angles, and when $B_y < 0$ strong eastward flows exist in the pre-midnight sector which would lead to decreasing bearing angles, as observed.

The long period, large bearing swings (feature B) are most probably a consequence of very large scale (>1000 km) ionospheric gradients across the polar cap. The high latitude model in PIM indicates that critical ionospheric frequencies at the latitude of the path mid-points under consideration usually range from less than 2.0 MHz to over 4.5 MHz during days in February and March 1994. Large gradients in foF2 are also observed as a result of both the solar terminator and the "tongue of ionisation" which results from the convection of dayside plasma over the central polar cap. As a result, the path from Iqaluit-Alert, which has an obliquity factor (corrected for earth curvature) of 3.2 is unable to sustain GCP propagation above frequencies of about ($2.0 \times 3.2 =$) 6.4 MHz during these periods and the radio waves reflect from regions of enhanced plasma density on either side of the GCP. At the end of GCP propagation this would occur progressively towards the west (towards the dusk terminator) and before GCP propagation resumed the path would be deviated from the enhanced ionosphere in the East (the dawnward terminator). This is in agreement with the observed trend in the bearing data. Since the signal frequency is close to the penetration frequency at these times, the ray will remain inside the ionosphere for a prolonged period and will therefore be subject to the maximum effect of ionospheric ray-path deviation [*Titheridge*, 1958].

6.1.4: Analysis of oblique incidence ionograms over the Iqaluit-Alert propagation path

Ionograms were recorded over the path from Iqaluit to Alert using the same method as for the ionograms for the Halifax-Leitrim path (Section 5.2) for the period January-March, 1996. Unfortunately, the DF system was operating rather badly during this period, so only a few days were available for analysis. These are discussed below.

6.1.4.1: 23rd January 1996, (a geomagnetically quiet period).

The bearings obtained on the 9.292 MHz signals from Iqaluit for the 23/1/96 are plotted in Figure 6.20. Vertical lines represent the times at which ionograms were recorded and are included for clarity. In the period 0300-1130 UT, the bearings are well displaced from the GCB of 188°. After local midnight (from 0500 UT onwards), bearing swings of period ~30 minutes are distinguishable, though these are superimposed on larger bearing variations which vary over periods of roughly 2 hours. The A_p value for this day was low (A_p=5) and the behaviour of the bearings (post-midnight, E-S-W bearing swings in trains) is typical of the low A_p days as described above, though this example exhibits particularly large long period underlying bearing trends.

The ionogram sequence for this day is presented in Figures 6.21. Between the hours of 0115 and 0415 UT the only mode of propagation at 9.292 MHz is a single E_s mode. However, the bearings range up to 20° above the GCB in this period. Thus an E_s mode in the polar cap may be well displaced from the GCP, contrary to the notion obtained from mid-latitude studies that an E_s mode represents propagation close to the GCP.

At 0515 UT the signals are suddenly acquired from a bearing of about 150° (30° below the GCB) and the ionogram for this time indicates the appearance of a second thin ionogram trace, stronger than the original trace and delayed by an extra 1.0ms. The relative delay between the two layers diminishes steadily to zero as the bearing offset also diminishes to zero at 0645 UT. Similar examples of multiple thin bands in the ionograms are evident in the ionograms of 0715 to 1215 UT and the delay of these bands above the main trace is reasonably well correlated with the associated, large changes in the bearing offset. From 1245 UT the ionogram trace reacquires a discernible high angle ray and has an MUF that exceeds the 9.292 MHz operating frequency. At this time the bearing deviations from the GCB become small (less than about ±5°).

The horizontal bands in the ionograms are often split into pairs over a similar range of frequencies (e.g. 0945, 1015 UT). As with the auroral backscatter echoes of Figure 2.2, the cause of this is probably due to both high and low angle ray paths being supported in the F region prior to reflection from an irregularity structure. However, the associated bearings rule out the auroral oval region as the source of these echoes.

The general shape of the ionogram traces (high MOF, lack of a high angle trace, low delay spread, and little or no dispersion) that occur in conjunction with the positive bearing swings suggests reflection from a thin, dense ionospheric structure. This is precisely the sort of trace that might be expected from reflections from the discrete sun-aligned arcs of ionisation observed in the morning-side polar cap under conditions of low geomagnetic activity. In addition, a large number of the ionograms exhibit multiple horizontal traces separated by up to 1.0 ms (see for example ionograms for 0445 and 0745 UT). Such features could represent reflections from multiple sun-aligned arcs over the propagation path.

6.1.4.2: 24th February 1996 (a geomagnetically active period)

Figure 6.22 presents 9.292 MHz bearings for the 24th February 1996. This was a geomagnetically active day (Ap=20) with peak activity in the morning (peak ap (3-6 UT)=56) and a rapid change to quiet conditions at noon (ap(12-15 UT)=6). The bearings swing from the higher, westerly bearings down to the true bearing and are observed only in the pre-midnight sector (before 0430 UT). This behaviour is typical of the bearing swings under these geomagnetic conditions and probably results from the motion of polar patches over the path. The single swing from the East prior to GCB propagation at 1200 UT is a recurrent feature in the data and probably results from reflections from a solar enhanced ionosphere in the east associated with the (sunrise) solar terminator. At 0115 UT the bearings show a 30° deviation above the GCB at the start of a downward swing. At this time the ionogram indicates that the propagation occurs via a detached, spread mode with considerable frequency and delay spread and slant. A similar ionogram mode is observed at 0245 UT and 0345 UT for which the strongest bearings are returned at approximately +30° and +40° respectively. These slanted, spread traces are similar to the 'nose-extensions' discussed in Section 5.2 and indicate large-scale, horizontal gradients in the ionospheric electron density near the Tx-Rx path. The active geophysical conditions suggest the presence of polar patches and their associated enhancements and gradients of electron density. Thus, polar patches are a most likely candidate cause of the slanted, spread ionogram traces.

The ionogram for 1145 UT presented in Figure 6.23 indicates the unusual modes present as the bearings 'tail-up' to the GCB over 30°.

6.1.4.3: 4th March 1996 – a geomagnetically quiet period

Another good example of ionograms that coincide with the sunrise tail-up in the bearings to the GCB is presented in Figures 6.24 and 6.25 4th March 1996 (0815 UT to 1145 UT) – a geomagnetically quiet period ($a_p = 4$). In both this and the previous example, the traces appear to consist of multiple, horizontal layers with little delay spread, and the higher delay traces appear at higher frequencies. This is effectively a 'striated nose-extension' and indicates both an increasing level of ionisation to the East (dawn side) of the path (explaining the slant) and a highly structured ionosphere with many discrete reflectors (such as arcs) which manifest themselves as the superimposed horizontal traces.

6.2: The Iqaluit - Leitrim path

The bearing measurements of Iqaluit from Leitrim are notable for the lack of any large deviations from the GCB. Bearing deviations rarely exceeded ±10°. Examples of the bearings are presented for the month of March 1994 at 5.832 MHz and 9.292 MHz in Figures 6.26 and 6.27 respectively. No propagation was observed at the highest frequency of 20.3 MHz.

Though the path mid-point lies within, or just equatorwards of the disturbed auroral ionosphere the path runs approximately perpendicular to the geomagnetic field and therefore parallel to the principal horizontal electron density gradients and normal to FAI scattering planes. This path orientation thus minimises the bearing deviations that result from ionospheric tilts and forward scattering, though one might still expect to observe considerable deviations in the elevation angle if these were measured.

6.3: The Halifax - Alert path

The path from Halifax to Alert is a 4182 km path for which propagation prediction programs generally predict a two-hop path as the most reliable mode. If the lengths of each hop were approximately the same, the first hop would be similar to the 1-hop Iqaluit-Leitrim path (though propagating in the reverse direction) with a reflection point in the auroral oval region. The second hop would be similar to the 1-hop, Iqaluit-Alert path with a predicted ionospheric reflection point (3/4-path distance) only 120 km due east of the midpoint of the Iqaluit-Alert path (within the polar cap). Since the Iqaluit-Leitrim path introduced few bearing deviations, one could predict minimal bearing deviations of the ray on the first hop of the Halifax-Alert path, with large bearing deviations on the second hop, similar to those on the Iqaluit-Alert path.

During the winter months, the 10.945 bearings from Halifax to Alert exhibited many of the same features observed on the 9.292 MHz signals on the Iqaluit to Alert path. On some occasions, the two data sets showed features that were well correlated in time, magnitude and general shape. As an example, Figure 6.28 present the bearings for the Iqaluit-Alert, 9.292 MHz and the Halifax-Alert, 10.945 MHz bearings on the 27th and 28th February. The striking similarity in the measurements suggest that the paths of the rays on the second hop of the Halifax-Alert propagation are very close to those of the single-hop Iqaluit-Alert path.

6.3.1: Bearing deviations at 5.097 MHz

Figure 6.29 presents the bearings measured at 5.097 MHz for March 1994. Note that the bearing measurements were of good quality only until the 17th March. The signal is absorbed in the hours around local noon and large swings in the bearings are observed, particularly in the hours around local mid-night. Bearing measurements with the smallest deviation from the GCB occur in the period 1800-0000 UT each day.

One notable feature is a frequently observed swing from approximately 100° to 220° at about 0900-1500 UT (clearest on the 3rd, 10th and 13th March). These are even more pronounced in January when they occur almost daily, and are presumably associated with very large-scale cross-polar cap gradients.

By the end of May 1994, the bearings deviations at 5.097 MHz are generally reduced to less than ~30° and the signals are strongly absorbed during the daytime. Figure 6.30 provides an example of the type of bearings observed at this time. The bearings tend towards the west (higher bearings) at the end of propagation, before the path enters the sunlit ionosphere and D-region absorption closes the GC propagation path.

6.3.2: Bearing deviations at 10.945 MHz

Figure 6.31 presents the bearings measured at 10.945 MHz for March 1994. The bearings tend to move towards the west before local midnight as the MUF is exceeded on the GCP and they return from the east after local midnight.

In the summer months, the 10.945 MHz propagation was observed over a 24-hour period except on geomagnetically active days when the propagation ceased in the few hours around local midnight. Examples of the typical bearing distribution during this month are given in Figure 6.32, which presents bearings from 17-21 May 1994. It is notable that it is the bearings during the hours around local noon that suffer the greatest deviations (generally 'spreading' to lower bearings) whereas the hours around local midnight often have a very low dispersion (see for example, 17-20 May in Figure 6.32).

6.3.3: Bearing deviations at 15.945 MHz

Figure 6.33 presents the bearings measured at 15.920 MHz for March 1994. The characteristics of these measurements differ only slightly from those of the 10.945 MHz signals.

An equipment error lead to two 'shadows' appearing in the bearing vs. time plots at approx. +/- 70° of the main signal (near the GCB).

7: Summary and conclusions

The HF Direction Finding receivers of this experimental campaign have returned unprecedentedly high time resolution data of important scientific and practical value. A list of the most important findings of this research is given below.

1. The times of day for which signals were received in an azimuthal range within ±10° of the great circle bearing on high latitude paths are not well predicted by standard frequency planning aids such as ICEPAC [*Tascione et al.*, 1987], VOACAP [*Teters et al.*, 1983] and CCIR recommendation 533 [*CCIR*, 1992].
2. Times of propagation on all seven paths of the experimental campaign are strongly related to the level of geomagnetic activity as measured by the global geomagnetic activity index, A_p. This investigation has established the patterns of propagation times with season and A_p levels on each path and furthermore, various models have been employed to account for these patterns.
3. Variations in the times of GCP propagation on the trans-Atlantic path from Halifax to Cheltenham are well modelled by the Halcrow-Nisbet [1977] model relating the local time extent of the mid-latitude trough to the K_p index of geomagnetic activity.
4. The sub-auroral trough produces large (±25°) diurnal trends in the bearings of 5.097 MHz signals from Halifax to Cheltenham during geomagnetically active periods. Signals appear to reflect from the equatorward side of the trough in the evening and then switch to poleward wall reflections mid-way through the night. During very active periods, reflections from both walls have been observed simultaneously, whilst GCB propagation has ceased to be supported.
5. Large, (up to 50°) bearing 'tails' have been observed on the 10.945 MHz and 15.920 MHz signals from Halifax to Cheltenham at the beginning and end of propagation. These occur on about 50% of days, with 90% tailing towards the equatorward side of the path. The tails are larger and more frequently observed at 10.945 MHz than at 15.920 MHz, and at the end of propagation (sunset) more than at the beginning of propagation (sunrise).
6. Propagation from bearings 10-50° poleward of the GCB has been observed on the Halifax-Cheltenham path at 10.945 MHz (and less often at 15.920 MHz). Such propagation is associated with large increases in Doppler spread index of the signal (up to 90 Hz) and generally occur in the 48 hour periods following the onset of geomagnetic storms (or A_p>50). This is thought to be a scatter mode of propagation involving reflections from field-aligned irregularities on the equatorward edge of the auroral oval.

7. Anomalous night-time propagation on 10.945 MHz signals from Halifax-Cheltenham have been observed during long periods of geomagnetic quiet (A_p<20) at bearings up to 50° equatorward of the GCB. These are associated with only small increases in Doppler spread index. Subsequent ray tracing studies by *Warrington et al.* [1999] have demonstrated that these observations are consistent with a seascatter (sea sidescatter) mode of propagation when the transmission frequency exceeds the MUF on the GCP.
8. Large (up to 100°) bearing tails are also observed for 70% of days on 5.097 MHz signals on the 911 km E-W path from Halifax to Leitrim. Signals generally arrived from polewards of the GCB at the beginning of propagation and tailed to the equatorward side at the end of propagation. Doppler spread index values remained moderate throughout (<20 Hz). The occurrence of this phenomenon was positively correlated with A_p. The local times of the maximum deviation in the bearings also shifted about 4 hours earlier during high levels of A_p.
9. Halifax signals were received from the north (bearing ~0-20°) at Leitrim for nighttime periods of several hours. These were associated with large increases in Doppler spread index (up to 60 Hz). The bearings of these signals did not 'tail' smoothly towards or away from the GCB. Often the bearings would increase (towards the GCB) and then decrease away from the GCB throughout the event indicating the approach and recession of the reflection point region. The bearings also lay closer to the GCB with larger A_p values. The latter two observations are consistent with a scattering region located near the equatorward wall of the auroral oval.
10. Ionograms taken on the Halifax to Leitrim path exhibited 'nose-extensions' on the 1F trace (similar to slant-F in backscatter ionograms) during periods of bearing tails. Horizontal bands (or 'spurs') were observed (similar to auroral backscatter echoes) during periods for which the bearings showed propagation from the North.
11. Small (±4°) diurnal changes in the bearing of 6.43 MHz signals on the Halifax-Leitrim path have been observed and attributed to systematic ionospheric tilts. These did not vary noticeably with A_p levels during April and May 1993.
12. The Wainwright-Leitrim path signals were subject to intense auroral absorption during high geomagnetically active periods. Recurrent swings in the bearing were observed on the 6.905 MHz signals in the pre-midnight sector during geomagnetically moderate periods and attributed to the westward convection of auroral blobs across the path at these times. (Similar swings were observed on the Halifax-Cheltenham, 5.097 MHz signals, superimposed on the large, diurnal poleward bearing displacements). A single ±20° swing was observed once per

day (generally at the end of GCB propagation) in the bearings of 10.195 MHz signals.

13. Paths entering the unilluminated polar cap ionosphere were subject to large (>50°) recurrent swings in the bearing, with modal repetition periods of around 40 minutes. The standard deviation of bearings reached a minimum at around an A_p of 10. For low A_p values, and/or positive values of B_z (the northward component of the IMF), the bearing swings were predominantly increasing (E-S-W) and were attributed to reflections from sun-aligned arcs. The local time distribution of these swings formed a broad peak centred about 0200LT. During periods of high A_p, (and/or negative B_z) decreasing (W-S-E) bearing swings were found to predominate in the pre-(local) midnight sector and were attributed to the presence of drifting polar patches of ionisation. A further analysis of B_y direction showed a large reduction in the pre-midnight, decreasing swings during negative B_z and positive B_y. This was attributed to the skew of polar patches to the dawn side of the polar cap expected from the change in the pattern of F-region convection flow.
14. Ionograms on the polar cap Iqaluit-Alert path showed multiple, thin traces during periods of low A_p and slant, spread nose-extensions during periods of high A_p. The former is attributed to reflections from auroral arcs, and the latter from the tilts produced by polar patches.
15. Large diurnal shifts in the bearing were observed at 5.832 MHz on the Iqaluit-Alert path and attributed to cross-polar cap gradients. The local time 'phase' of these changes varied with changes in the level of A_p.
16. The one-hop, north-south aligned, trans-auroral Iqaluit-Leitrim path exhibited only small (<10°) deviations in the bearings whereas the two-hop, north-south aligned path from Halifax to Alert exhibited many of the same characteristics as those of the Iqaluit-Alert path. These observations indicate that polar cap contributes far more than the auroral region to the azimuthal deviations of rays on north-south aligned propagation paths.

The results of this study should enable the operators of DF sites to estimate the level of confidence they can have in the bearings they measure based upon factors such as geomagnetic activity, local time, frequency, signal strength and Doppler shift. In this way, confidence indication can be placed on each line of bearing (LOB) employed in determining a transmitter location. Location accuracy should thus increase when the LOBs are 'weighted' according to the criteria discovered in the present investigation.

8: References

Barry, G.H. and R.B. Fenwick 1975 "Techniques for Real-time HF Channel Measurement and Optimum Data Transmission", AGARD Conf. Proc. **173**, *Radio Systems and the Ionosphere*, Ed. W.T. Blackband, Advisory Group for Aerospace Research and Development, North Atlantic Treaty Organisation, p.15-1.

Bates, H.F. and P.R. Albee 1970 "Aspect Sensitivity of F-layer HF Backscatter Echoes", J. Geophys. Res., **75**, p.165.

Bates H.F., P.R. Albee and R.D. Hunsucker 1966 "On the Relationship of the Aurora to Non Great-circle High Frequency Propagation", J. Geophys. Res., **71,** (5), p.1413.

Bates H.F., A.E. Belon and R.D. Hunsucker 1973 "Aurora and the Poleward edge of the Main Ionospheric Trough", J. Geophys. Res., **78**, p.648.

Bilitza D., (Ed.) 1990 "International Reference Ionosphere 1990". NSSDC 90-22, Greenbelt Maryland, 1990.

Buchau J., B.W. Reinisch, E.J. Weber and J.G. Moore 1983 "Structure and Dynamics of the Winter Polar Cap F region", Radio Sci., **18**, (6), p.995.

Buchau J., E.J. Weber, D.N. Anderson, H.C. Carlson Jr., J.G. Moore, B.W. Reinisch and R.C. Livingstone 1985 "Ionospheric Structures in the Polar Cap: Their Origin and Relation to the 250 MHz Scintillation", Radio Sci. **20**, (3), p.325.

Cannon, P.S. 1989 "Morphology of the High Latitude Ionosphere and its Implications for HF communication systems", IEE Proceedings **136**, Pt.1, No. 1, p.1.

Carlson H.C. Jr. 1994 "The Dark Polar Ionosphere: Progress and Future Challenges", Radio Sci. **29**, (1), p.157.

Carlson H.C. Jr., V.B. Wickwar, E.J. Weber, J. Buchau, J.G. Moore and W. Whiting 1984 "Plasma Characteristics of Polar Cap F-Layer Arcs" Geophys. Res. Lett. **11**, (9), p.895

Carlson, H.C., R.A. Heelis, E.J. Weber and J.R. Sharber 1988 "Coherent Mesoscale Convection Patterns during Northward Interplanetary Magnetic Field", J. Geophys. Res., **93**, p.14501.

CCIR 1990a "Ionospheric Properties (Question 25/6)", Report 725-3, XVIIth Plenary Assembly, Düsseldorf, 1990, Reports of the CCIR (also decisions), Annex to Vol. VI, *Propagation in Ionised Media*, CCIR International Radio Consultative Committee, Geneva, p.1.

CCIR 1990b "Ground and Ionospheric Side- and Back-scatter (Question 32/6)", Report 726-2, XVIIth Plenary Assembly, Düsseldorf, 1990, Reports of the CCIR (also decisions), Annex to Vol. VI, *Propagation in Ionised Media,* CCIR International Radio Consultative Committee, Geneva, p.103.

CCIR 1992 CCIR Recommendation 533-3 "CCIR HF Propagation Prediction Method (1978-1982-1990-1992)", ITU CCIR Recommendations RPI Series *Propagation in Ionised Media*, Geneva, p.57.

Chapman S. 1931 "The absorption and dissociative or ionizing effect of monochromatic radiation in an atmosphere on a rotating Earth." Proc. Roy. Soc. **43**, p.26.

Char B.W., K.O. Geddeas, G.H. Gonnet and S.M. Watt 1985 "Maple users guide (4th Ed.)" Whatcom, Ontario, Canada.

Chestnut W.G. 1972 "Polar propagation effects on VHF-UHF radars" AGARD Conf. Proc. **97**, *Radar propagation in the arctic*, Ed. J. Frihagen, p.5-1.

Choi, D.S., B. Weijers, R.J. Norris and N.B. Meyers. 1992 "The Spatial and Temporal Characteristics of High Frequency Auroral Backscatter" AGARD Conf. Proc. **528**, *Proceedings of the AGARD 40th Symposium of the Electromagnetic Wave Propagation Panel Symposium on Radiolocation Techniques, London, 1-5 June* Advisory Group for Aerospace Research and Development, North Atlantic Treaty Organisation, p.6-1.

Daniell, R.E. Jr., L.D. Brown, D.N. Anderson, M.W. Fox, P.H. Doherty, D.T. Decker, J.J. Sojka and R.W. Schunk, 1995 "PIM: A Global Ionospheric Parameterization Based on First Principles Models", Radio Sci. **30**, p.1499.

Davies K. 1990 "Ionospheric Radio", IEE Electromagnetic Waves Series 31, Peter Peregrinus Ltd., London, UK.

Davies K. and C.M. Rush 1985 "High frequency ray-paths in ionospheric layers with horizontal gradients", Radio Sci. **20**, (1), p.95.

Feinblum D.A. and R.J. Horan | 1973 | "HILON - A model of the Ionospheric Effects at Ft. Churchill 1968" Tech. Rep. Bell Labs/Western Electric (US army contract DAHC 60-71-C-0005) New Jersey.

Feldstein Y.I. | 1963 | "On Morphology of Auroral and Magnetic Disturbances at High Latitudes", Geomagn. Aeron. **3**, p.183.

Foppiano A.J. and P.A. Bradley | 1983 | "Prediction of Auroral Absorption of High-Frequency Waves at Oblique Incidence", Telecomm. J., **50**, p.547.

Frank L.A., J.D. Craven, D.A. Gurnett, S.D. Shawhan, D.R. Weimer, J.L. Burch, J.D. Winningham, C.R. Chappell, J.H. Waite, R.A. Heelis, N.C. Maynard, M. Sugiura, W.K. Peterson and E.G. Shelley | 1986 | "The Theta Aurora", J. Geophys. Res., **91**, p.3177.

Georges T.M. | 1967 | "Ionospheric Effects of Atmospheric Waves", ESSA Tech. Rep. IER 57-ITSA 54

Gething, P.J.D. | 1991 | "Radio Direction Finding and Superresolution" IEE Electromagnetic Waves Series 33, Peter Peregrinus Ltd., London, UK.

Gussenhoven M.S. | 1982 | "Extremely High Latitude Auroras", J. Geophys. Res., **87**, p.2401.

Hagg E.L. and W. Rolfe | 1963 | "A study of trans-Atlantic radio propagation modes at 41.5 Mc/s" Can. J. Phys. **41**, p.220.

Halcrow B.W. and J.S. Nisbet | 1977 | "A Model of the F2 Peak Electron Densities in the Main Trough Region of the Ionosphere", Radio Sci. **12**, p.815.

Hargreaves, J.K., M.T. Feeney, H. Ranta and A. Ranta | 1987 | "On the Prediction of Auroral Radio Absorption on the Equatorial Side of the Absorption Zone", Radio Sci., **49**, (3), p.259.

Hartz T.R., A.G. Montbriand and E.L. Vogan | 1963 | "A Study of Auroral Absorption at 30 MHz" Can. J. Phys, **41**, p.581.

Haselgrove, J. | 1954 | "Ray Theory and a New Method for Ray Tracing", Report on the Conference on the Physics of the Ionosphere, Cambridge, 1954, (Physical Society, London) p.355.

Helms W.J. and A.D. Thompson	1973	"Ray-tracing Simulation of Ionization Trough Effects upon Radio Waves", Radio Sci. **8**, (12), p.1125.
Holzworth R.H. and C.-I. Meng	1975	"Mathematical Representation of the Auroral Oval", Geophys. Res. Lett. **2**, (9), p.377.
Ismail S., D.D. Wallis and L.L. Cogger	1977	"Characteristics of Polar Cap Sun-aligned Arcs", J. Geophys. Res., **82**, p.4741.
Ismail S. and C-I Meng	1982	"A Classification of Polar Cap Auroral Arcs", Planet Space Sci. **30**, p.319.
Jenkins, R.W.	1992	"Preliminary Analysis of Kestrel Data", CRC Technical Memorandum DRL/TM083/92, Communications Research Centre, Ottawa, Ont., Canada, January 31, 1992.
Jenkins R.W., E.L. Hagg and L.E. Montbriand	1979	"Direction and Doppler Characteristics of Medium and Long Path HF Signals Within the Night-time Sub-auroral Region", AGARD Conf. Proc. **233**, Advisory Group for Aerospace Research and Development, North Atlantic Treaty Organisation, p.20-1.
Jones R.M. and J.J. Stephenson	1975	"A Versatile Three-Dimensional Raytracing Computer Program for Radio Waves in the Ionosphere", Rep. 75-76, Office of telecommunications, Boulder, Colorado, USA.
Jones T.B. and J.S.B. Reynolds	1975	"Ionospheric Perturbations and their Effects on the Accuracy of HF Direction Finders", Rad. Elec. Eng. **45**, p63
Jones T.B. and E.M. Warrington	1992	"Large Bearing Errors Observed at a High Latitude DF Site", AGARD Conf. Proc. **528**, *Proceedings of the AGARD 50th Symposium of the Electromagnetic Wave Propagation Panel on Radiolocation Techniques, London, 1-5 June*, Advisory Group for Aerospace Research and Development, North Atlantic Treaty Organisation, p.18-1.
Jones T.B., E.M. Warrington and J.E. Perry	1992	"Systematic Bearing Errors of HF Signals Observed Over a North-South Propagation Path", AGARD Conf. Proc. **528**, *Proceedings of the AGARD 50th Symposium of the Electromagnetic Wave Propagation Panel on Radiolocation Techniques, London, 1-5 June*, Advisory Group for Aerospace Research and Development, North Atlantic Treaty Organisation, p.17-1.

Karpachev A.T. 1992 "Global Variations of foF2 in the Night Trough Region", Geomagnetism and Aeronomy **32**, (5), p.665.

Kohnlein W. and W.J. Raitt 1977 "Position of the Mid-latitude Trough in the Topside Ionosphere as Deduced from ESRO 4 Observations", Planet. Space Sci. **25**, p.600.

Lassen K. and C. Danielsen 1978 "Quiet Time Patterns of Auroral Arcs for Different Directions of Interplanetary Magnetic Field in the Y-Z Plane", J. Geophys. Res. **83**, p.5277.

Lockwood, M. 1993 "Modelling the high latitude ionosphere for time varying plasma convection." Proceedings of the IEE, part H, **140**, (2), p.91.

MacNamara L.F. 1991 "The Ionosphere: Communications, Surveillance and Direction Finding" Orbit Foundation Series, Kreisler Publ. Co., Malabar, Florida, USA.

Minullin, R.G. 1986 "The Azimuthal Arrival Angles of Radiowaves Reflected by the E_s layer", Geomagnetism and Aeronomy, **26**, (4), p.460.

Miya, K., M. Ishikawa and S. Kanaya 1957 "On the Bearing of Ionospheric Radio Waves", Report of Ionospheric Research in Japan, **11**, (3), p.130.

Moffett R.J. and S. Quegan 1983 "The Mid-latitude Trough in the Electron Concentration of the Ionospheric F-layer: a Review of Observations and Modelling", J. Atmos. Terr. Phys. **45**, (5), p.315.

Montbriand, L.E. 1988 "Auroral Backscatter Observed at HF from Ottawa", Radio Sci., **23**, p.850.

Muldrew D.B. 1983 "Alouette-ISIS Radio Wave Studies of the Cleft, the Auroral Zone, and the Main Trough and of their Associated Irregularities", Radio Sci. **18**, (6), p.1140.

NTIA/ITS 2000 U.S. Department of Commerce NTIA/ITS Institute for Telecommunication Sciences High Frequency Propagation Models web page. *http://elbert.its.bldrdoc.gov/hf.html*

Piggott W.R. 1975 "High Latitude Supplement" Report UAG-50, World Data Center (WDC-A), National Academy of Sciences, 2101 Constitution Avenue, N.W. Washington, D.C., U.S.A., October 1975

Ratcliffe J.A.	1959	"The magneto-ionic theory", Cambridge University Press, Cambridge.
Rairden R.L. and S.B. Mende	1989	"Properties of 6300-Å Auroral Emissions at the South Pole", J. Geophys. Res., **94**, p.1402.
Rino C.L., R.L. Livingstone, R.T. Tsunoda, R.M. Robinson, J.F. Vickrey, C. Senior, M.D. Cousins, J. Owen and J.A. Klobuchar	1983	"Recent Studies of the Structure and Morphology of the Auroral Zone F-region Irregularities", Radio Sci. **18**, p.1167.
Robinson R.M., R.T. Tsunoda, J.F. Vickrey and L. Geurin	1985	"Sources of F-region Ionisation Enhancements in the Night-time Auroral Zone", J. Geophys. Res. **90**, (A8), p.7533.
Rodger A.S. and M. Pinnock	1980	"The Variability and Predictability of the Main Ionospheric Trough" in *Exploration of the Polar Upper Atmosphere*,. Eds. C.S. Deehr and J.A. Holtet; D. Reidel Publ. Co., p.463.
Rodger A.S., C. Morrell and J.R. Dudeney	1983	"Studies of Sporadic E (E_s) associated with the Main Ionospheric Trough", Radio Sci. **18**, (6), p.937.
Rodger A.S., M. Pinnock, J.R. Dudeney, K.B. Baker and R.A. Greenwald	1994	"A New Mechanism for Polar Patch Formation", J. Geophys. Res., **99**, p.6425.
Rohan P.	1991	"Introduction to Electromagnetic Wave Propagation",1st Ed., Artech House, Inc., 685 Canton Street, Norwood, MA 02062.
Rycroft M.J. and S.J. Burnell	1970	"Statistical Analysis of Movements of the Ionospheric Trough and the Plasmapause", J. Geophys. Res. **75**, p.5600.
Stepanov A.E., Yu.I.Gal'perin, C. Beghin and A.A. Serov	1993	"Large Scale Plasma Blobs of Enhanced Ionospheric Plasma at Polar Latitudes: Measurements from Aureol-3", Cosm. Res. **30** (4), p.433.
Swider, W.	1988	Wallchart entitled "Aerospace Environment", Air Force Geophysics Laboratory, Hanscom Air Force Base, Massachusetts, U.S.A.
Tascione T.F.	1988	"Introduction to the Space Environment" Orbit Book Co., Malabar, Florida, USA.

Tascione, T.F., K.W. Kroehl, and B.A. Hausman — 1987 — A technical description of the ionospheric conductivity and electron density profile model (ICED, version 196-II), Syst. Doc Vol. VII, Air Weather Serv., U.S. Air Force, Scott Air Force Base, Ill.

Tedd B.L., H.J. Strangeways and T.B. Jones — 1984 — "The influence of large-scale TIDs on the bearings of geographically spaced HF transmissions", J. Atmos. Terr. Phys., **46**, (2), p.109.

Tedd B.L., H.J. Strangeways and T.B. Jones — 1985 — "Systematic Ionospheric Electron Density Tilts (SITs) at Mid-latitudes and their Associated HF bearing Errors", J. Atmos. Terr. Phys. **47**, (11), p.1085.

Teters, L.R., J.L. Lloyd, G.W. Haydon and D.L. Lucas — 1983 — Estimating the Performance of Telecommunication Systems Using the Ionospheric Transmission Channel, Institute for Telecommunication Sciences NTIA Report 83-127, July 1983.

Titheridge J.E. — 1958 — "Variations in the Direction of Arrival of High-Frequency Radio Waves", J. Atmos. Terr. Phys.**13**, p.17.

URSI — 1972 — "The URSI Handbook of ionogram interpretation and reduction." 2nd Ed. Nov 1972, Revision of Chapters 1-4, WDC-A Report UAG-23A, Eds. Piggott, W.R and K. Rawer.

Vickrey, J.F., C.L. Rino and T.A. Potemra — 1980 — "Chatanika/Triad observations of unstable ionization enhancements in the auroral F-region", Geophys. Res. Lett. **7**, p.789.

Wakai N., H. Ohyama and T. Koizumi — 1986 — "Manual of Ionogram Scaling", Revised Ed; Radio Research Laboratory, Ministry of Posts and Telecommunications, Japan. July 1986.

Warrington E.M., T.B. Jones, S.M. Orrell and B.S. Dhanda — 1991 — "Amplitude and Frequency Variations of HF Signals Propagated Over High Latitude Paths", IEE Conf Publ. **333**, *Proceedings of the 7th International Conference on Antennas and Propagation., April 1991*, p.889.

Warrington E.M. and T.B. Jones — 1992 — "Bearing Determination and Bearing Quality Indication from a Goniometric HF DF System", AGARD Conf. Proc. **528**, *Proceedings of the AGARD 50th Symposium of the Electromagnetic Wave Propagation Panel on Radiolocation Techniques, London, 1-5 June*, Advisory Group for Aerospace Research and Development, North Atlantic Treaty Organisation, p.20-1.

Warrington E.M., N.C. Rogers and T.B. Jones | 1997 | "Large HF Bearing Errors for Propagation Paths Contained Within the Polar Cap", IEE Proc. Microw. Antennas Propag., **144**, (4), p.241.

Warrington E.M., T.B. Jones, N.C. Rogers and A.J. Stocker | 1999 | "High latitude off-great circle propagation effects with reference to HF communication systems and radiolocation", in *RTO Meeting Proceedings* ***26****, (RTO-MP-26), November 1999 NATO Research and Technology Organisation (RTO) Information Systems Technology (IST) symposium on "Tactical Mobile Communications", Lillehammer, Norway, 14-16 June 1999*, North Atlantic Treaty Organisation, p.17-1.

Weber E.J., J. Buchau, J.G. Moore, J.R. Sharber, R.C. Livingstone, J.D. Winningham and B.W. Reinisch. | 1984 | "F Layer Ionisation Patches in the Polar Cap" J. Geophys. Res. **89**, (A3), p.1683.

Weber E.J., R.T. Tsunoda, J. Buchau, R.E. Sheehan, D.J. Strickland, W. Whiting and J.G. Moore | 1985 | "Co-ordinated Measurements of Auroral Zone Plasma Enhancements", J. Geophys. Res. **90**, (A7), p.6497.

Weber E.J., J.A. Klobuchar, J. Buchau, H.C. Carlson Jr., R.C. Livingstone, O.de la Beaujardiere, M. McCready, J.G. Moore and G.J. Bishop. | 1986 | "Polar Cap F Layer Patches: Structure and Dynamics", J. Geophys. Res. **91** (A11), p.12121.

Weber E.J., M.C. Kelley, J.O. Ballenthin, S. Basu, H.C. Carlson, J.R. Fleischman, D.A. Hardy, N.C. Maynard, R.F. Pfaff, P Rodriguez, R.E. Sheehan and M. Smiddy | 1989 | "Rocket Measurements within a Polar Cap Arc", J. Geophys. Res., **94**, p.6692.

Whalen J.A. | 1989 | "The Daytime F layer Trough and its Relation to Ionospheric-Magnetospheric Convection", J. Geophys. Res. **94**, (17), p.169.

Whalen J.A. | 1994 | "Properties of the F Layer Plasma in the Midday Throat Ridge and Trough", Radio Sci. **29**, (1), p.219.

Yevlashina, M.L., V.S. Mingalev and G.A. Alad'yev | 1986 | "Effect of the Principal Ionospheric Trough on the Propagation of Short Radio Waves", Geomagnetism and Aeronomy, **26**, (1), p.63.

Appendix A: The Halcrow-Nisbet model of the sub-auroral trough

Halcrow and Nisbet [1977] have published a parameterised model of the location of the walls of the sub-auroral trough, based upon top-sounder data from satellites. The positions of the top and bottom of the trough are reproduced below (with some typographical corrections).

$$\Lambda_{st} = 48° + 5°\left\{1 + \left[1 + \left(\frac{T^2 - 4}{5.65T + 0.1}\right)^{22}\right]^{-0.5} - \left[1 + \left(\frac{T^2 - 8}{12.35T + 0.1}\right)^{14}\right]^{-0.5}\right\}$$

$$\Lambda_{sb} = 54° - 0.5(K_p - 1/3) + 7°\left\{1 + \left[1 + \left(\frac{T^2 - 4}{5.8T + 0.1}\right)^{22}\right]^{-0.5} - \left[1 + \left(\frac{T^2 - 8}{13.5T + 0.1}\right)^{16}\right]^{-0.5}\right\}$$

$$\Lambda_{nb} = 64° - 1.0(K_p - 1/3) + 9°\left[\exp(-1.9\times10^{-5}T^{5.42}) + \exp(-2.15\times10^{-3})(24 - T)^{4.55}\right]$$

$$\Lambda_{nt} = 67° - 1.25(K_p - 1/3) + 9°\left[\exp(-1.7\times10^{-5}T^{5.35}) + \exp(-4.66\times10^{-4})(24 - T)^{4.1}\right]$$

where T = LT + 12hrs if LT < 12
T = LT − 12hrs if LT >= 12,
(LT = local time)

Λ_{st}, Λ_{nb}, etc. are the invariant latitudes as shown in Figure 1.7. Subscripts $_s$ and $_n$ represent the south and north walls respectively, and $_b$ and $_t$ represent the bottom of the trough (where the trough is fully formed) and the top of the trough (where the trough is not present).

The closing of the trough at sunrise occurs at local times when the solar-zenith angle lies between 95° and 87°.

The opening of the trough begins at a local time 1.5 hours after the solar-zenith angle has reached

$$87° - 3°(K_p - 1/3)$$

and the trough is fully formed at a local time 1.5 hours after the zenith angle has reached

$$91° - 3°(K_p - 1/3).$$

Appendix B: Transmitter, receiver and propagation path details

	Geographic Latitude (°N)	Geographic Longitude (°E)	Corrected Geomagnetic Latitude (°N)	Local Midnight (UT hh:mm)	CGLT Midnight (UT hh:mm)
TRANSMITTERS					
Halifax (CFH)	44.92	296.02	54.25	04:45	03:56
Iqaluit (CZD)	63.73	291.46	73.26	04:34	04:06
Wainwright (CZB)	52.80	249.70	61.12	07:21	07:56
RECEIVERS					
Alert	82.50	297.67	86.98	04:09	21:13
Cheltenham	51.80	357.80	48.50	00:09	23:12
Leitrim	45.34	284.41	56.42	05:02	04:55
PATH MIDPOINTS					
Hal - Alert	63.71	296.27	72.54	04:15	03:39
Hal - Cheltenham	52.63	324.59		02:27	
Hal - Leitrim	45.28	290.24	55.62	04:39	04:26
Iqa - Alert	73.13	292.87	81.72	04:29	03:29
Iqa - Cheltenham	62.04	330.81		01:57	
Iqa - Leitrim	54.58	287.13		04:51	
Wai - Leitrim	50.38	268.40		06:07	

Table B1: Location of transmitters, receivers and path midpoints and times of local midnight.

GREAT CIRCLE BEARING (degrees)			
	Alert	Cheltenham	Leitrim
Halifax	181.9	285.5	88.8
Iqaluit	188.5	315.6	9.7
Wainwright	-----	-----	300.9

Table B2: Great Circle Bearings of transmitters.

GREAT CIRCLE PATH LENGTH (km)			
	Alert	Cheltenham	Leitrim
Halifax	4182	4491	911
Iqaluit	2095	3946	2093
Wainwright	----	----	2633

Table B3: Great Circle path lengths.

TRANSMITTER FREQUENCIES (MHz)			
Halifax	5.097	10.945	15.920
Iqaluit	5.832	9.292	20.300
Wainwright	6.905	10.195	20.900

Table B4: Transmitter frequencies. NB: Prior to November 1993 the Halifax transmitter broadcast a CW signal at 6.43 MHz, 10.945 MHz and 15.920 MHz.

Appendix C: Method employed in determination of bearings

The method used to determine the bearings of incoming signals was that described by *Warrington and Jones,* [1992]. This appendix summarises the parts of this procedure pertinent to the results obtained in this thesis.

C.1: Determination of 'snap' bearings

RF signals from the sum beam output of the PUSHER circularly-disposed antenna array were demodulated in the system receiver and combined with goniometer positional information for initial processing. An average beam pattern called a 'composite scan' was formed from several successive rotations of the goniometer (to eliminate any effects due to modulation).

The position of maximum symmetry of the composite scan (also called the goniometer beam pattern) was determined by 'folding' the composite scan about a particular bearing (the fold point) and calculating the area between the original and the folded curve within a fixed window (see Figure C.1). The width of this window was 1.1 times the width of the main peak in the DF waveform, as calculated for an elevation angle of 20°. The fold point was moved until the area between the curves was minimised. A 'snap bearing' was assigned to this position of maximum symmetry, but only recorded if the peak amplitude of the composite scan exceeded 150% of the minimum amplitude, and only if a minimum existed within ±12° of the peak.

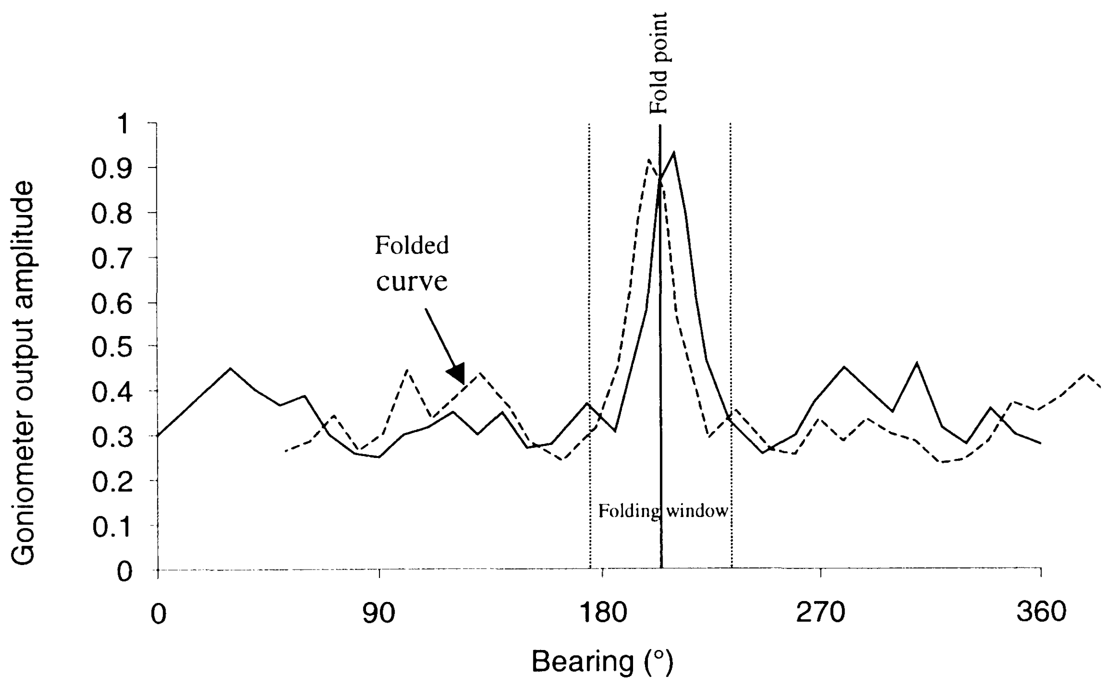

Figure C.1: Illustration of the process employed to determine the snap bearing as the point of best symettry. The fold point is moved such that the area between the original and folded curve is minimised [after *Warrington and Jones*, 1992].

For each snap bearing, a value of 'asymmetry' was assigned. This was defined as the area between the two curves (folded at the point of maximum symmetry) divided by the area under the original beam pattern within the folding window.

C.2: Determination of 'composite' bearings

To allow multiple directions of arrival to be recorded, averaging of the snaps was performed in 10° wide bins. Each bin overlapped the next by 5° to ensure that the placing of the bins did not affect the calculation. This procedure relied on the presence of modulation and fading to ensure that enough snaps were present for each azimuthal angle of arrival.

The bin containing the most snaps, if more than four, was used to calculate a composite bearing, as described in the following paragraph. These snaps were then removed from this bin and from the overlapping bins on either side. The procedure was then repeated until no bin contained four or more snaps.

Composite bearings were determined as a weighted average of the snap bearings in the bin. The weighting factor applied to each snap was approximately proportional to the reciprocal of the square of the expected error of the snap, based on its associated asymmetry value, as derived from computer modelling. The weighting of each snap was also dependent on the radio frequency, since this affected the width of the main lobe of the DF waveform.

Appendix D: Estimation of the position of a point reflector based on group delay and bearing measurements

A first-order estimate of the position of a reflection point may be made from the group delay measured on oblique ionograms and the bearing measured at the time the ionogram was taken.

The position of the reflection point is calculated from the simultaneous solution of three equations representing a sphere (the virtual height of reflection), a group path ellipsoid and the bearing plane. The geometry represented by the equations is portrayed in Figure D.1.

Equation (1) is a sphere of radius R+h (where R is the radius of the Earth and h is an assumed virtual height of reflection).

$$x^2 + y^2 + z^2 - (R+h)^2 = 0 \qquad \text{...(D1)}$$

where R = radius of Earth,
h = assumed virtual height of reflection (=300 km),

Equation (D2) is an ellipsoid with a major axis given by the group path, d, with foci at the locations of the transmitter and receiver.

$$\frac{x^2}{a^2} + \frac{\left(y^2 + (z - R')^2\right)}{b^2} - 1 = 0 \qquad \text{...(D2)}$$

where $a = \dfrac{d}{2}$,

$b^2 = \dfrac{d^2 - L^2}{4}$,

$L = 2R\sin\left(\dfrac{D}{2R}\right)$, (where D = GCP length),

and $R' = R\cos\left(\dfrac{D}{2R}\right)$

Note that axes have been oriented such that the transmitter and receiver are located at co-ordinates (L/2,0,R') and (-L/2,0,R') respectively.

The group path, d was estimated from ionograms by measuring the time difference between the time delay of the trace at the frequency of transmission and the time delay of the E_s trace. A virtual height of 120 km was assumed for the E_s region path that was assumed to propagate along the GCP.

Equation (D3) represents the great circle plane containing the receiver and the line of bearing.

$$x + \cot(\beta).y + \frac{L}{2R'}.z = 0 \qquad ...(D3)$$

where β = (measured bearing) - (GCP bearing).

The simultaneous solutions to Equations D1-D3 were found using a commercial computer software package called MAPLE [*Char et al.*, 1985] and are far too lengthy to include here. A maximum of 4 solutions exist, though two of these arise from the π ambiguity in $\cot(\beta)$ in equation (D3) and may be discarded following scrutiny of the value of β. In practice it is found that unique solutions only exist where the group path, d exceeds a critical value such that the pseudo-elliptic locus of simultaneous solutions to equations (D1) and (D2) has a major axis greater than L.

The solution vectors (x, y, z) were rotated about the z axis by an angle equal to that required between the GCP and the meridian passing through its midpoint and then about the y and z axes by the angles of GCP midpoint co-latitude and longitude respectively. Latitude and longitude were then found by the usual Cartesian to spherical co-ordinate relations.

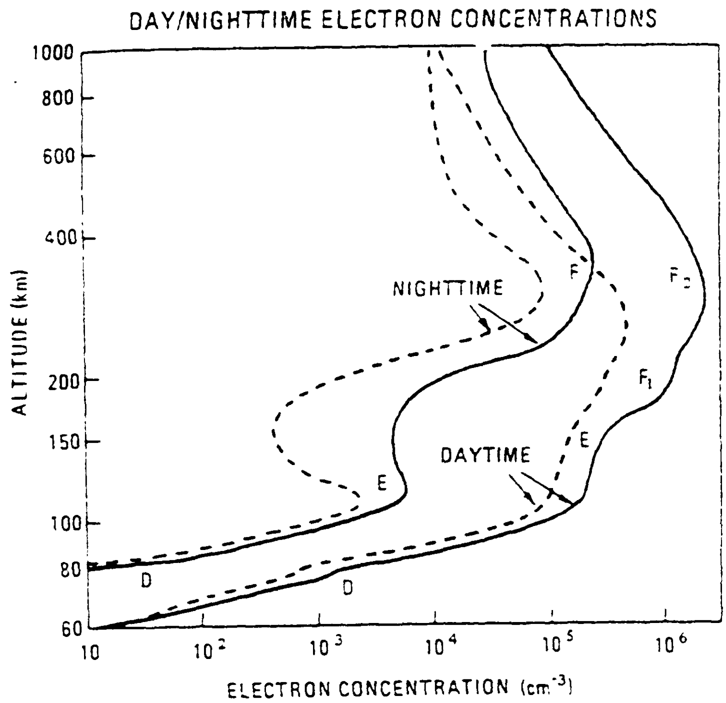

Figure 1.1: Typical electron density profiles of the ionosphere. Example profiles are shown for solar maximum (solid lines) and solar minimum (dashed lines). [From *Swider*, 1988].

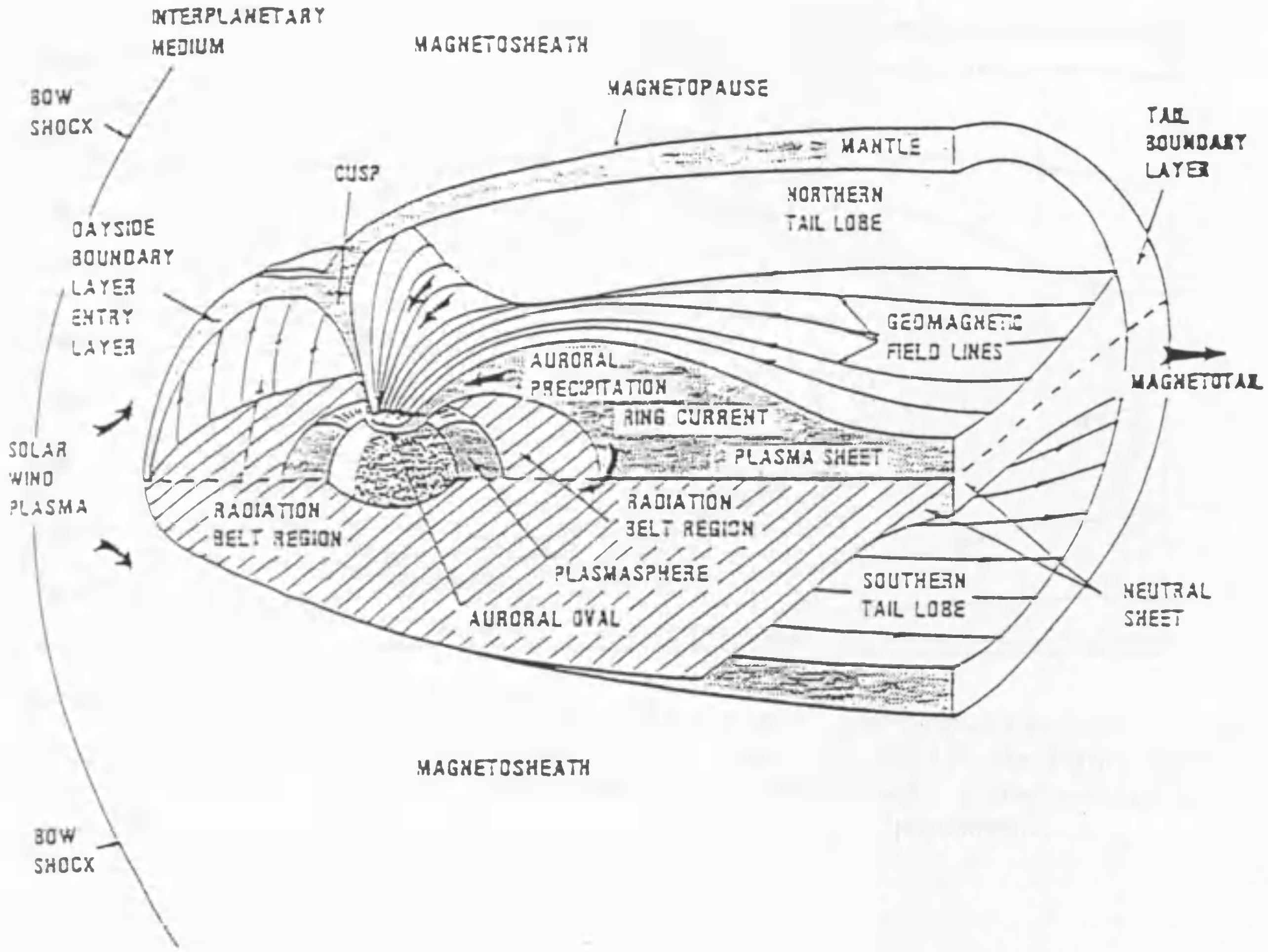

Figure 1.2: Nomenclature of the Magnetosphere [from *Tascione 1988*].

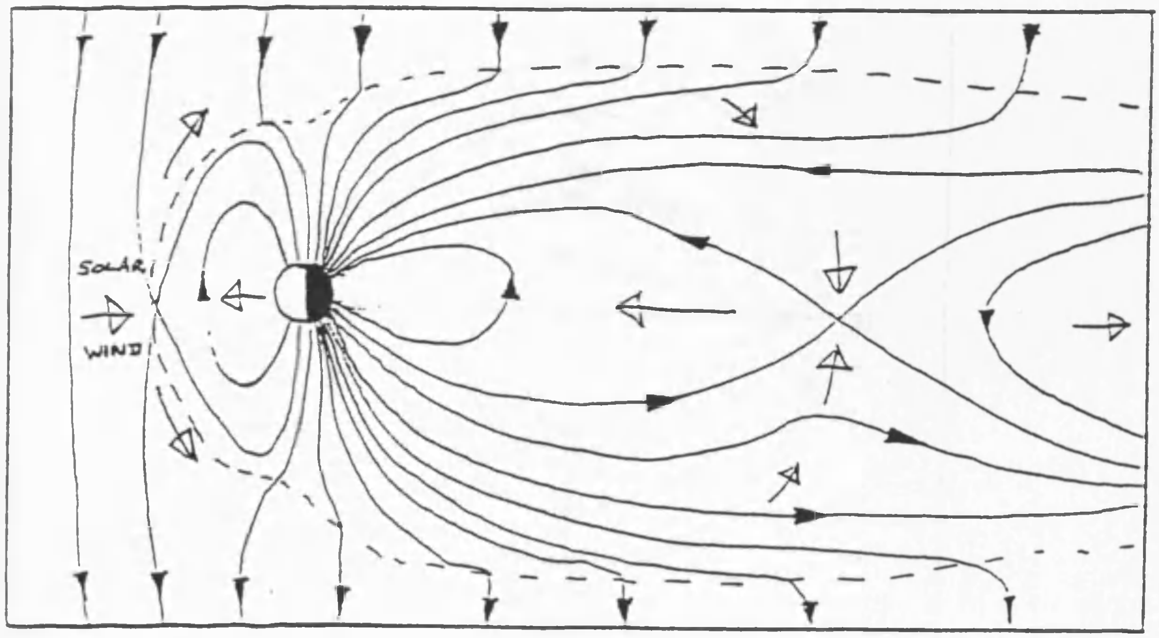

Figure 1.3: Magnetospheric convection of the magnetic field (solid arrows) for a southward IMF. Open arrows indicate the motion of magnetic flux tubes and the plasma confined within these tubes. The dotted line represents the
magnetopause boundary.

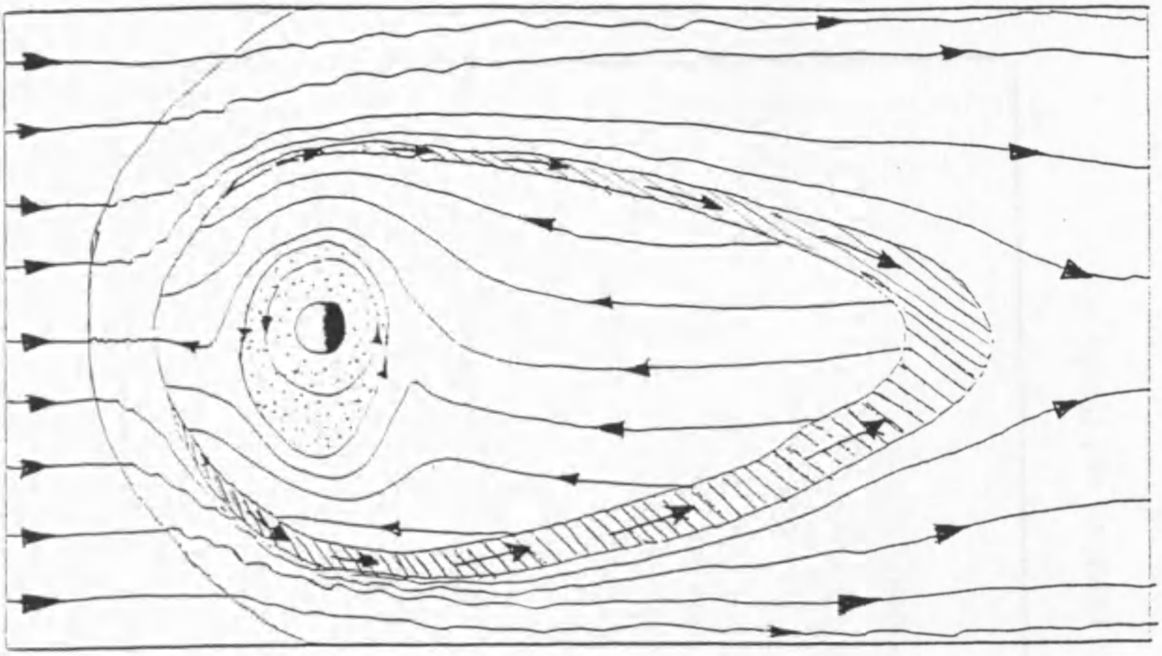

Figure 1.4: Plasma flow (solid arrows) in the magnetospheric equatorial plane. The dotted region represents the plasmasphere, which corotates with the Earth. The hatched region represents the boundary layers in which viscous interaction helps to drive the return convective flow. Sunward flow is driven by reconnection.

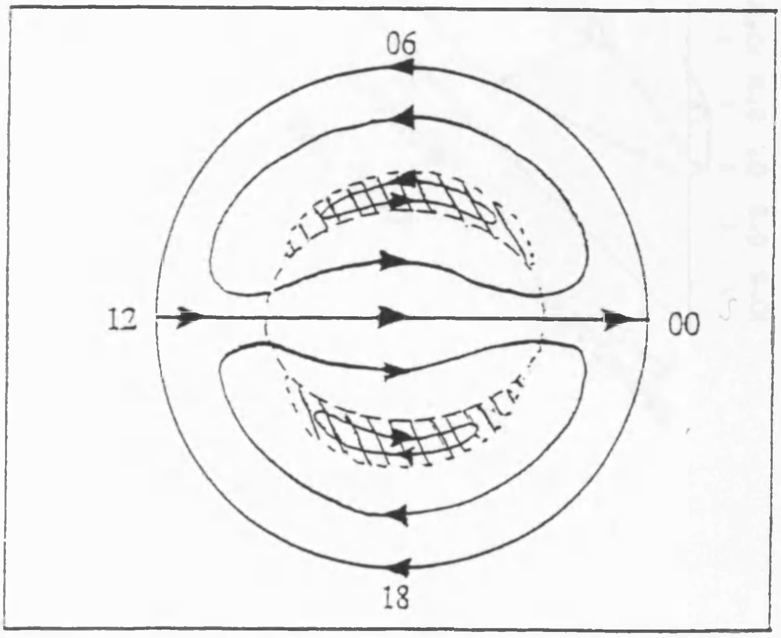

Figure 1.5: The characteristic two-cell convection pattern in the high latitude, F-region ionosphere for a southward IMF. The hatched region maps to the viscous flow in the magnetospheric boundary layers. Numbers indicate local times.

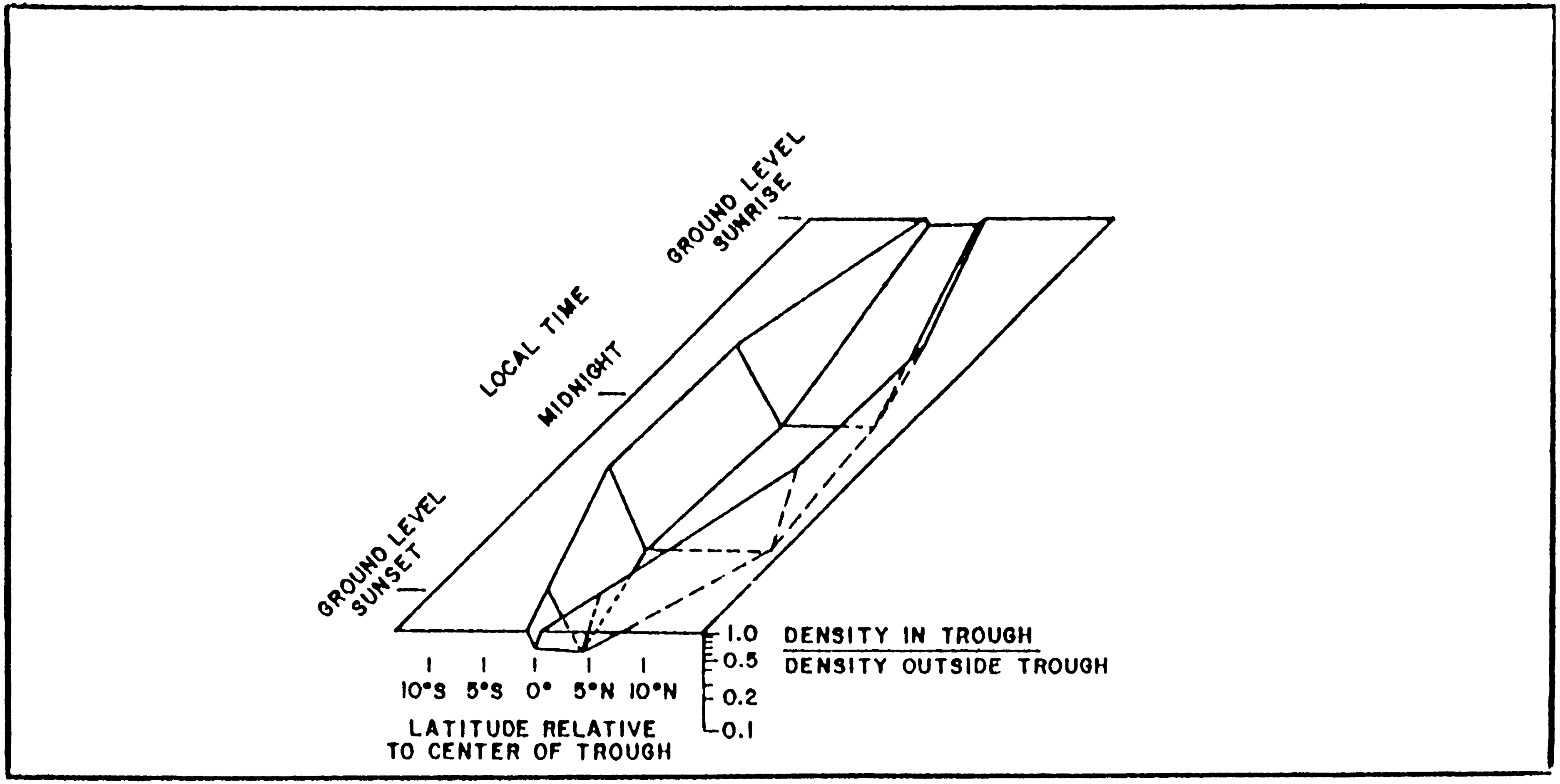

Figure 1.6: The structure of the sub-auroral trough [from *Feinblum and Horan*, 1973].

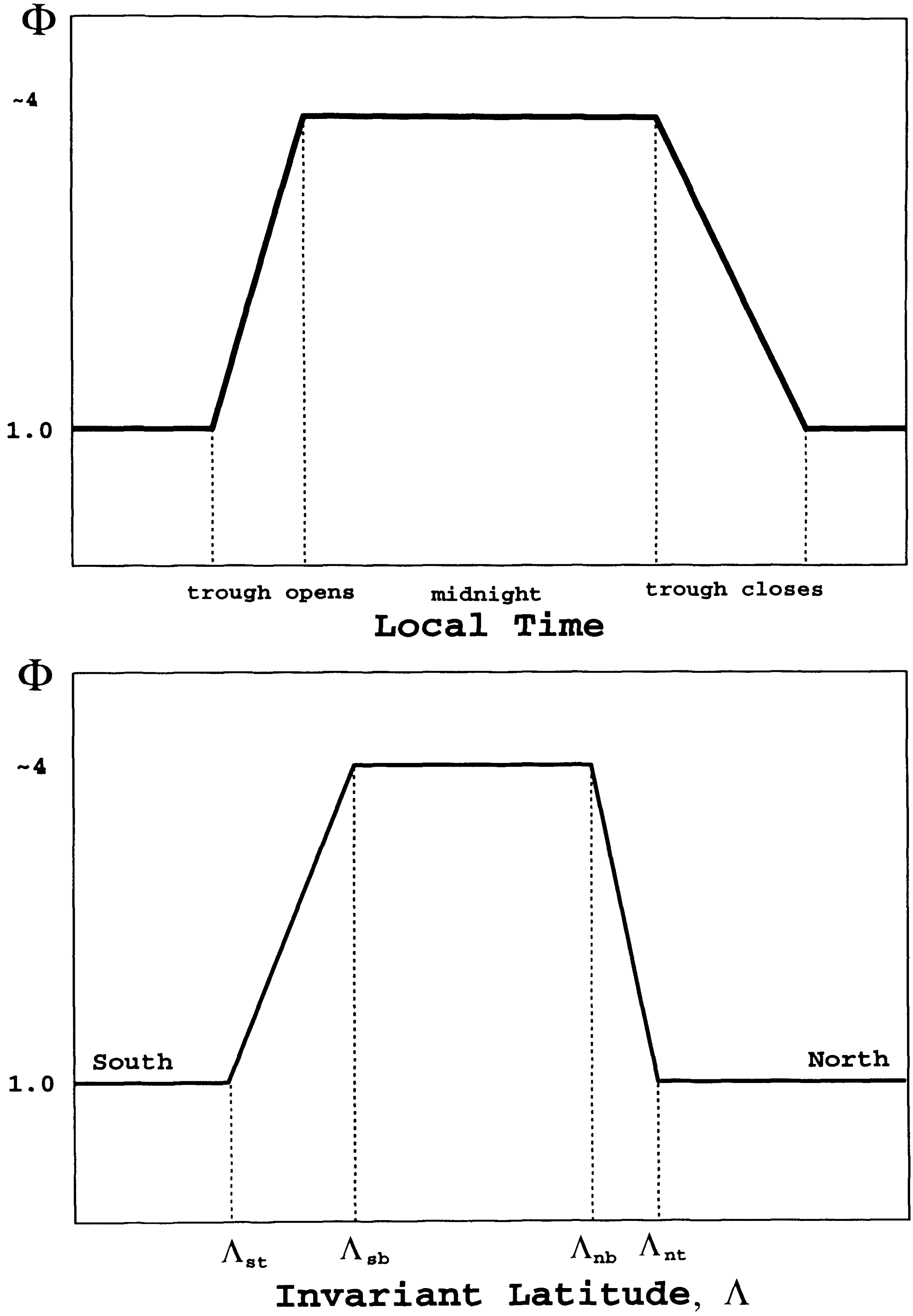

Figure 1.7: Mathematical representation of the *Halcrow and Nisbet* [1977] model of the sub-auroral trough. Here Φ represents the reciprocal of the correction factor to the CCIR predictions of F_2 peak electron density.

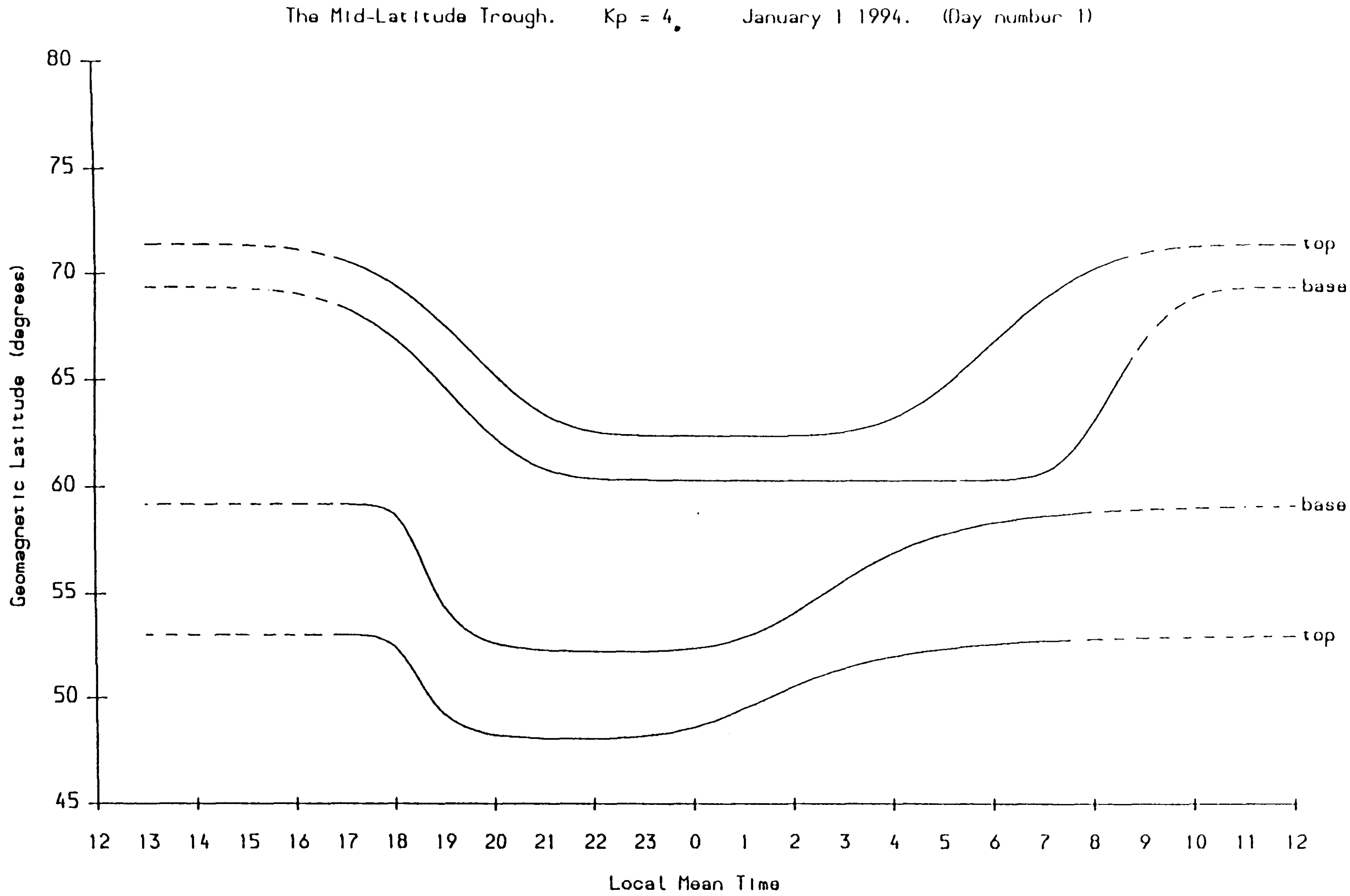

Figure 1.8: The Mid-Latitude Trough wall positions [from *Halcrow and Nisbet, 1977*].

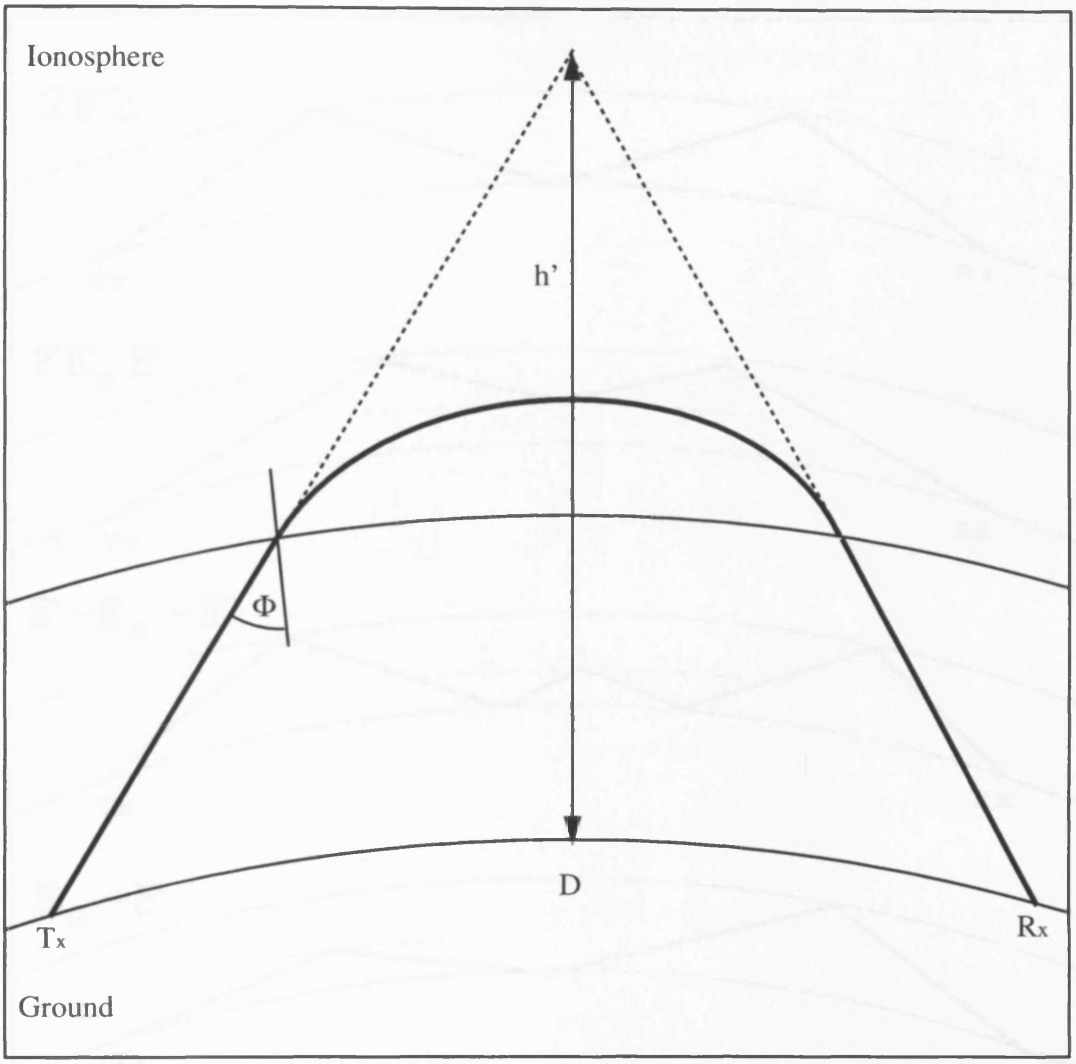

Figure 1.9: A typical HF ray path in the ionosphere.

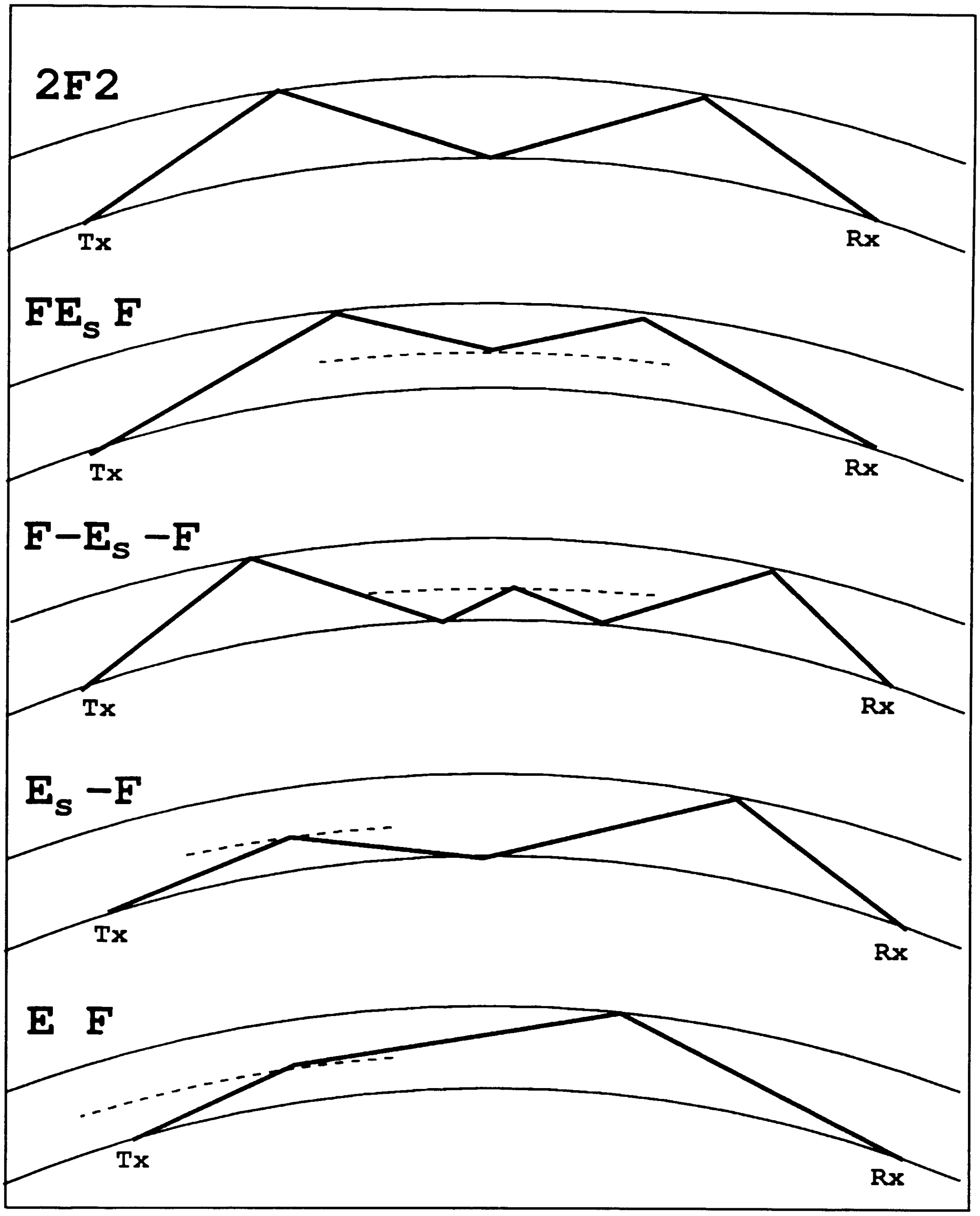

Figure 1.10: Illustration of various modes of propagation in the ionosphere. Here the dashed lines represent layers of sporadic-E.

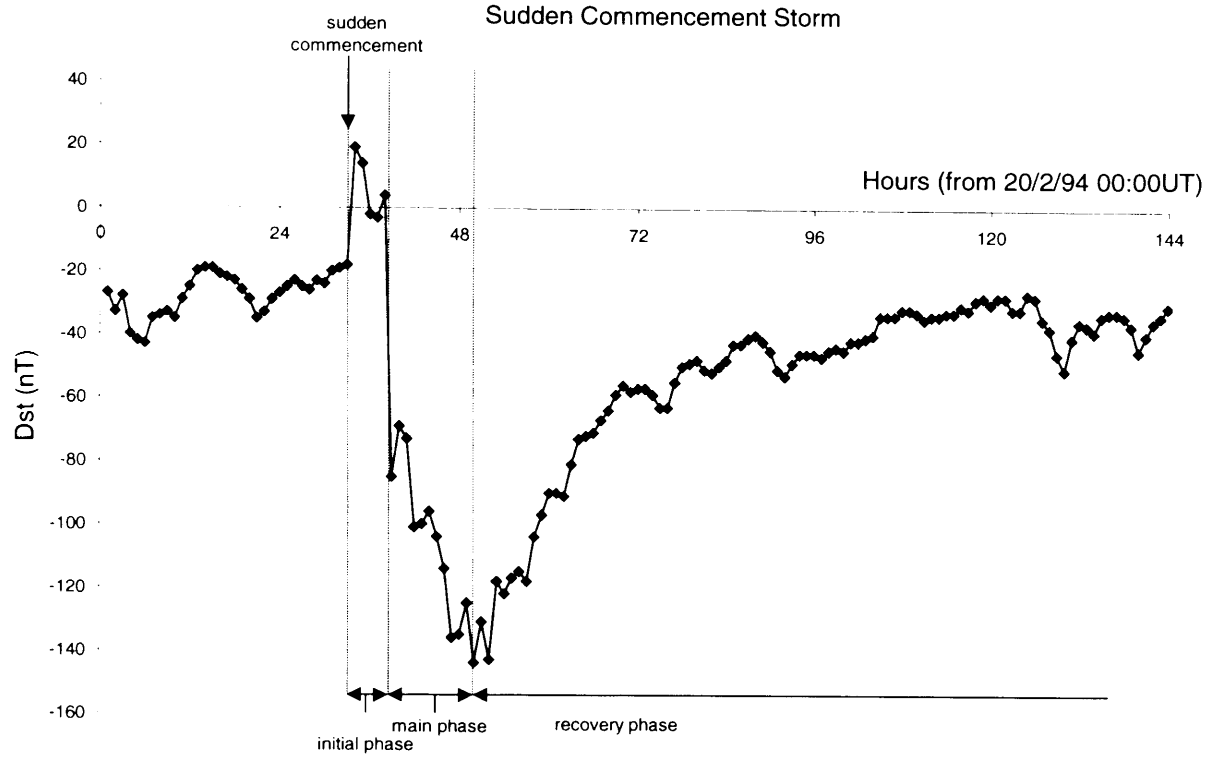

Figure 1.11a: Dst variation during the period 20-25 February 1994 showing the typical characteristics of a solar flare induced, sudden commence geomagnetic storm.

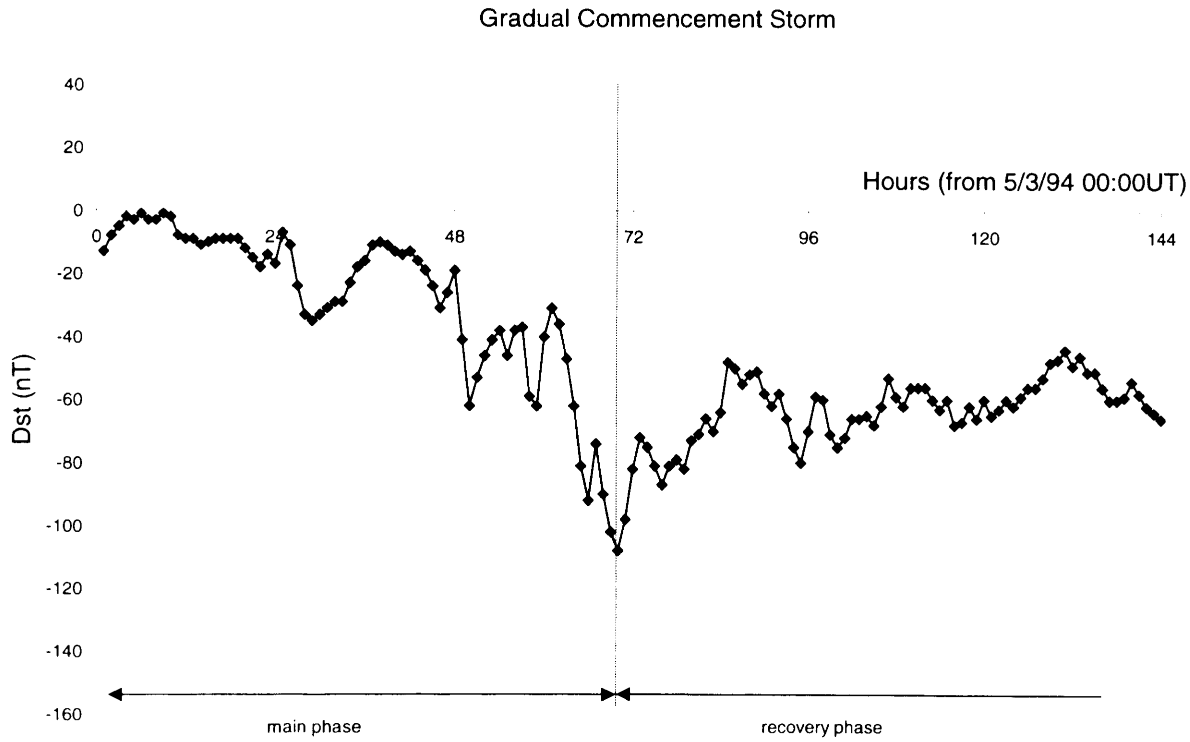

Figure 1.11b: Dst variation during the period 5-10 March 1994 showing the typical characteristics of a gradual commencement type storm. Note the extended period of main and recovery phases and the lack of any discernible initial phase.

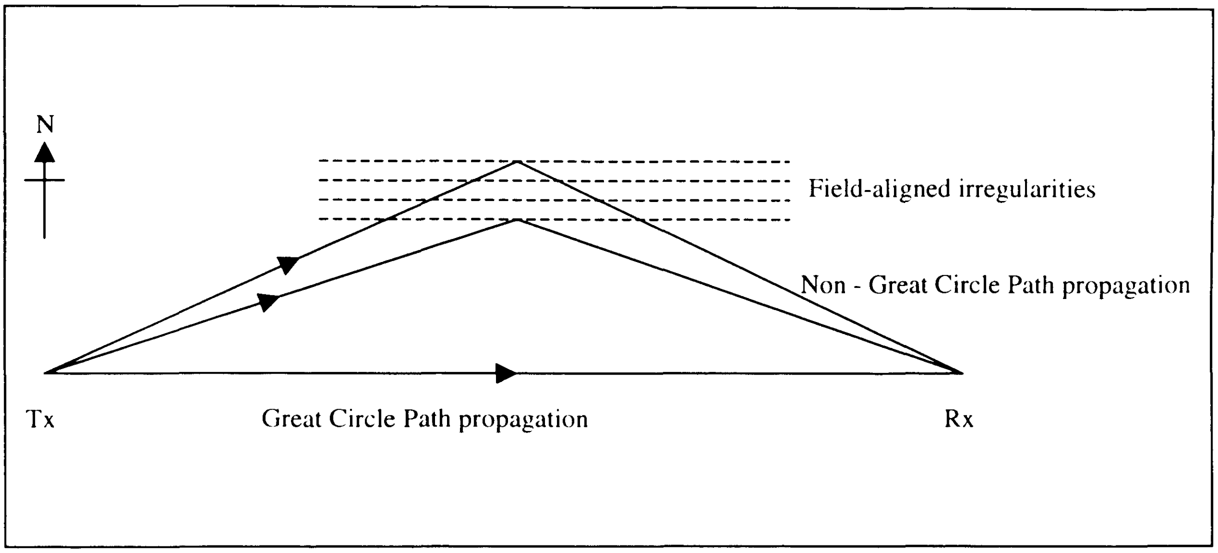

Figure 2.1: Non-great circle propagation due to field-aligned irregularities (FAIs).

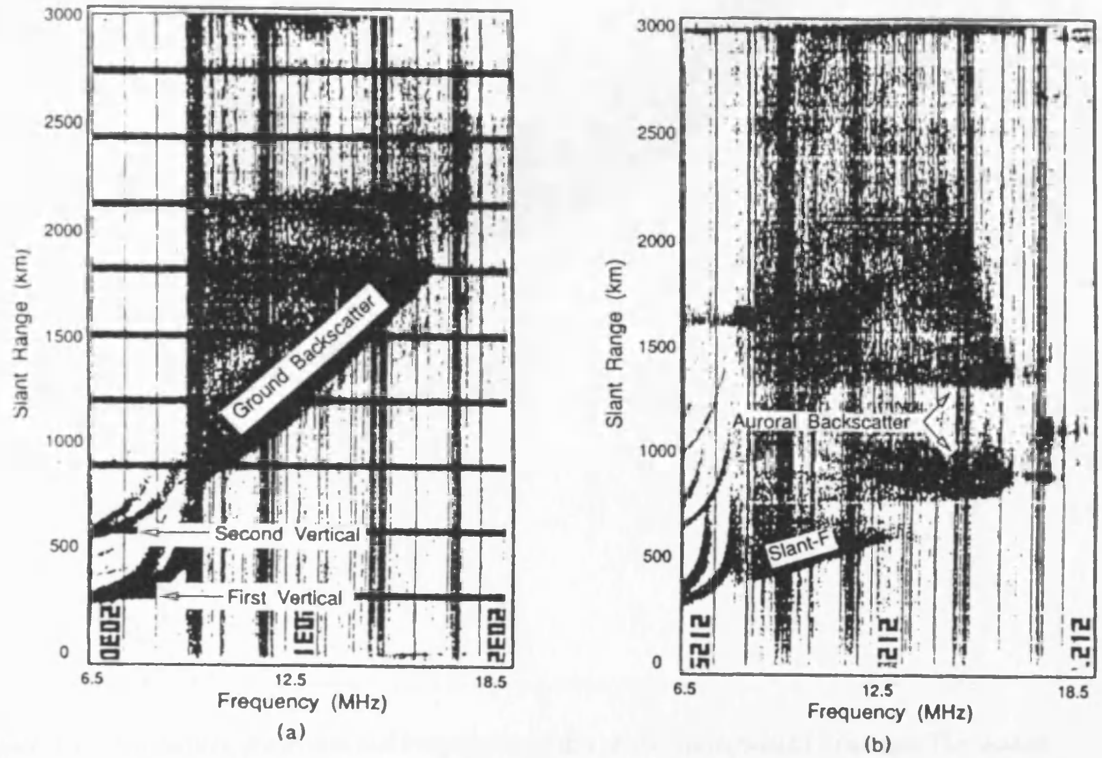

Figure 2.2: North-look, backscatter ionograms showing (a) ground backscatter under normal propagation conditions and (b) additional echoes, slant-F and auroral backscatter. (Reproduced from *Choi et al.* [1992]).

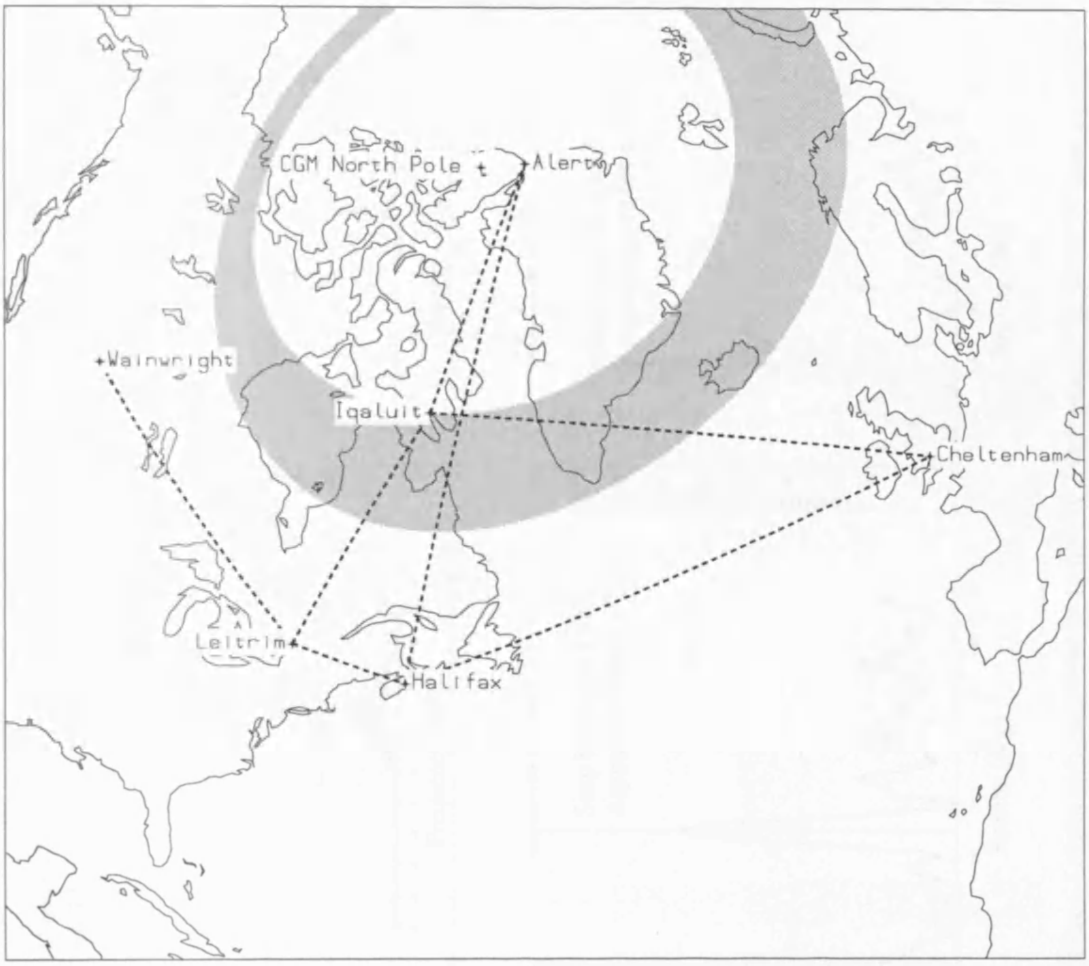

Figure 3.1: Transmitters, Receivers and Propagation Paths of the Springboard Campaign. The shaded region represents the approximate extent of the visual auroral zone based on a model by *Holzworth and Meng*, [1970] for an Ap value of 15.

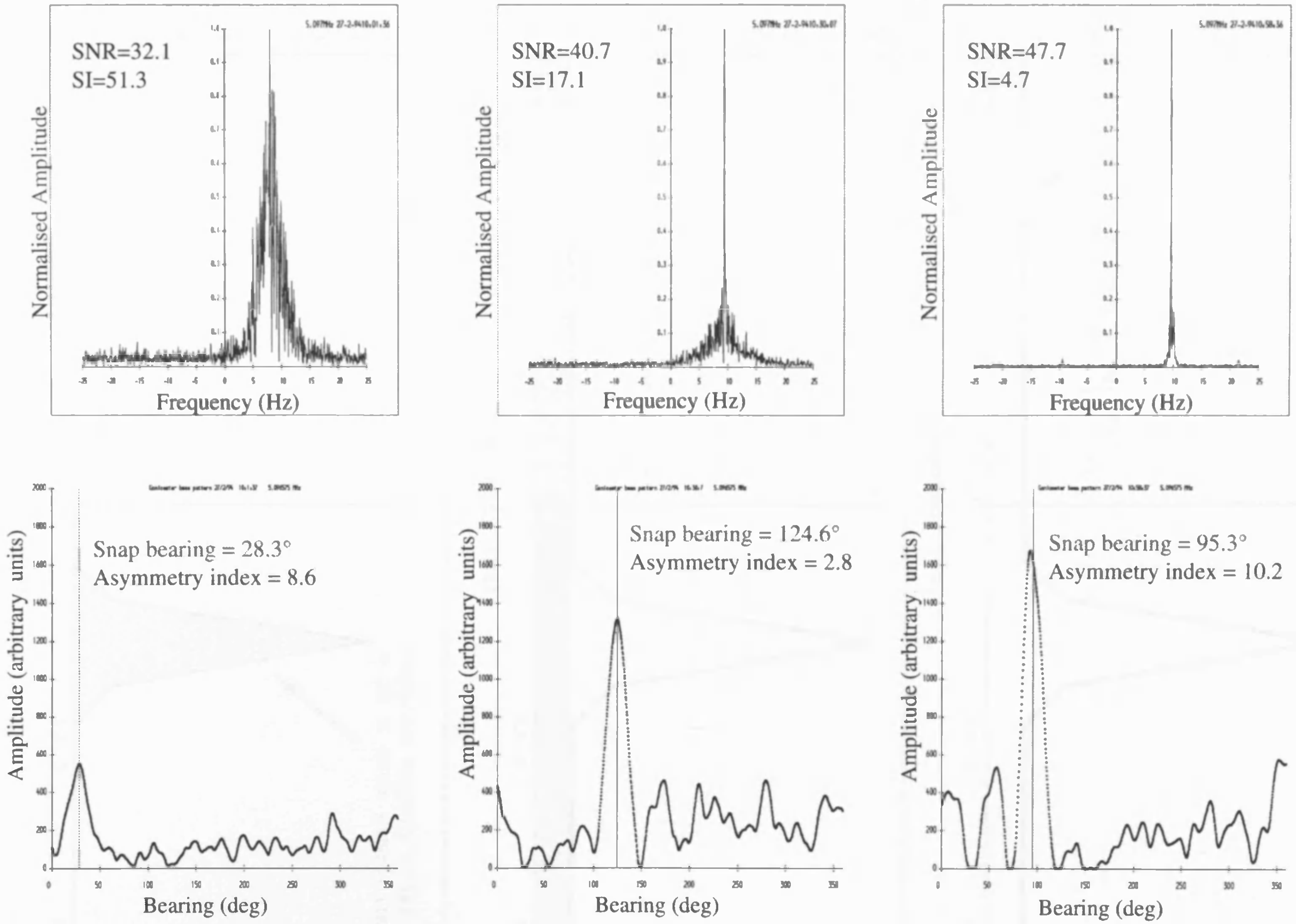

Figure 3.2: Receiver and Goniometer measurements at 5.097MHz over the Halifax – Leitrim path on 27/2/94 at 10:01:36UT (left panels), 10:30:07UT (centre panels) and 10:58:36UT (right panels).

Top panels: Normalised signal spectra showing a 10Hz applied offset. SNR and Doppler spread index (SI) values are also shown.

Bottom panels: Goniometer beam patterns. The vertical lines indicate the assigned 'snap' bearing, together with an asymmetry index.

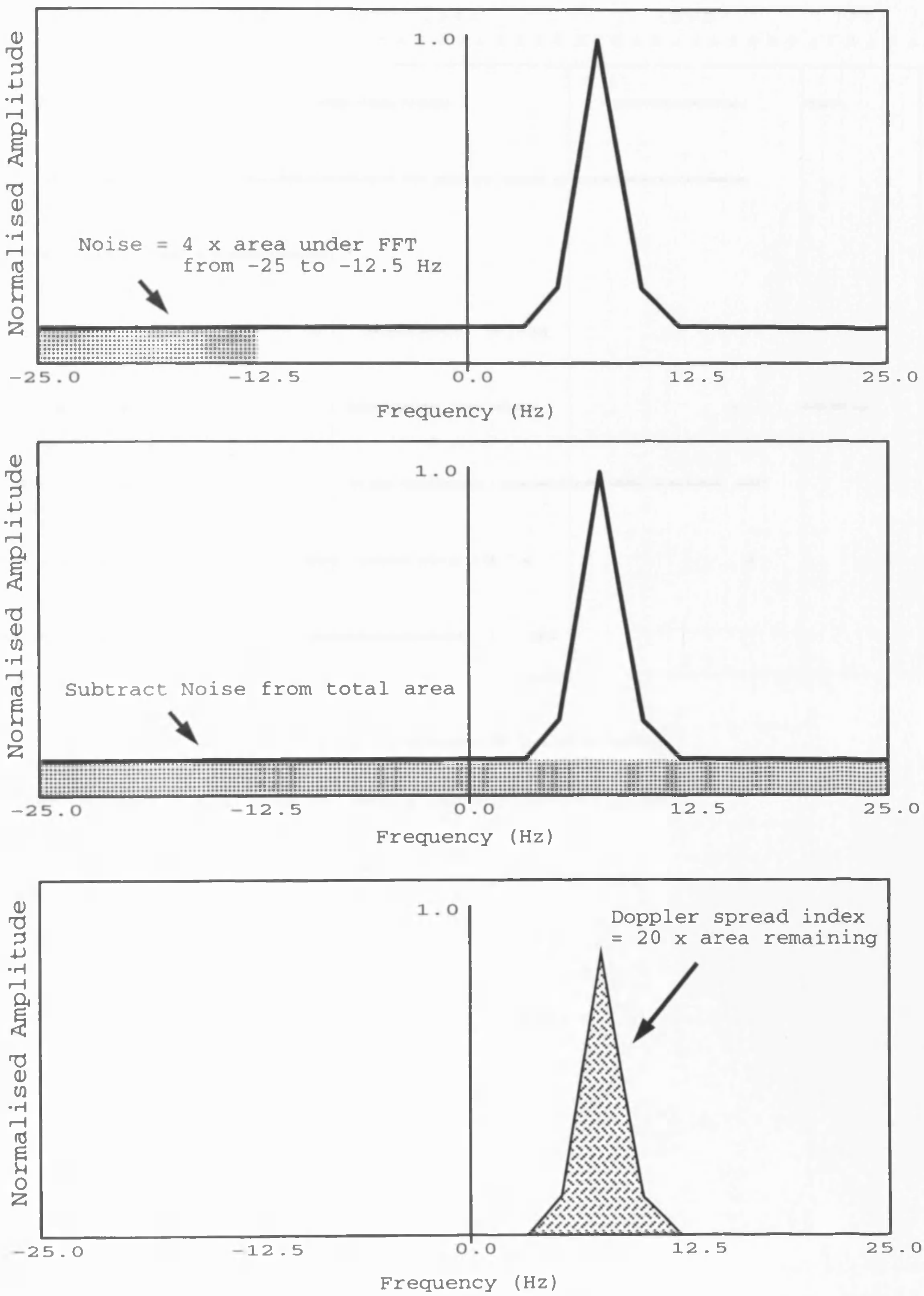

Figure 3.3: Calculation of SNR and Doppler spread index from normalised signal spectra.

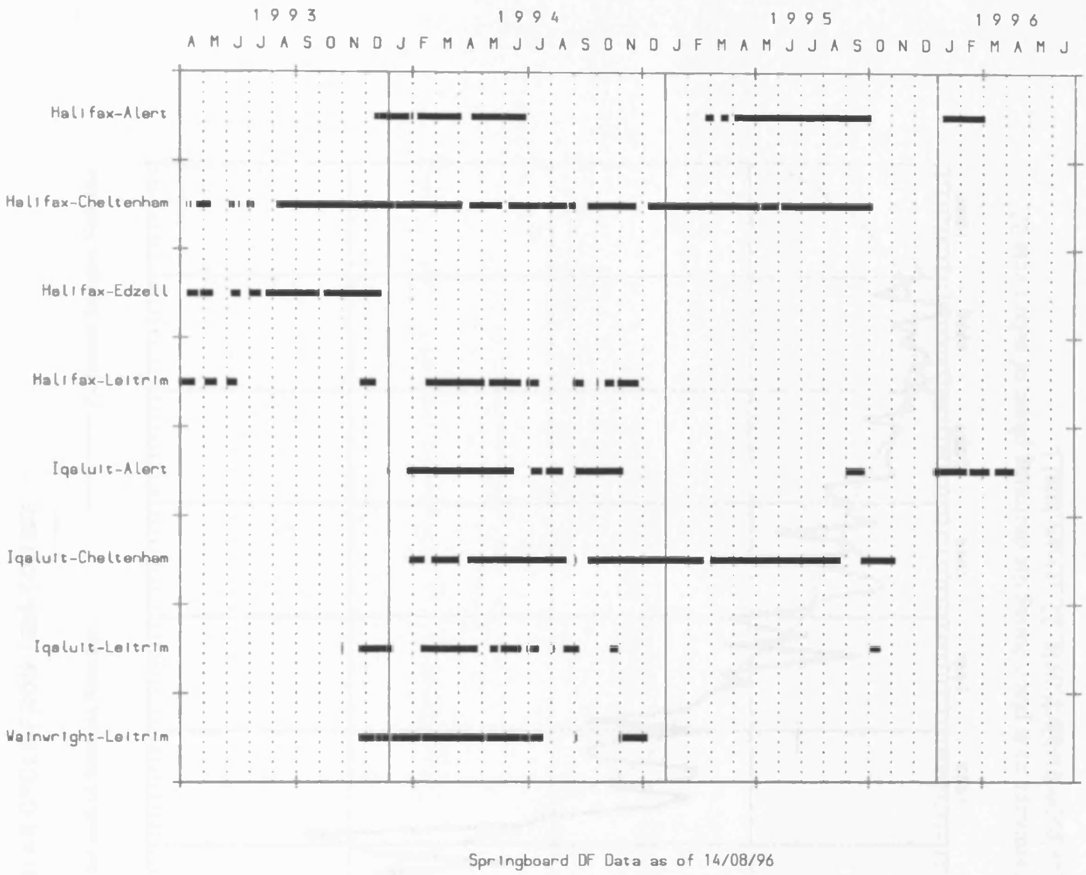

Figure 4.1: Dates for which processed bearing measurements are available.

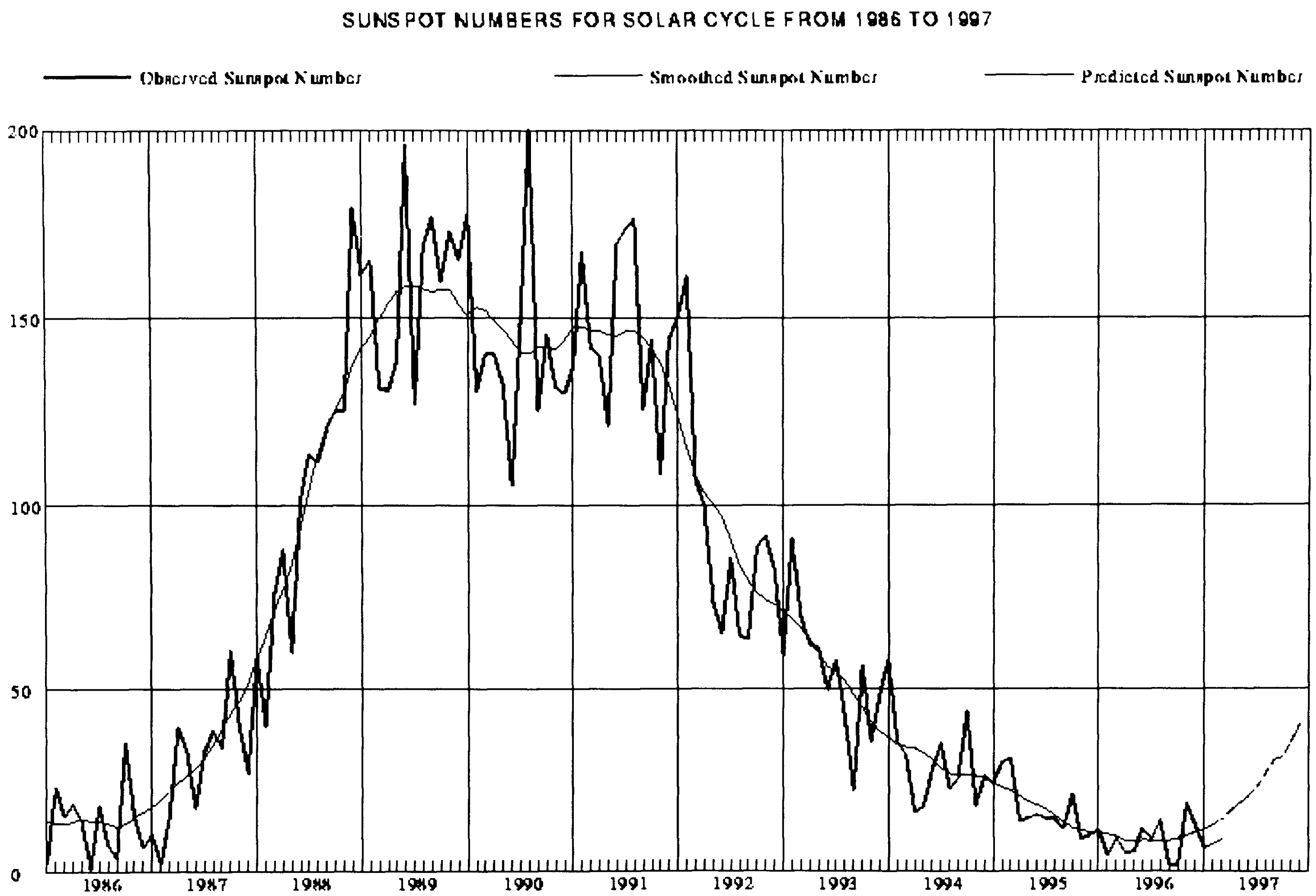

Figure 4.2: Solar activity for solar cycle 22. The experimental campaign took place during the declining phase of solar cycle 22 [*from Thompson, R.*, http://www.ips.gov.au/papes/richard/cycle_22_review.html].

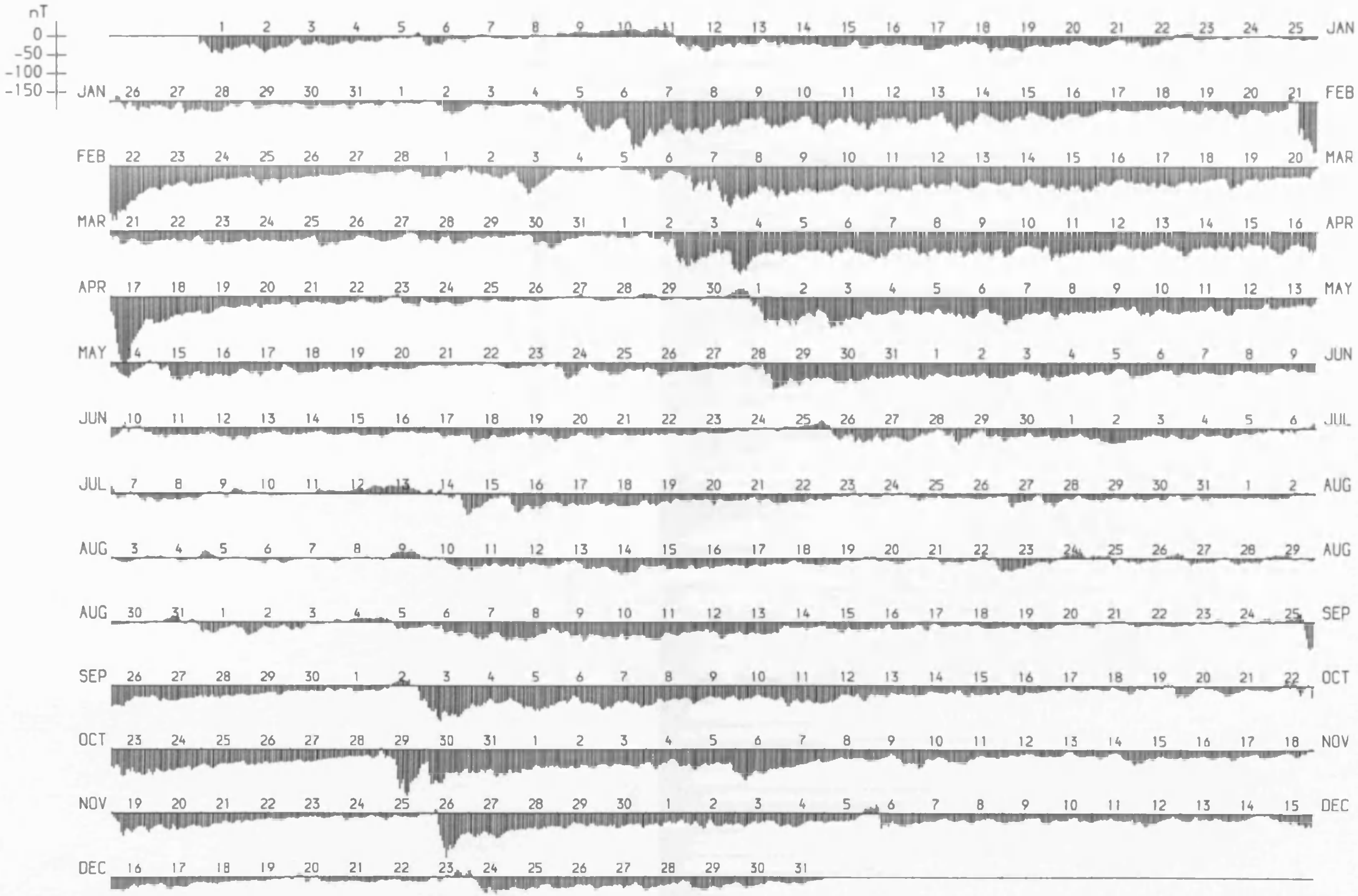

Figure 4.3: The D_{st} geomagnetic activity index for 1994.

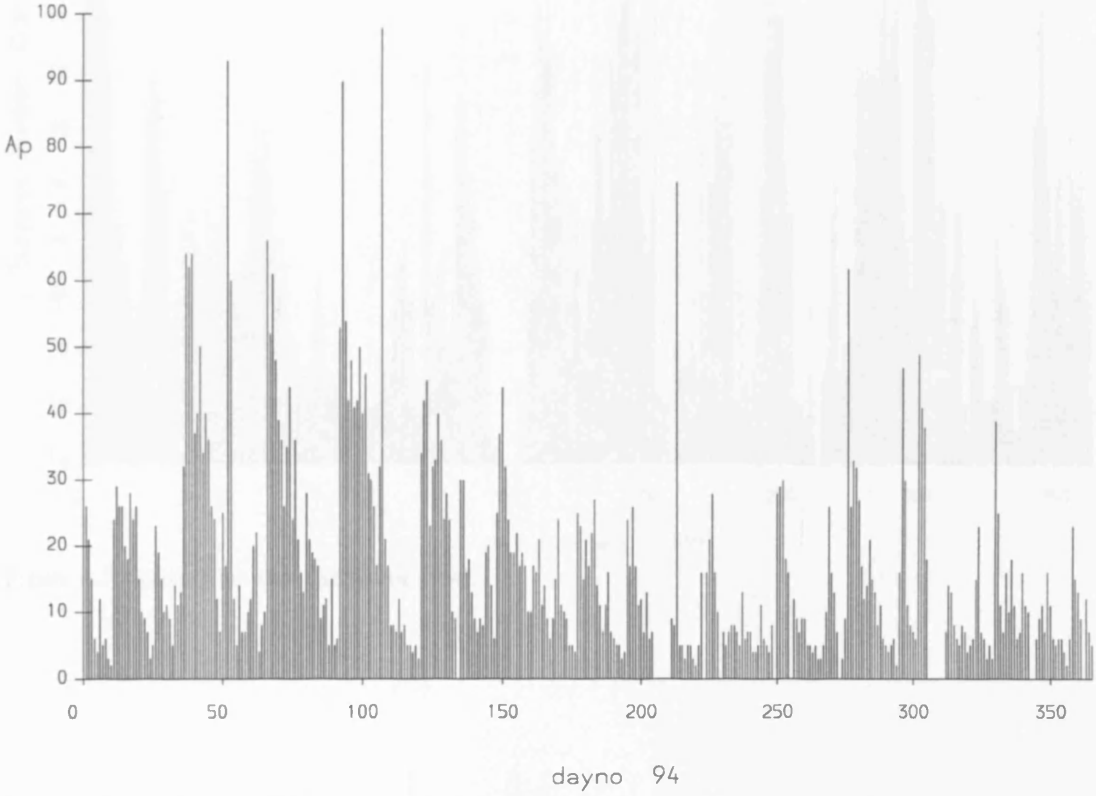

Figure 4.4: The Ap geomagnetic activity index for 1994.

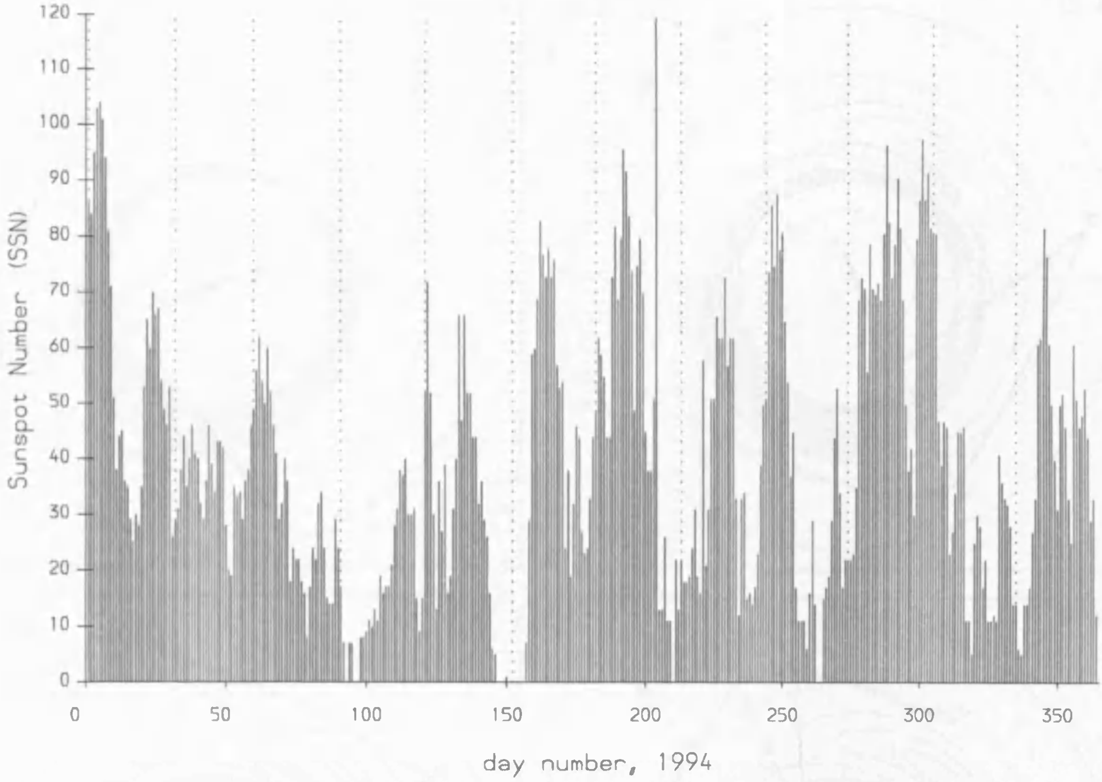

Figure 4.5: Sunspot number (SSN) for 1994.

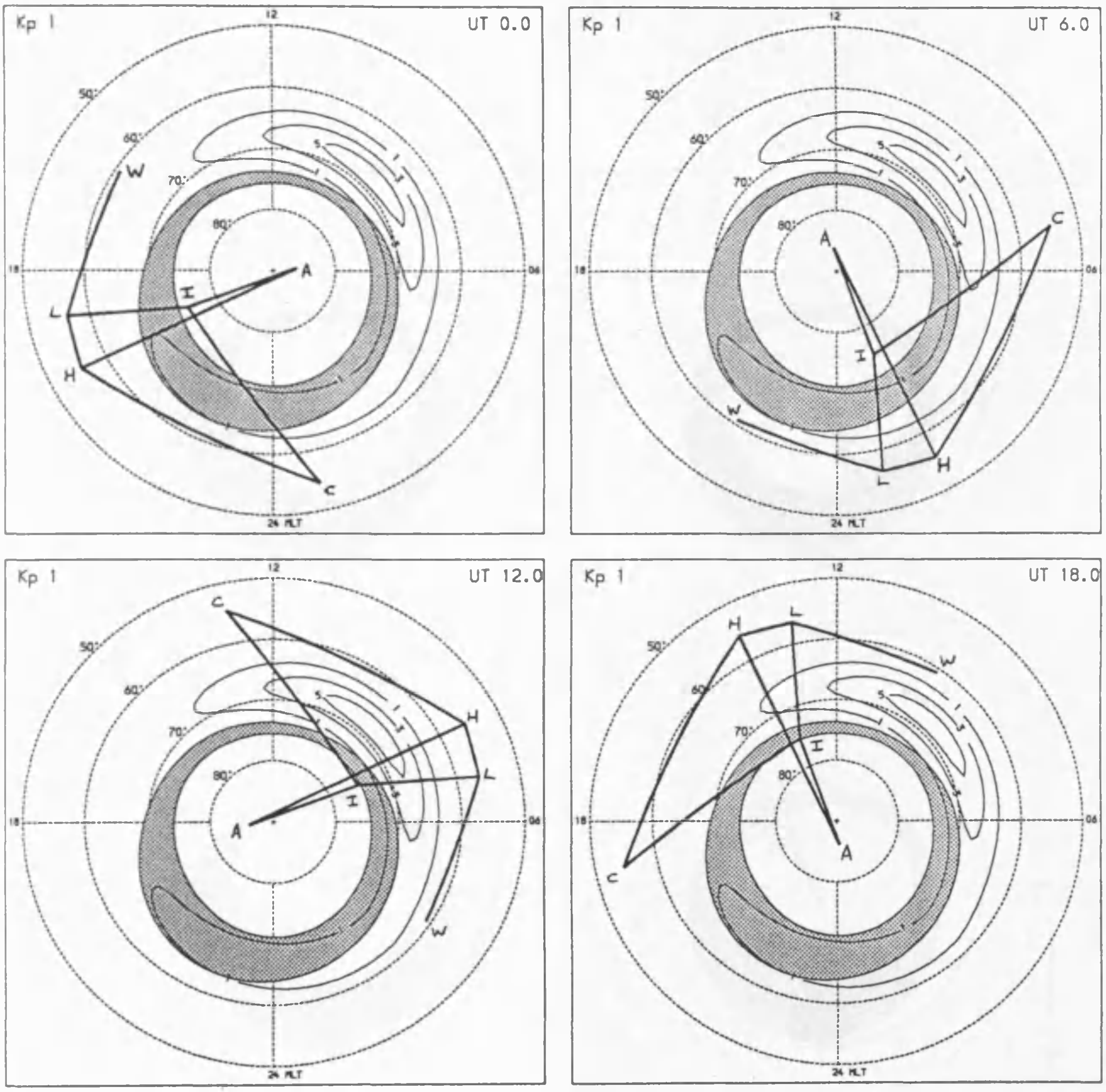

Figure 4.6: Paths of the Springboard campaign (plotted in Corrected Geomagnetic Coordinates). The shaded region represents the model extent of the visual aurorae [*Holzworth and Meng*, 1975] and the contours represent the percentage of days on which the absorption measured by a riometer at 30 MHz exceeds 1dB according to the model of *Foppiano and Bradley* [1983]. The results are presented for Kp values of 1.

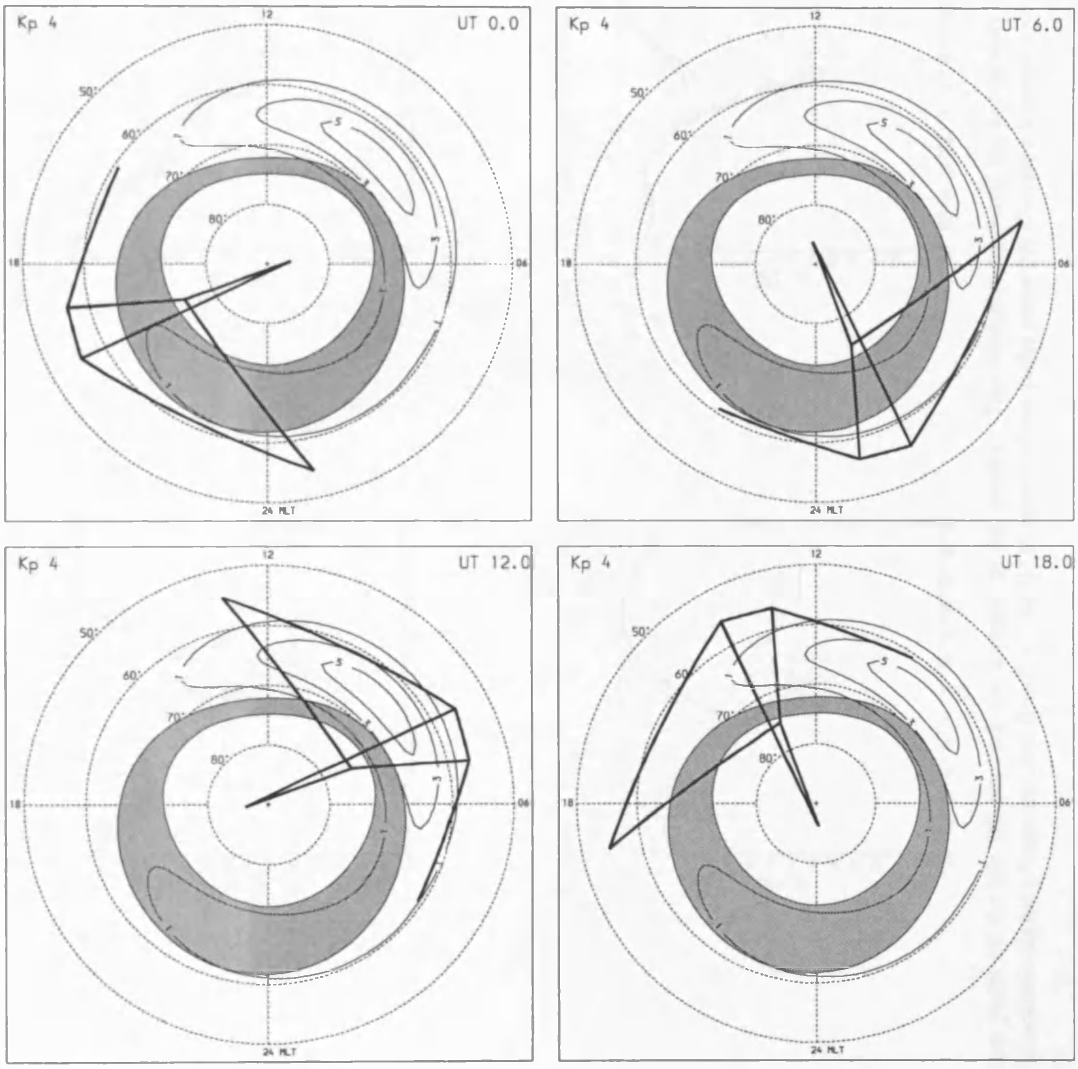

Figure 4.7: The *Foppiano and Bradley* [1983] model of Q1, and the *Holzworth and Meng* [1975] model of the aurora (shaded regions) at a Kp value of 4. The great-circle propagation paths of the HF DF network are shown at four different times of day (UT).

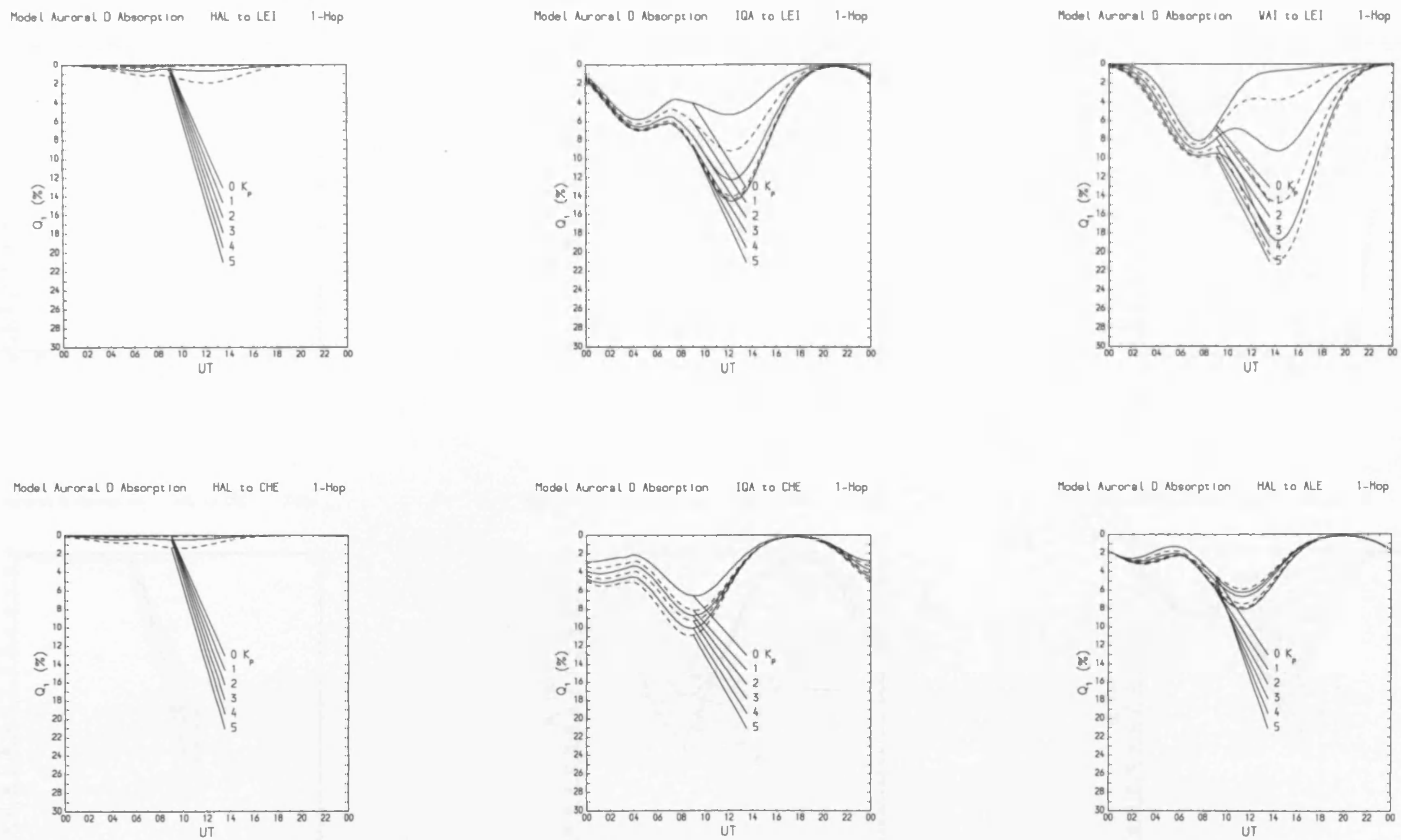

Figure 4.8: Diurnal variation of absorption on 1-hop paths of the HF DF network for a range of Kp values. The contours represent the probability sum of Q_1 (the probability of 1dB absorption on a 30MHz trans-ionospheric signal [*Foppiano and Bradley*, 1983]) at points where paths cross the D-region ionosphere (at an altitude of 80km, based on virtual apogee at 250km).

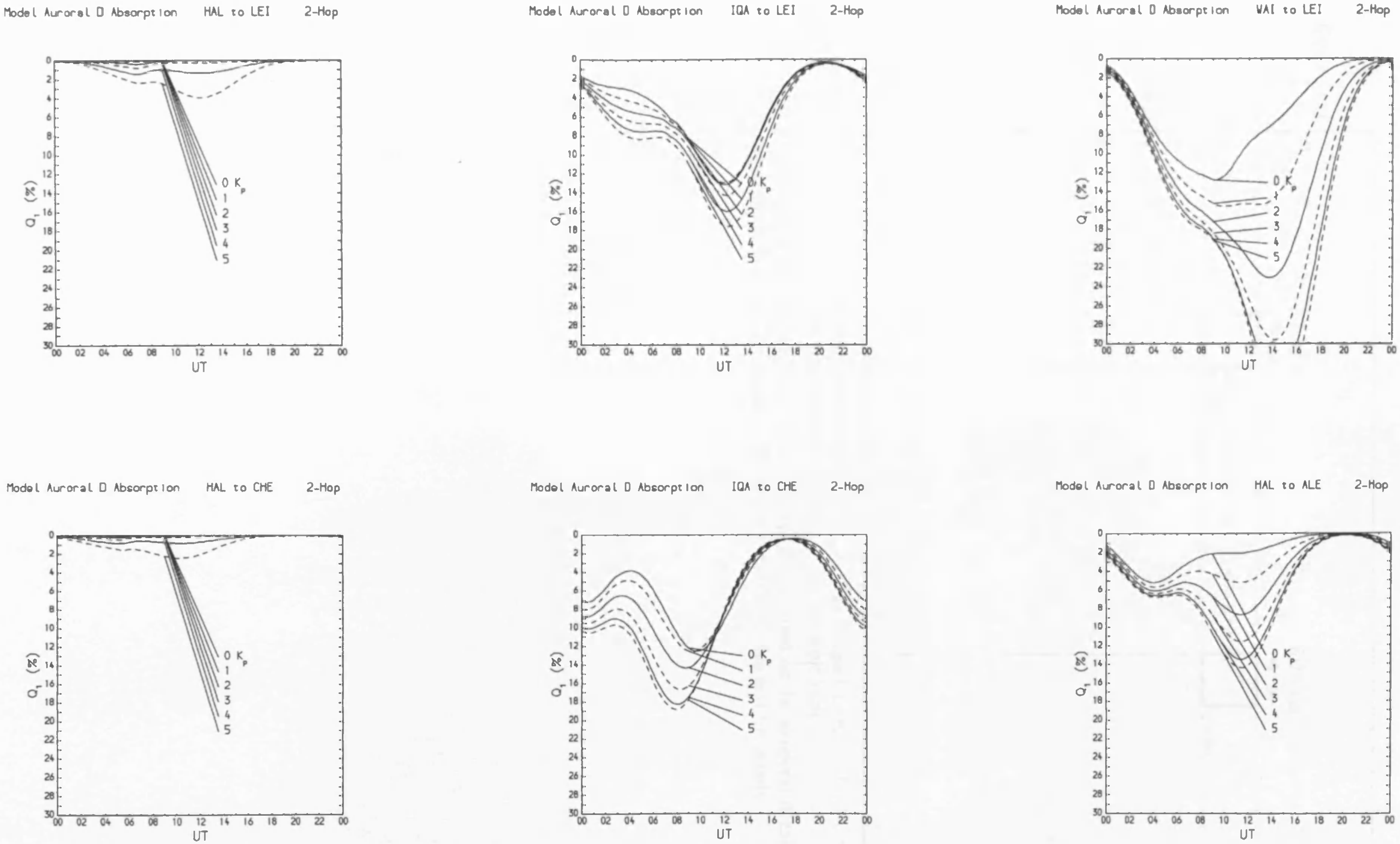

Figure 4.9: The same measurements as for Figure 4.8 but for 2-hop propagation.

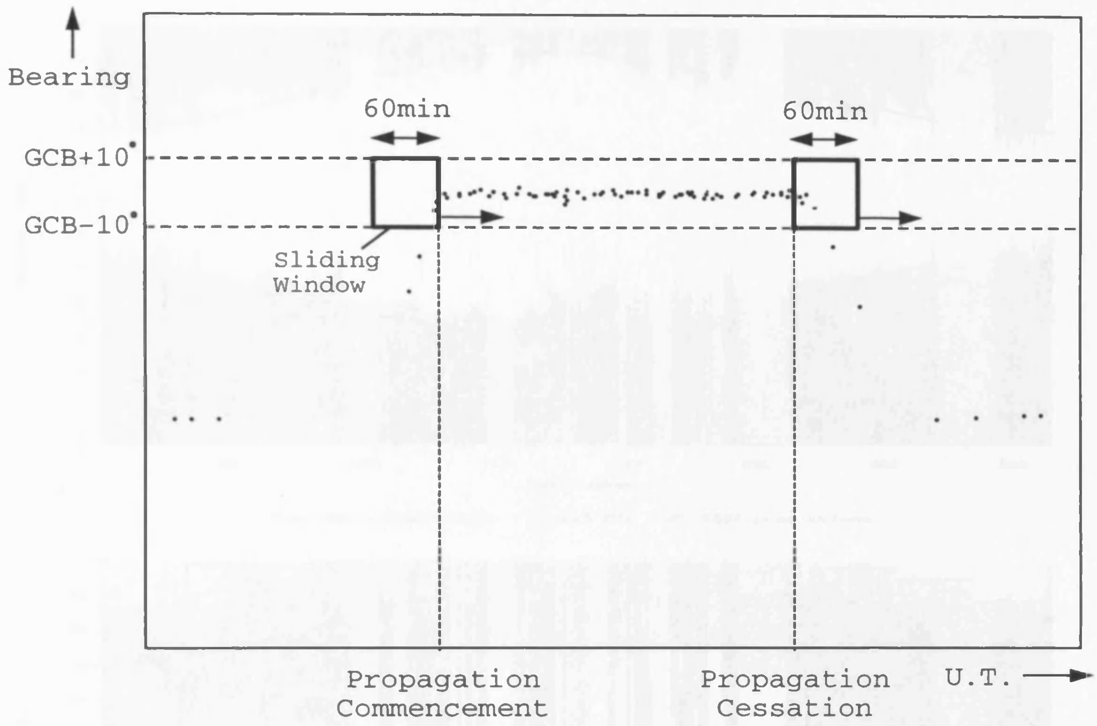

Figure 4.10: Illustration of the calculation of times of propagation based on the temporal density of composite bearing returns from the DF system within ±10° of the GCB. See text for details.

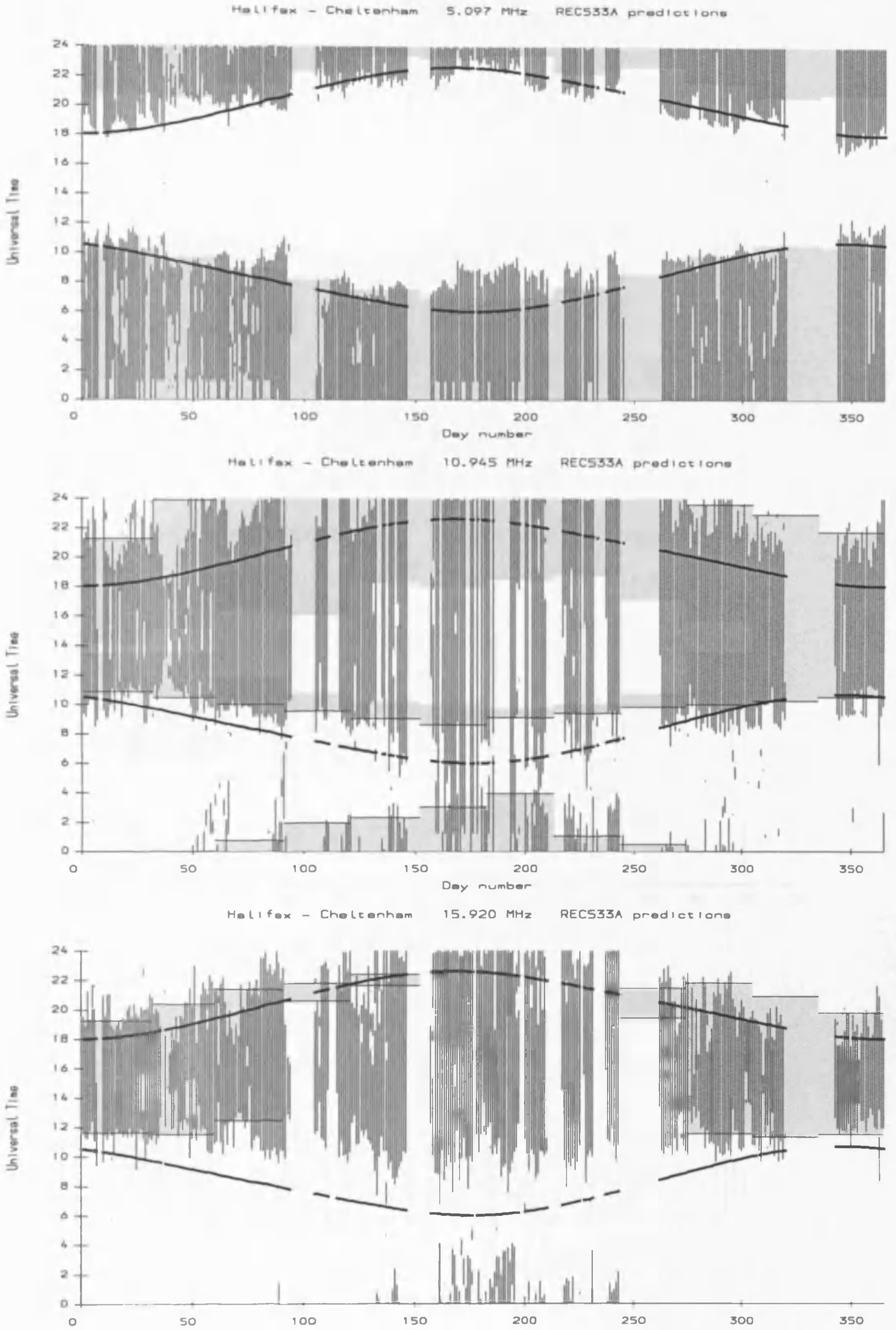

Figure 4.11: Times of propagation on the Halifax - Cheltenham path for 1994. The vertical lines indicate times of propagation based on bearing returns from the DF system, the shaded blocks represent CCIR Rec.533 model predictions and times of ground sunrise and sunset at the path midpoint are indicated by the solid curves.

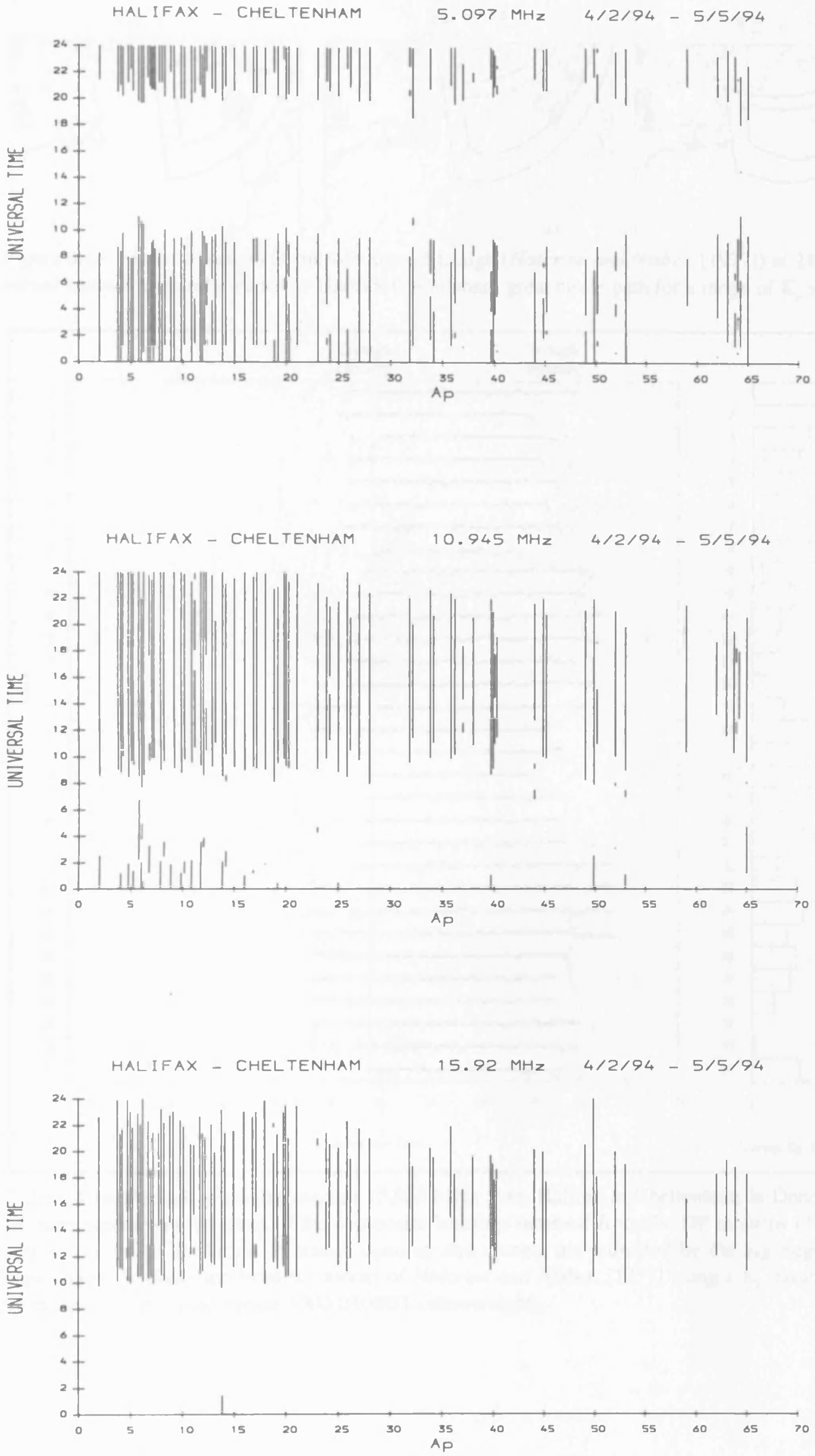

Figure 4.12: Times of propagation on the Halifax-Cheltenham path for 4/2/94 - 5/5/94 based on bearing returns from the DF system, arranged according to A_p index.

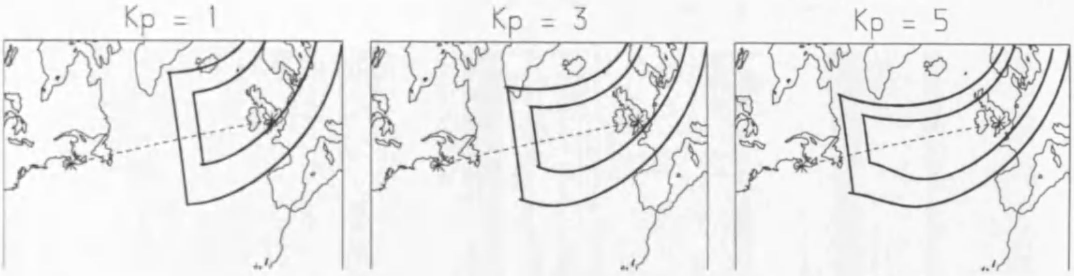

Figure 4.13: Model positions of the sub-auroral trough (*Halcrow and Nisbet*, [1977]) at 2100UT for a vernal equinox day, relative to the Halifax-Cheltenham great circle path for a range of K_p values.

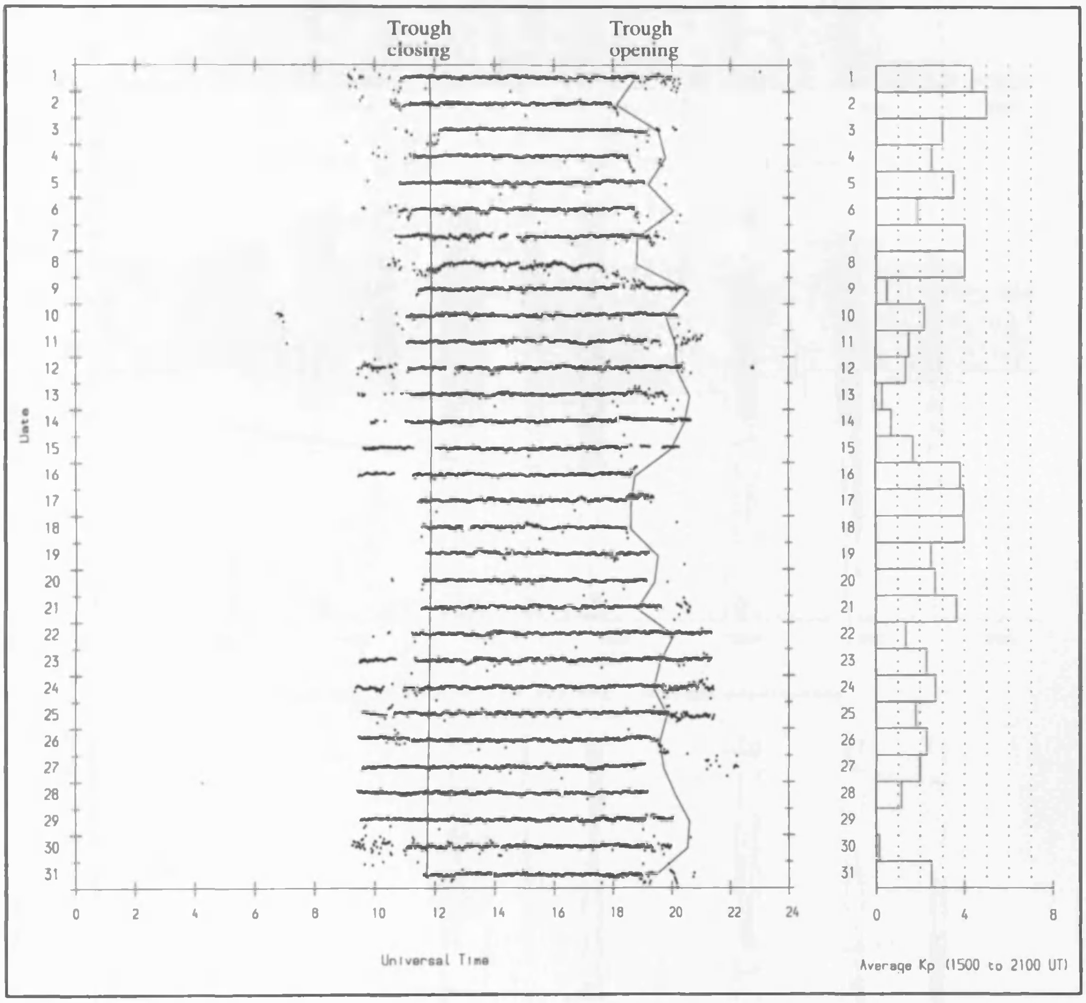

Figure 4.14: Periods of propagation at 15.920 MHz from Halifax to Cheltenham in December 1993 are here represented by plots of the composite bearings returned from the DF in strips of width 20°, centred on the GCB. Times of trough opening and closing are indicated by the zigzagged, vertical lines which are predicted from the model of *Halcrow and Nisbet*, [1977] using a K_p parameter given by the average K_p in the period 1500-2100UT (shown right).

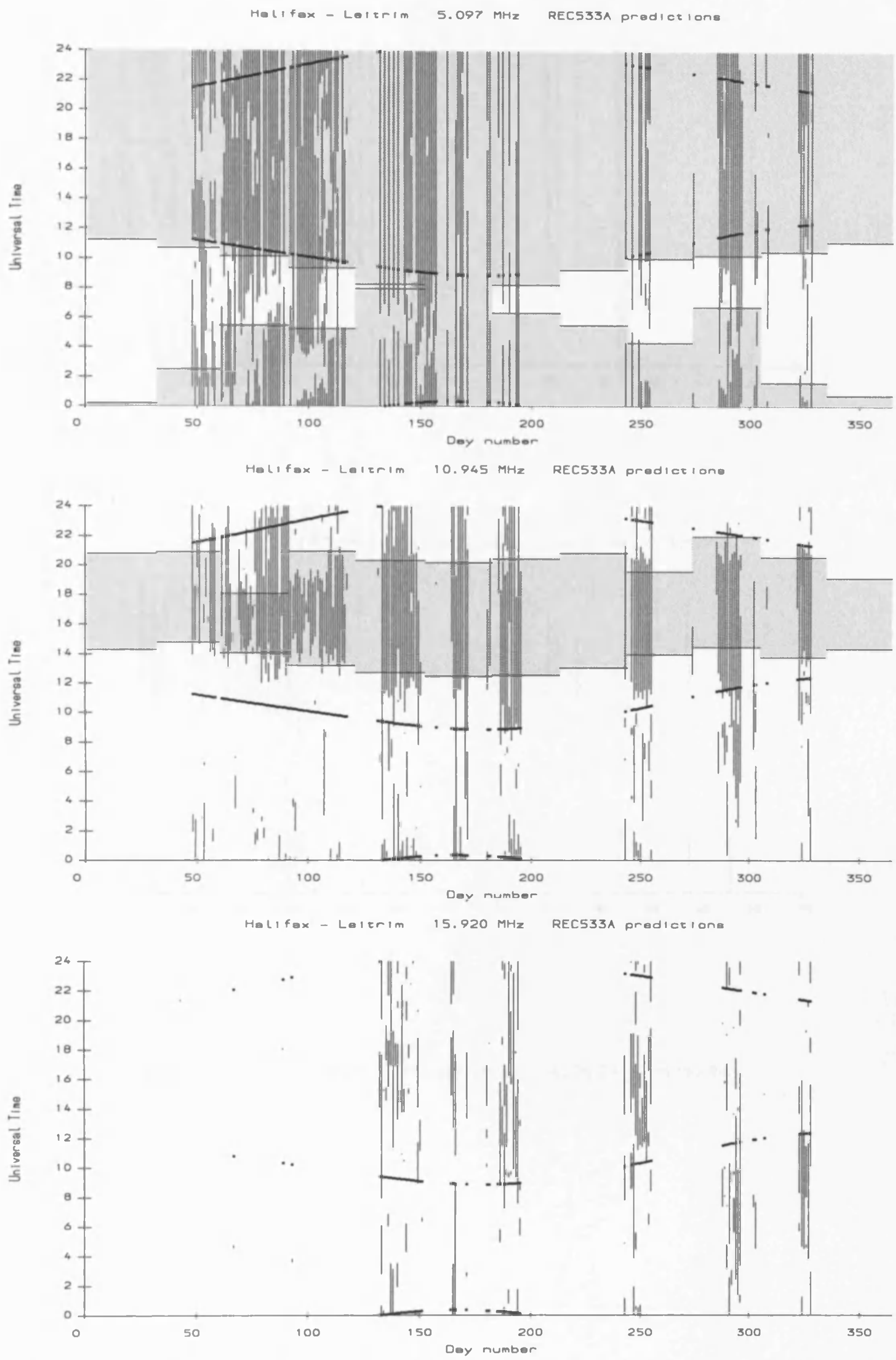

Figure 4.15: Times of propagation on the Halifax - Leitrim path for 1994. The vertical lines indicate times of propagation based on bearing returns from the DF system, the shaded blocks represent CCIR Rec.533 model predictions and times of ground sunrise and sunset at the path midpoint are indicated by the solid curves.

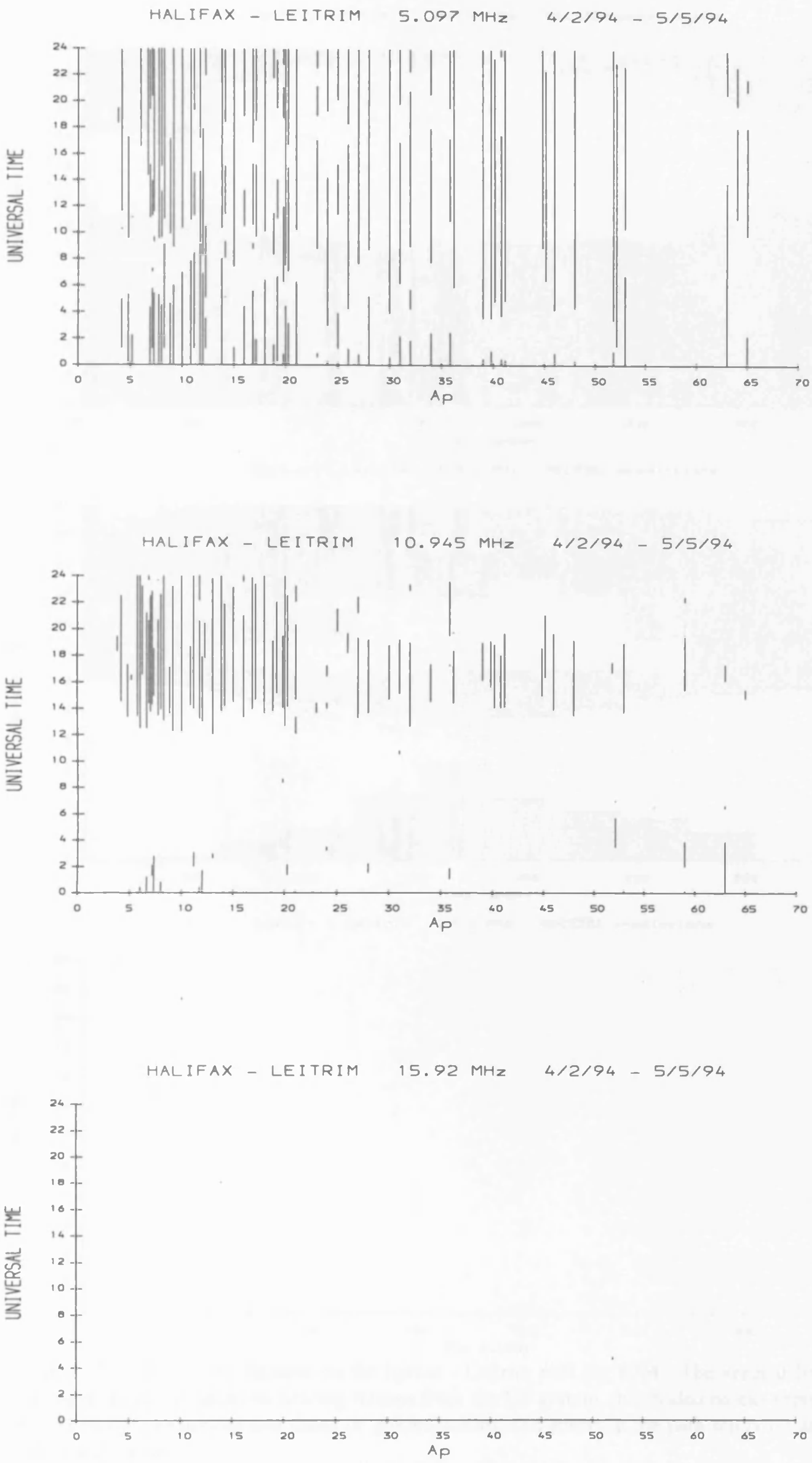

Figure 4.16: Times of propagation on the Halifax-Leitrim path for 4/2/94 - 5/5/94 based on bearing returns from the DF system, arranged according to A_p index.

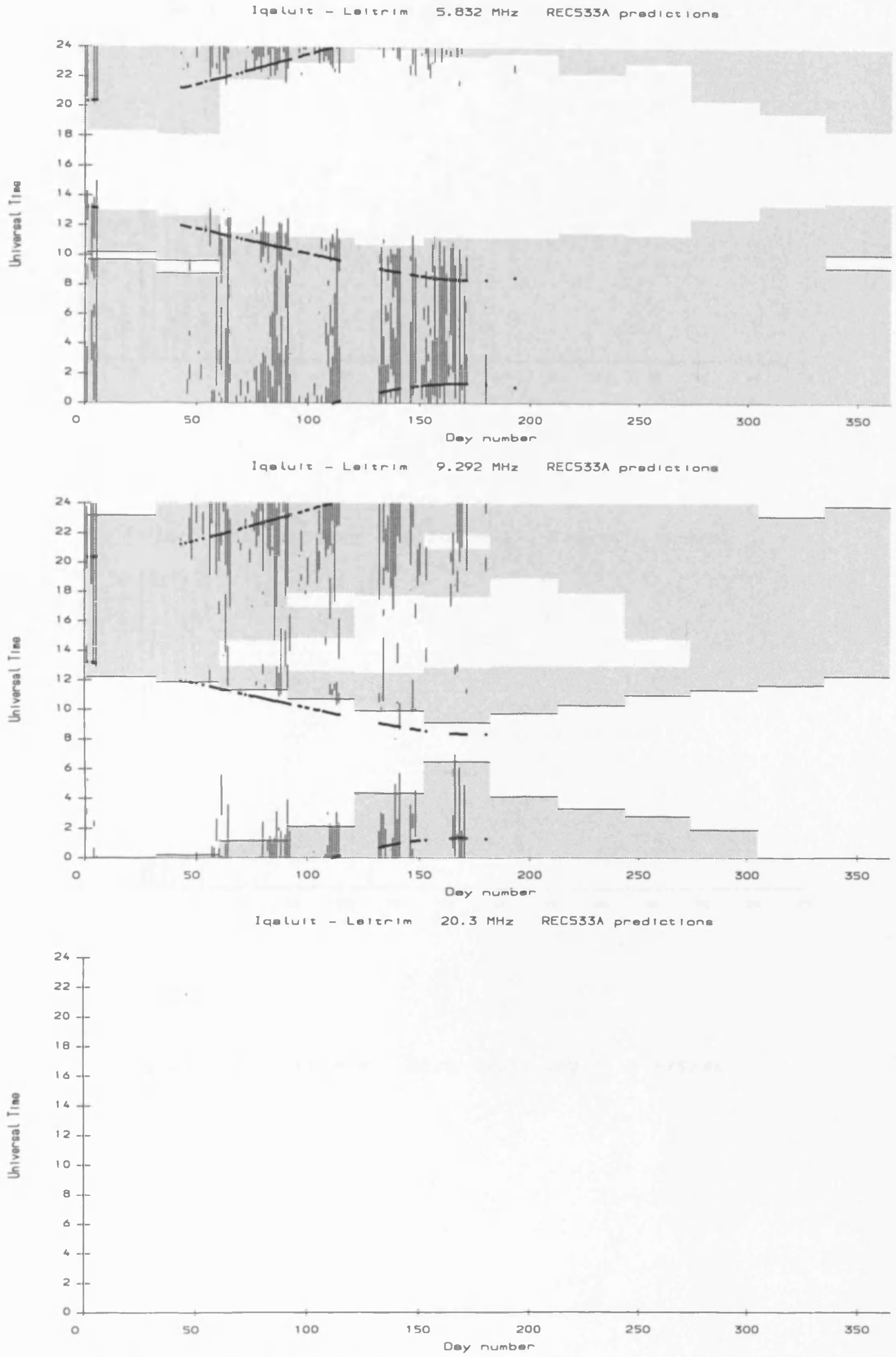

Figure 4.17: Times of propagation on the Iqaluit - Leitrim path for 1994. The vertical lines indicate times of propagation based on bearing returns from the DF system, the shaded blocks represent CCIR Rec.533 model predictions and times of ground sunrise and sunset at the path midpoint are indicated by the solid curves.

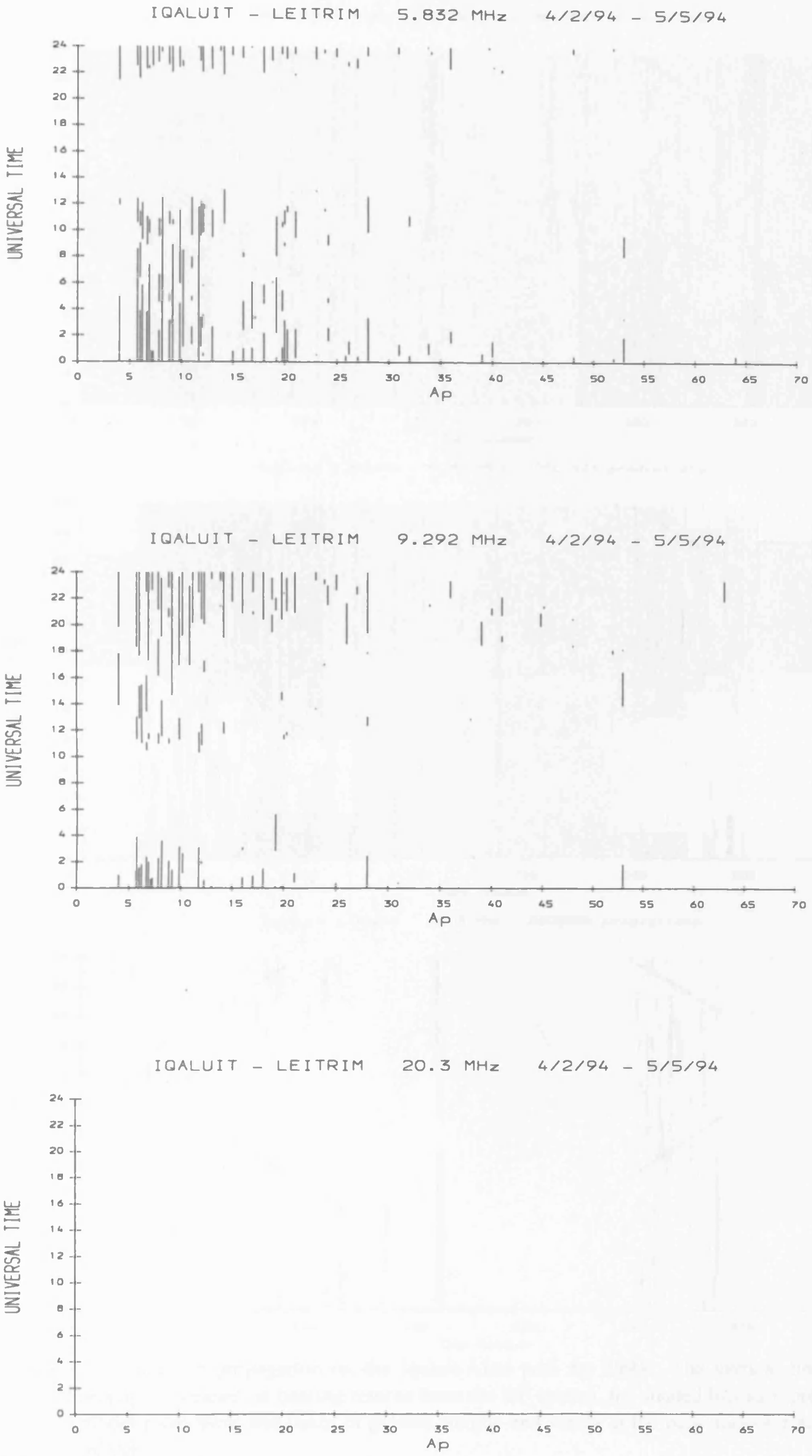

Figure 4.18: Times of propagation on the Iqaluit-Leitrim path for 4/2/94 - 5/5/94 based on bearing returns from the DF system, arranged according to A_p index.

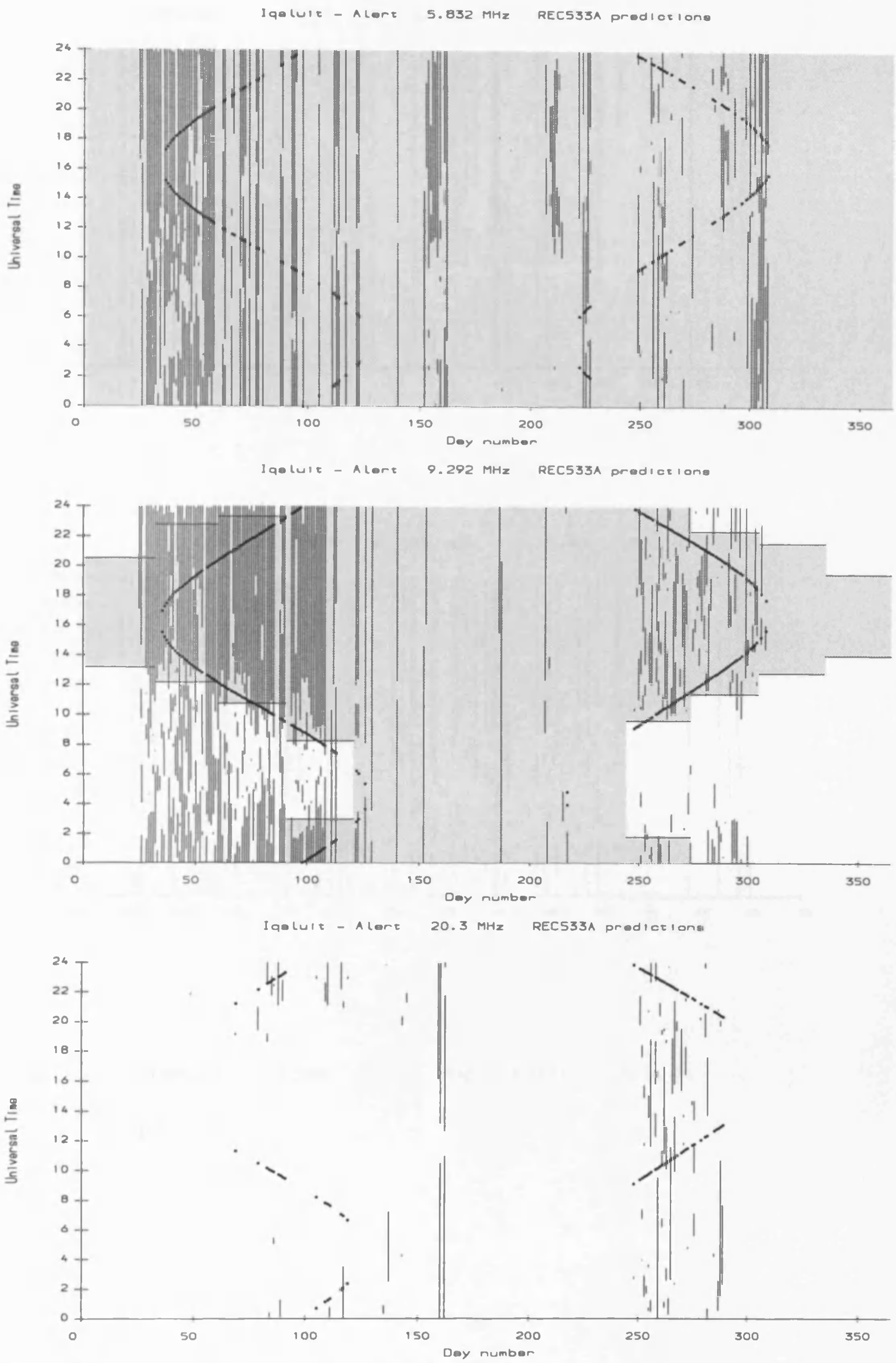

Figure 4.19: Times of propagation on the Iqaluit-Alert path for 1994. The vertical lines indicate times of propagation based on bearing returns from the DF system, the shaded blocks represent CCIR Rec.533 model predictions and times of ground sunrise and sunset at the path midpoint are indicated by the solid curves.

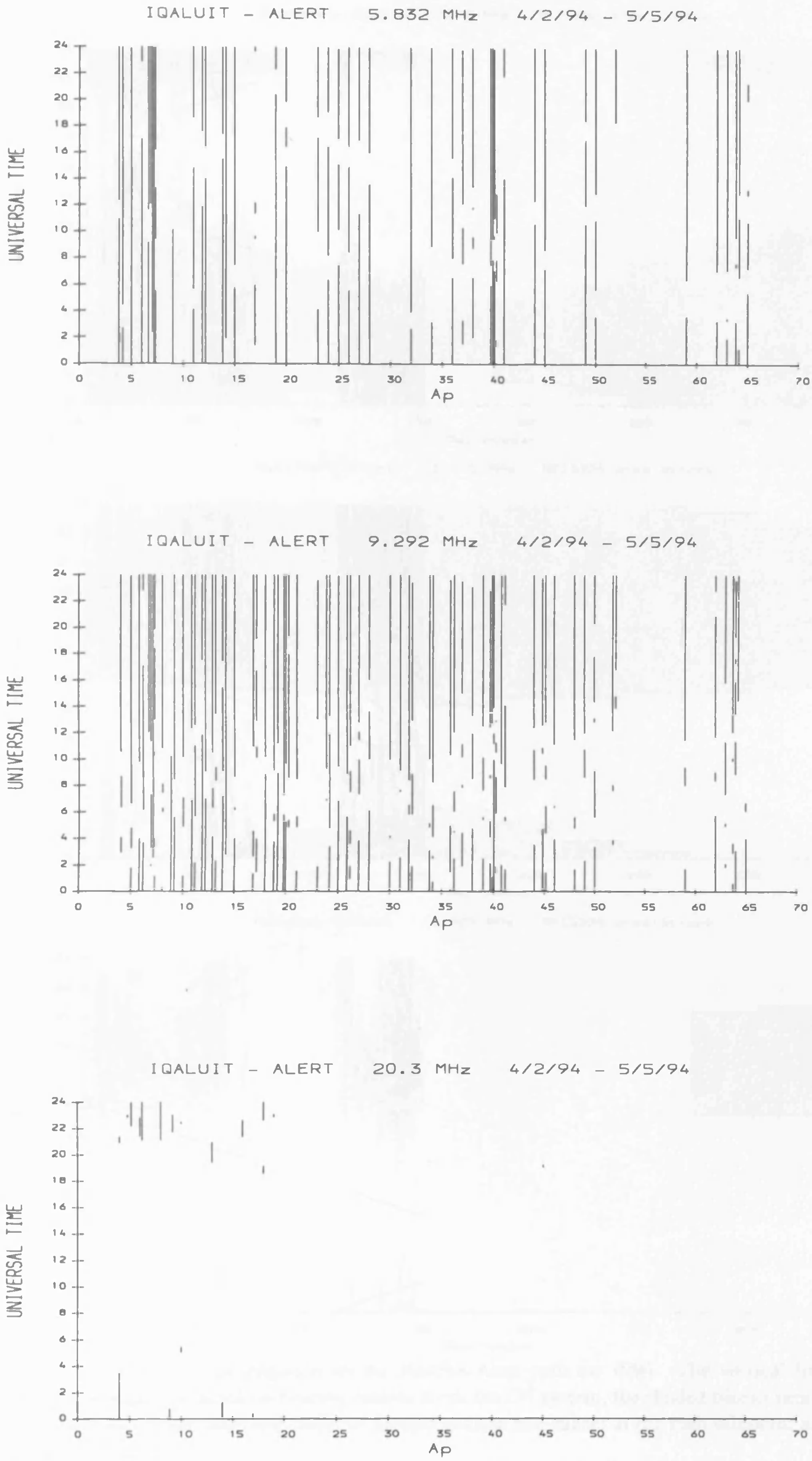

Figure 4.20: Times of propagation on the Iqaluit-Alert path for 4/2/94 - 5/5/94 based on bearing returns from the DF system, arranged according to A_p index.

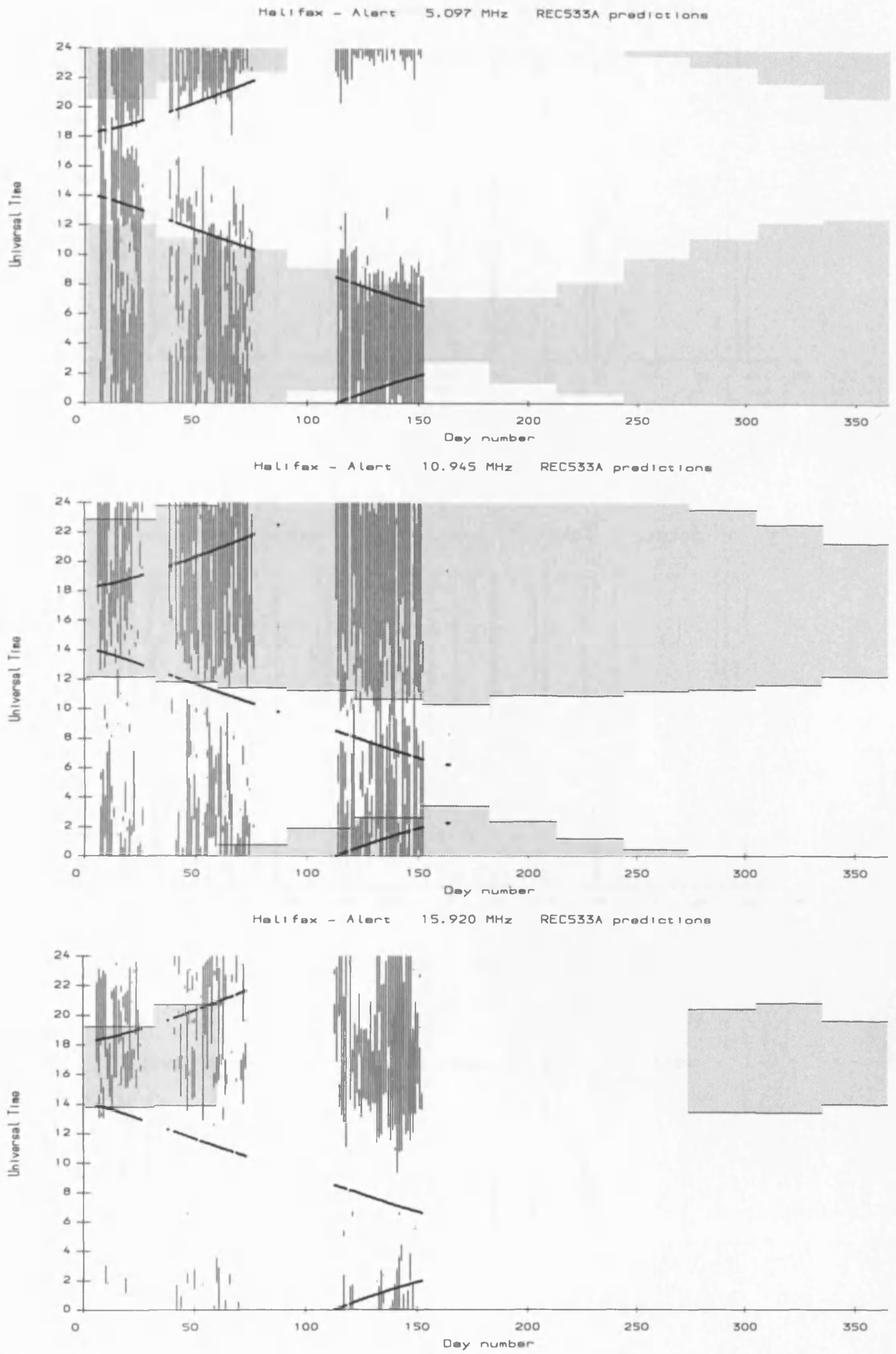

Figure 4.21: Times of propagation on the Halifax-Alert path for 1994. The vertical lines indicate times of propagation based on bearing returns from the DF system, the shaded blocks represent CCIR Rec.533 model predictions and times of ground sunrise and sunset at the path midpoint are indicated by the solid curves.

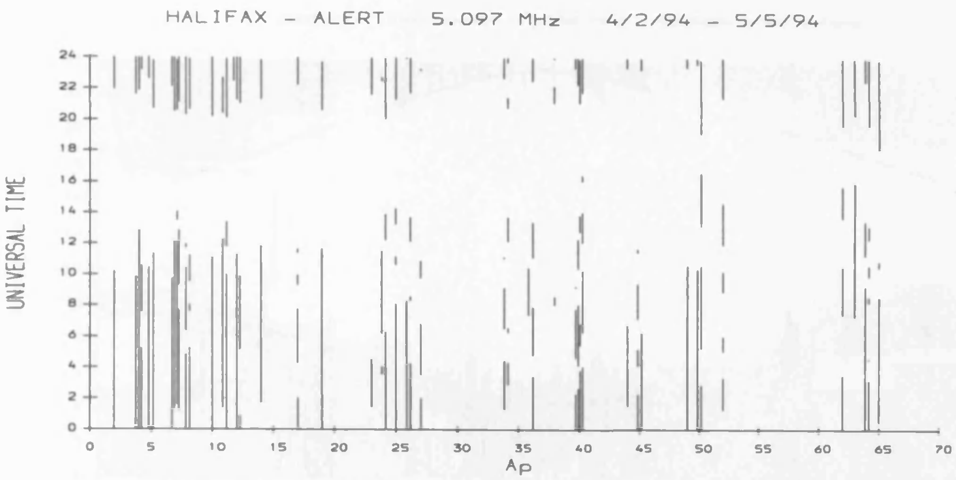

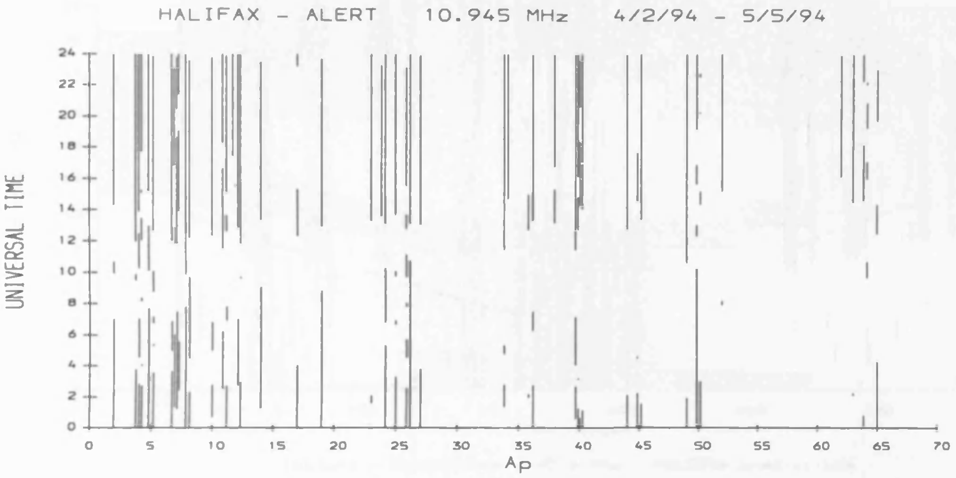

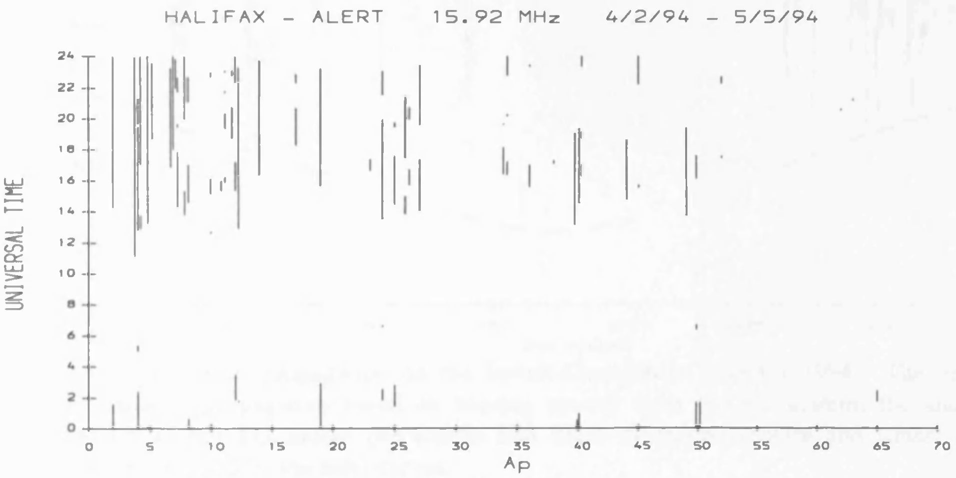

Figure 4.22: Times of propagation on the Halifax-Alert path for 4/2/94 - 5/5/94 based on bearing returns from the DF system, arranged according to A_p index.

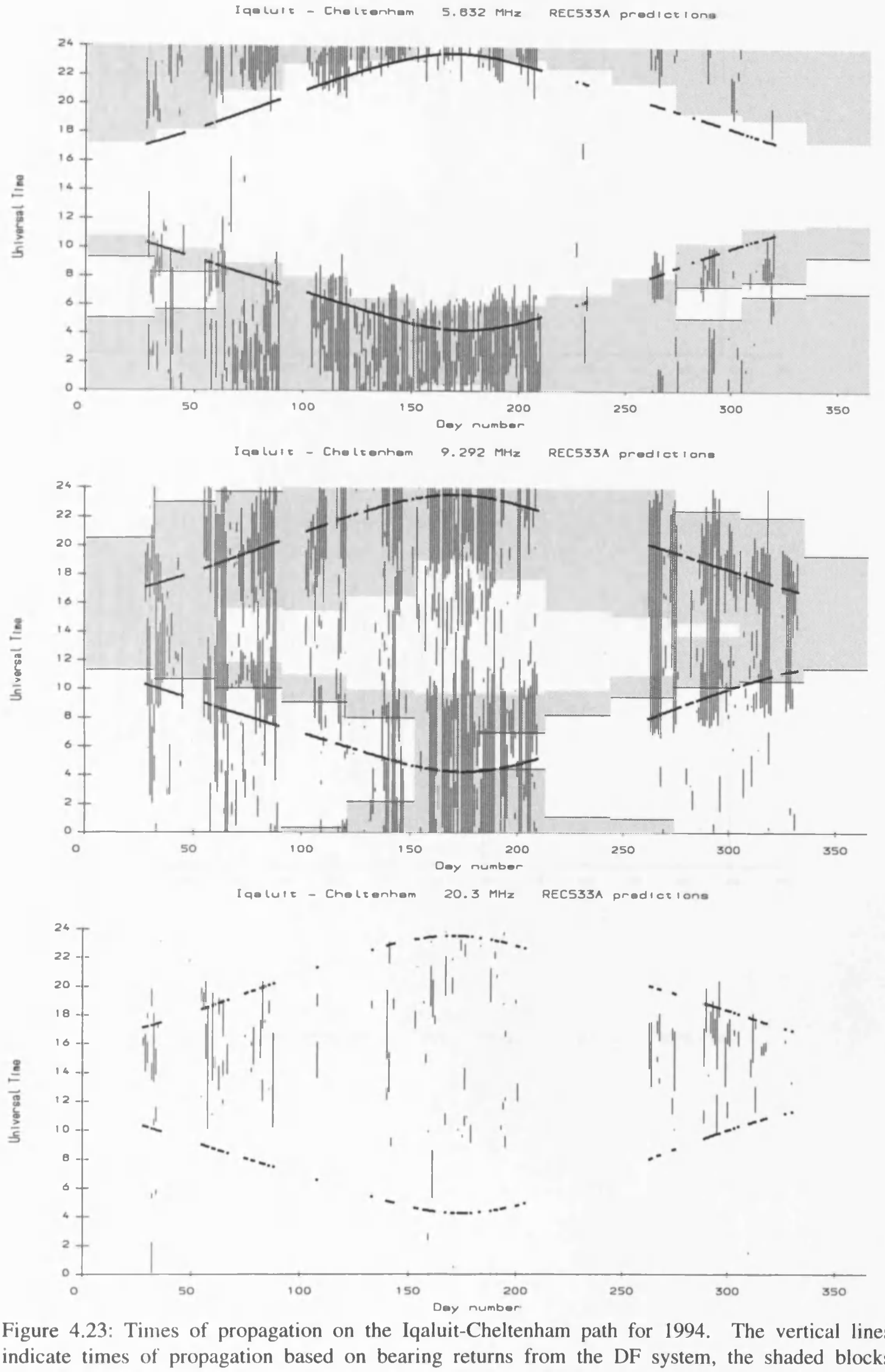

Figure 4.23: Times of propagation on the Iqaluit-Cheltenham path for 1994. The vertical lines indicate times of propagation based on bearing returns from the DF system, the shaded blocks represent CCIR Rec.533 model predictions and times of ground sunrise and sunset at the path midpoint are indicated by the solid curves.

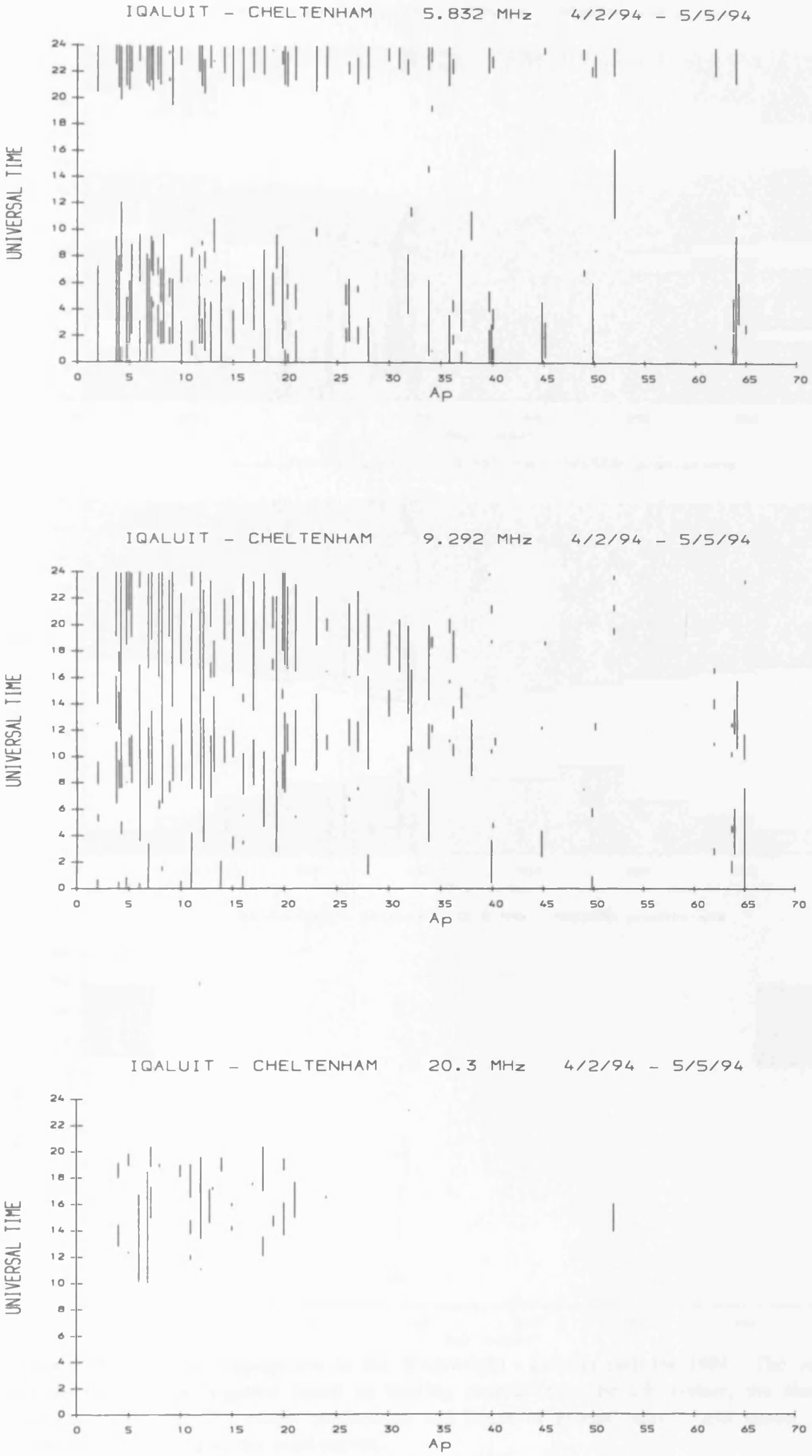

Figure 4.24: Times of propagation on the Iqaluit-Cheltenham path for 4/2/94 - 5/5/94 based on bearing returns from the DF system, arranged according to A_p index.

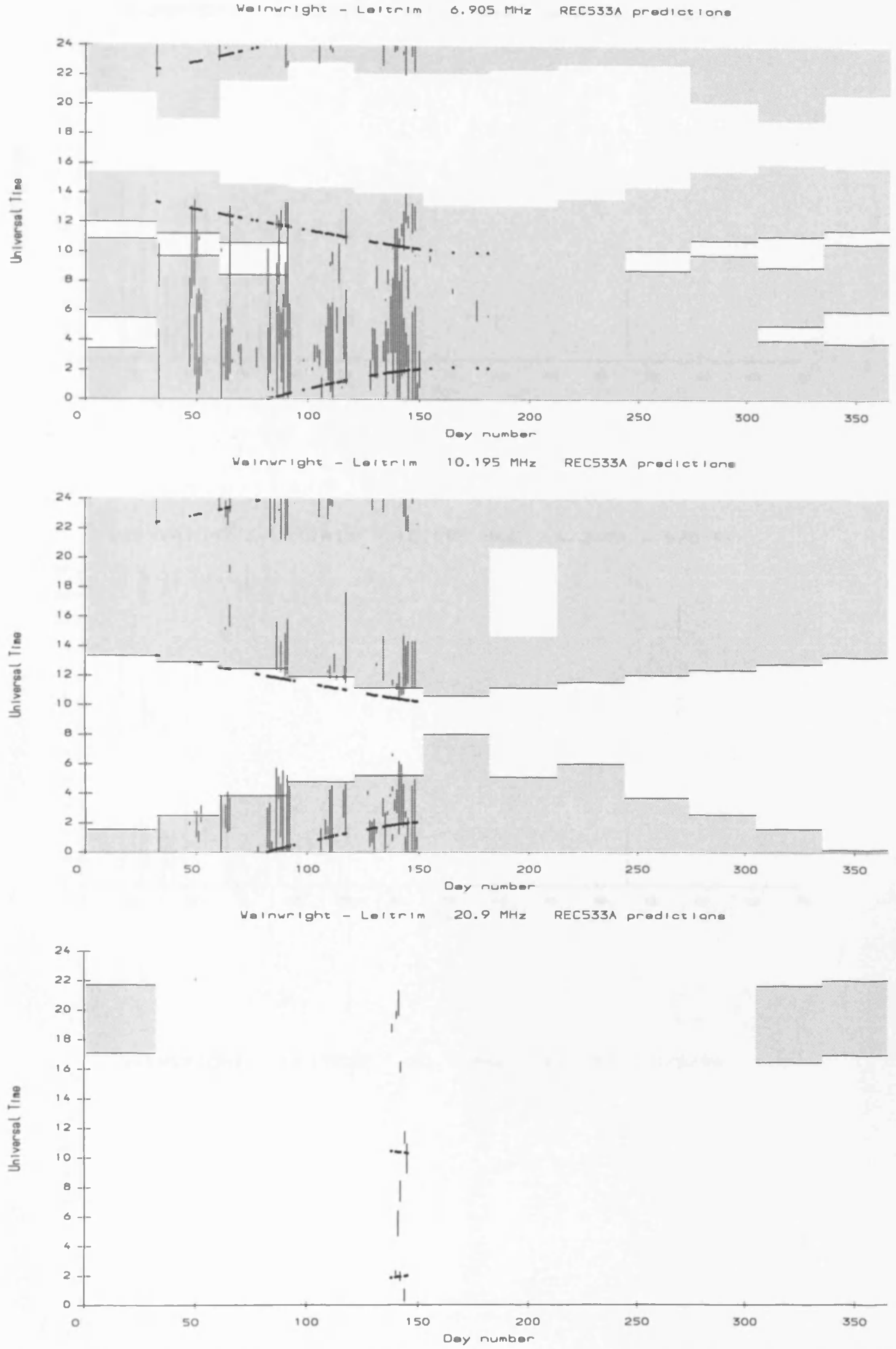

Figure 4.25: Times of propagation on the Wainwright - Leitrim path for 1994. The vertical lines indicate times of propagation based on bearing returns from the DF system, the shaded blocks represent CCIR Rec.533 model predictions and times of ground sunrise and sunset at the path midpoint are indicated by the solid curves.

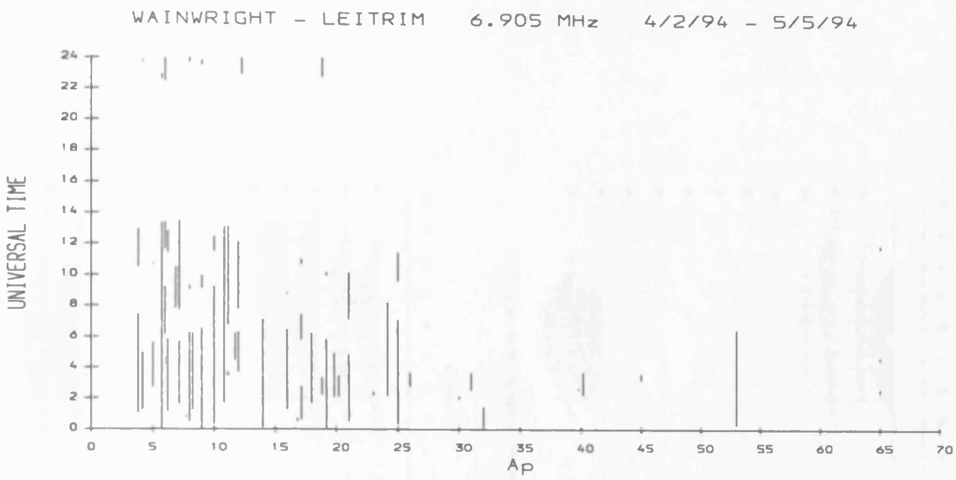

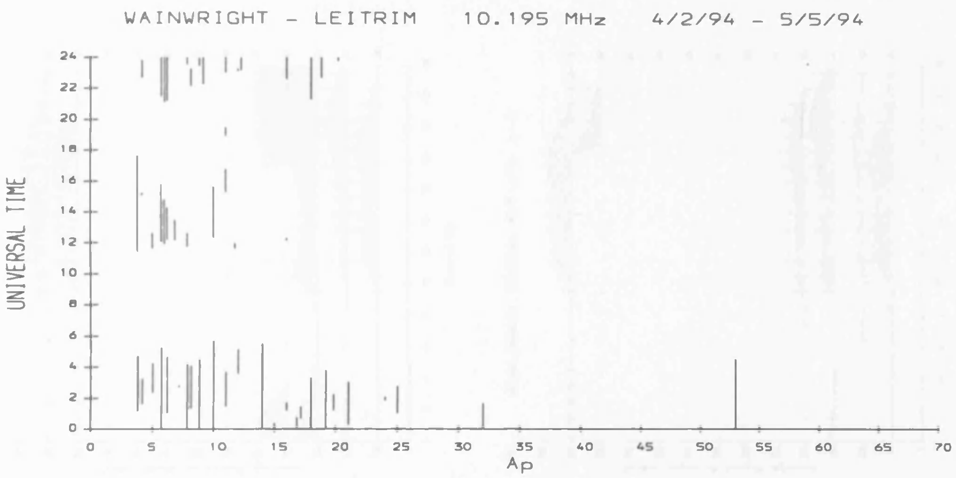

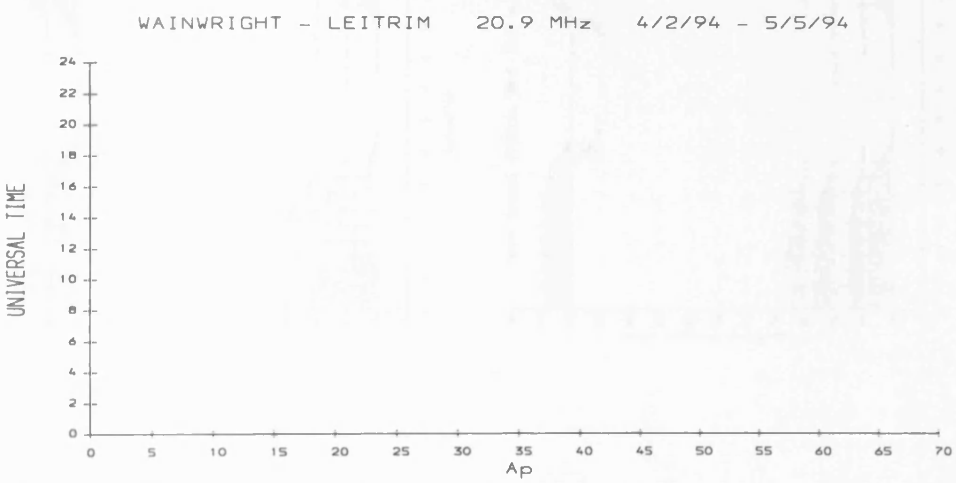

Figure 4.26: Times of propagation on the Wainwright-Leitrim path for 4/2/94 - 5/5/94 based on bearing returns from the DF system, arranged according to A_p index.

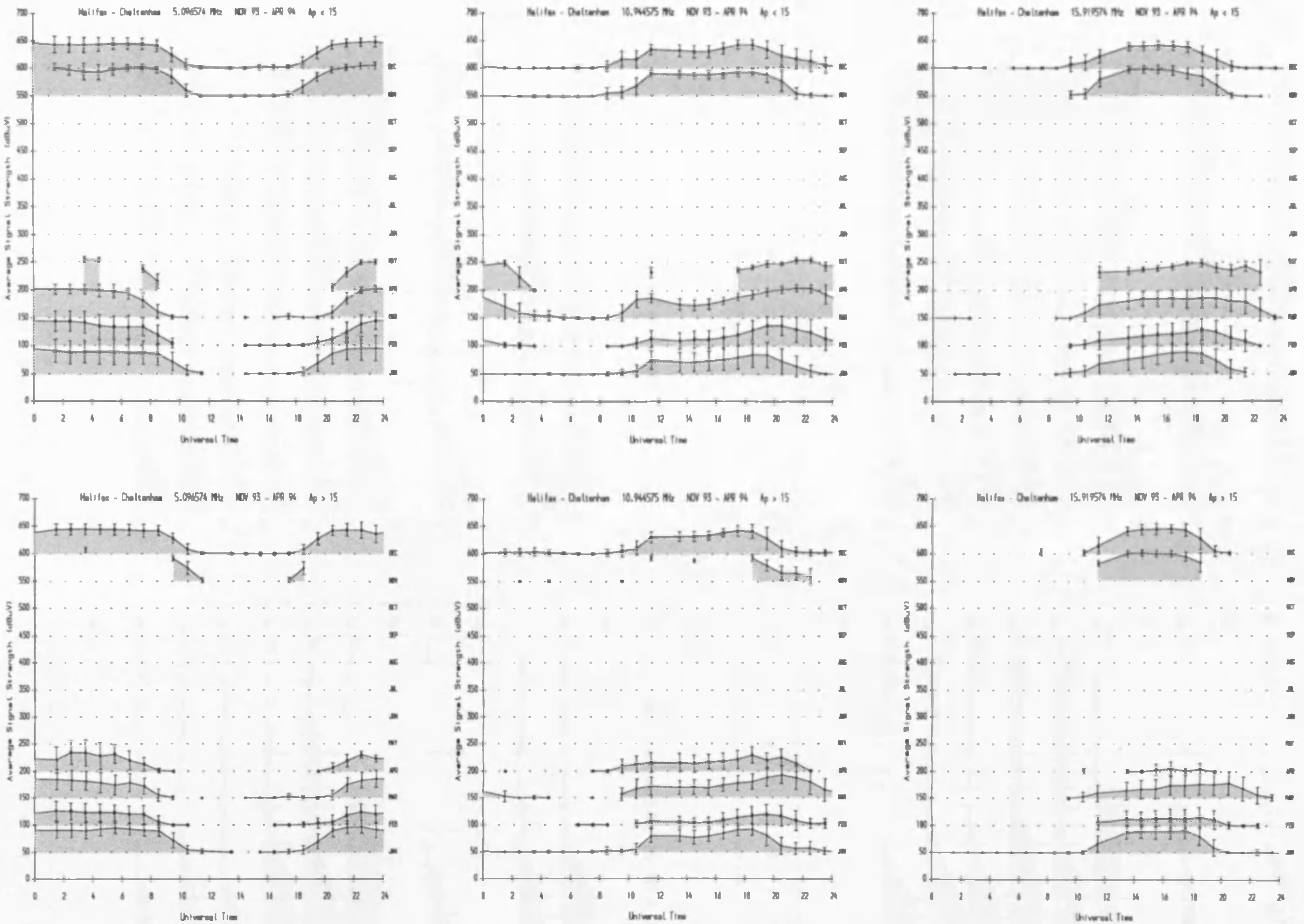

Figure 4.27: Mean signal strengths of transmissions from Halifax to Cheltenham for each UT hour and month in the period 12/93 to 11/94. The data is divided into geomagnetically quiet (Ap<15) periods (top panels) and active (A_p≥15) periods (bottom panels). Each curve is offset by +50dB and the error bars represent ±1 standard deviation of each hourly average value.

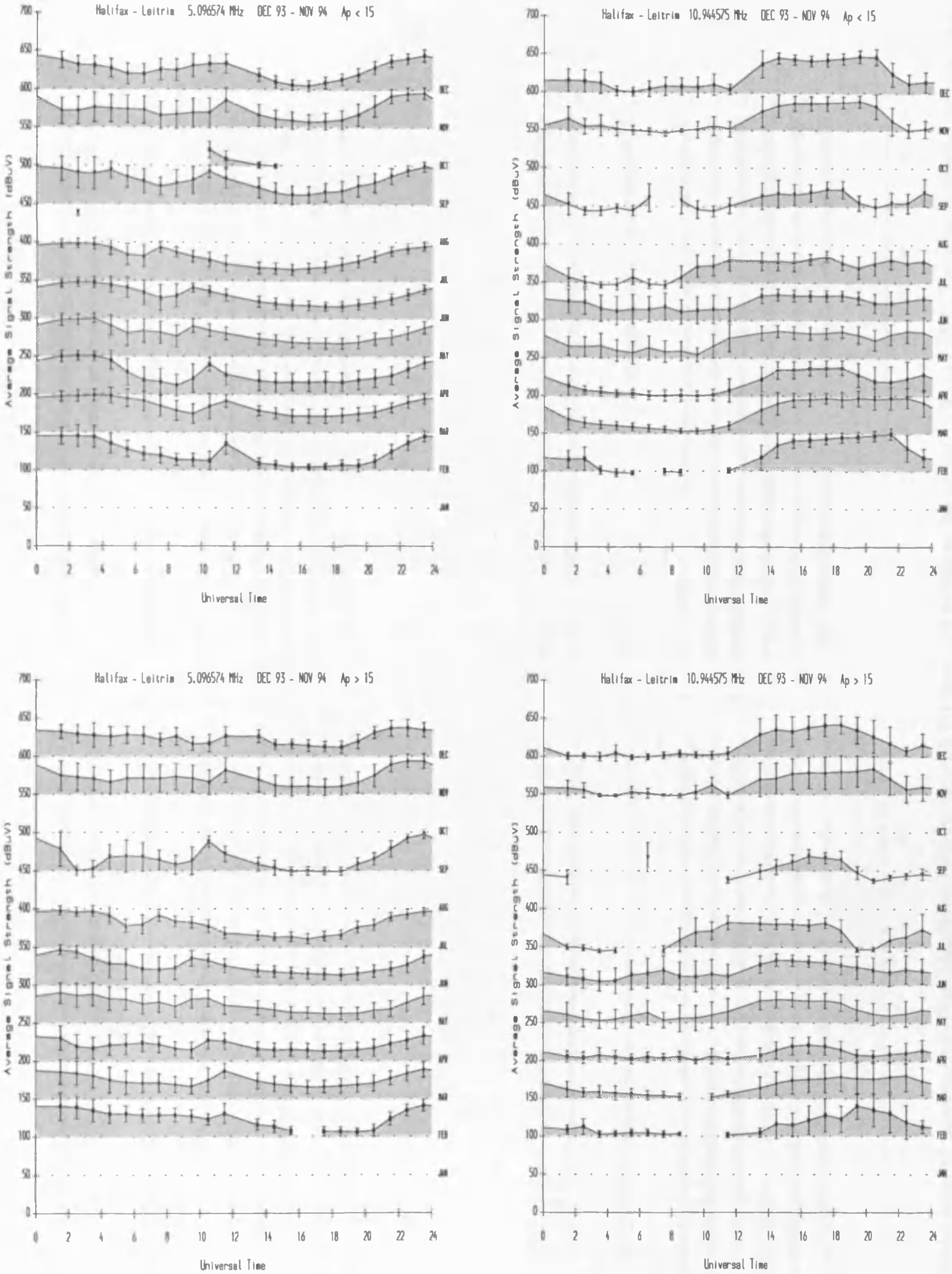

Figure 4.28: Mean signal strengths of transmissions from Halifax to Leitrim for each UT hour and month in the period 12/93 to 11/94. The data is divided into geomagnetically quiet (A_p<15) periods (top panels) and active (A_p>=15) periods (bottom panels). Each curve is offset by +50dB and the error bars represent ±1 standard deviation of each hourly average value.

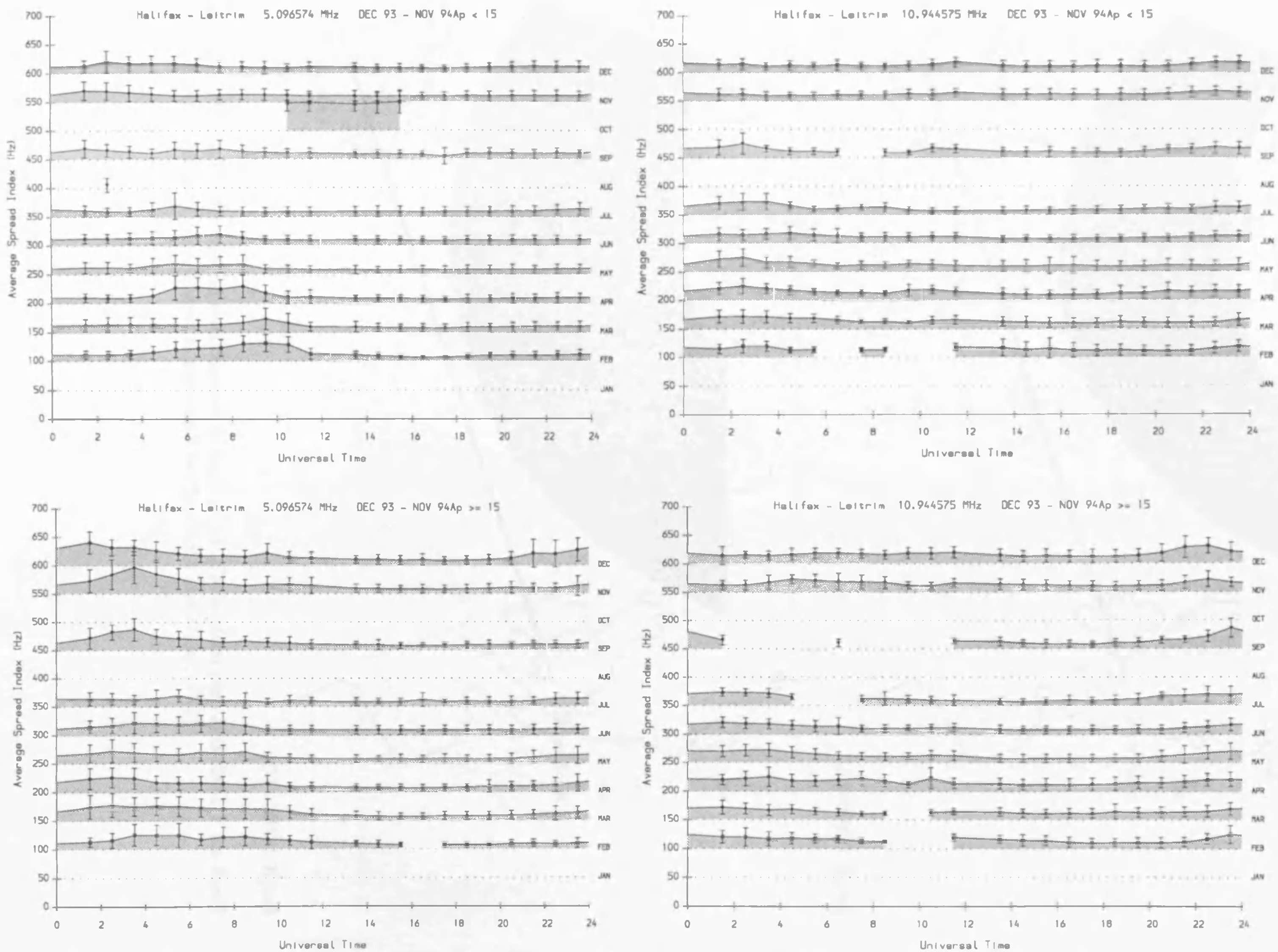

Figure 4.29: Mean Doppler spread index of transmissions from Halifax to Leitrim for each UT hour and month in the period 12/93 to 11/94. The data is divided into geomagnetically quiet (Ap<15) periods (top panels) and active (Ap>=15) periods (bottom panels). Each curve is offset by +50Hz and the error bars represent ±1 standard deviation of each hourly average value.

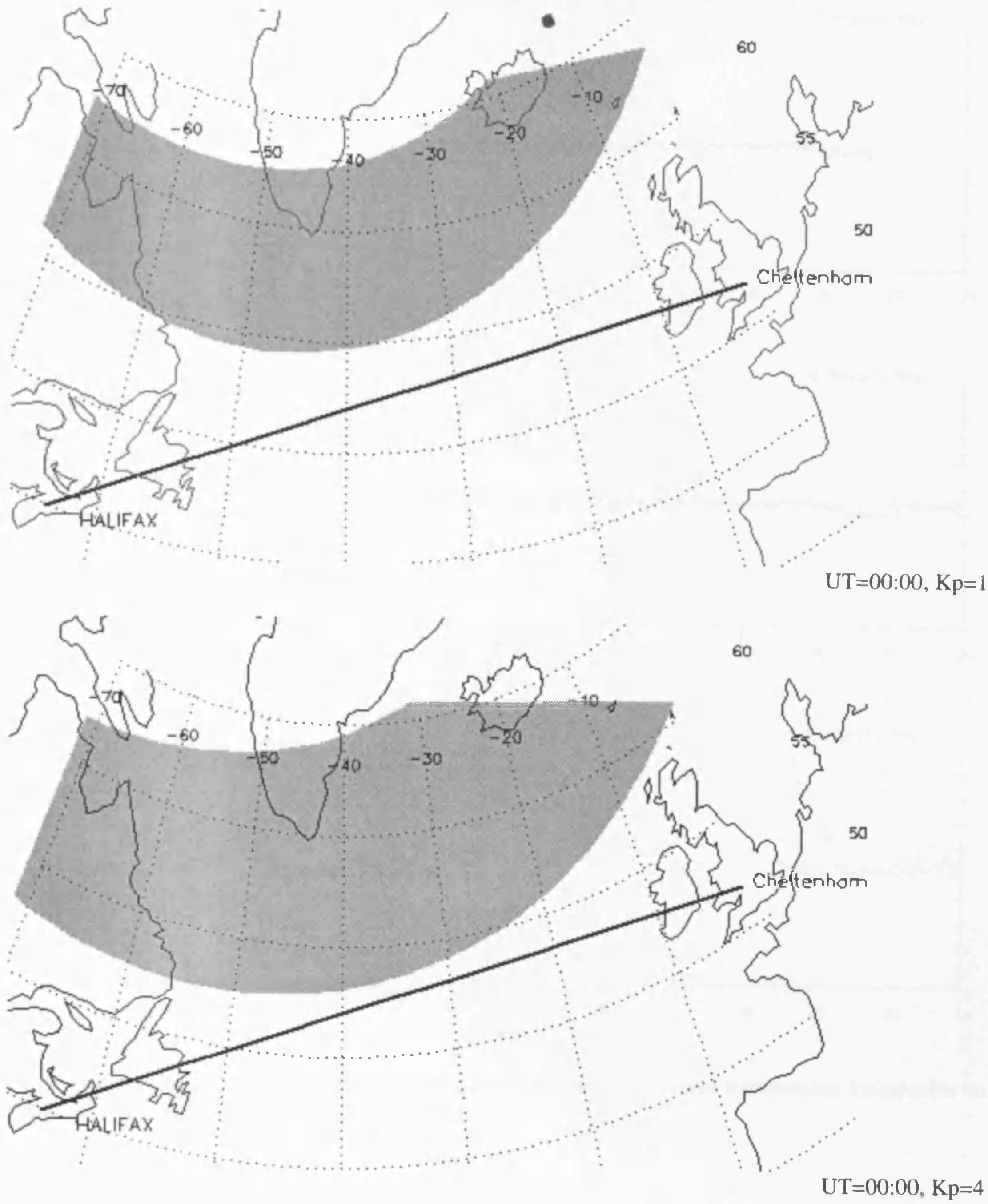

Figure 5.1: Position of the auroral oval relative to the Halifax- Cheltenham path at 00:00 UT for Kp=1 (upper panel) and Kp=4 (lower panel) as modelled by *Holzworth and Meng*, [1975].

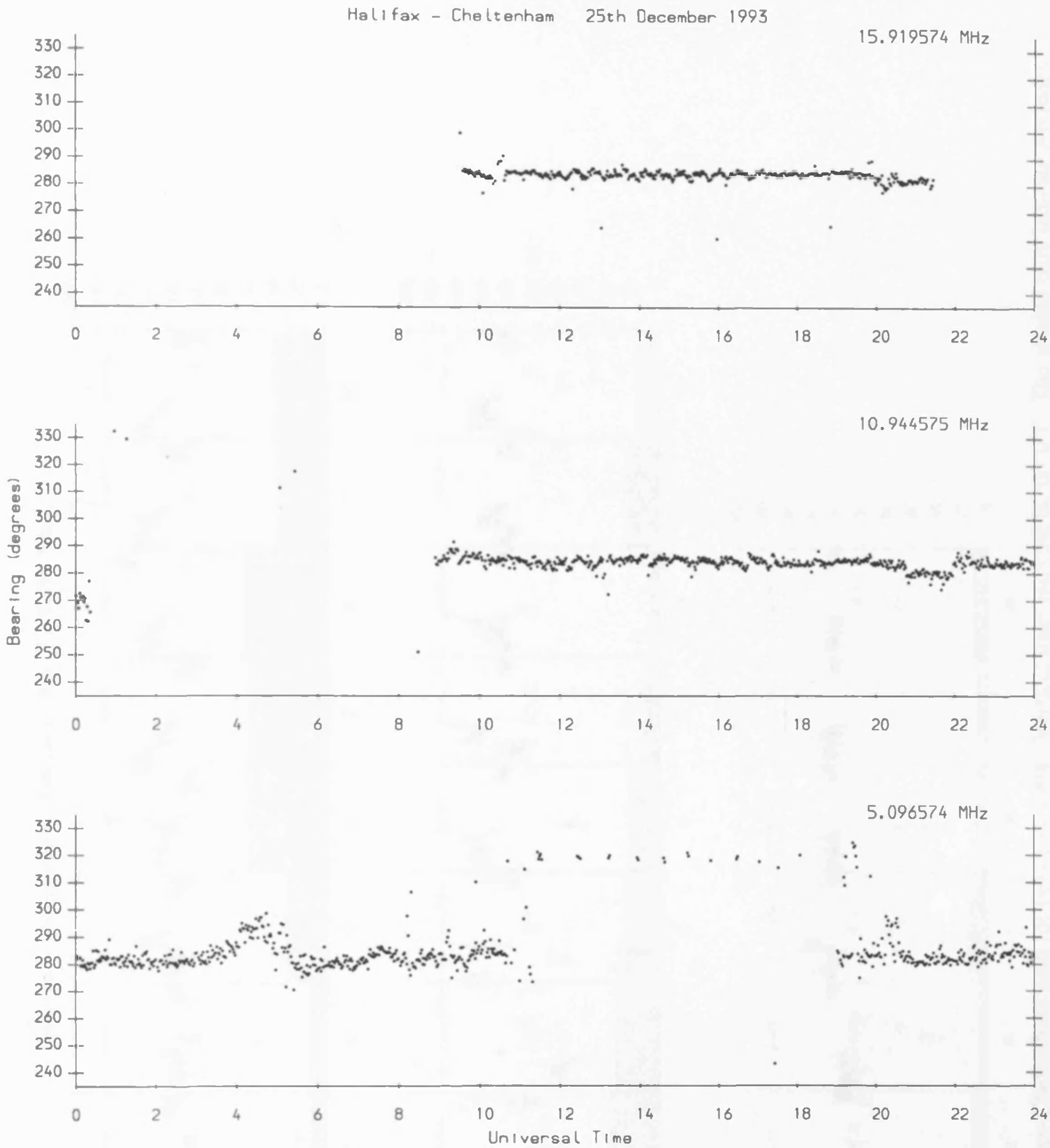

Figure 5.2: Bearings of Halifax signals received at Cheltenham at all three transmission frequencies on 25th Dec 1993. The true bearing (GCB) is 285°.

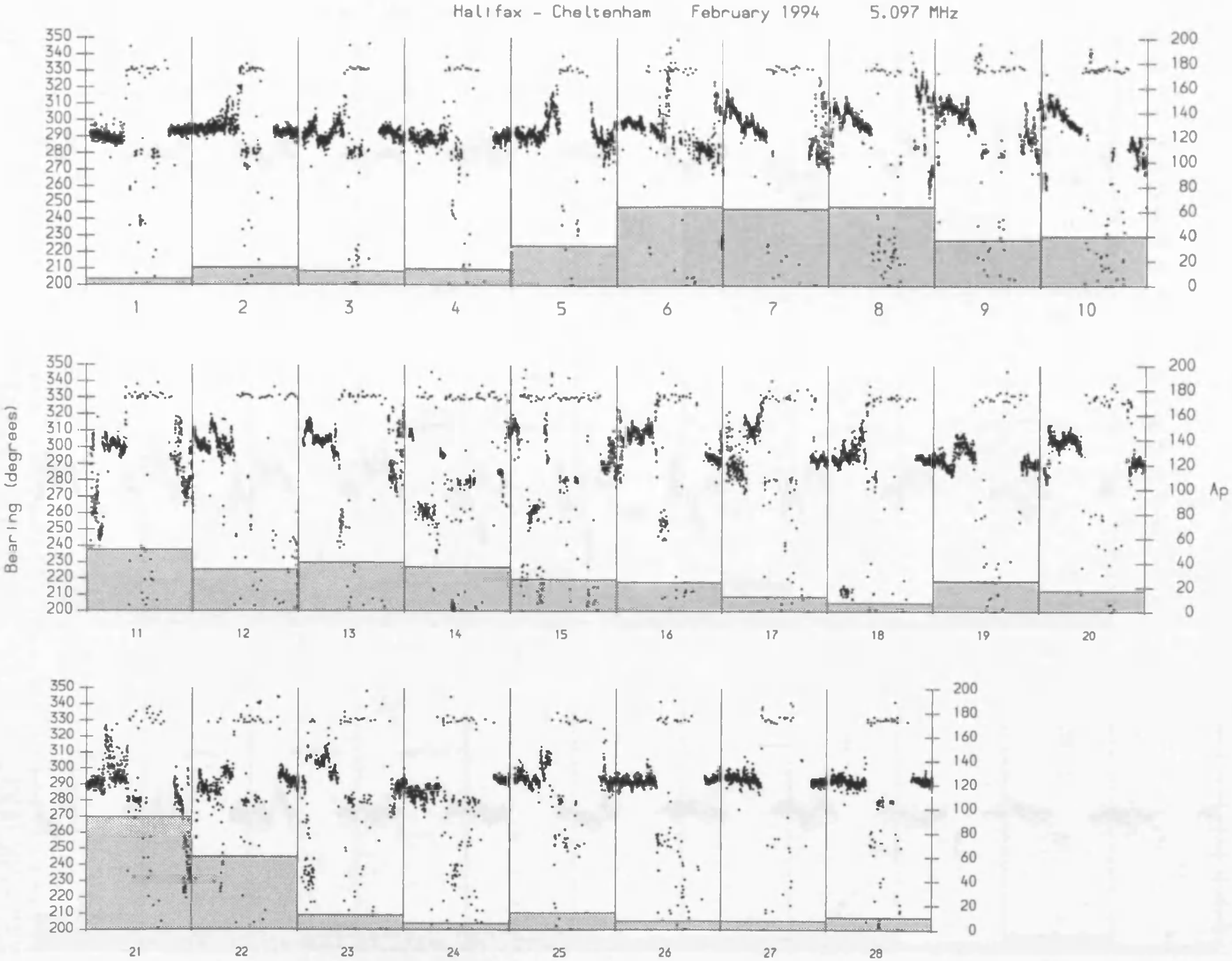

Figure 5.3: Bearings of 5.097MHz signals on the Halifax-Cheltenham path for February 1994. Vertical lines indicate 00:00 UT. The shaded bars indicate Ap index.

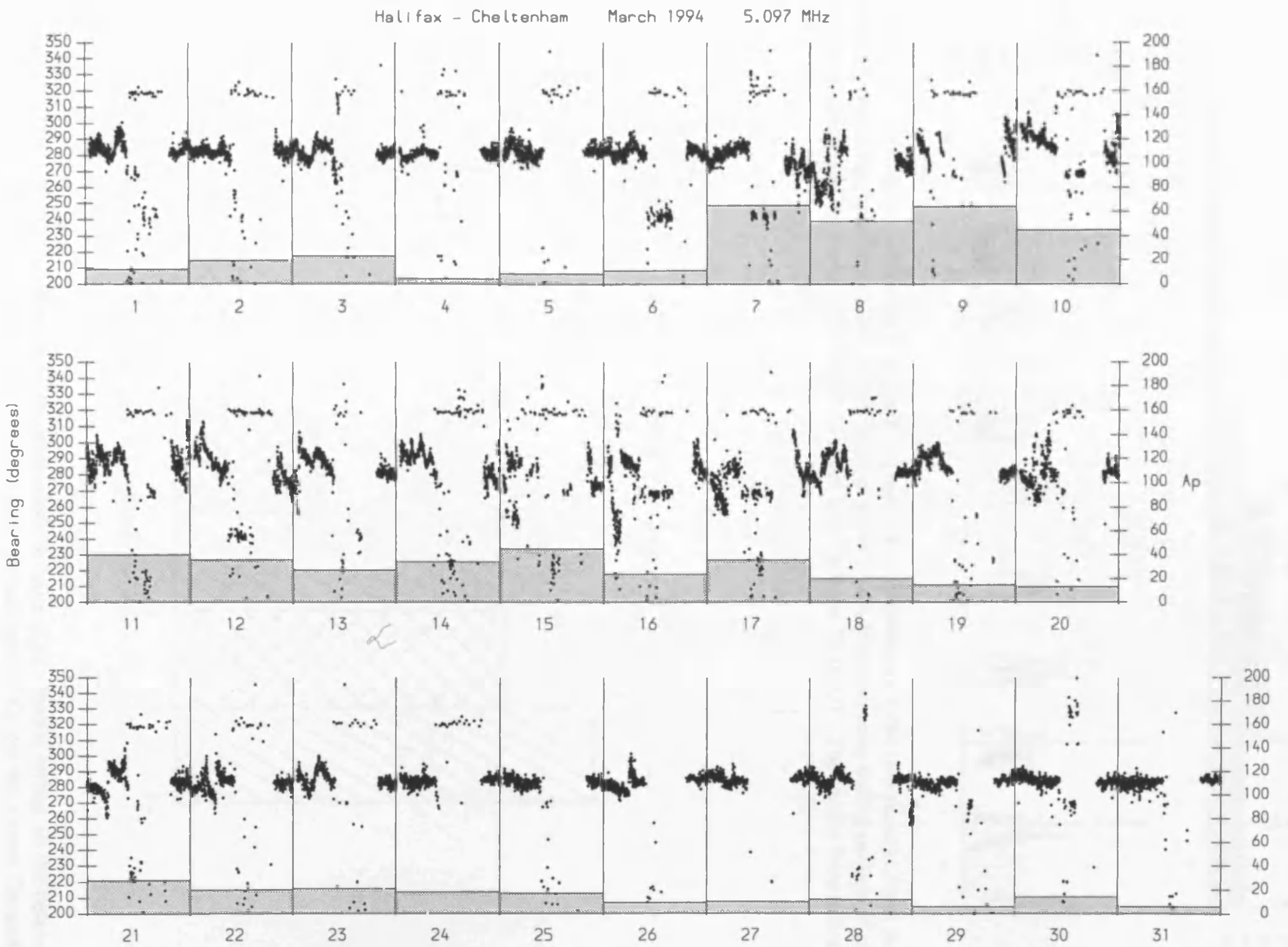

Figure 5.4: Bearings of 5.097MHz signals on the Halifax-Cheltenham path for March 1994. Vertical lines indicate 00:00 UT. The shaded bars indicate Ap index.

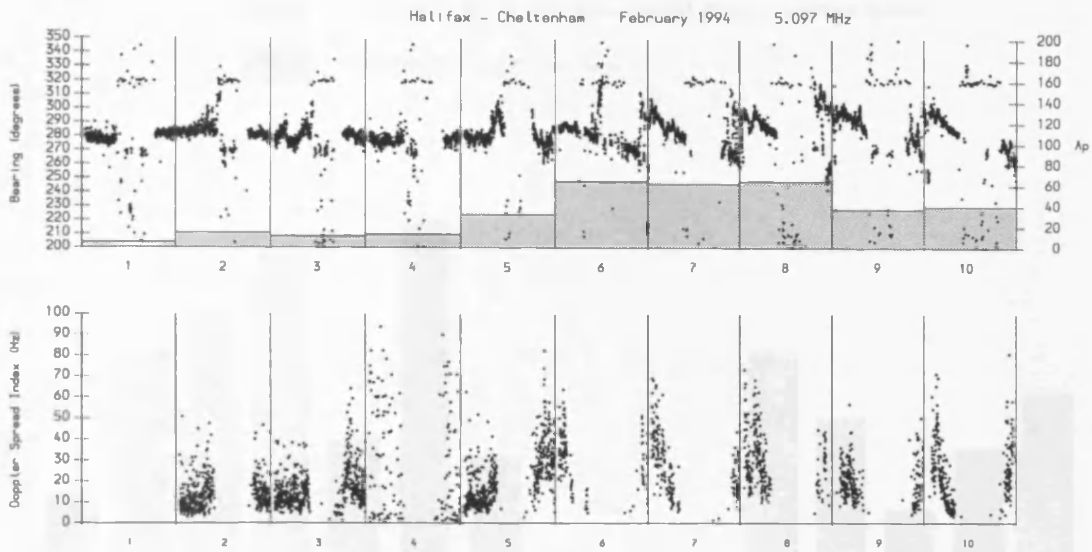

Figure 5.5: Bearing deviations on 5.097MHz signals for 1-10 February 1994 (top panel). Note how the associated Doppler spread index values (bottom panel) show large increases during periods of off-GCP propagation to the north of the path. Vertical lines indicate 00:00 UT. The shaded bars indicate Ap index.

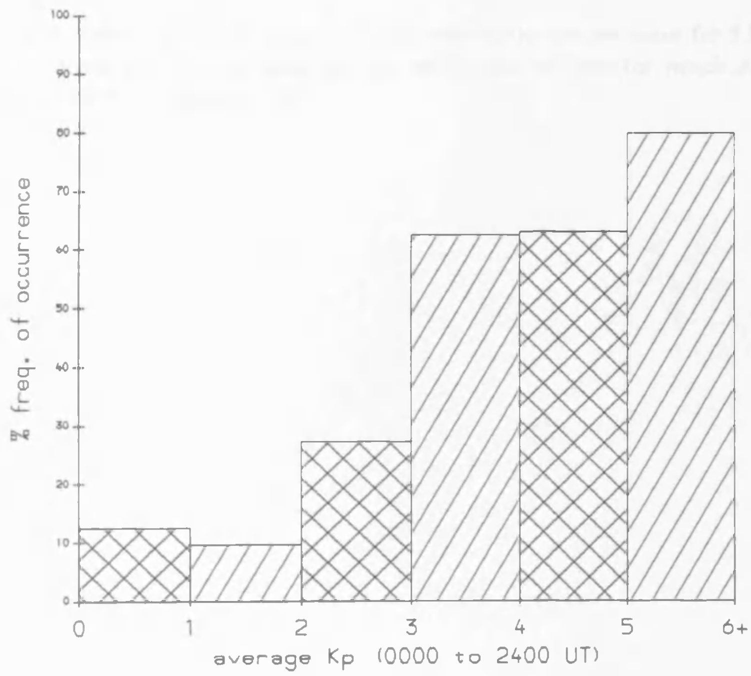

Figure 5.6: Frequency of occurrence of the characteristic large-scale, diurnal swings in the bearings of 5.097 MHz signals on the Halifax-Cheltenham path, plotted against Kp for the period December 1993 to April 1994.

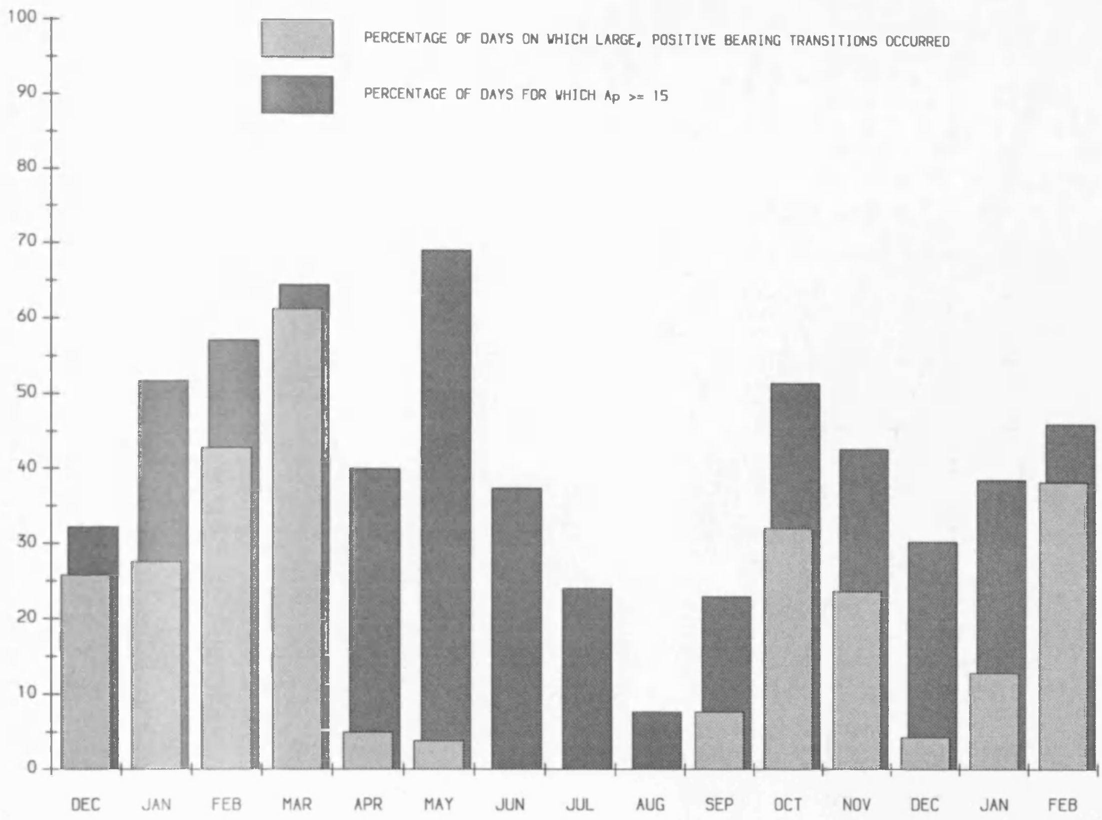

Figure 5.7: Percentage of days in which large northerly bearing deviations occur for 5.097MHz signals on the Halifax-Cheltenham path (white bars) and the percentage of days for which Ap>=15 for each month from December 1993 to February 1995.

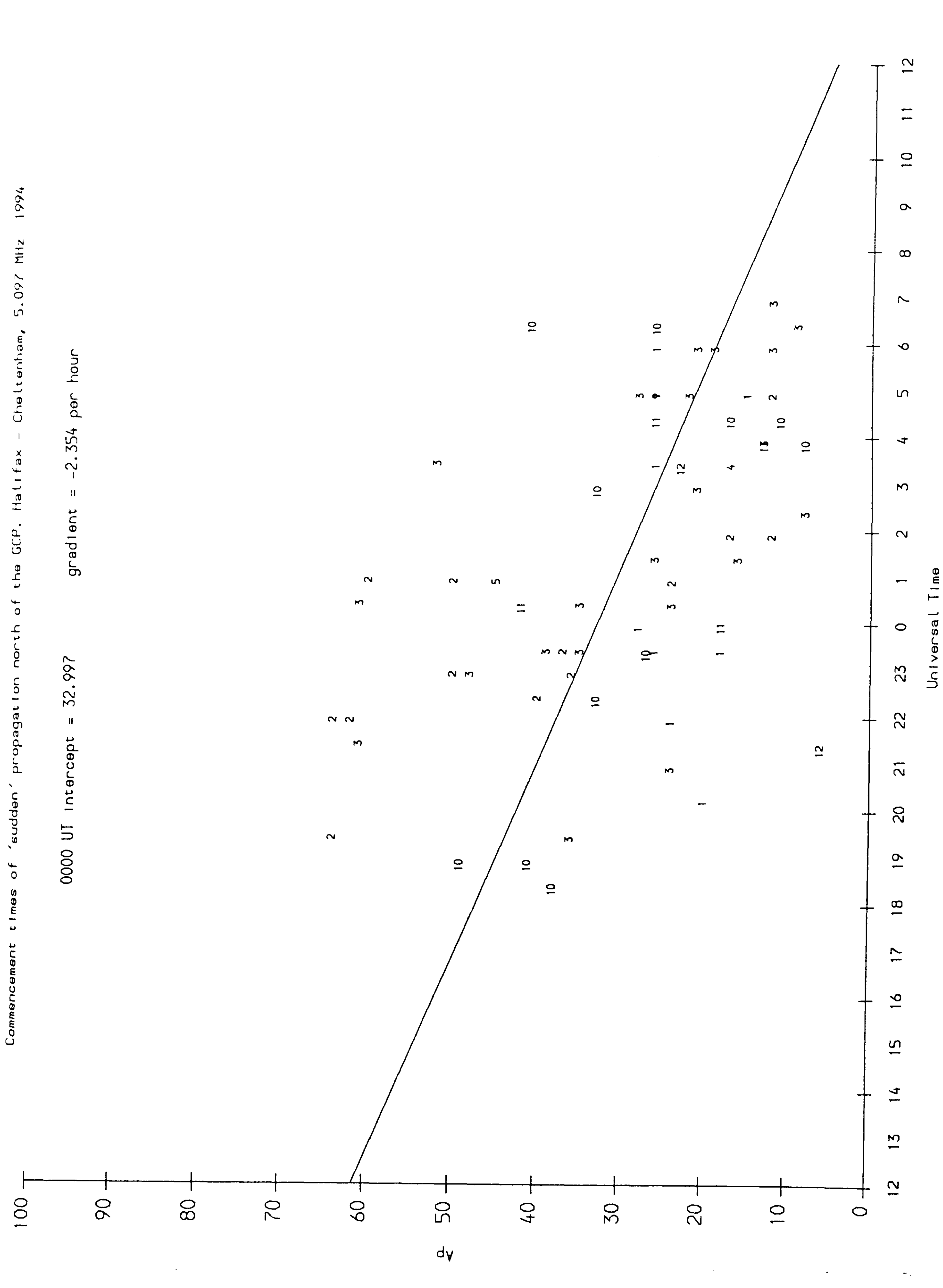

Figure 5.8: Times of acquisition of bearings well to the north of the GCB on the 5.097MHz, Halifax-Cheltenham transmissions as a function of Ap index. Numeric data points represent the month of the year, 1994 (1=Jan., 2=Feb., etc.).

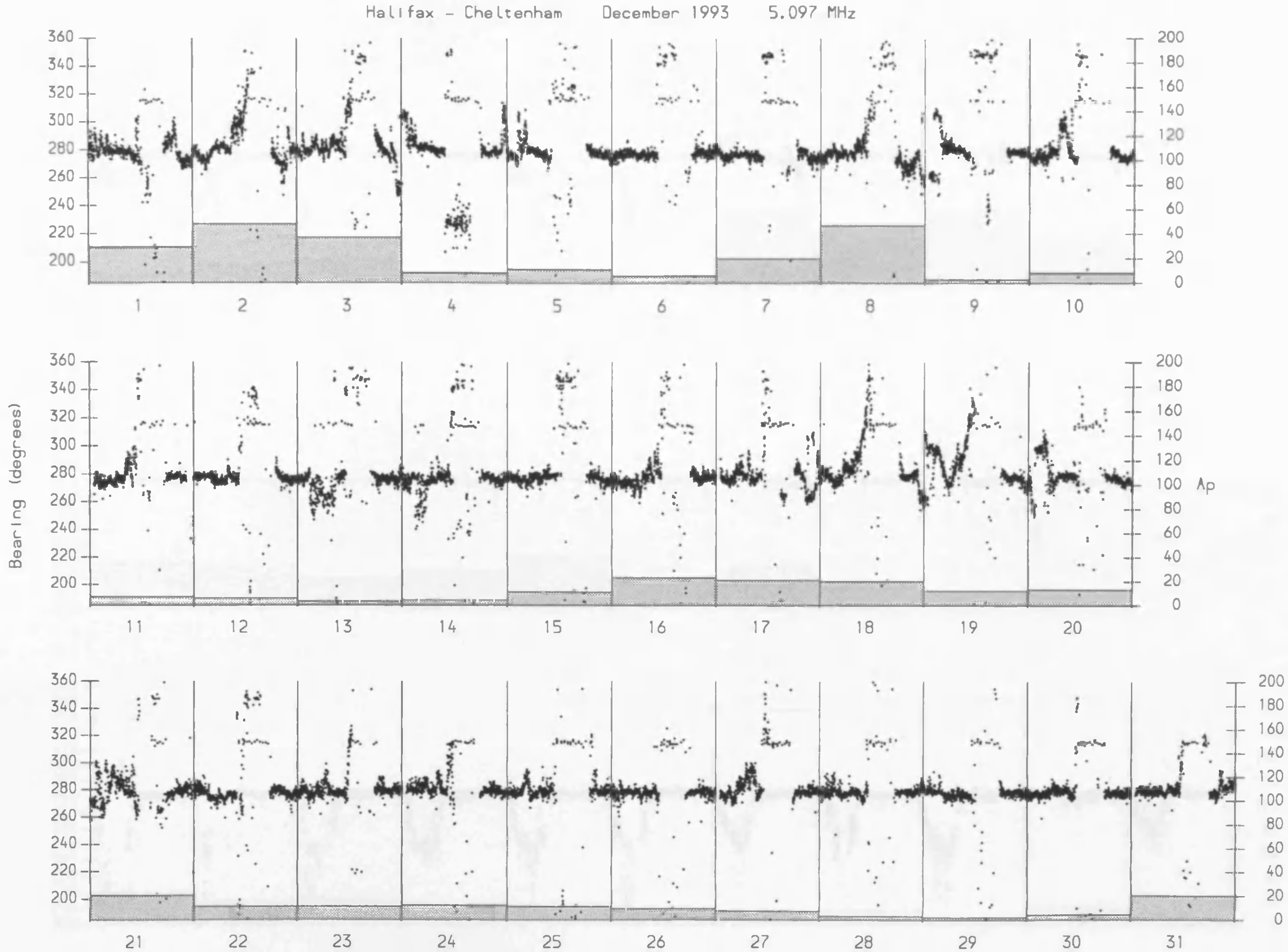

Figure 5.9: Bearings of 5.097MHz signals on the Halifax-Cheltenham path for December 1993. Vertical lines indicate 00:00 UT. The shaded bars indicate Ap index.

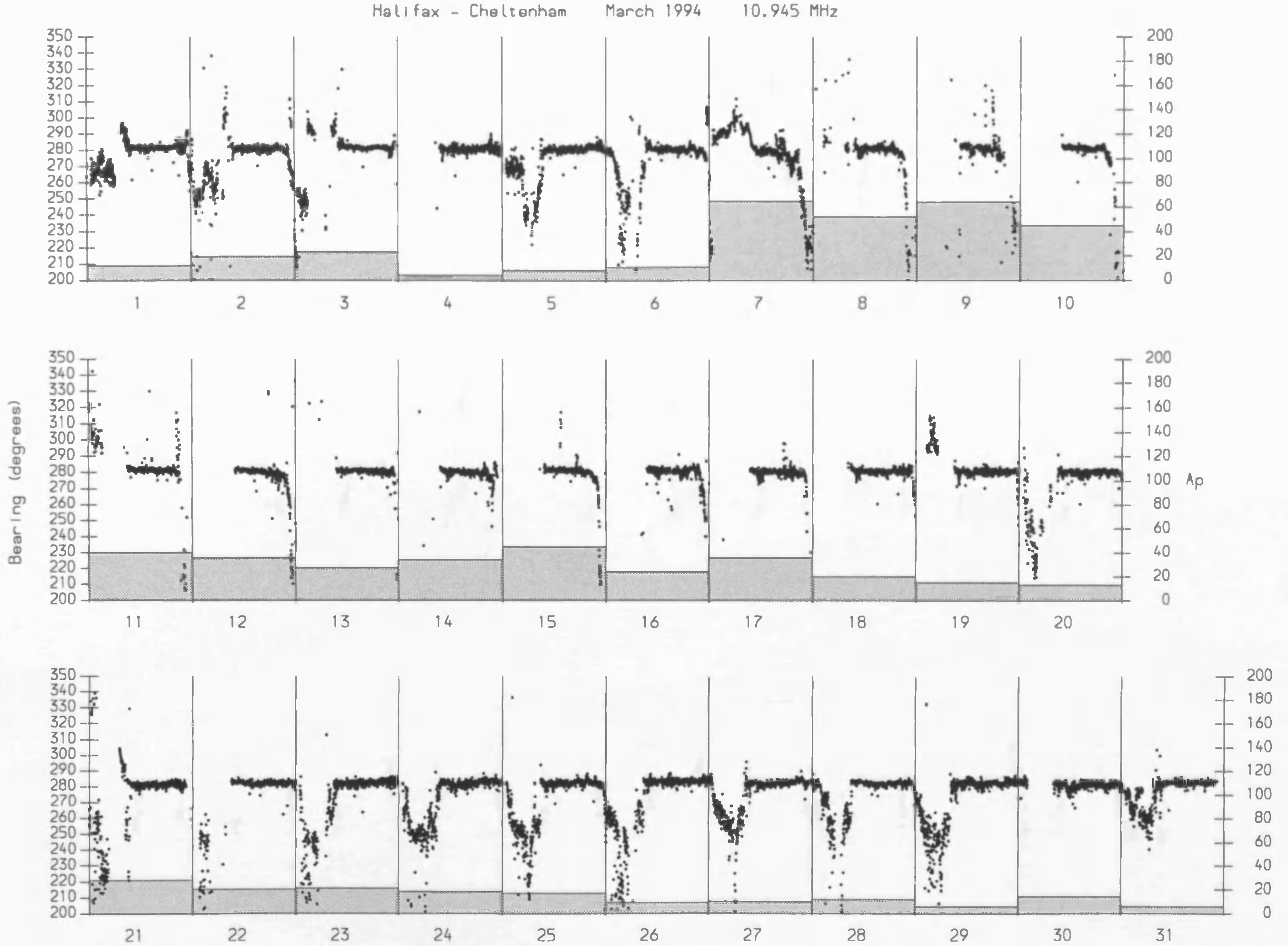

Figure 5.10: Bearings of 10.945MHz signals on the Halifax-Cheltenham path for March 1994. Vertical lines indicate 00:00 UT. The shaded bars indicate Ap index.

Figure 5.11: Bearings of 15.920MHz signals on the Halifax-Cheltenham path for March 1994. Vertical lines indicate 00:00 UT. The shaded bars indicate Ap index.

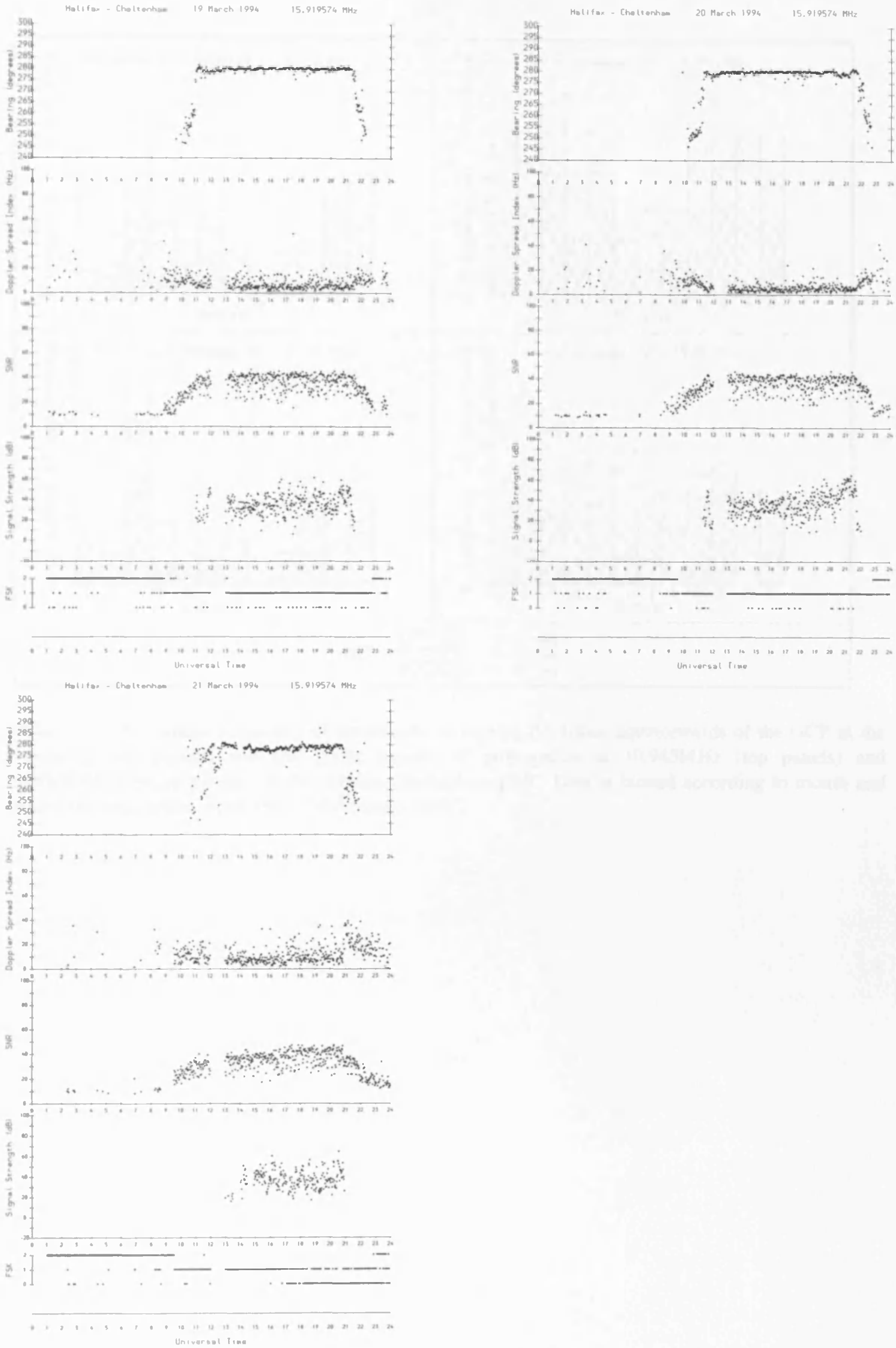

Figure 5.12: Example of tails in the bearing to the south of the true bearing (with associated Doppler spread index, SNR, signal strength and signal recognition index) for 15.919 MHz signals from Halifax to Cheltenham on 19-21 March 1994.

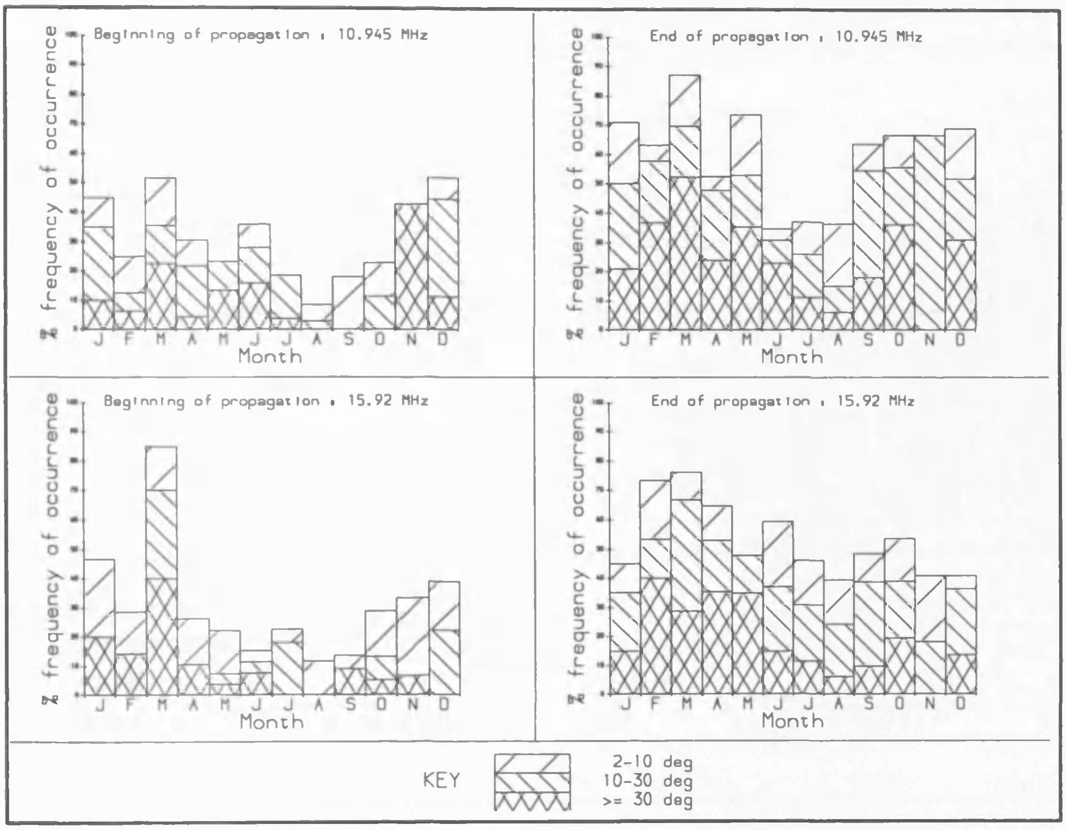

Figure 5.13: Percentage frequency of occurrence of bearing devations equatorwards of the GCP at the beginning (left panels) and end (right panels) of propagation at 10.945MHz (top panels) and 15.920MHz (bottom panels) on the Halifax-Cheltenham path. Data is binned according to month and covers the time period April 1993 - November 1994.

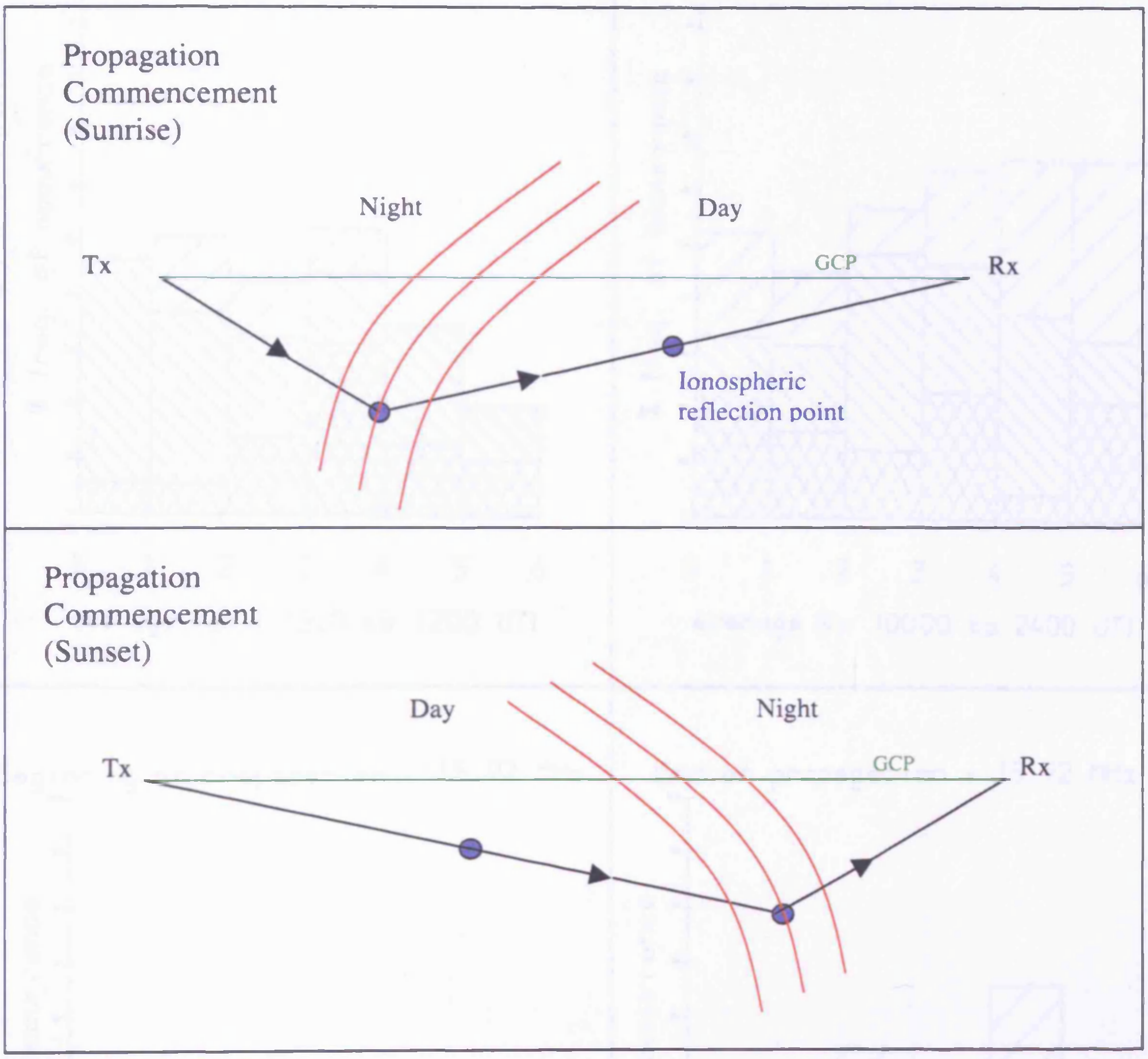

Figure 5.14: Schematic to illustrate the relative size of bearing tails at sunrise (top) and sunset (bottom) (see text for explanation).

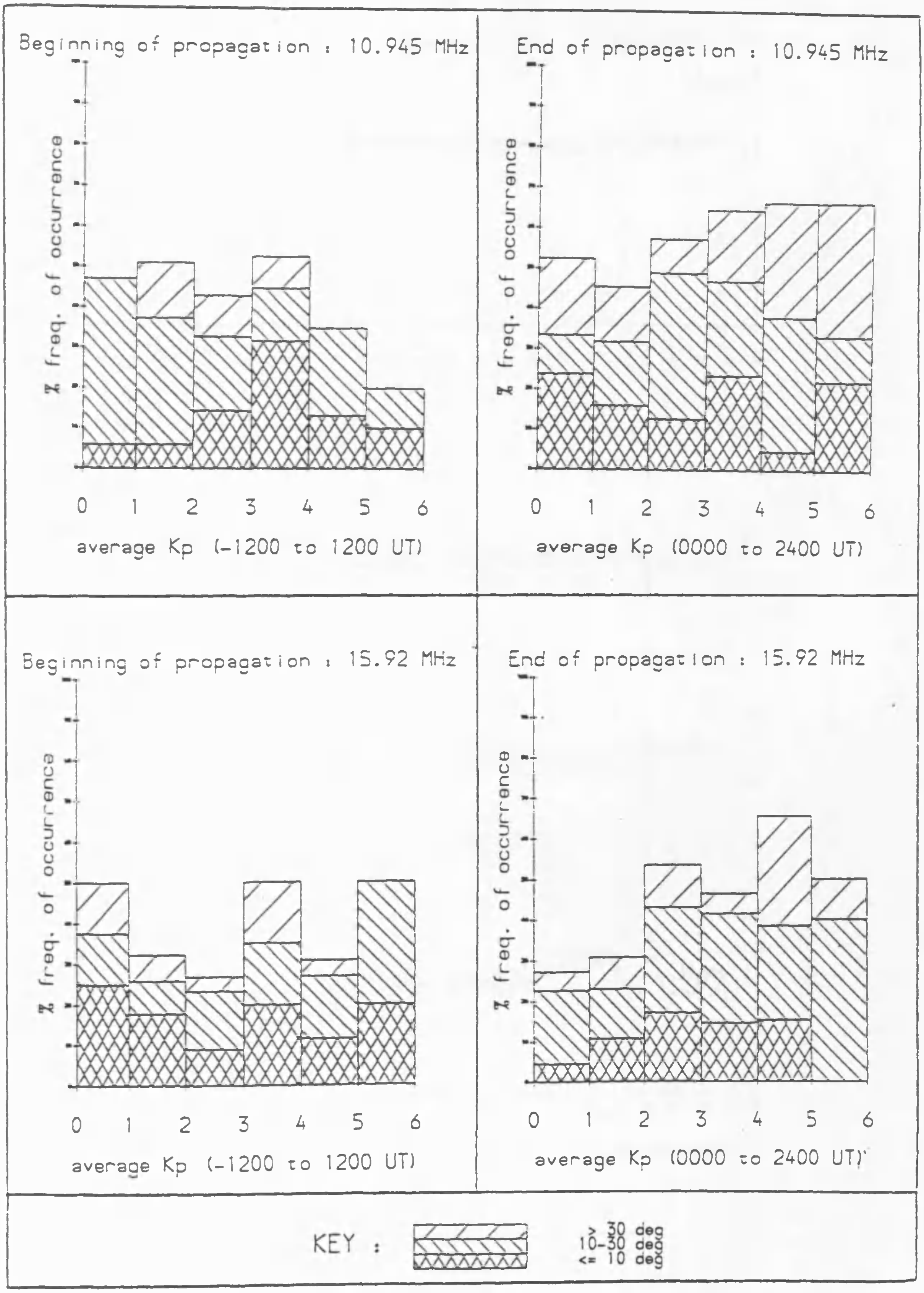

Figure 5.15: Percentage frequency of occurrence of bearing devations equatorwards of the GCP at the beginning (left panels) and end (right panels) of propagation at 10.945MHz (top panels) and 15.920MHz (bottom panels) on the Halifax-Cheltenham path. Data is binned according to Kp index and covers the time period April 1993 - November 1994.

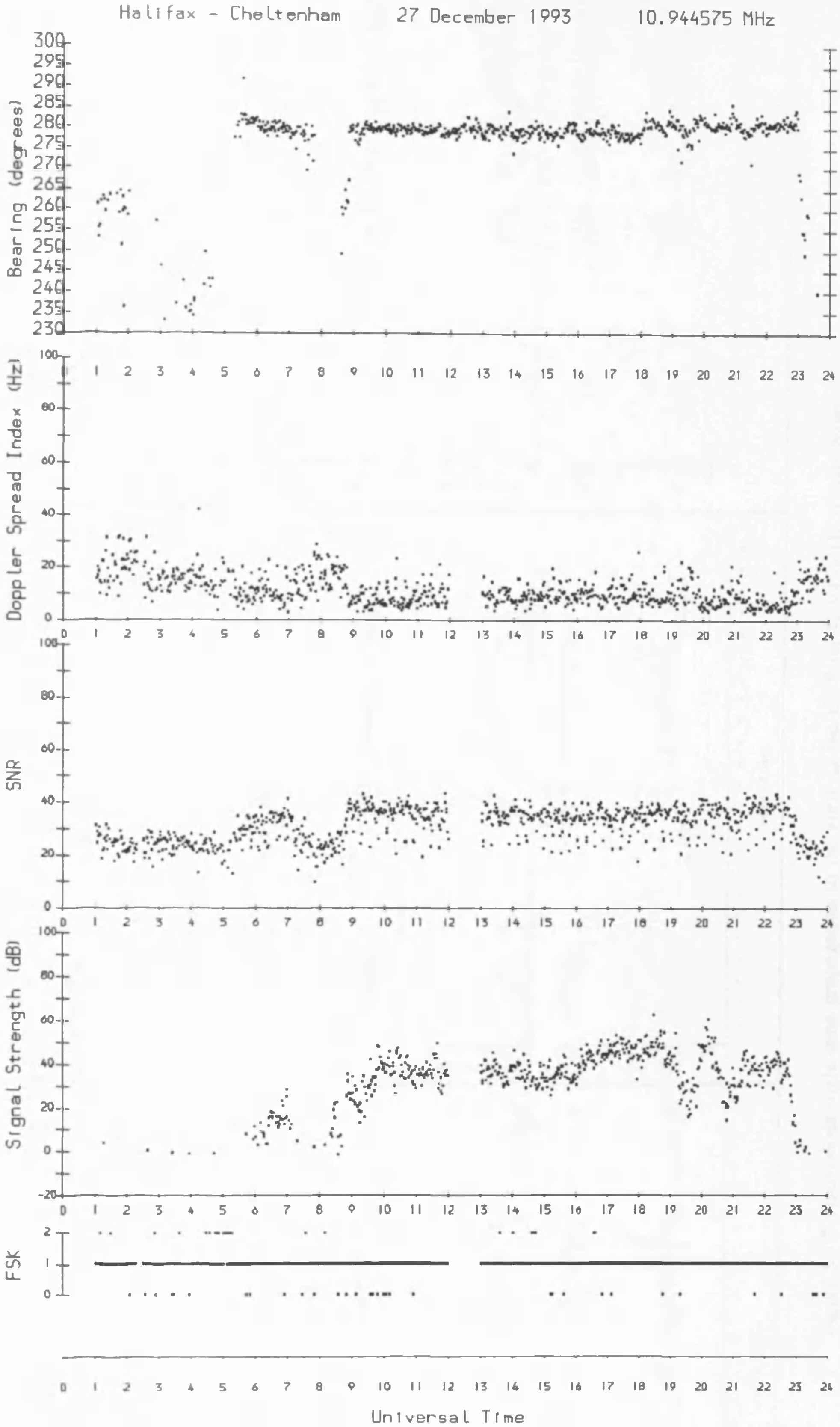

Figure 5.16: Example of an extra period of propagation lasting 2-3 hours before the 'usual' time of propagation at 8-9UT. Measurements are for the 10.945MHz signals on the Halifax-Cheltenham path on the 27th December 1993. Bearing, Doppler spread index, SNR, signal strength and signal recognition index ("FSK") are all shown.

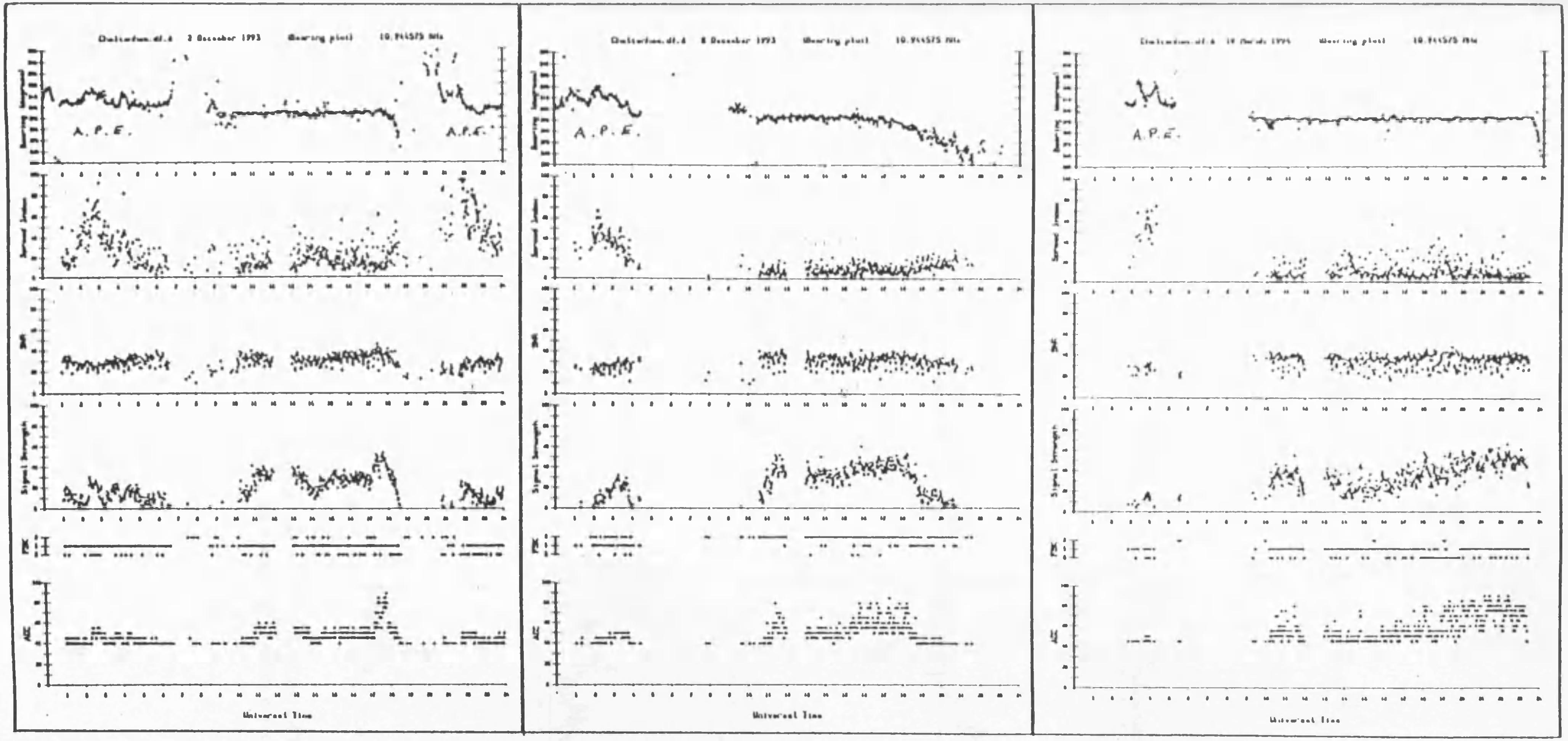

Figure 5.17 Anomalous night-time propagation to the north of the GCP on 10.945MHz signals from Halifax to Cheltenham on three days. The fields are (from top) bearing, Doppler spread index, SNR, signal strength, FSK signal recognition index and AGC setting.

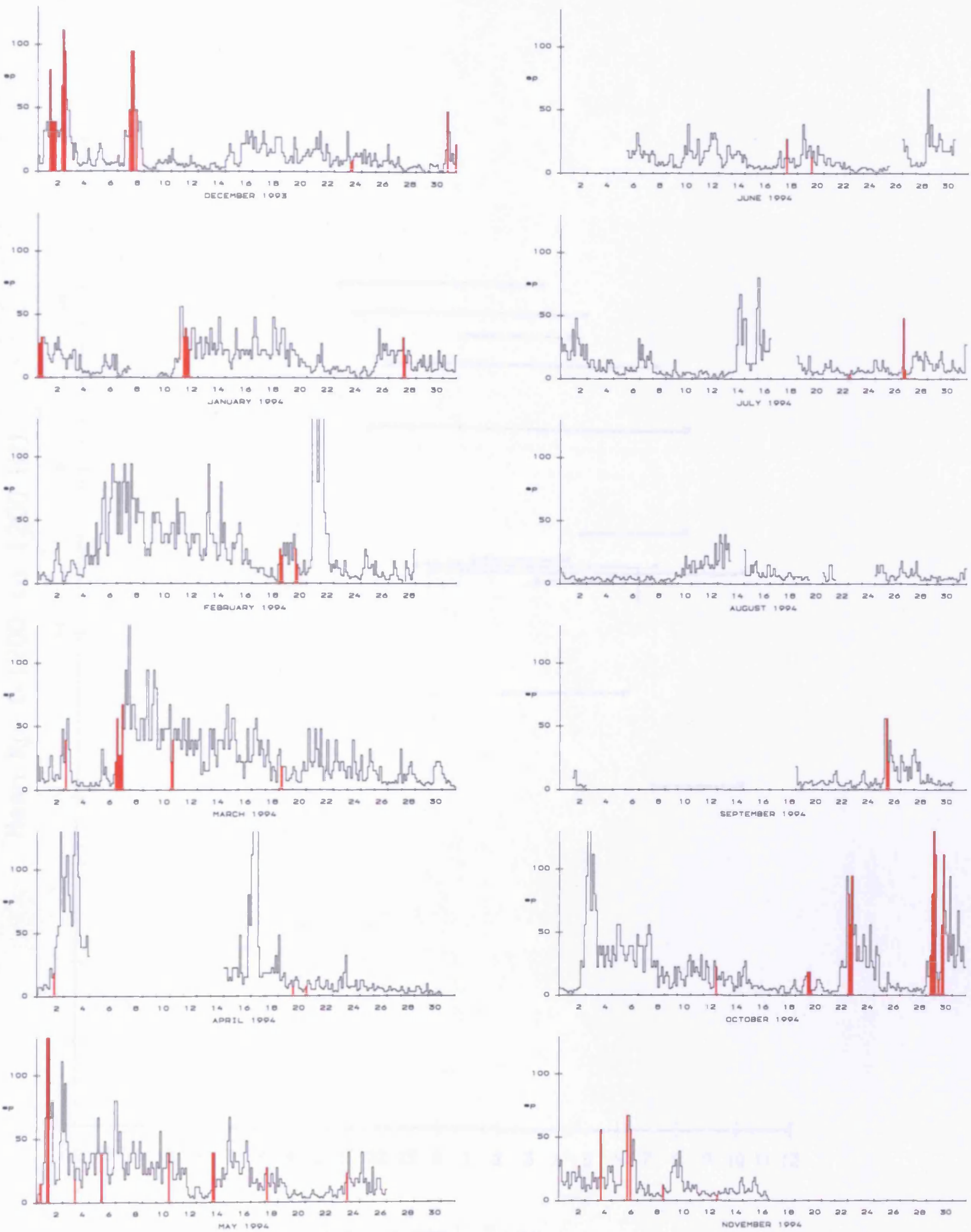

Figure 5.18: Times of anomalous night-time propagation to the north of the GCP on 10.945MHz signals from Halifax to Cheltenham are indicated by the vertical bars on this plot of the 3-hourly a_p index.

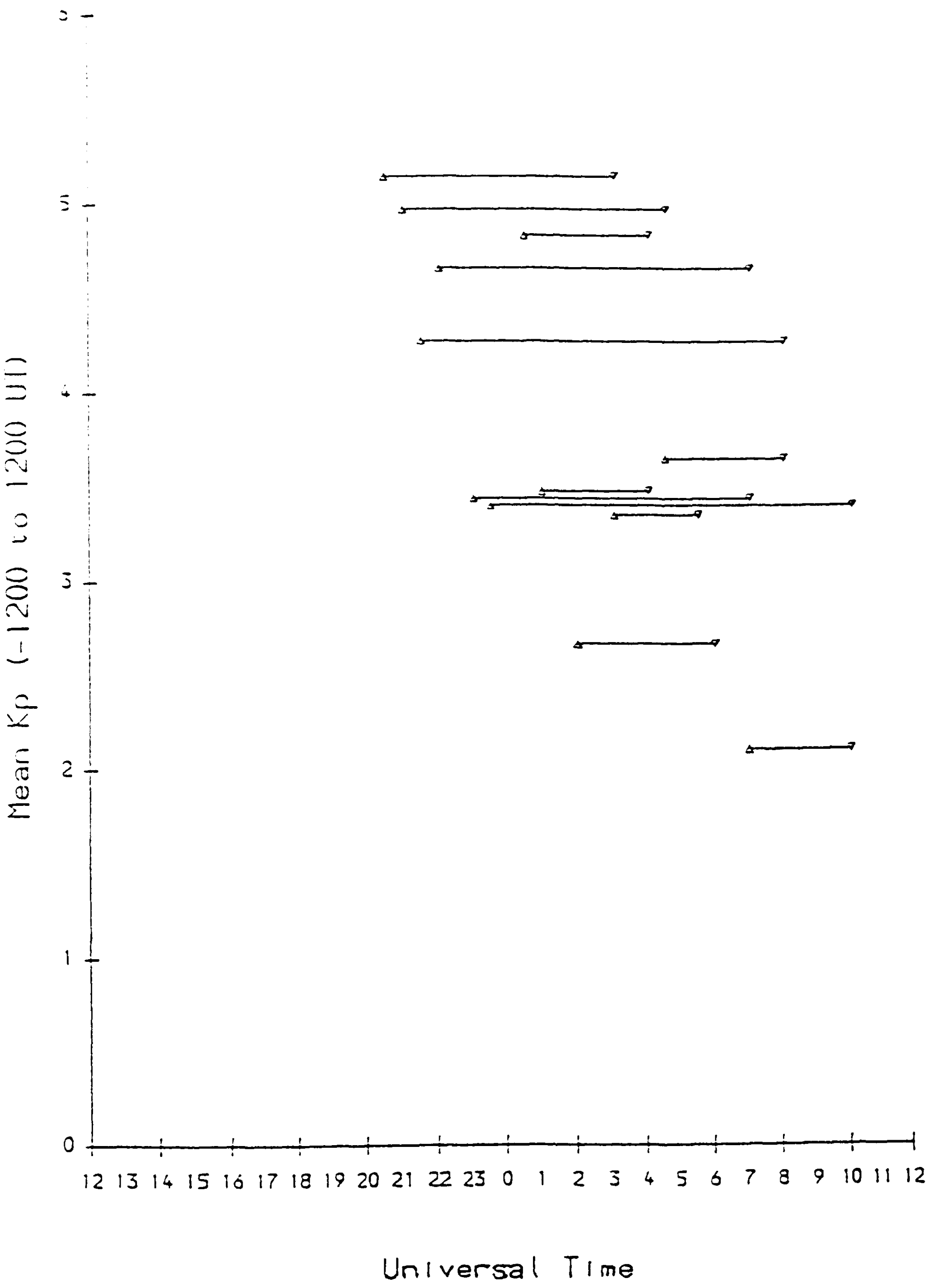

Figure 5.19: Times (UT) of anomalous night-time propagation to the north of the GCP on 10.945MHz signals from Halifax to Cheltenham, plotted against Kp (averaged 1200UT-1200UT).

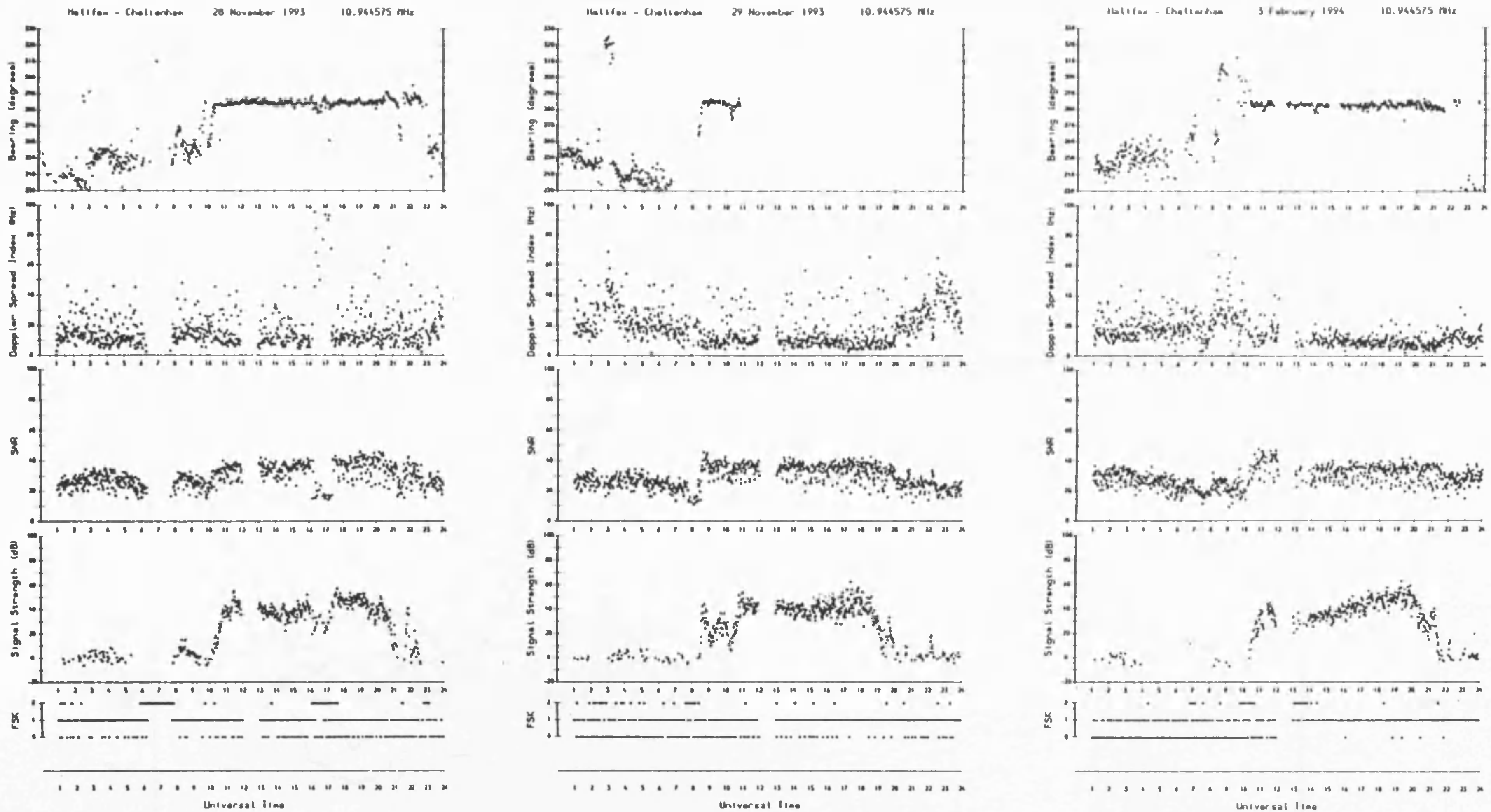

Figure 5.20: Example of 10.945MHz bearings on the Halifax-Cheltenham path showing large U-shaped equatorward deviations during the night.

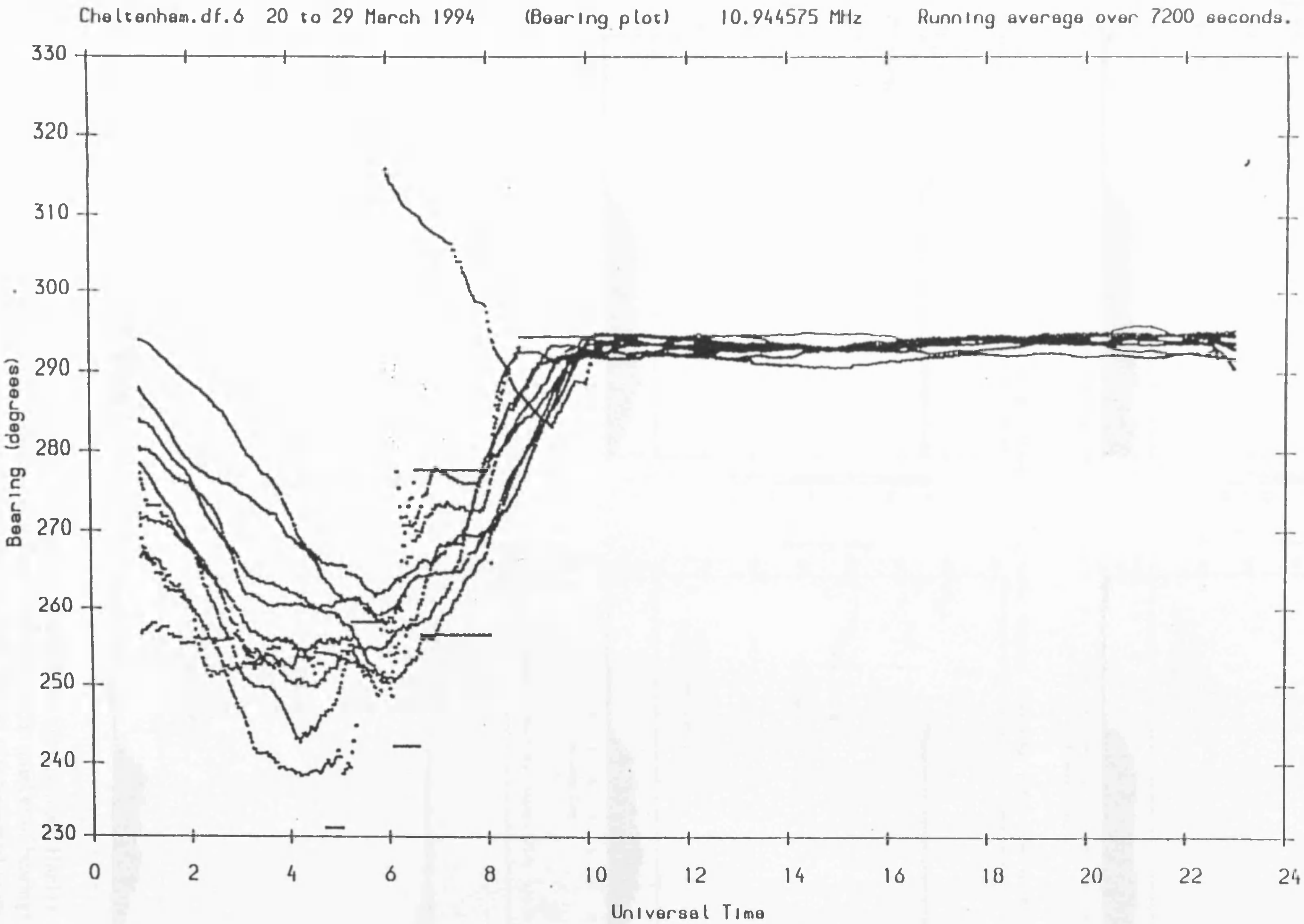

Figure 5.21: 2 hour running averages of the bearings of 10.945MHz signals from Halifax-Cheltenham for all days from 20-29th March 1994.

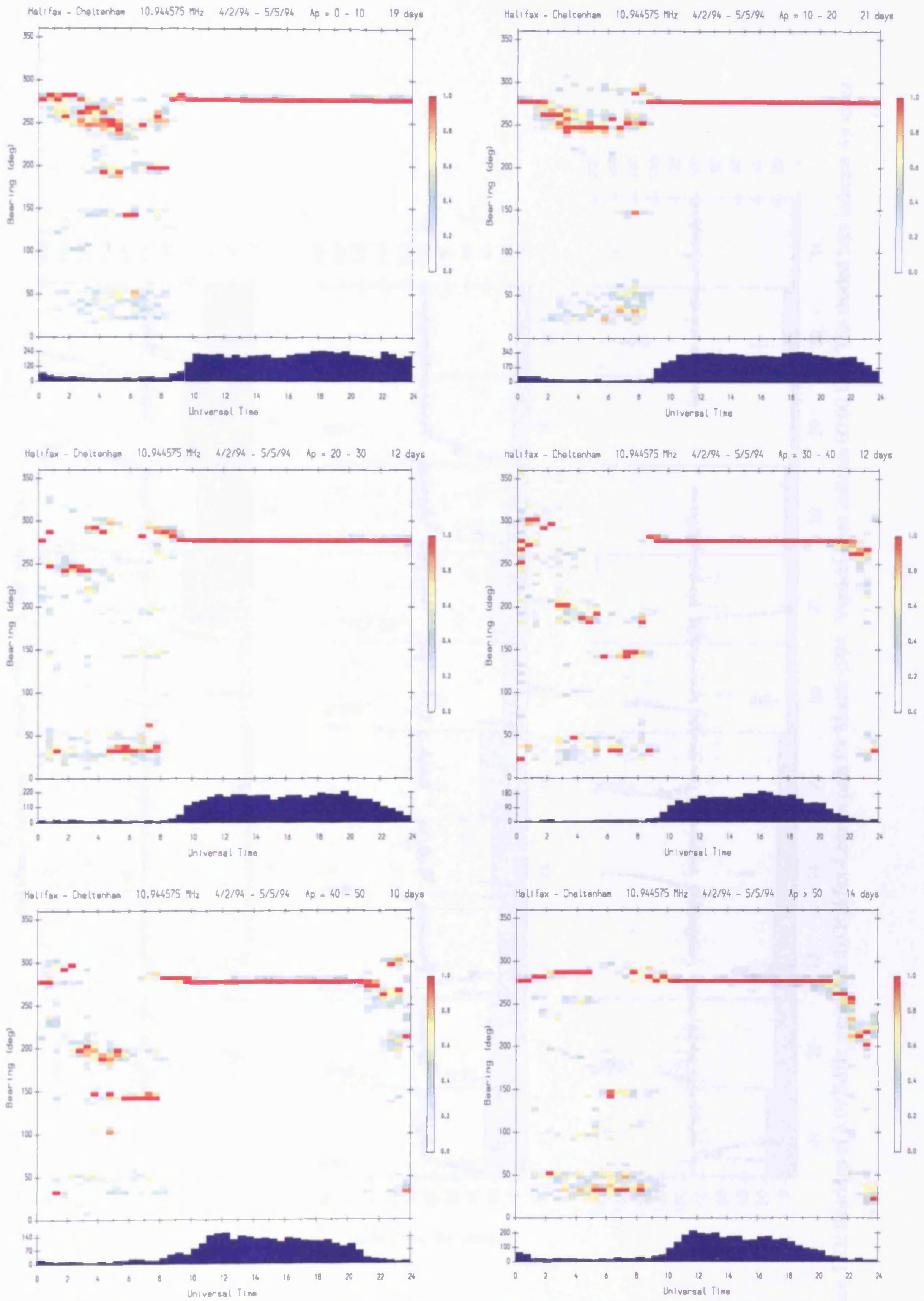

Figure 5.22: Contour plots of the distribution of bearings of 10.945MHz signals from Halifax-Cheltenham for 4/2/94-5/5/94. Each frame represents a different Ap range. The number of bearings is normalised for each UT bin and the total number of bearings in each UT bin is represented in the underlying histograms.

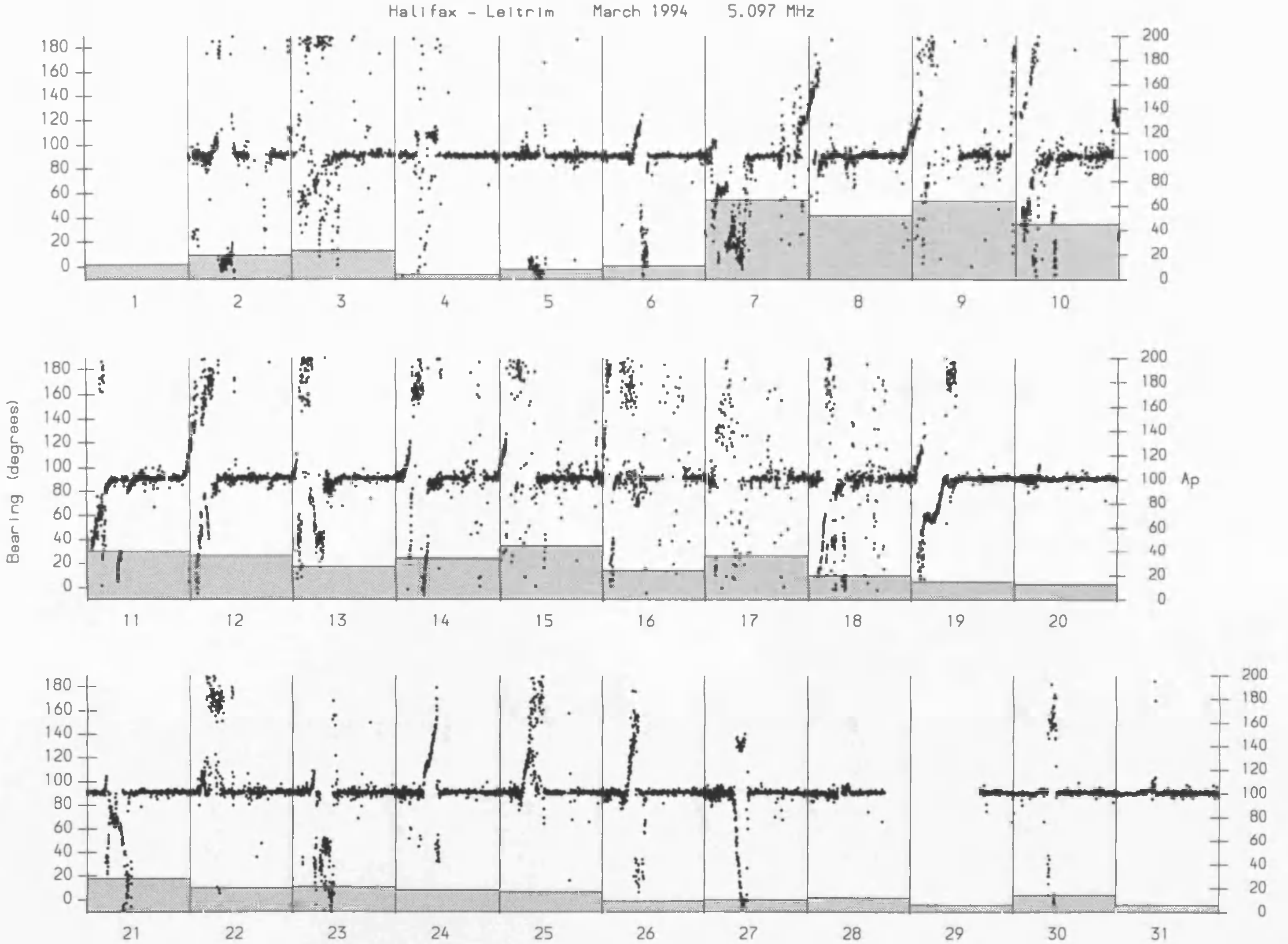

Figure 5.23: Bearings of 5.097MHz signals on the Halifax-Leitrim path for March 1994. Vertical lines indicate 00:00 UT. The shaded bars indicate Ap index.

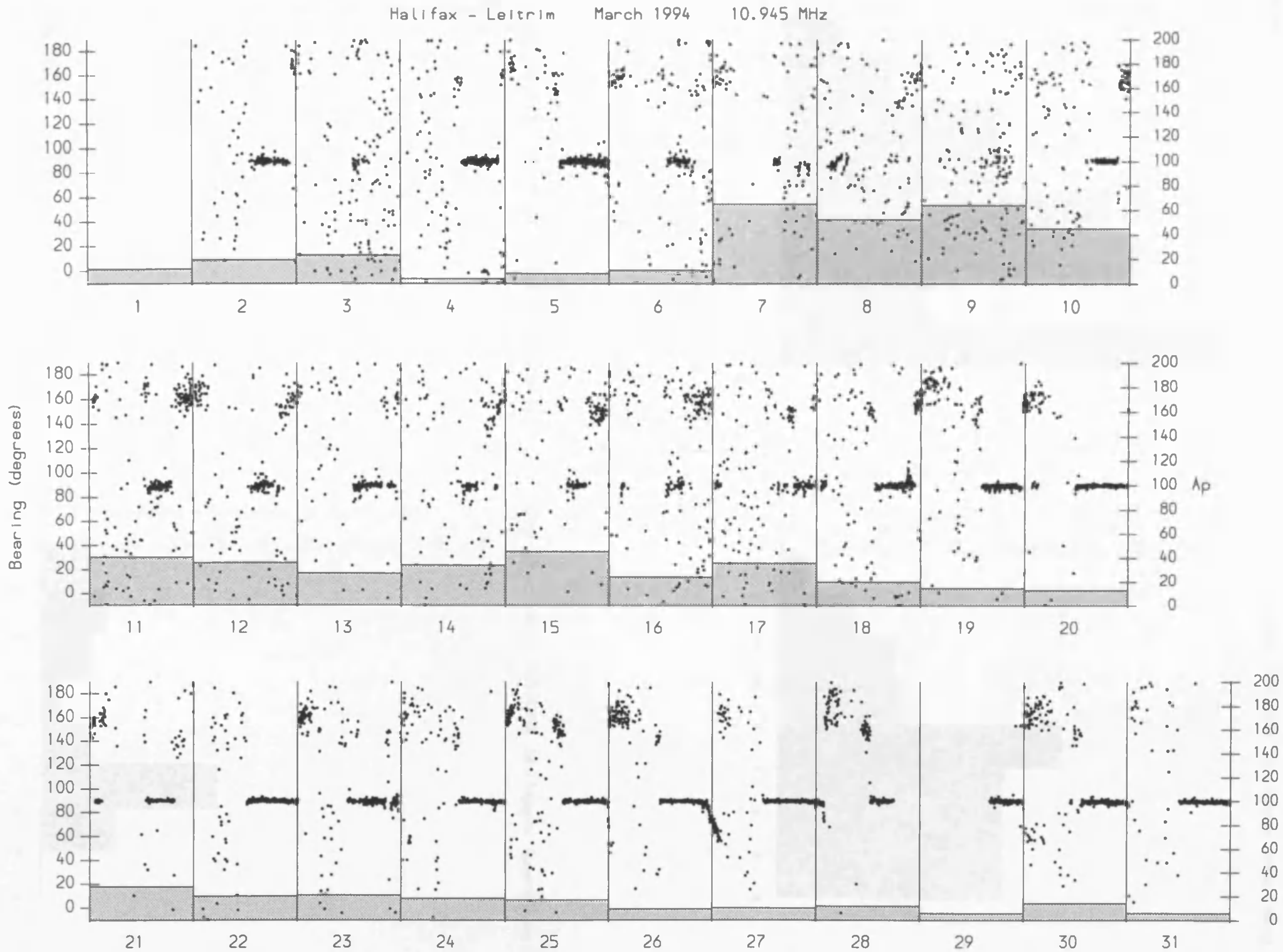

Figure 5.24: Bearings of 10.945MHz signals on the Halifax-Leitrim path for March 1994. Vertical lines indicate 00:00 UT. The shaded bars indicate Ap index.

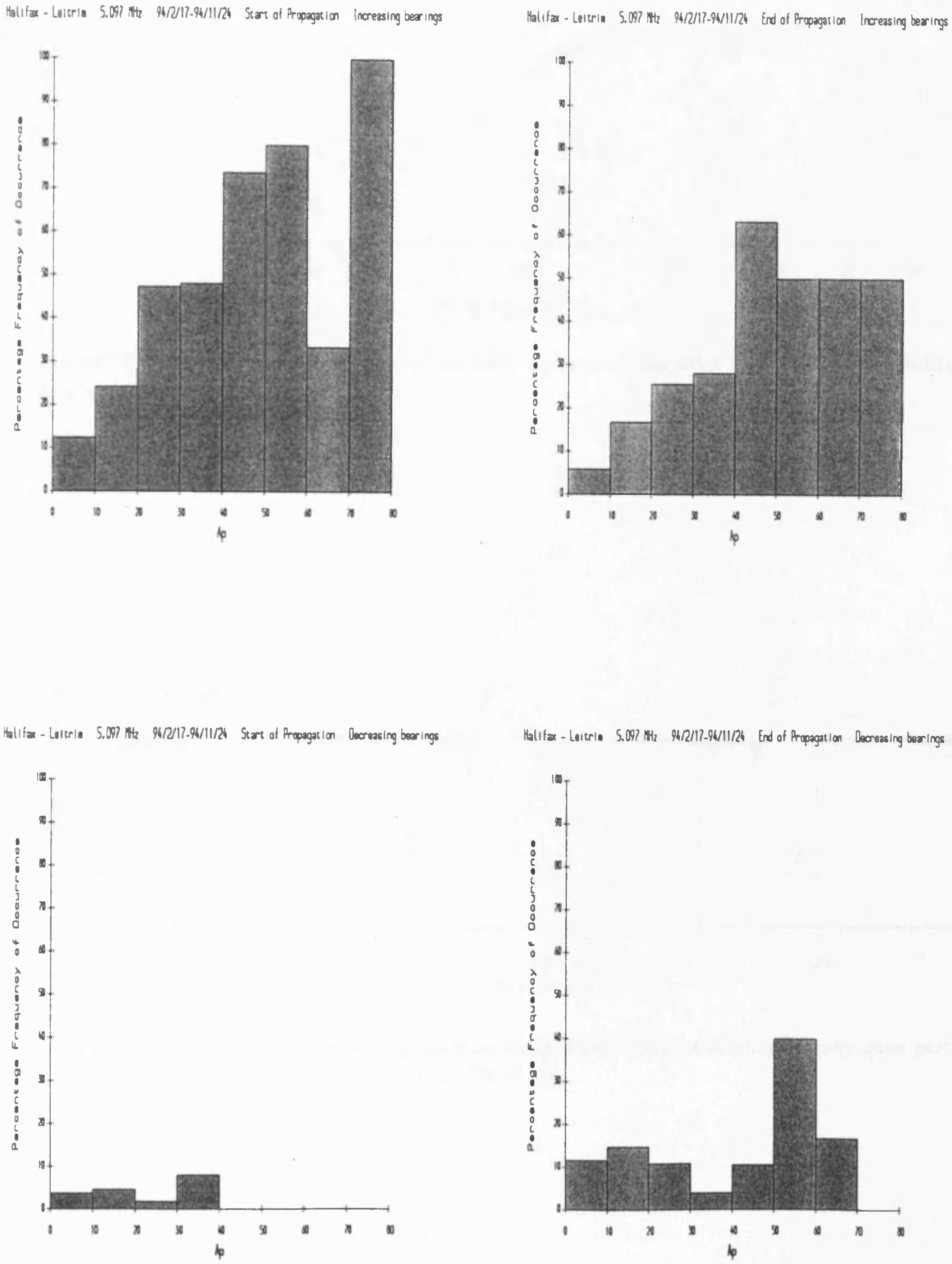

Figure 5.25: Percentage frequency of occurrence of bearing tails at the beginning (left panels) and end (right panels) of normal propagation at 5.097MHz plotted against ranges of Ap for all days in the period 17/2/94-24/11/94. The top panels indicate tails which increase in bearing with time and the bottom panels represent tails with decreasing bearings.

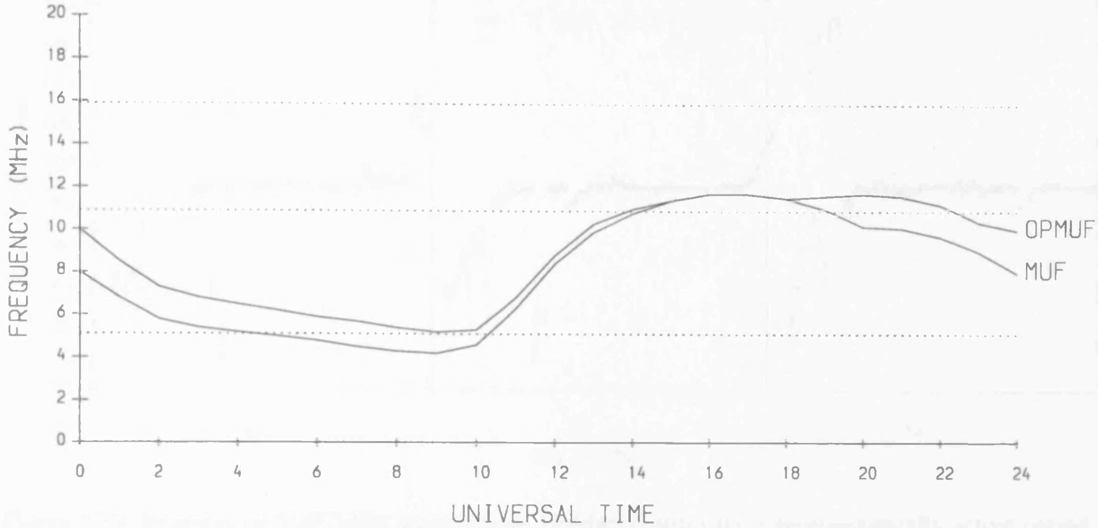

Figure 5.26: REC533 model prediction of the MUF and operational MUF (OPMUF) on the Halifax-Leitrim path for April 1994.

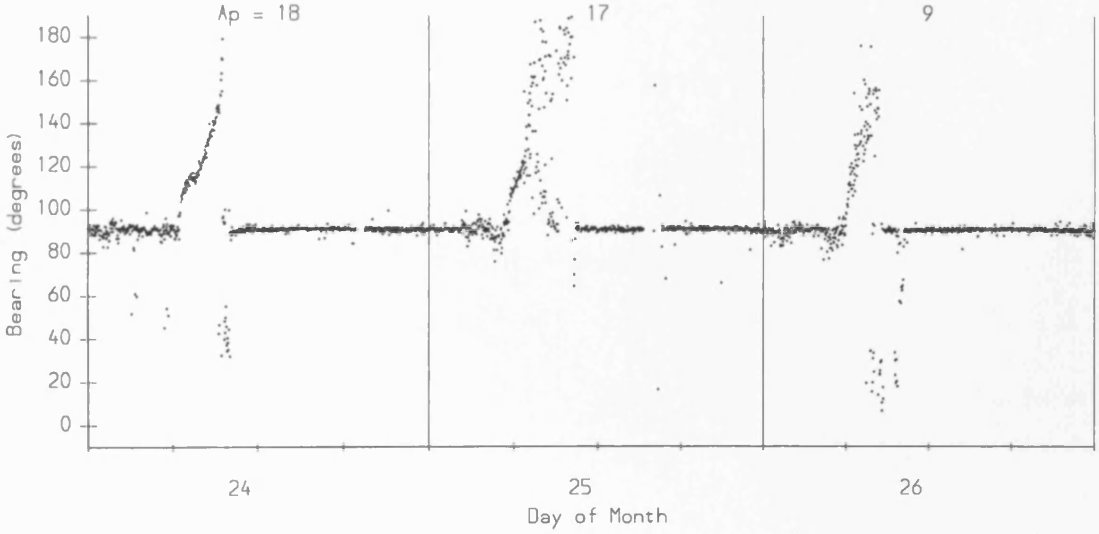

Figure 5.27: Bearings of 5.097MHz signals from Halifax-Leitrim for a geomagnetically quiet period (24-26th March 1994). Vertical lines indicate 00:00 UT.

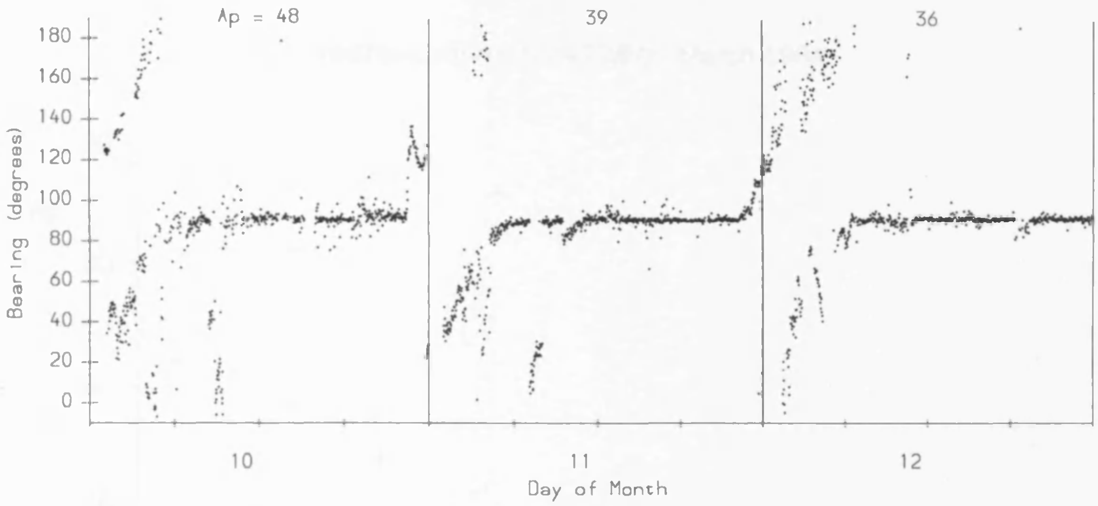

Figure 5.28: Bearings of 5.097MHz signals from Halifax-Leitrim for a geomagnetically active period (10-12th March 1994). Vertical lines indicate 00:00 UT.

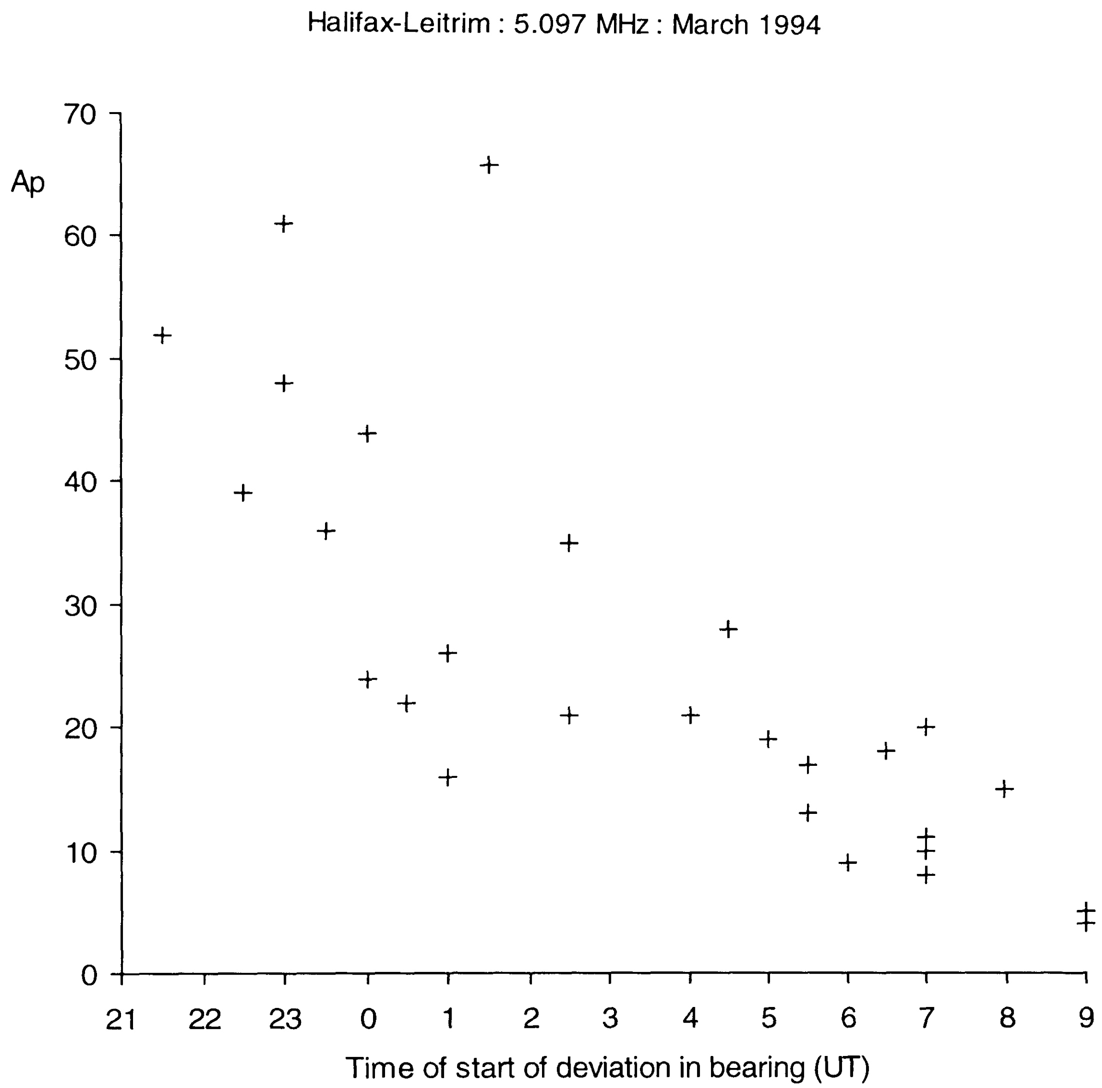

Figure 5.29: Times (UT) of the start of off-GCP propagation of 5.097MHz signals from Halifax to Leitrim plotted against Ap.

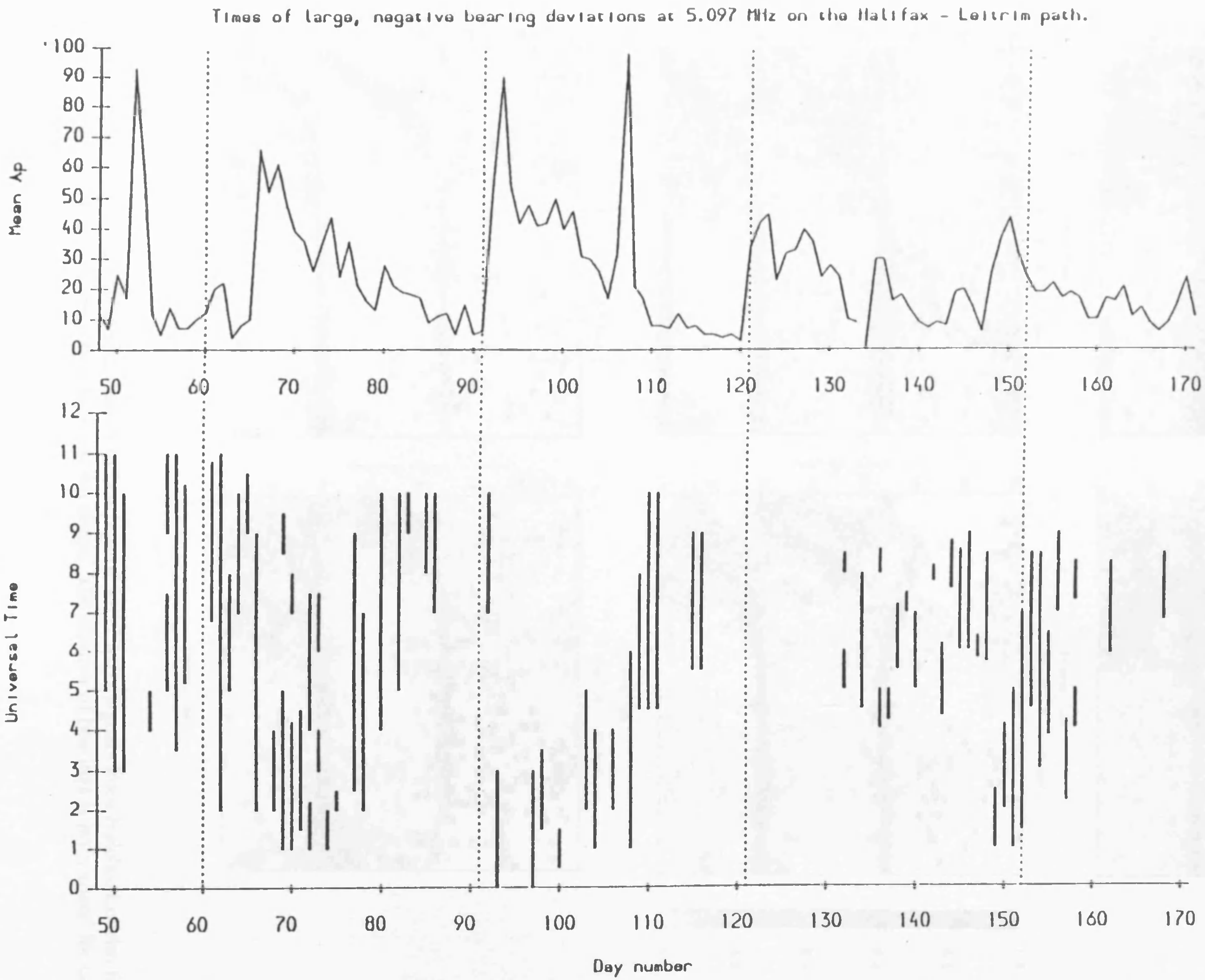

Figure 5.30: Times (UT) of large bearing deviations from the GCB of 5.097MHz signals from Halifax to Leitrim (vertical bars) plotted aginst day number for dates in the range 20/2/94-20/6/94. Ap index is plotted alongside.

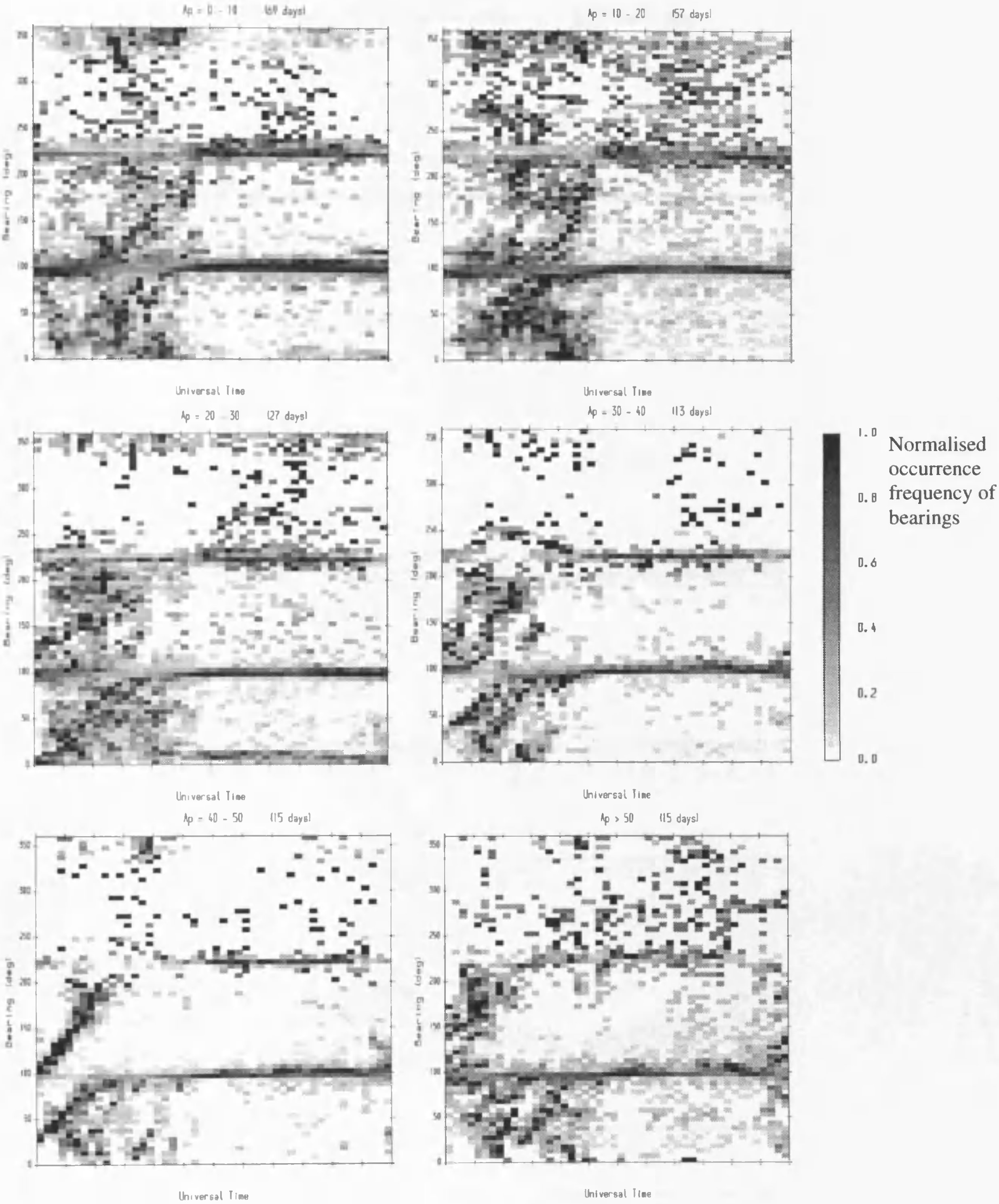

Figure 5.31: Contour plots of the distribution of bearings of 5.097 MHz signals from Halifax-Leitrim for all data in 1994. Each frame represents a different Ap range. The number of bearings is normalised for each 5° bearing bin.

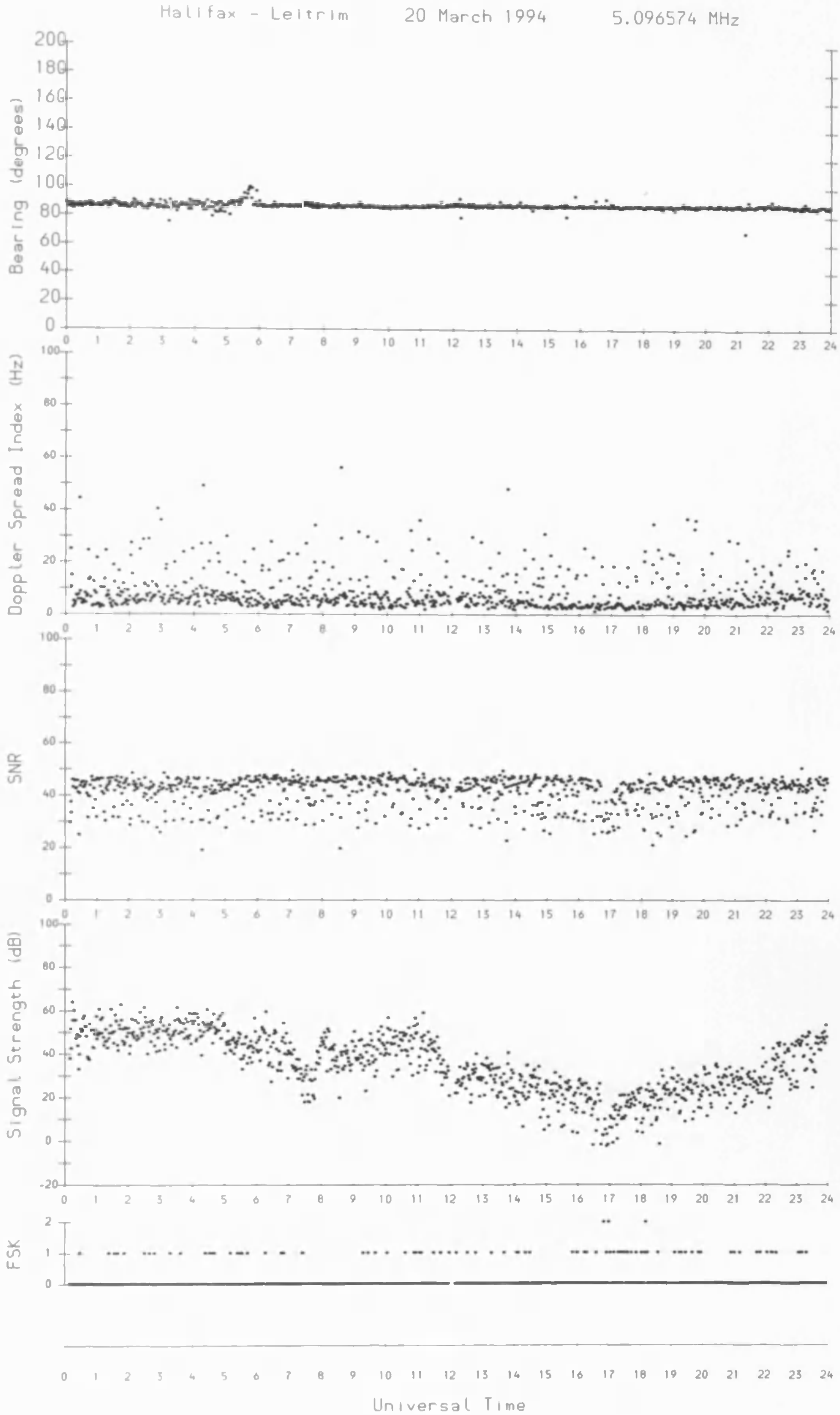

Figure 5.32: Bearings and signal characteristics of 5.097MHz signals from Halifax to Leitrim on 20th March 1994. The fields are (from top) bearing, Doppler spread index, SNR, signal strength, and signal recognition index.

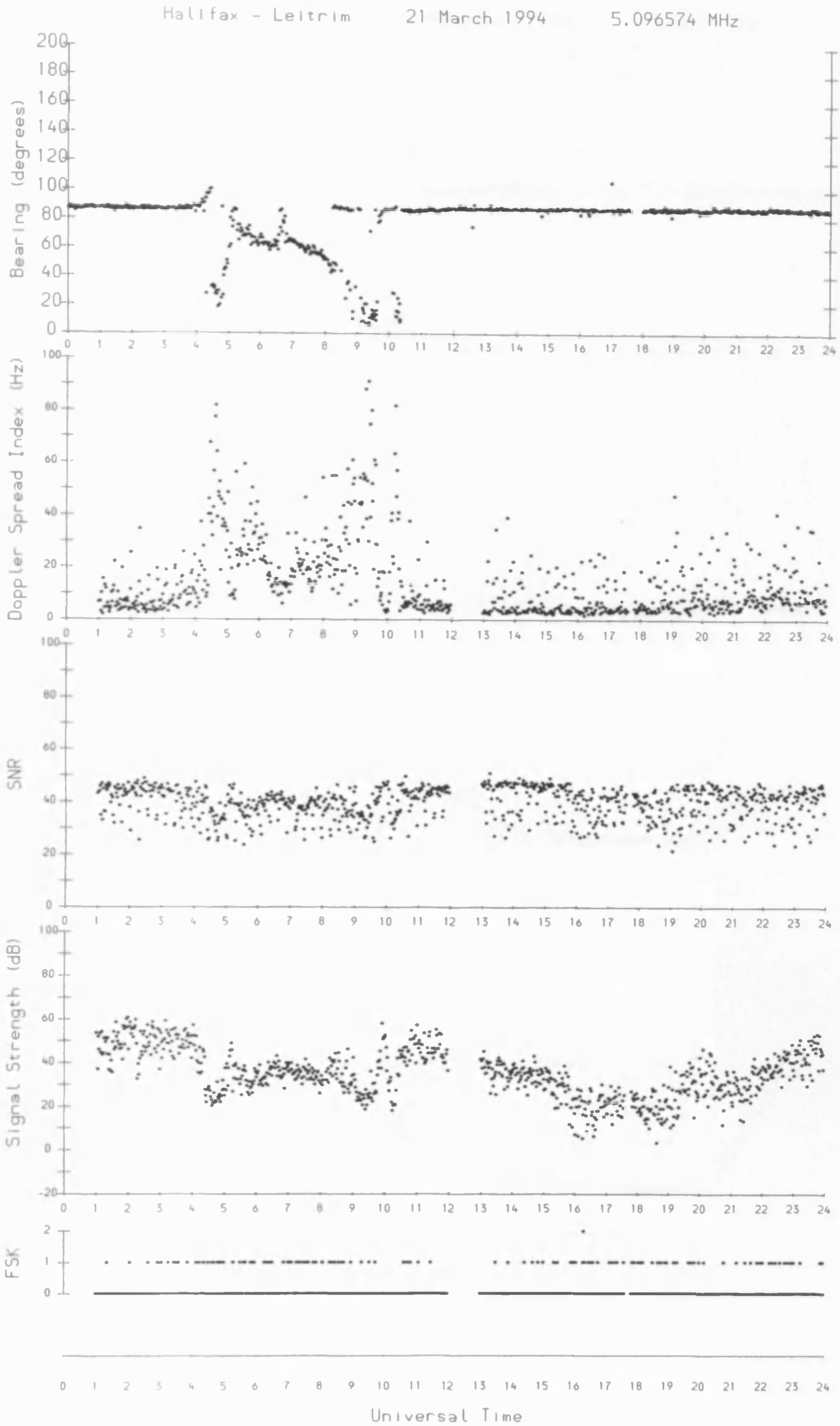

Figure 5.33: Bearings and signal characteristics of 5.097MHz signals from Halifax to Leitrim on 21st March 1994. The fields are (from top) bearing, Doppler spread index, SNR, signal strength, and signal recognition index.

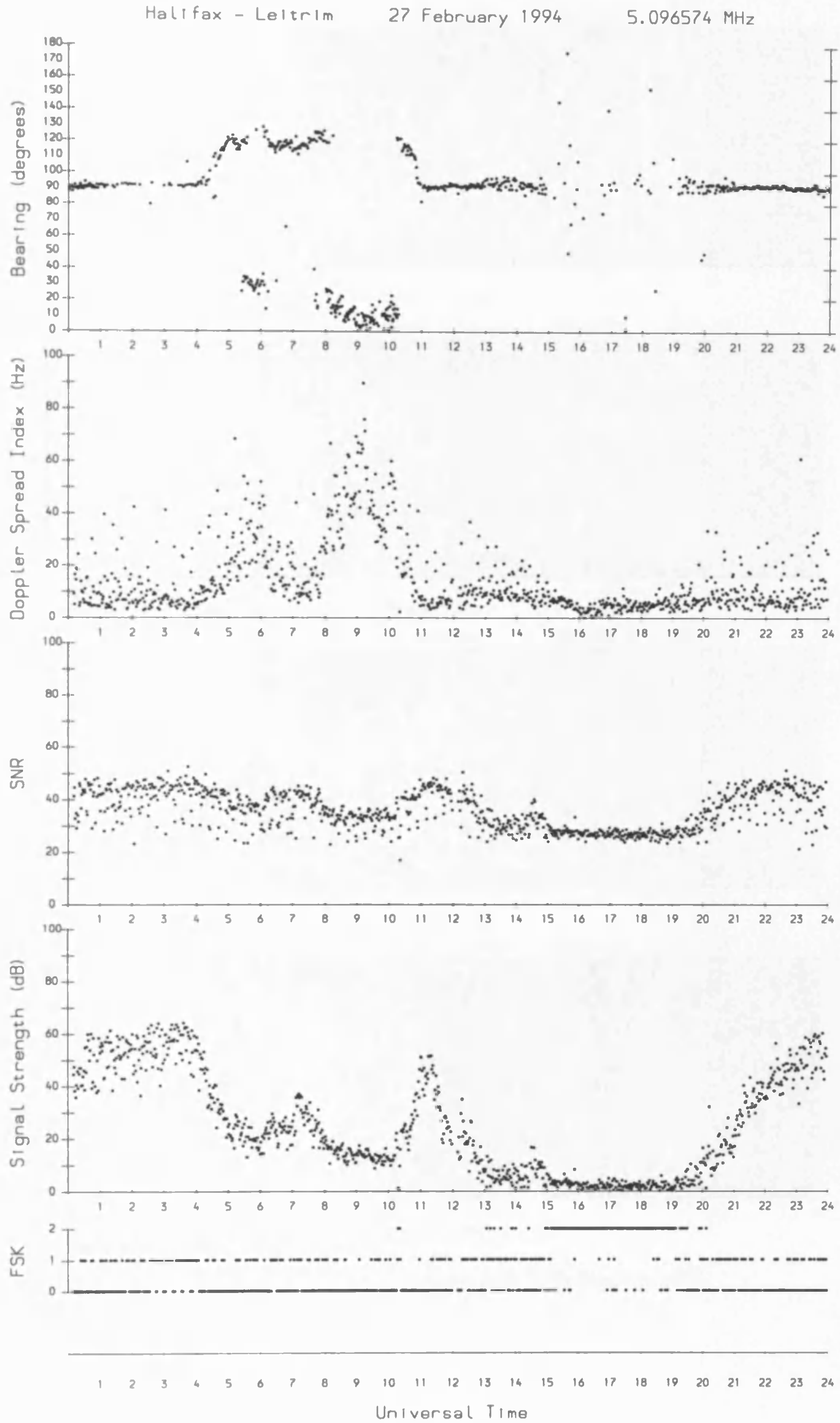

Figure 5.34: Bearings and signal characteristics of 5.097MHz signals from Halifax to Leitrim on 27th February 1994. The fields are (from top) bearing, Doppler spread index, SNR, signal strength, and signal recognition index ("FSK").

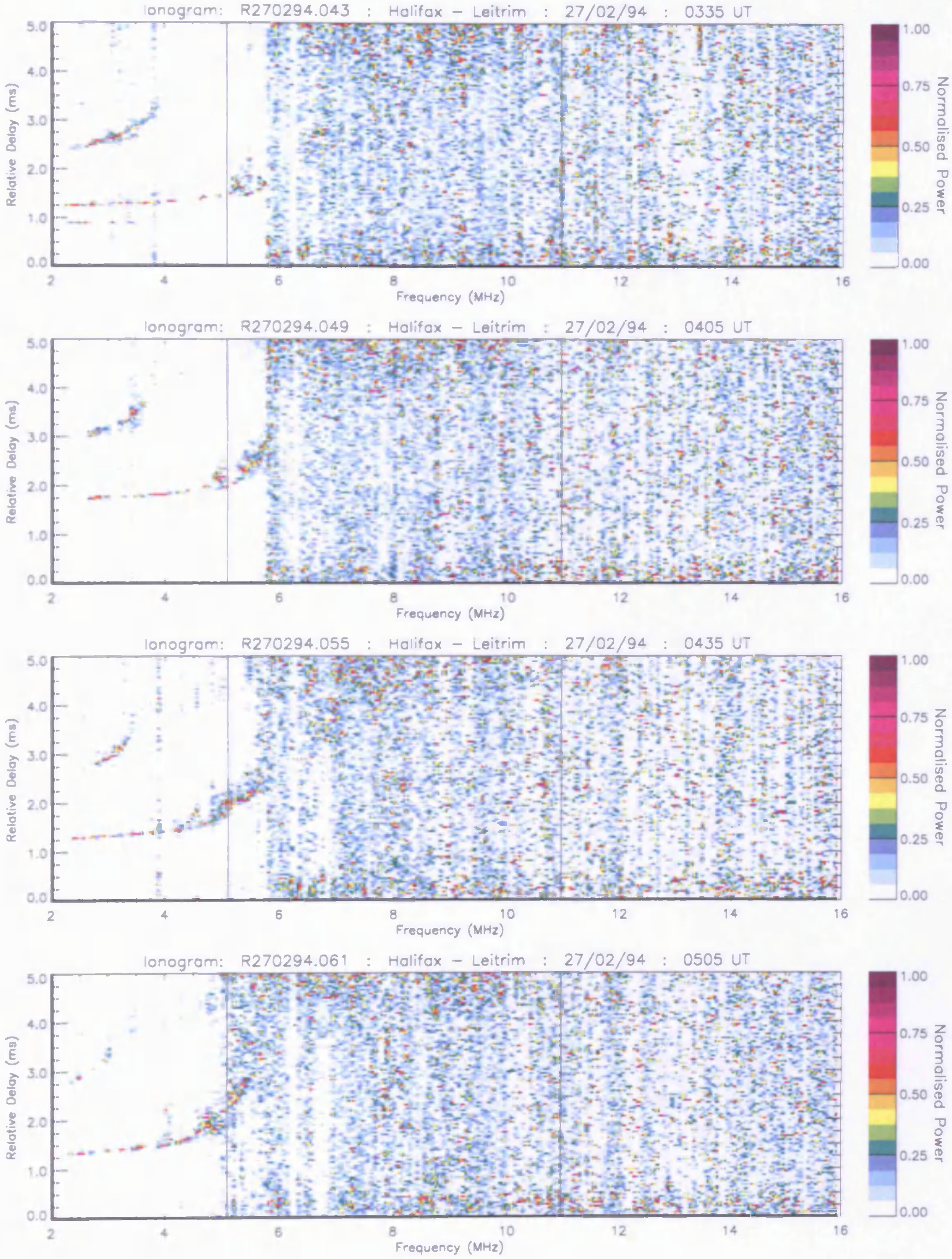

Figure 5.35: Ionogram sequence for Halifax-Leitrim path, 27th February 1994.

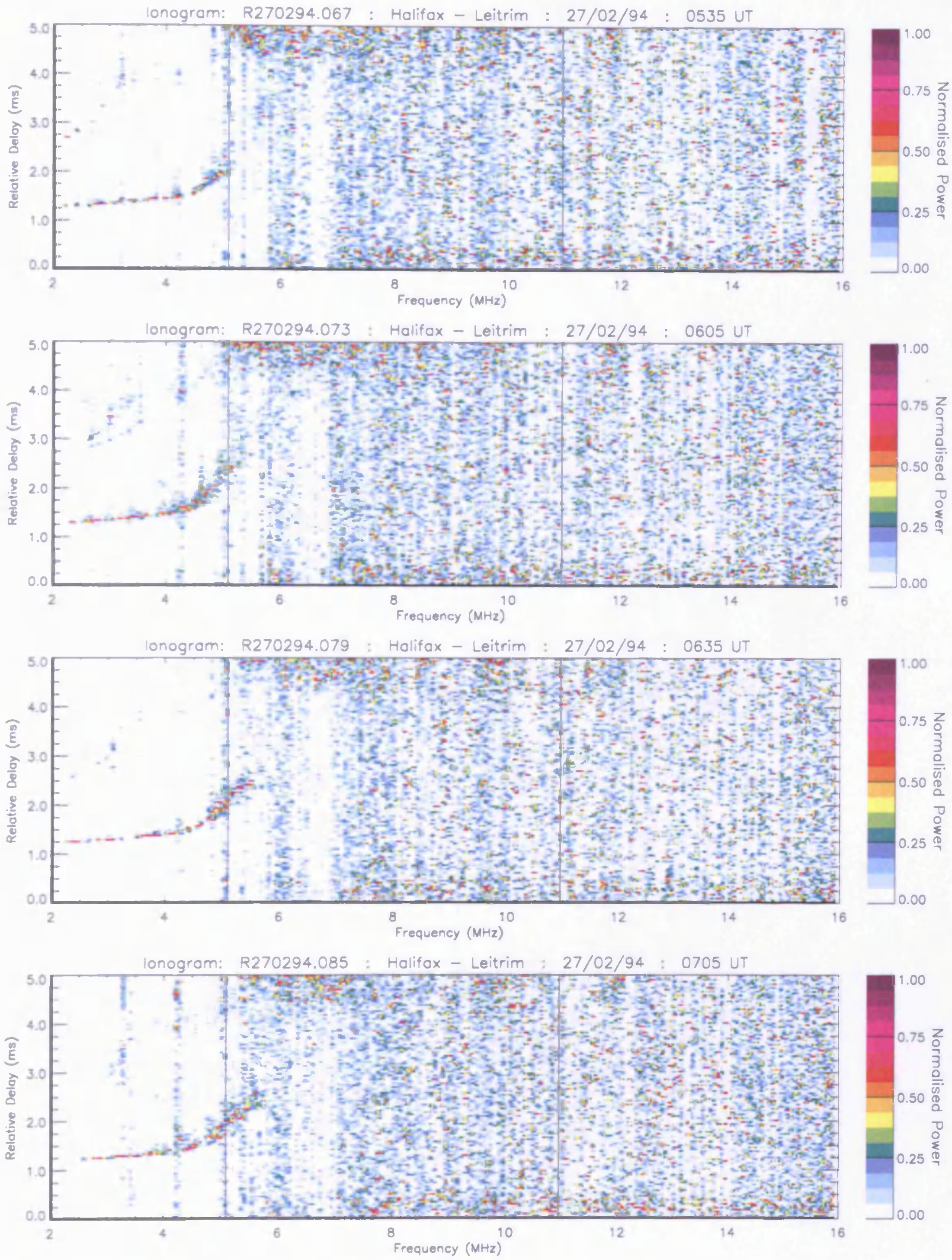

Figure 5.35 (ctd.): Ionogram sequence for Halifax-Leitrim path, 27th February 1994.

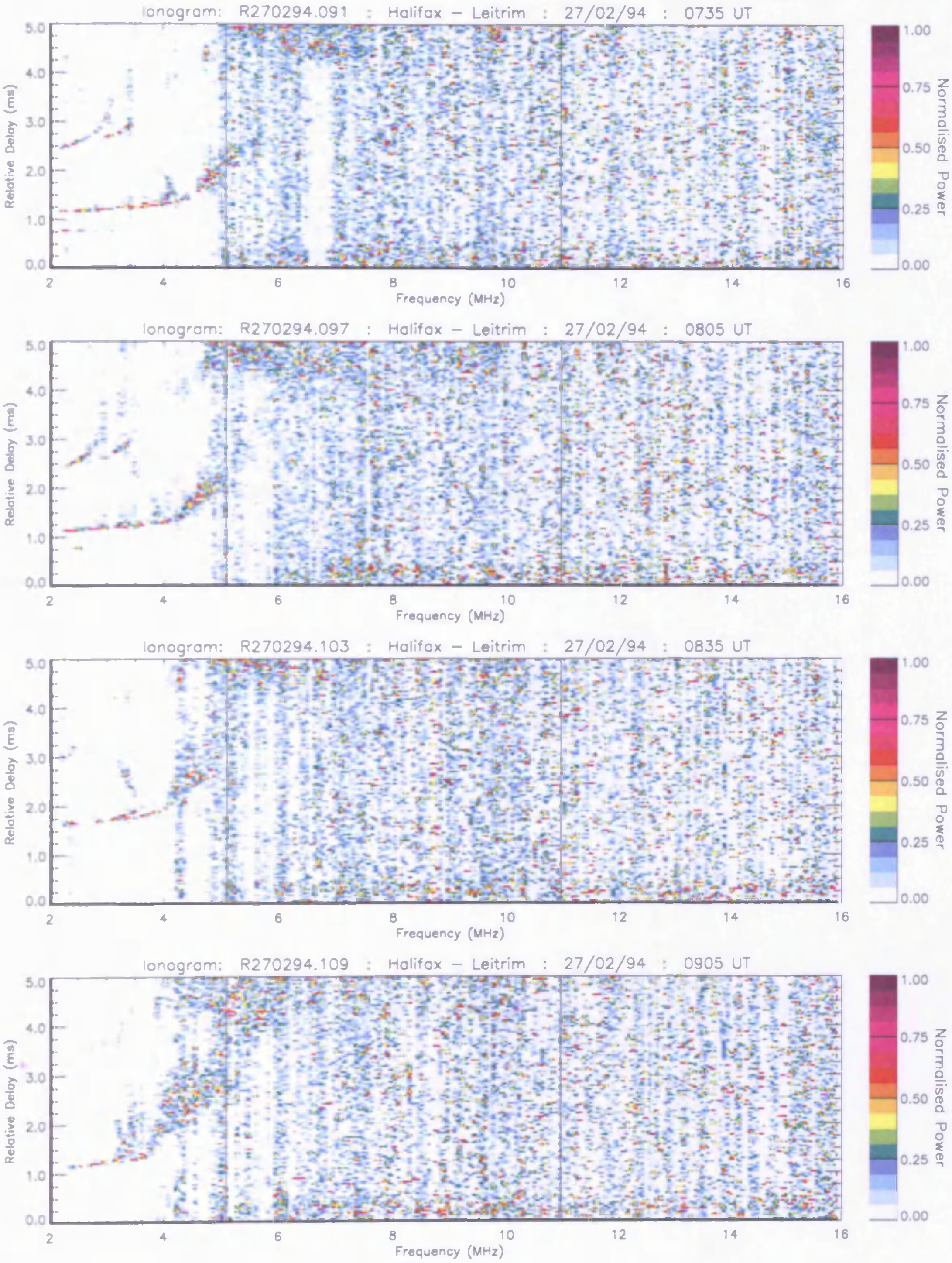

Figure 5.35 (ctd.): Ionogram sequence for Halifax-Leitrim path, 27th February 1994.

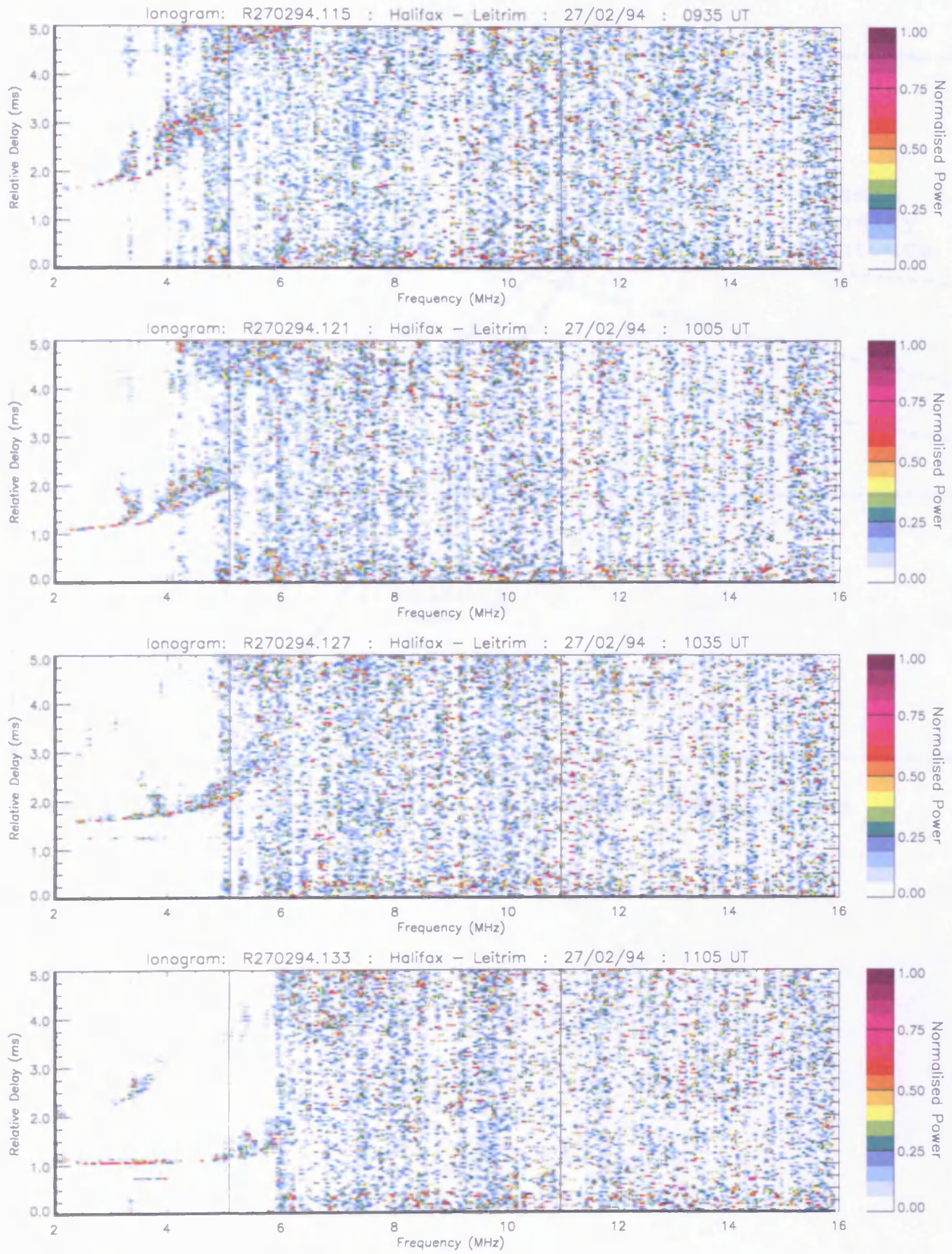

Figure 5.35 (ctd.): Ionogram sequence for Halifax-Leitrim path, 27th February 1994.

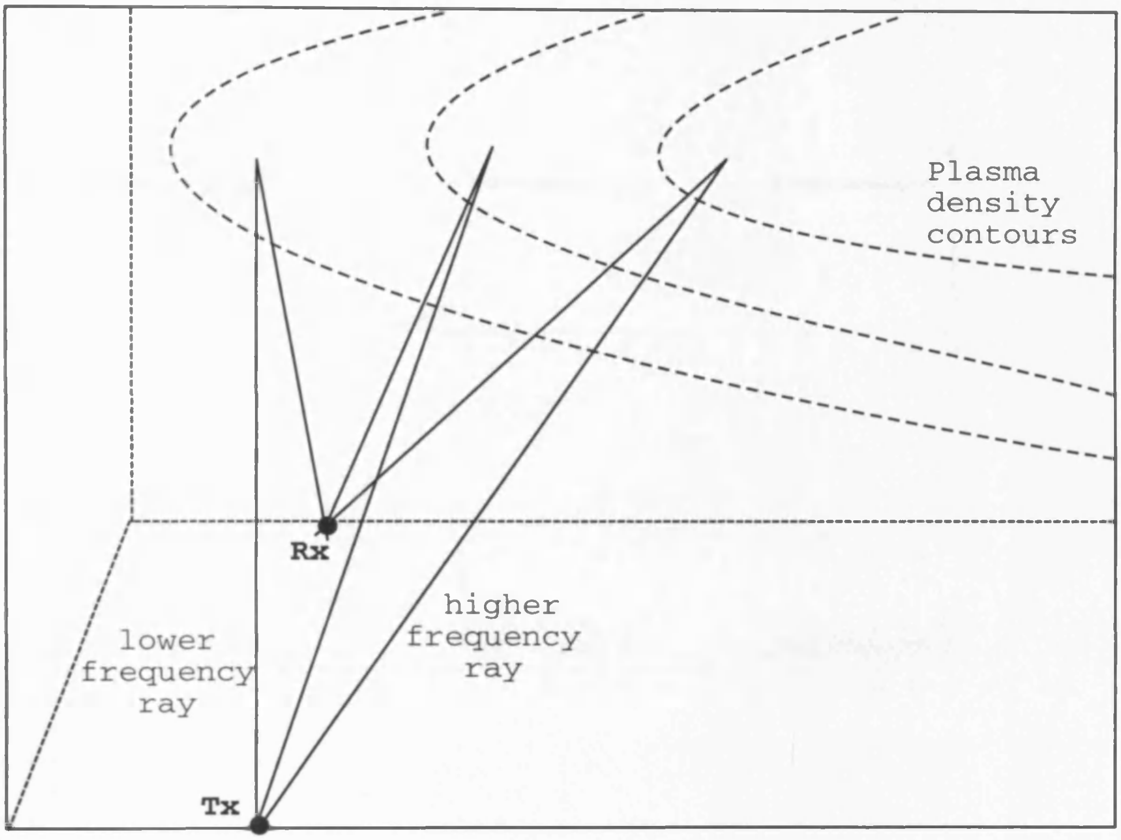

Figure 5.36: Schematic to illustrate the formation of 'nose extensions' on oblique ionograms.

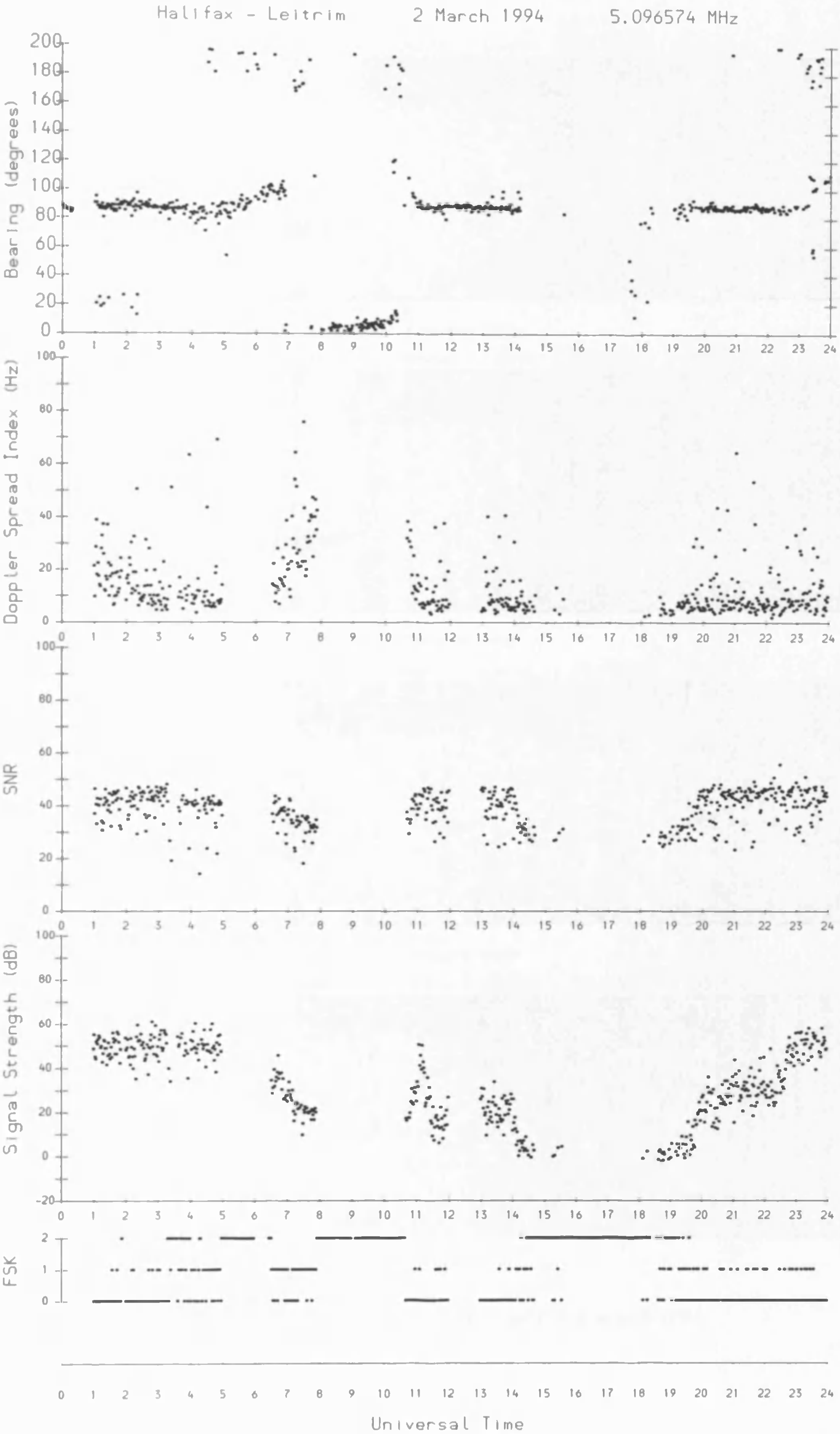

Figure 5.37: Bearings and signal characteristics of 5.097MHz signals from Halifax to Leitrim on 2nd March 1994. The fields are (from top) bearing, Doppler spread index, SNR, signal strength, and signal recognition index.

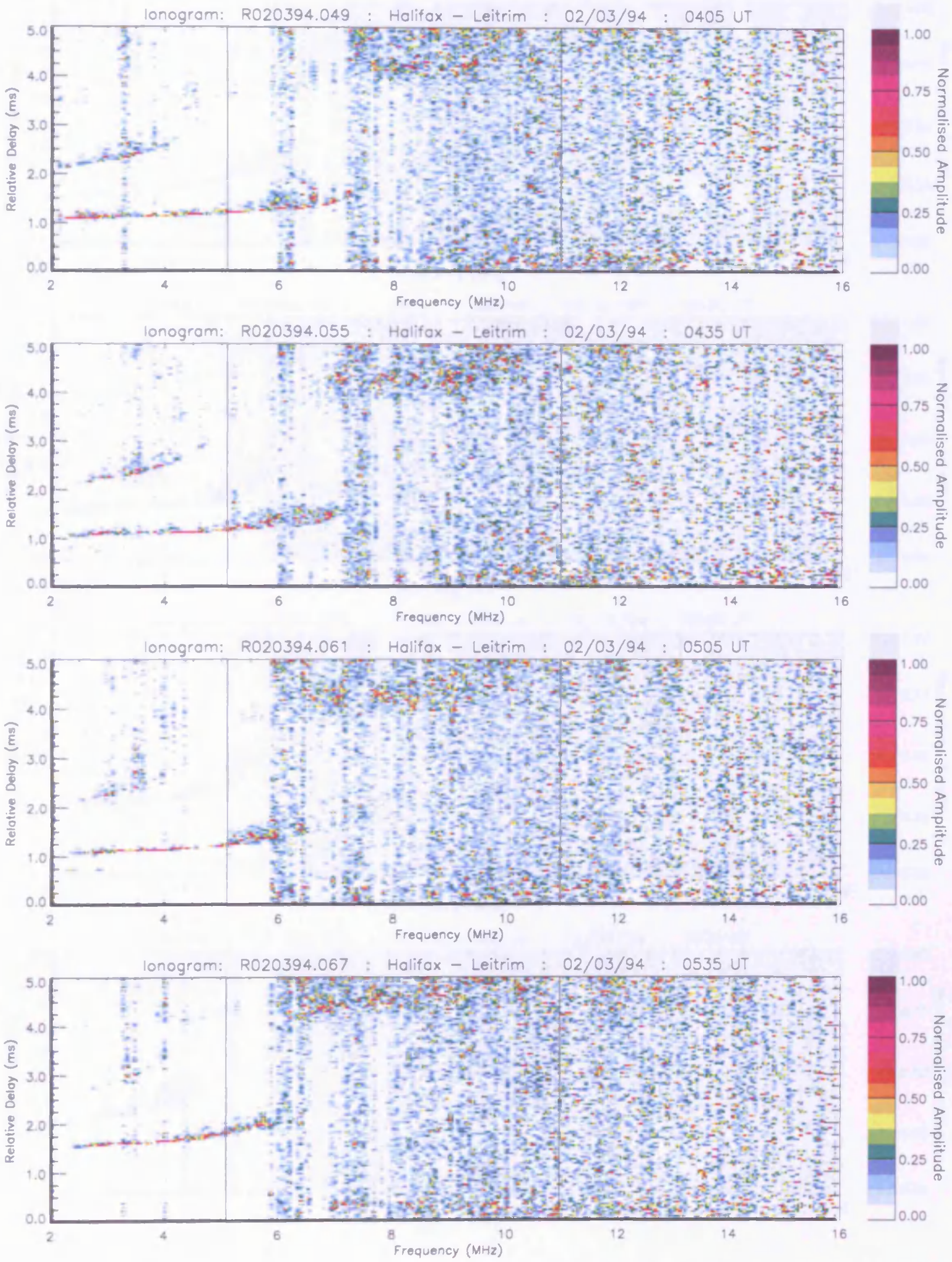

Figure 5.38: Ionogram sequence for Halifax-Leitrim path, 2nd March 1994.

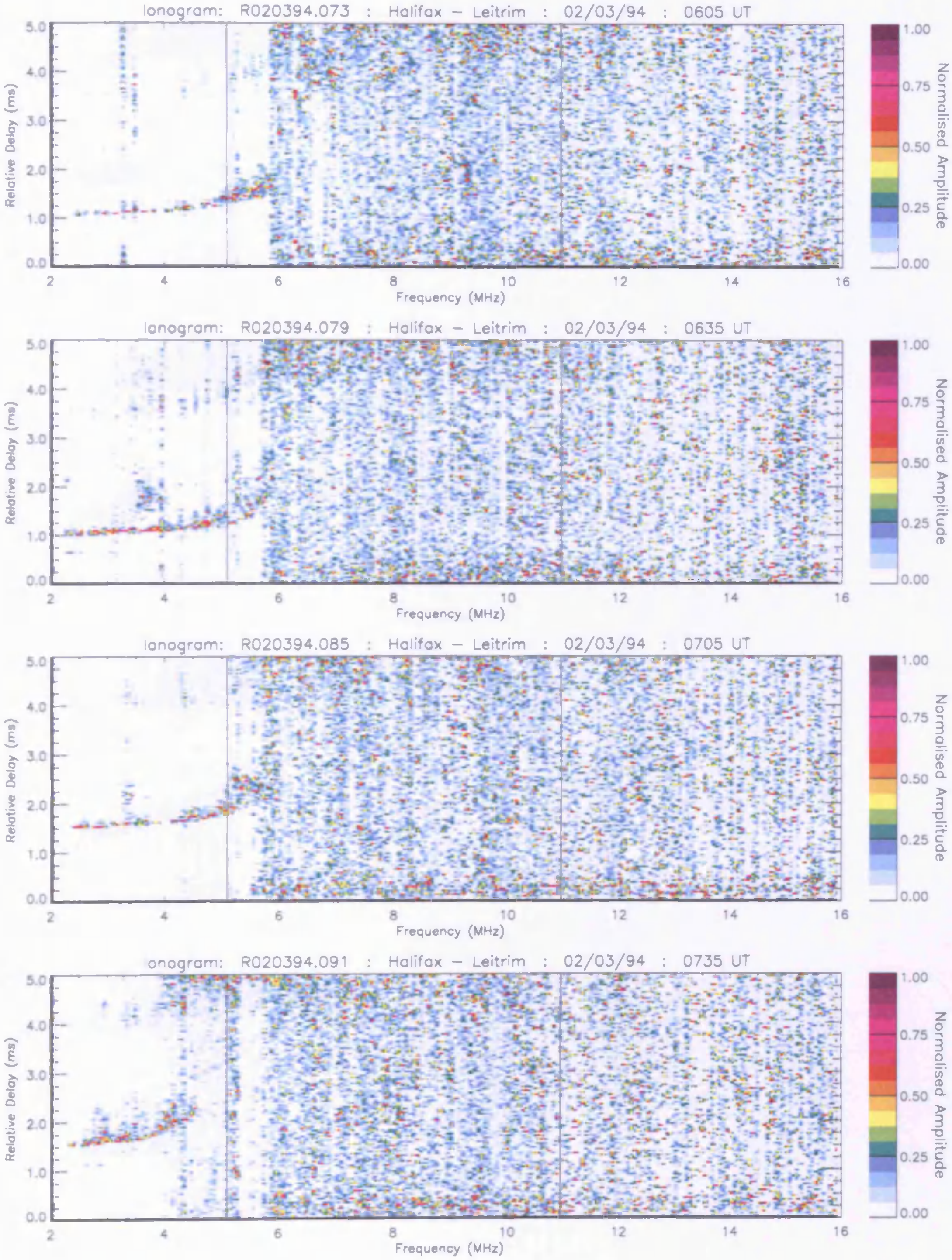

Figure 5.38 (ctd.): Ionogram sequence for Halifax-Leitrim path, 2nd March 1994.

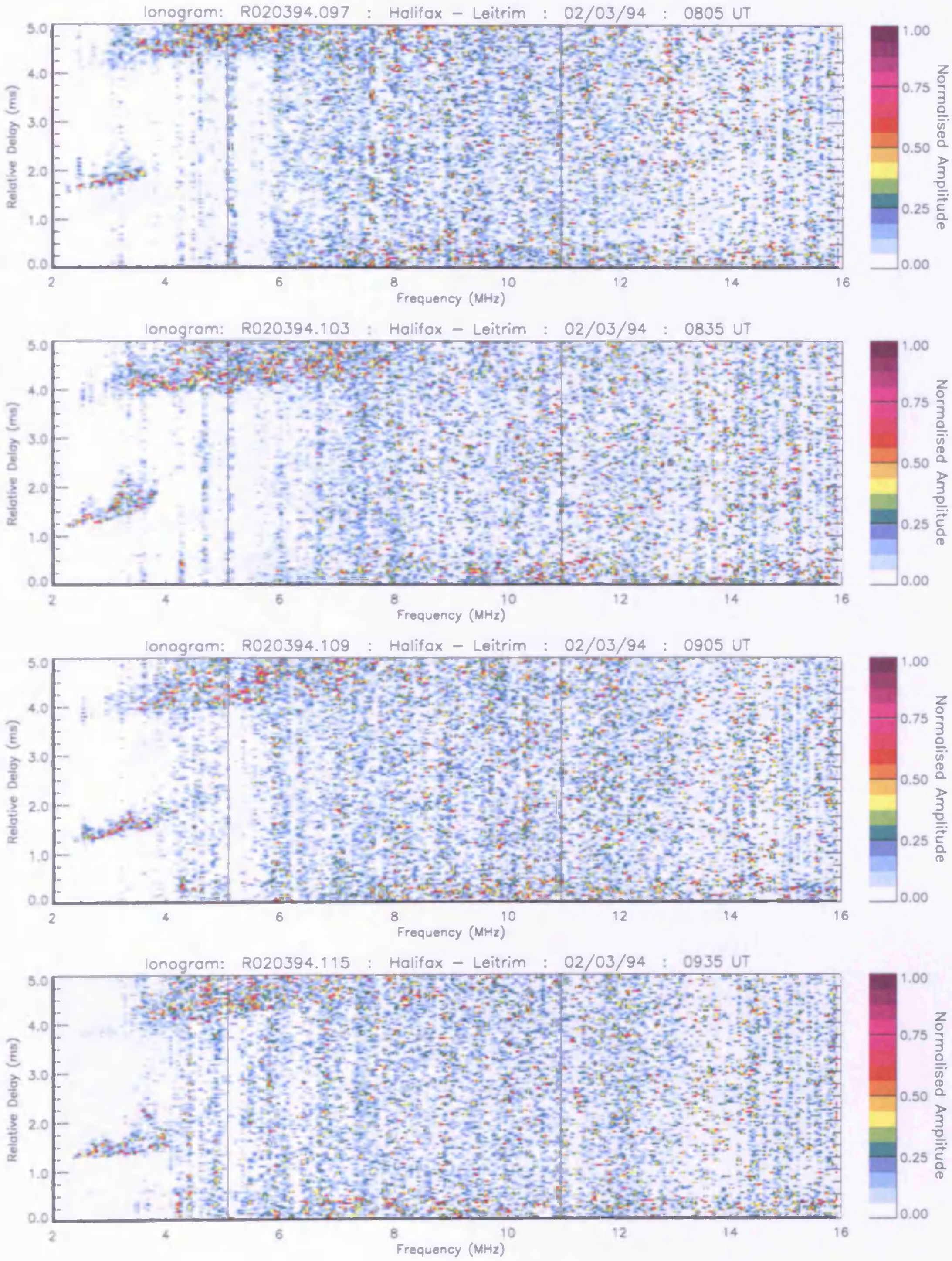

Figure 5.38 (ctd.): Ionogram sequence for Halifax-Leitrim path, 2nd March 1994.

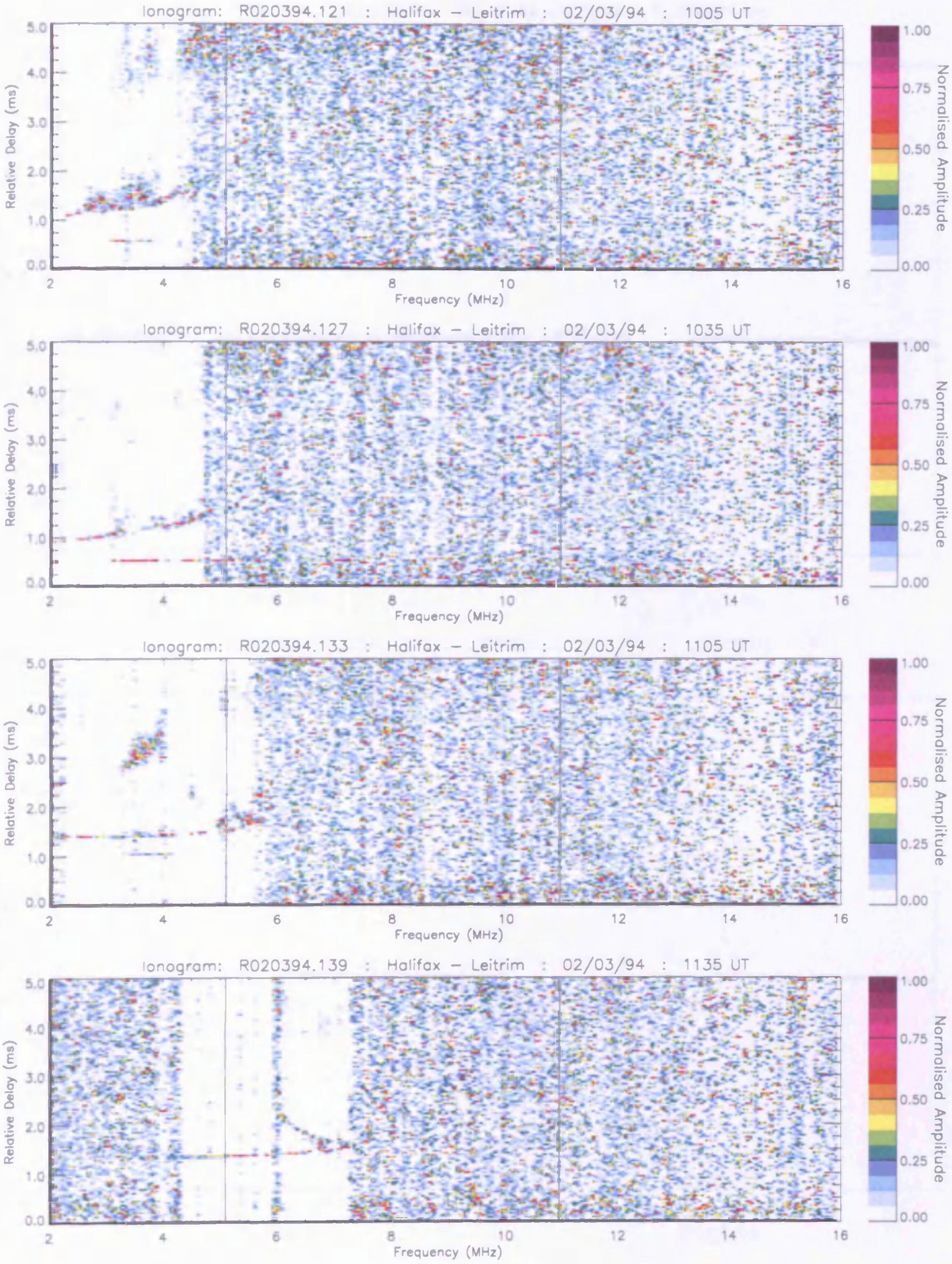

Figure 5.38 (ctd.): Ionogram sequence for Halifax-Leitrim path, 2nd March 1994.

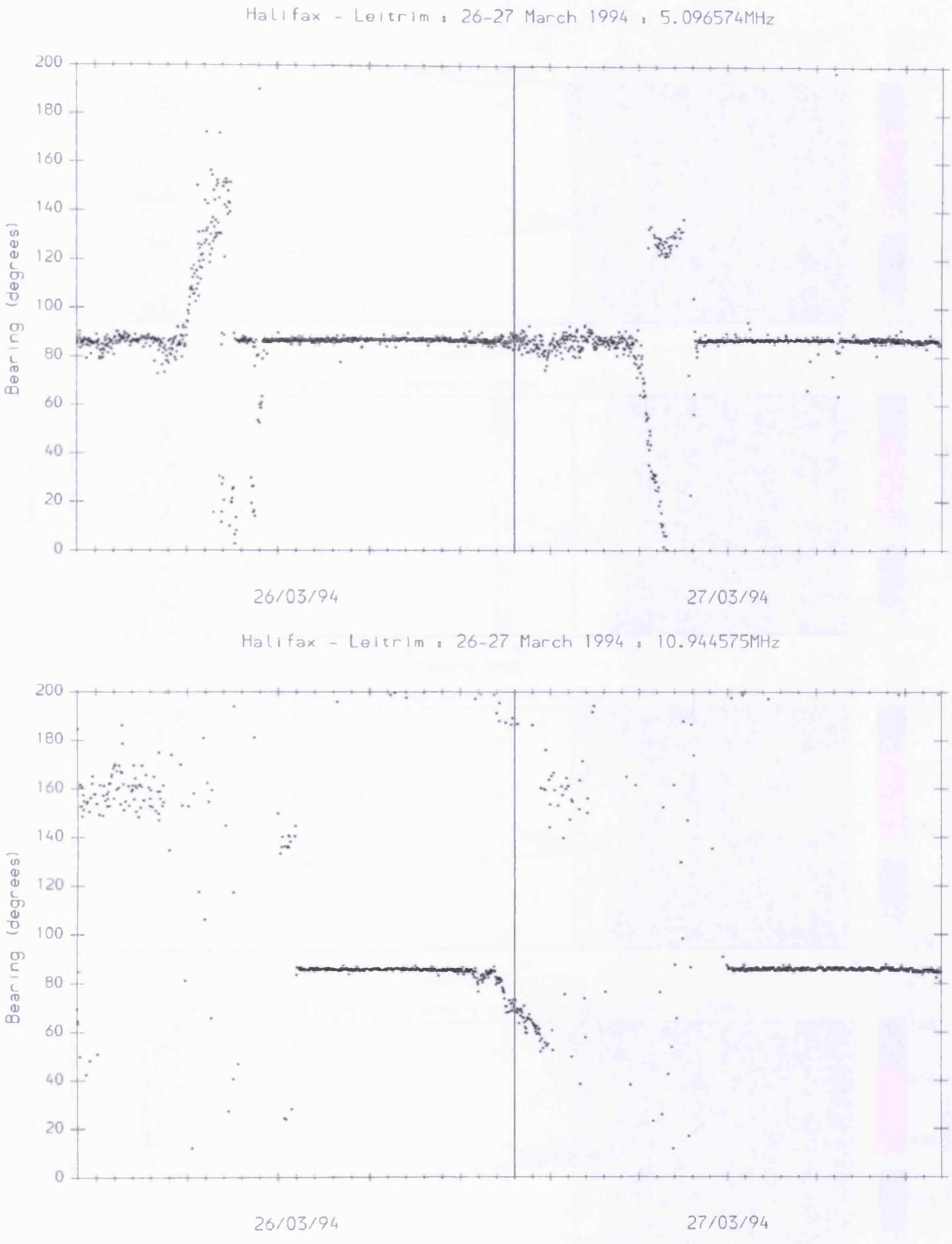

Figure 5.39: Bearings of 5.097MHz and 10.945MHz signals from Halifax to Leitrim on 26th/27th March, 1994.

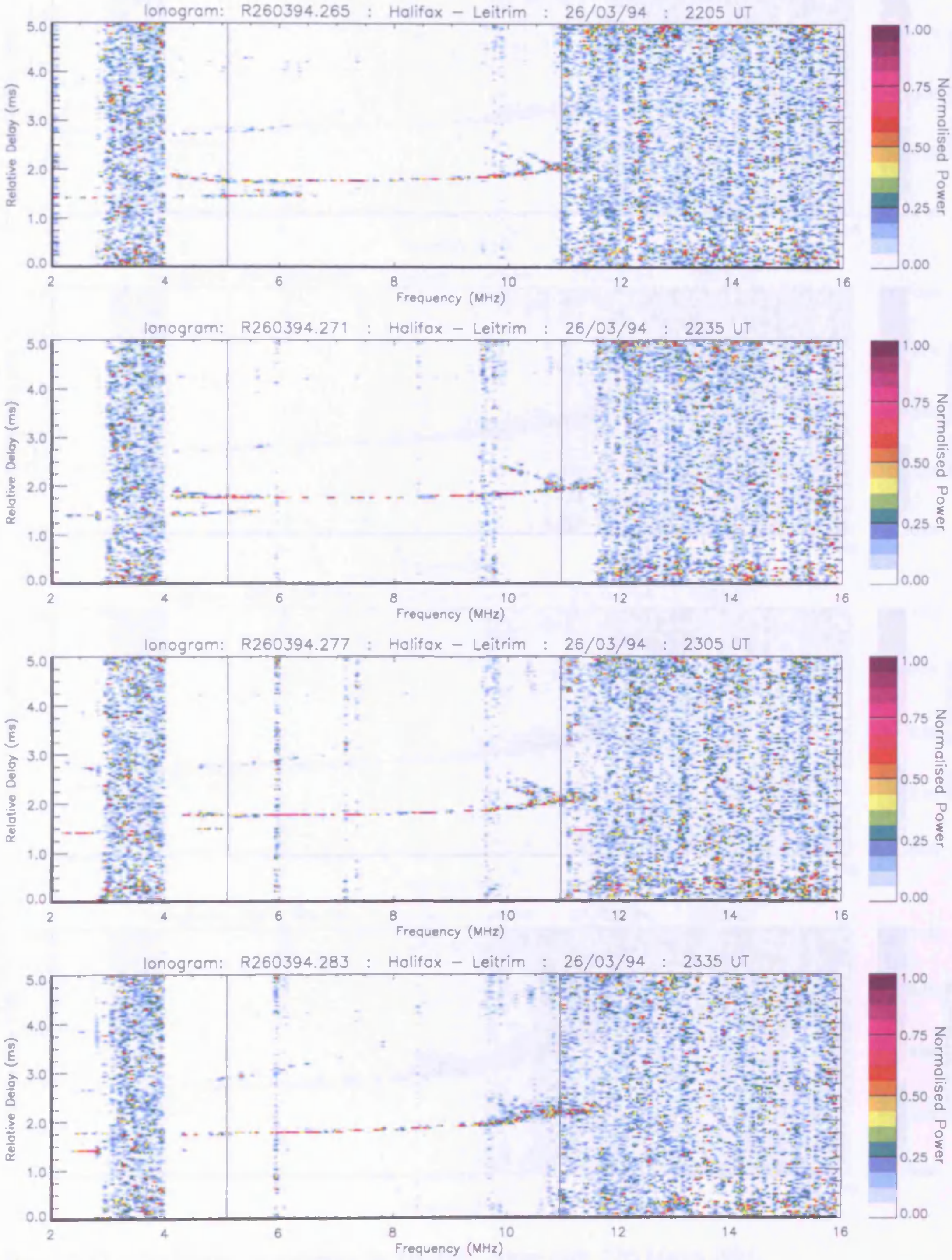

Figure 5.40: Ionogram sequence for Halifax-Leitrim path, 26th March 1994.

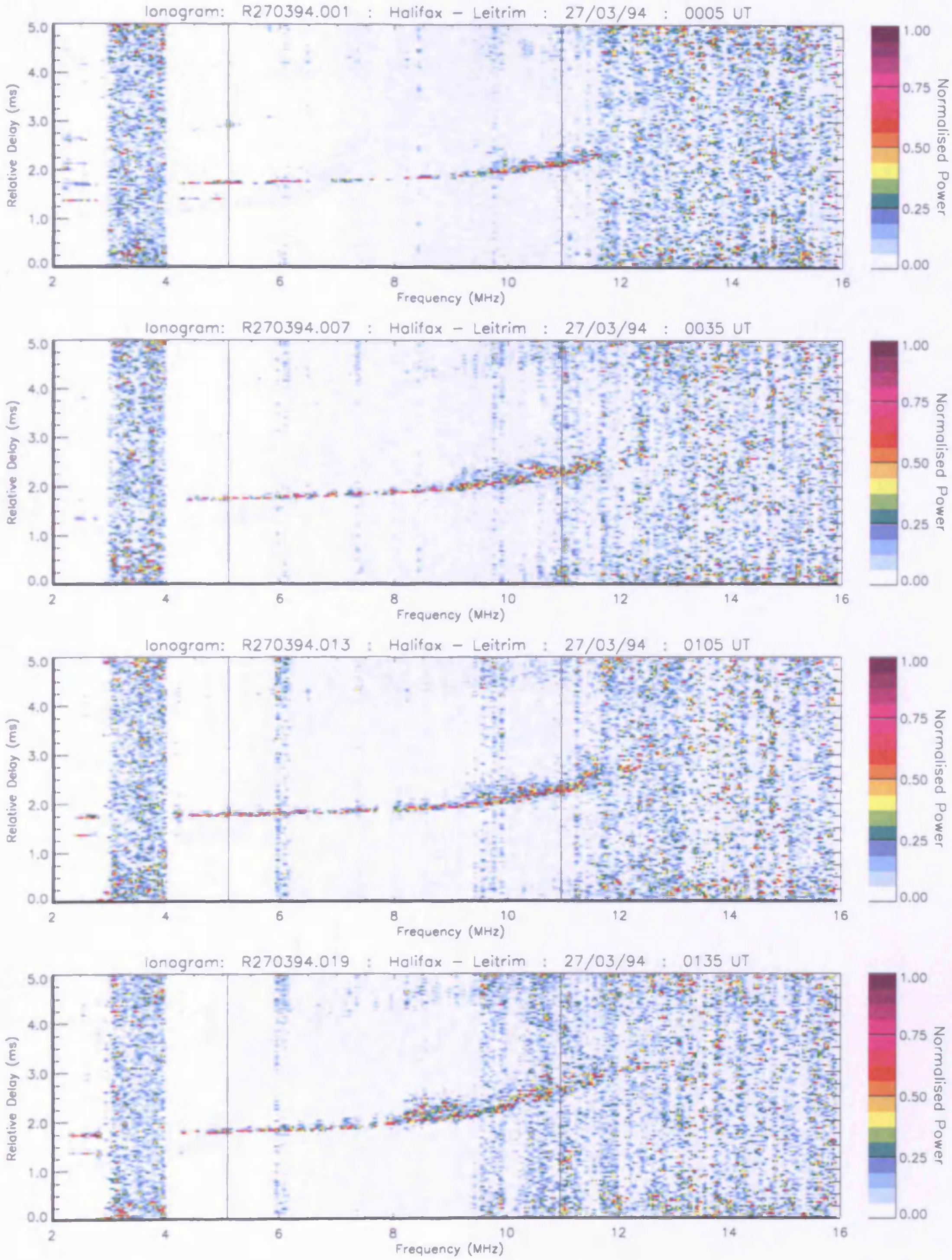

Figure 5.40 (ctd.): Ionogram sequence for Halifax-Leitrim path, 27th March 1994.

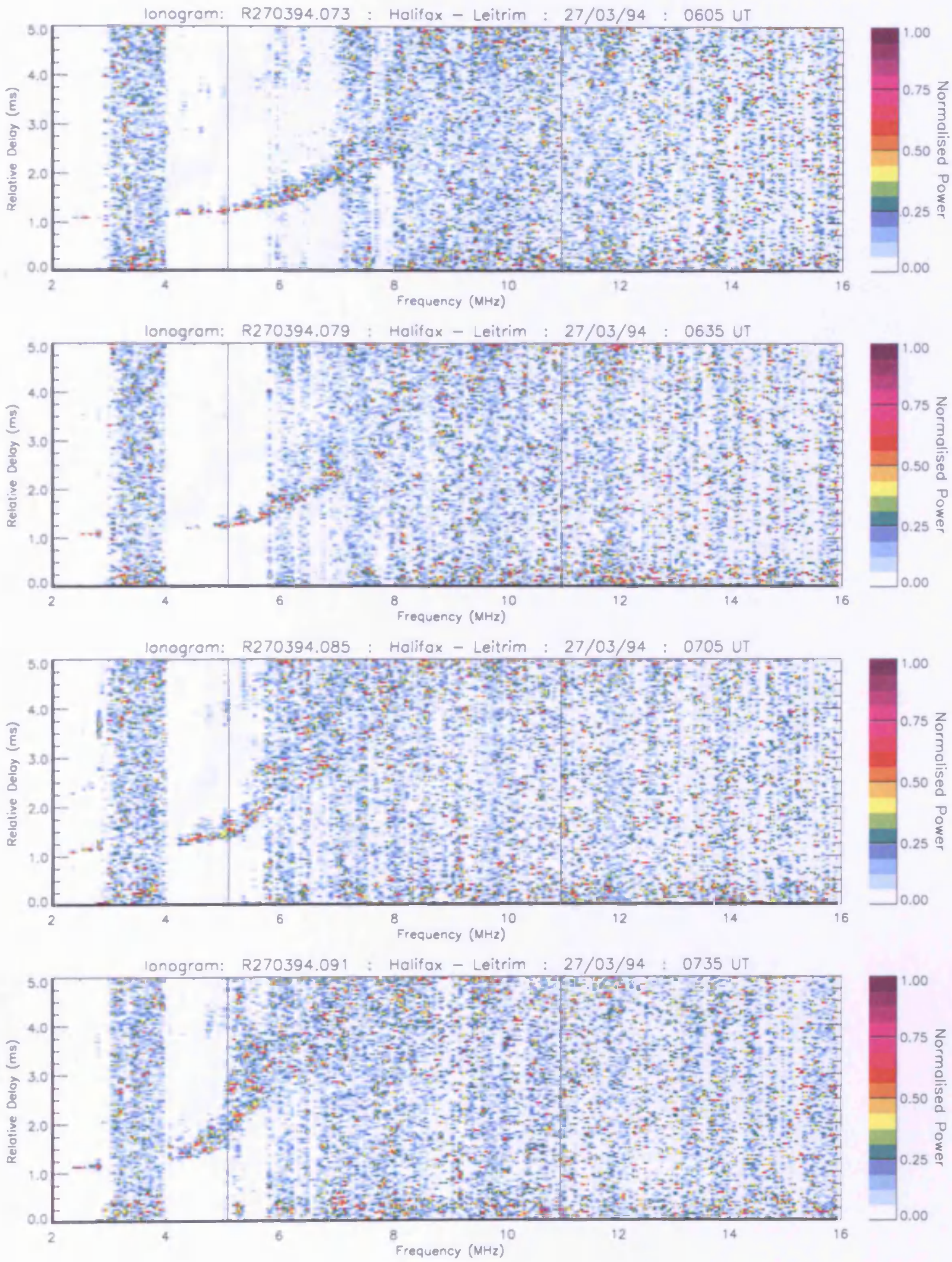

Figure 5.40 (ctd.): Ionogram sequence for Halifax-Leitrim path, 27th March 1994.

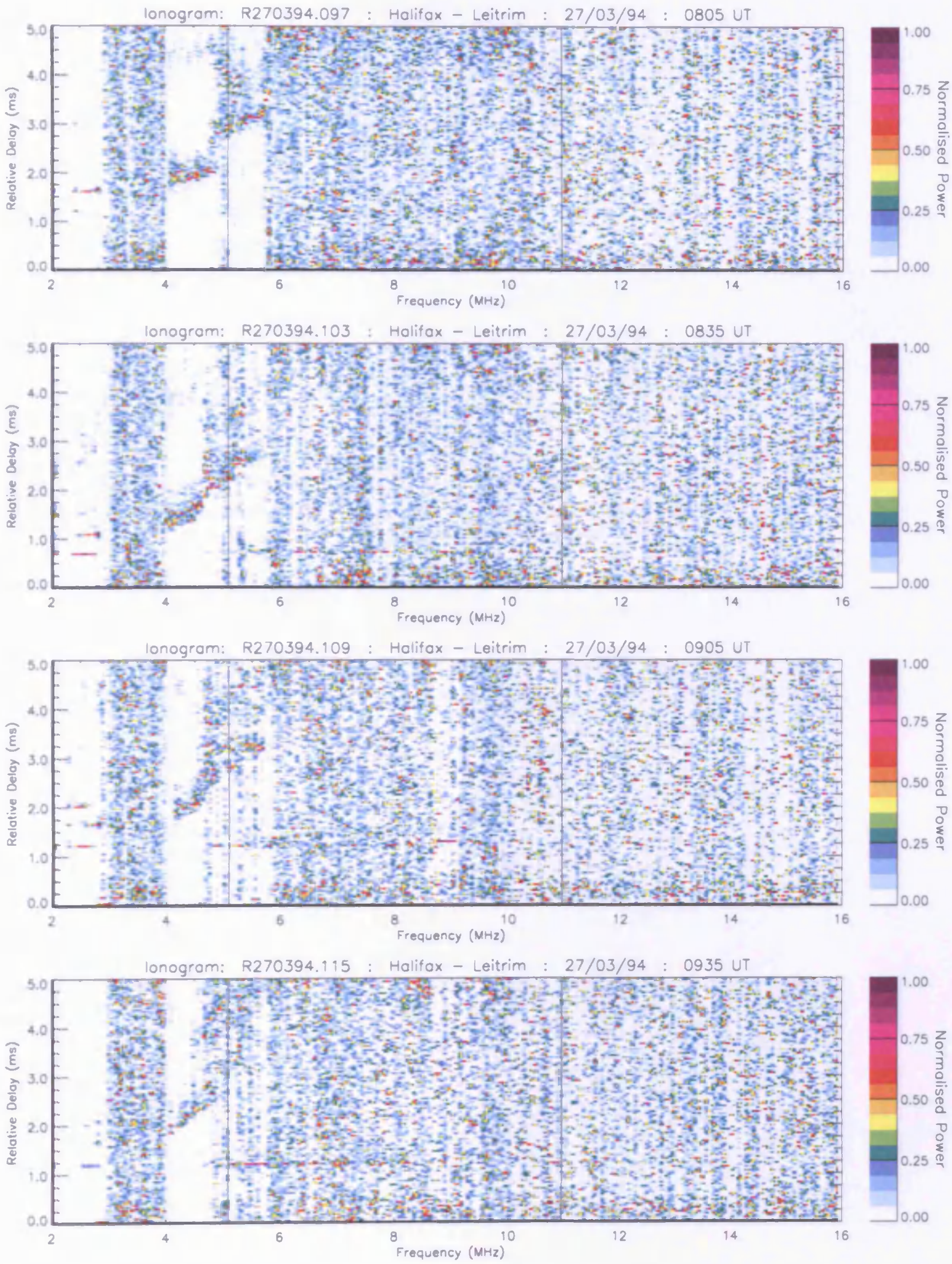

Figure 5.40 (ctd.): Ionogram sequence for Halifax-Leitrim path, 27th March 1994.

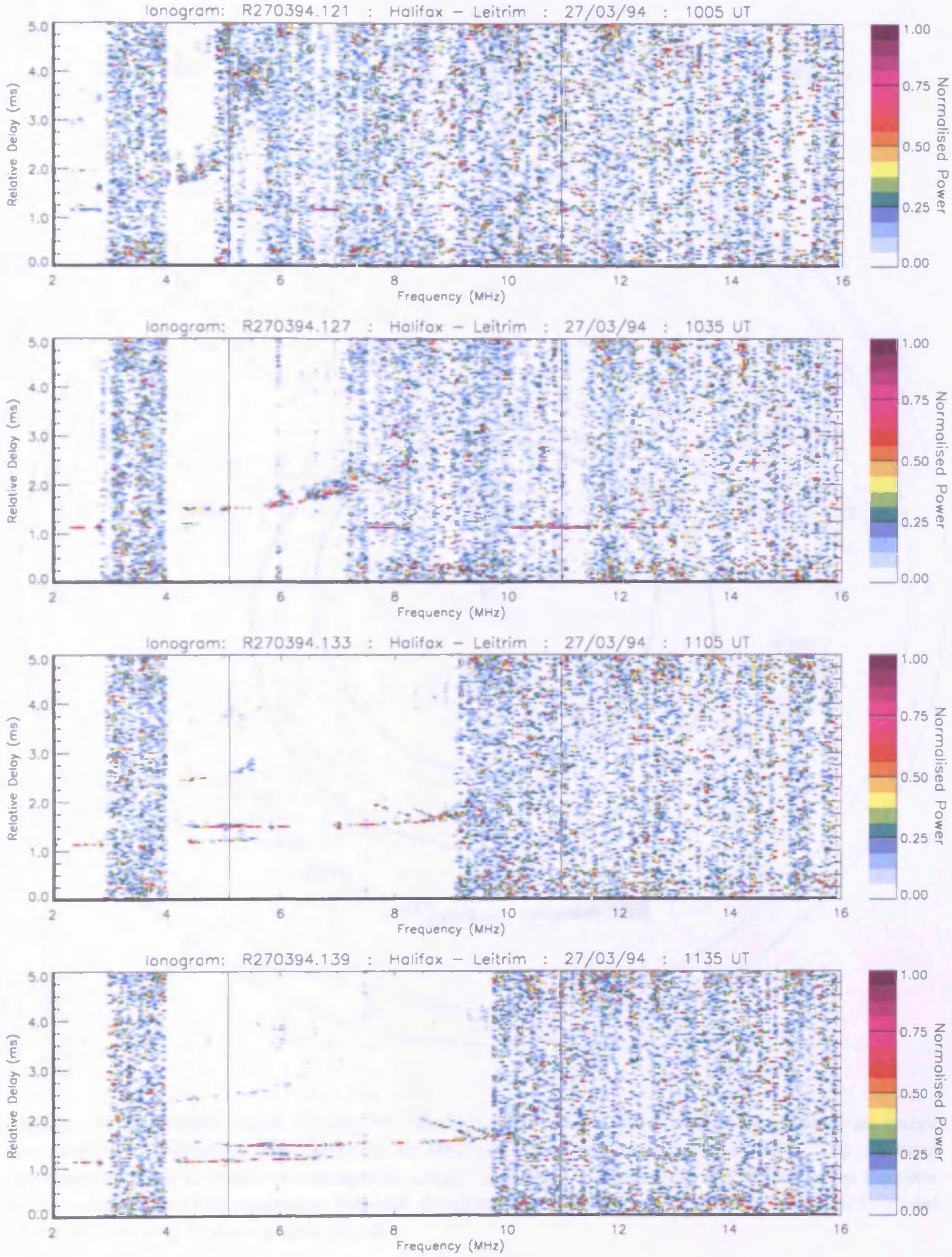

Figure 5.40 (ctd.): Ionogram sequence for Halifax-Leitrim path, 27th March 1994.

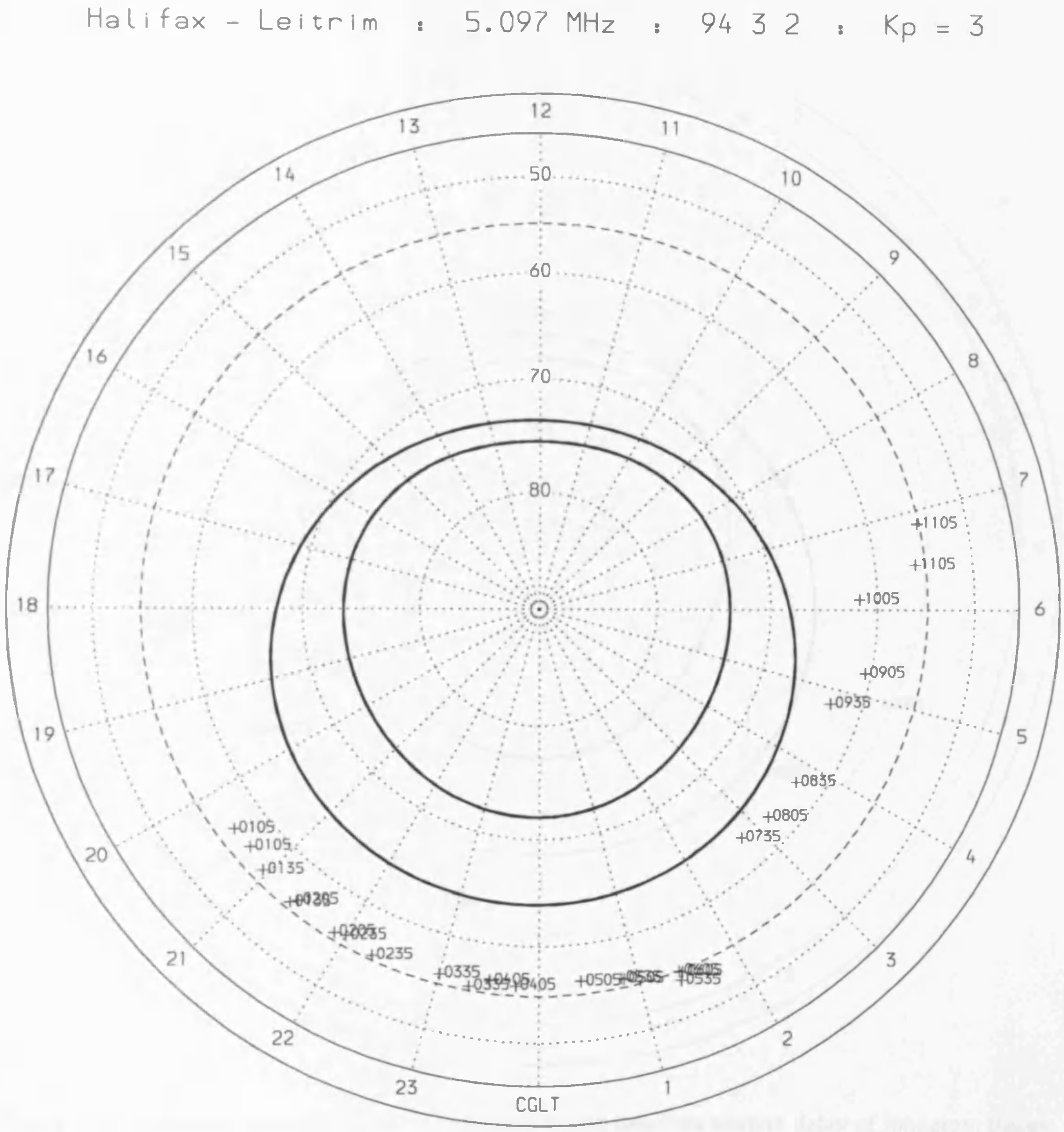

Figure 5.41: Estimated virtual location of reflection region based on relative delay of ionogram traces and associated bearings at 5.097MHz on the Halifax-Leitrim path on 2nd March 1994. The solutions are represented in Corrected Geomagnetic Local Time and CG latitude by a '+' followed by the time (UT). The dashed line represents the path midpoint latitude and the *Holzworth-Meng* [1975] model of the auroral oval location is also shown.

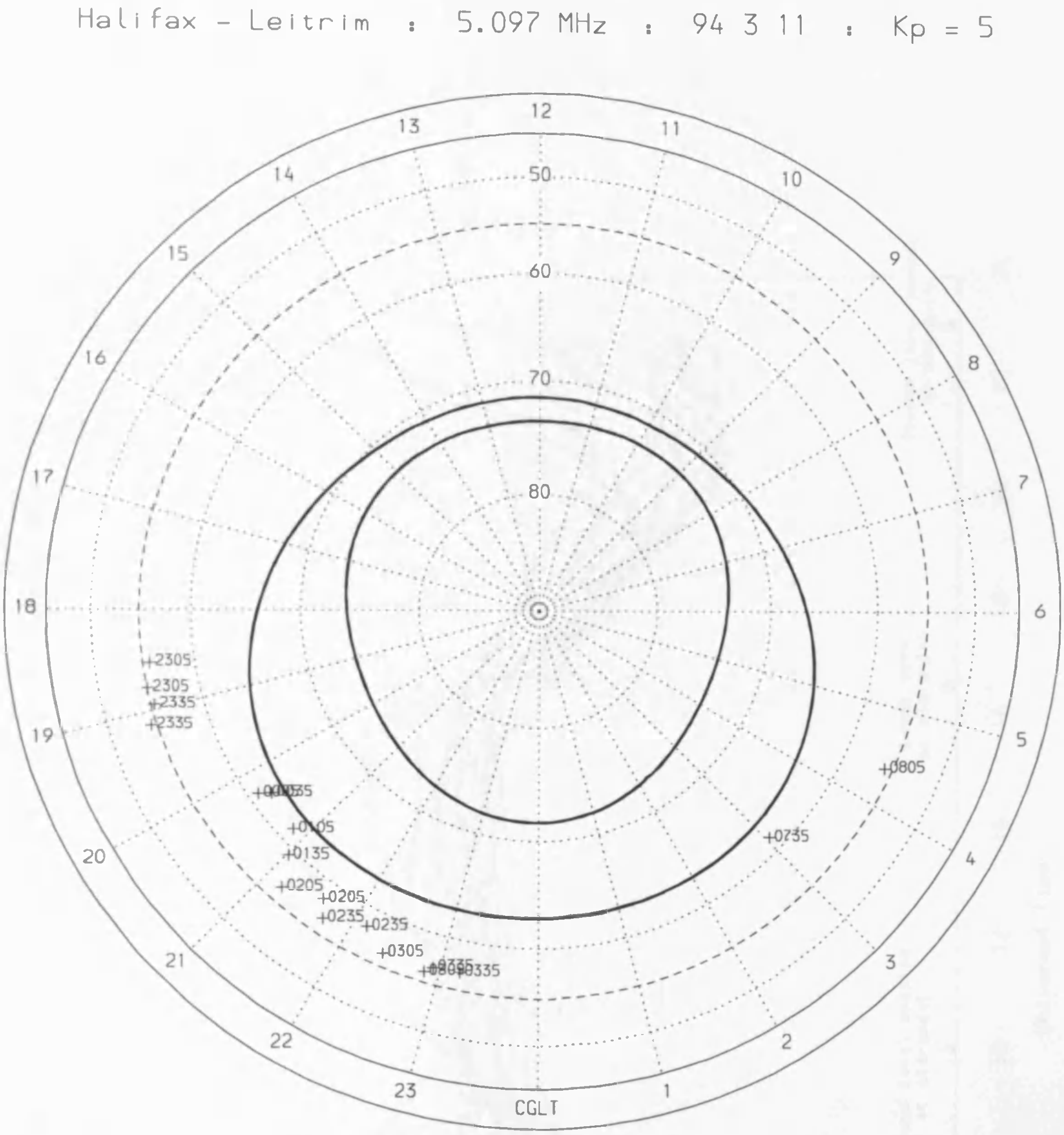

Figure 5.42: Estimated virtual location of reflection region based on relative delay of ionogram traces and associated bearings at 5.097MHz on the Halifax-Leitrim path on 11th March 1994. The solutions are represented in Corrected Geomagnetic Local Time and CG latitude by a '+' followed by the time (UT). The dashed line represents the path midpoint latitude and the *Holzworth-Meng* [1975] model of the auroral oval location is also shown.

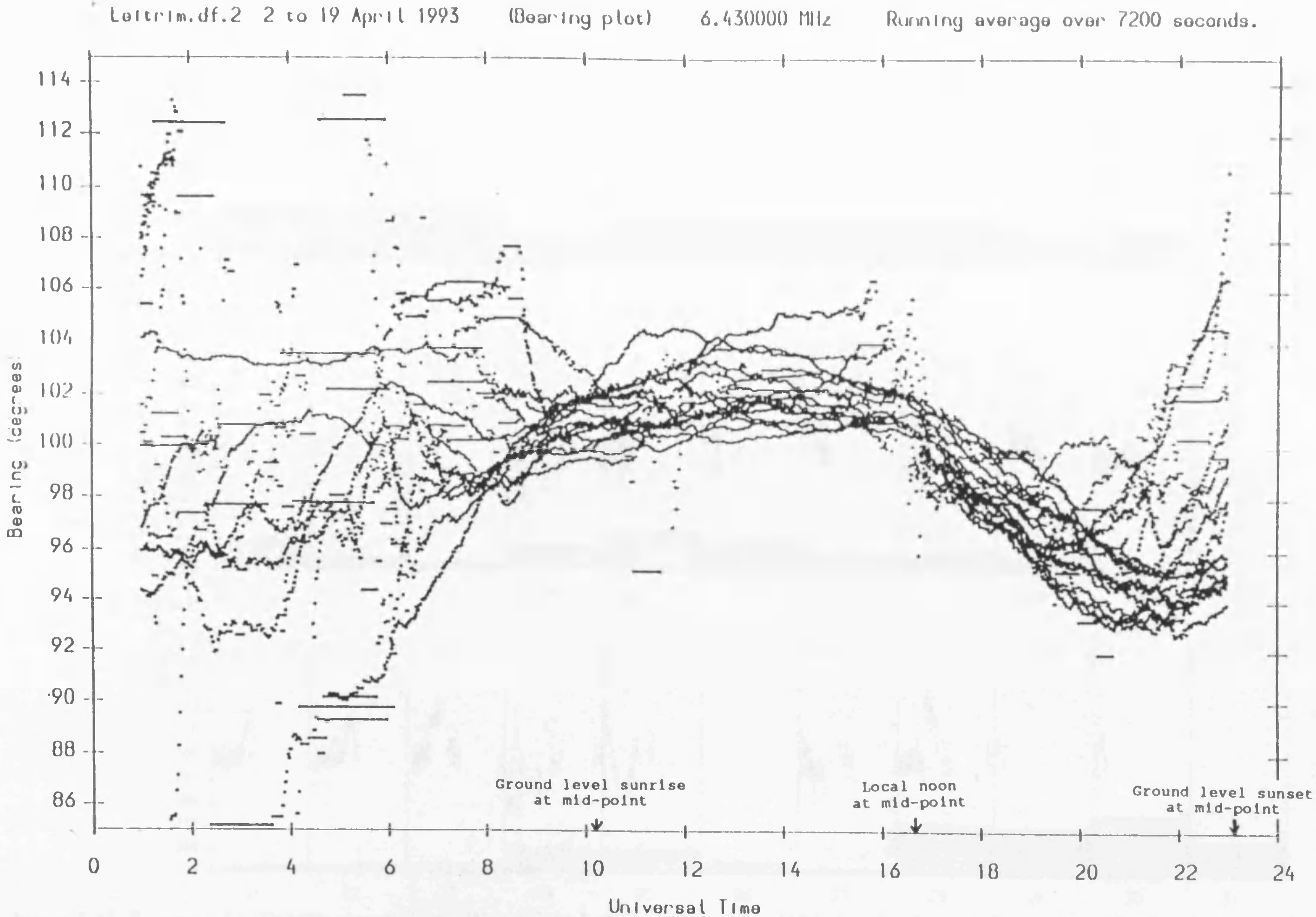

Figure 5.43: Bearings of the 6.43MHz signal from Halifax to Leitrim in April 1993, displaying systematical diurnal variations. The bearings shown are 2 hour, running averages.

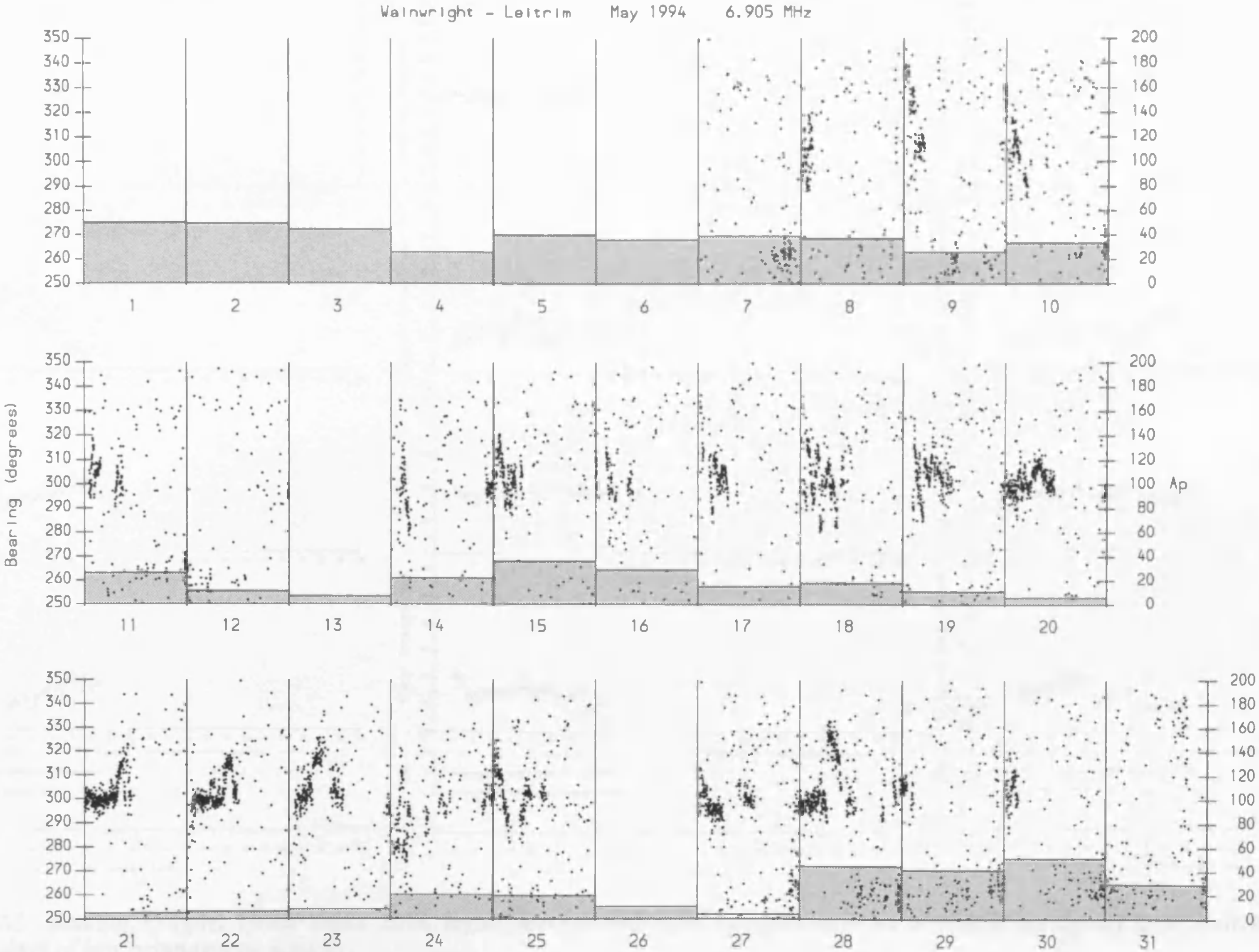

Figure 5.44: Bearings of 6.905MHz signals on the Wainwright-Leitrim path for May 1994. Vertical lines indicate 00:00 UT. The shaded bars indicate Ap index.

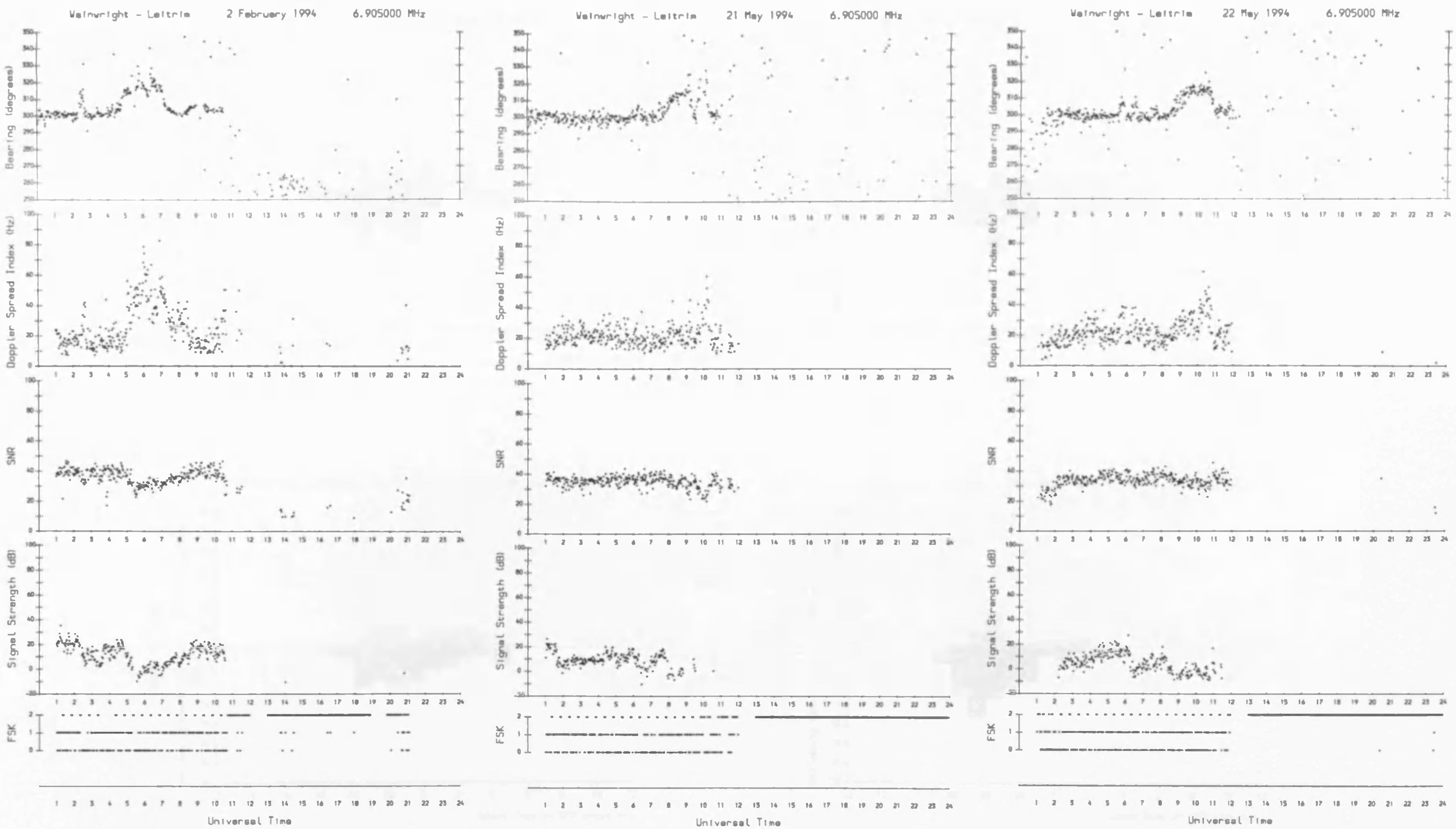

Figure 5.45: Bearing, Doppler spread index, SNR, signal strength and signal recognition index of 6.905MHz signals from Wainwright to Leitrim for three days of low geomagnetic activity.

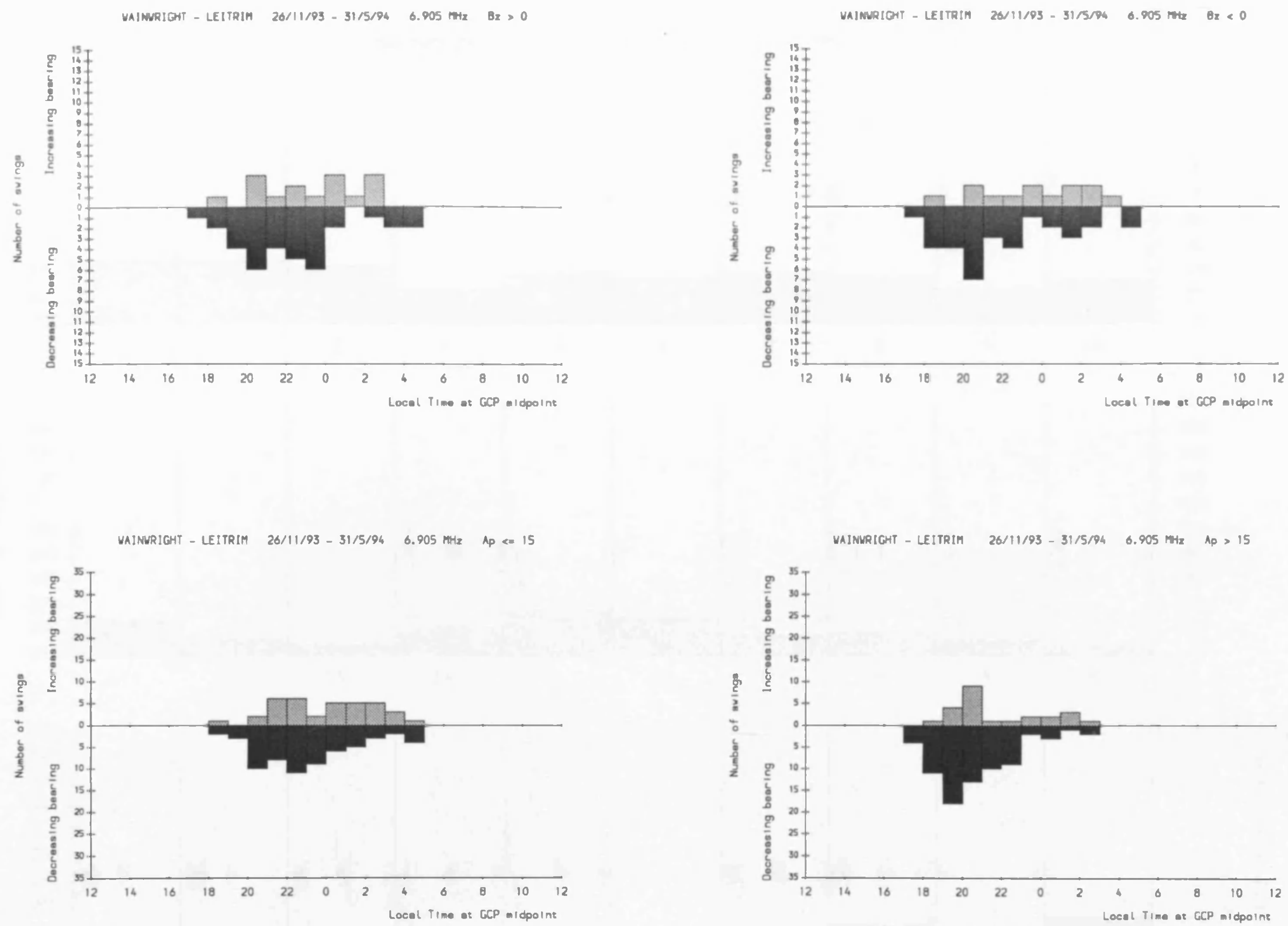

Figure 5.46: Number of swings in the bearing for each LT hour (at GCP midpt) on 6.905MHz signals from Wainwright to Leitrim for the period 26/11/93 - 31/5/94. Measurements are divided according to whether the bearings increased (light bars) or decreased (dark bars) with time for IMF Bz +ve (top left) or -ve (top right) or Ap<=15 (bottom left) or Ap>15 (bottom right).

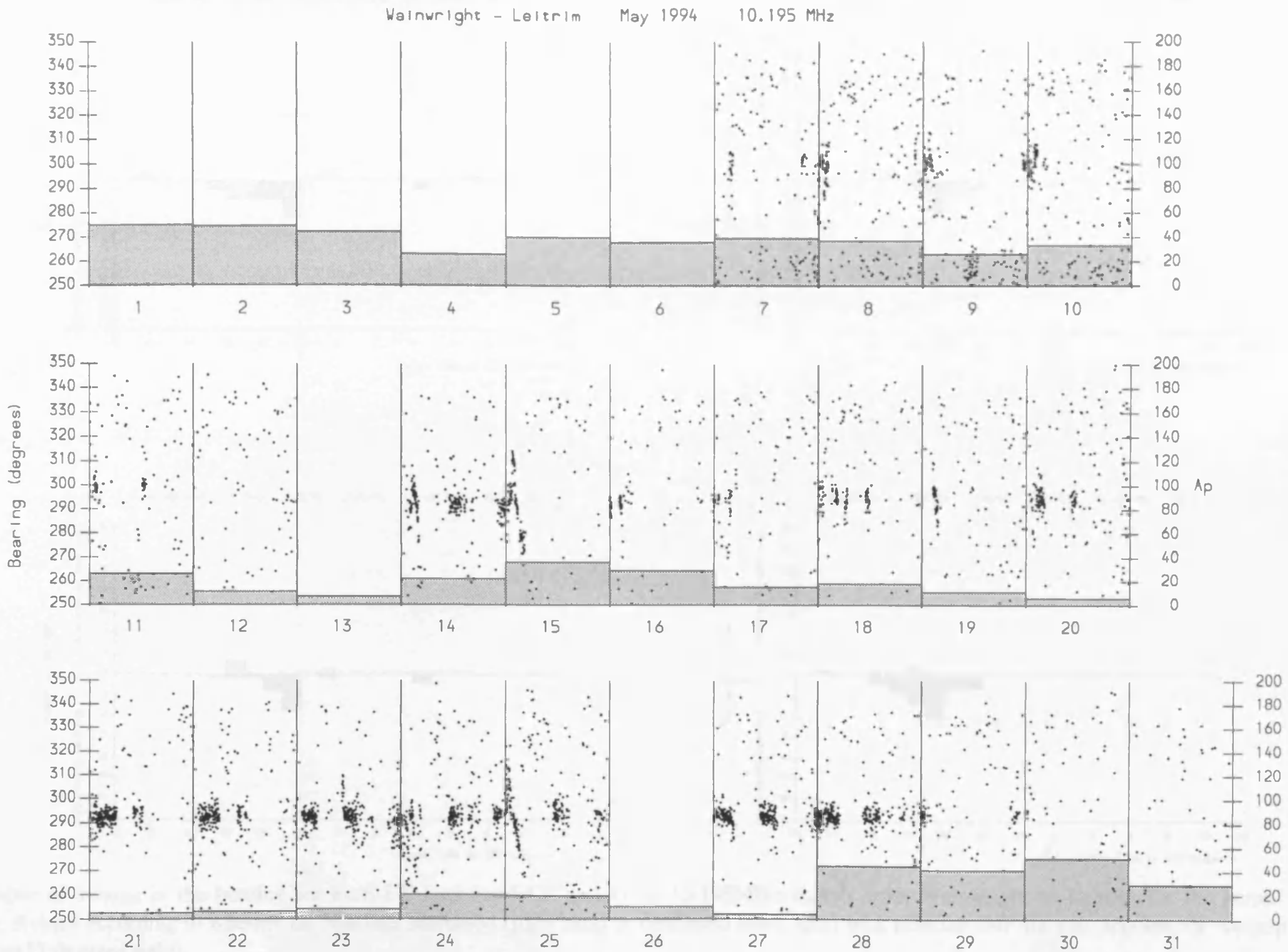

Figure 5.47: Bearings of 10.195MHz signals on the Wainwright-Leitrim path for May 1994. Vertical lines indicate 00:00 UT. The shaded bars indicate Ap index.

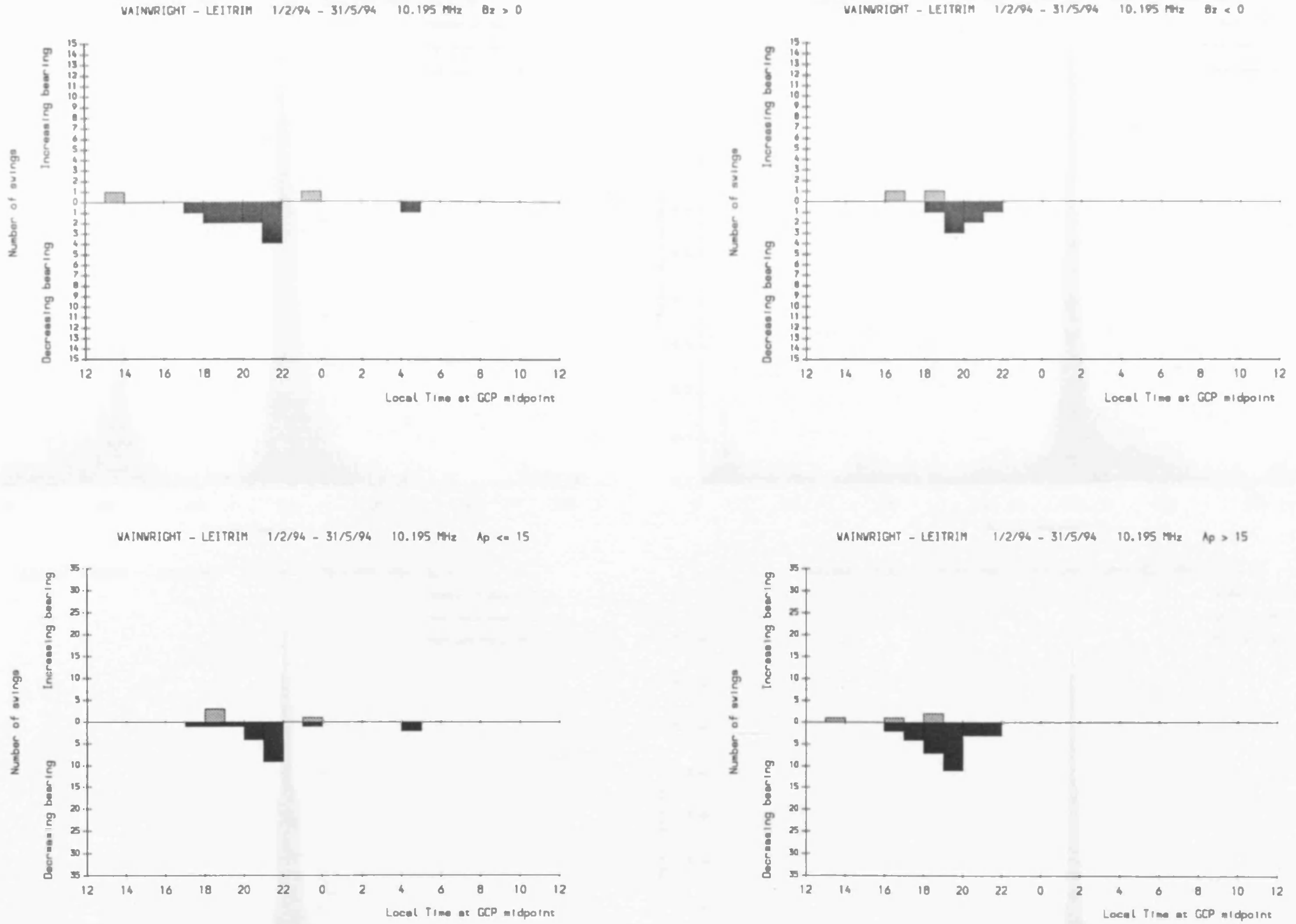

Figure 5.48: Number of swings in the bearing for each LT hour (at GCP midpt) on 10.195MHz signals from Wainwright to Leitrim for the period 1/2/94 - 31/5/94. Measurements are divided according to whether the bearings increased (light bars) or decreased (dark bars) with time for IMF Bz +ve (top left) or -ve (top right) or Ap<=15 (bottom left) or Ap>15 (bottom right).

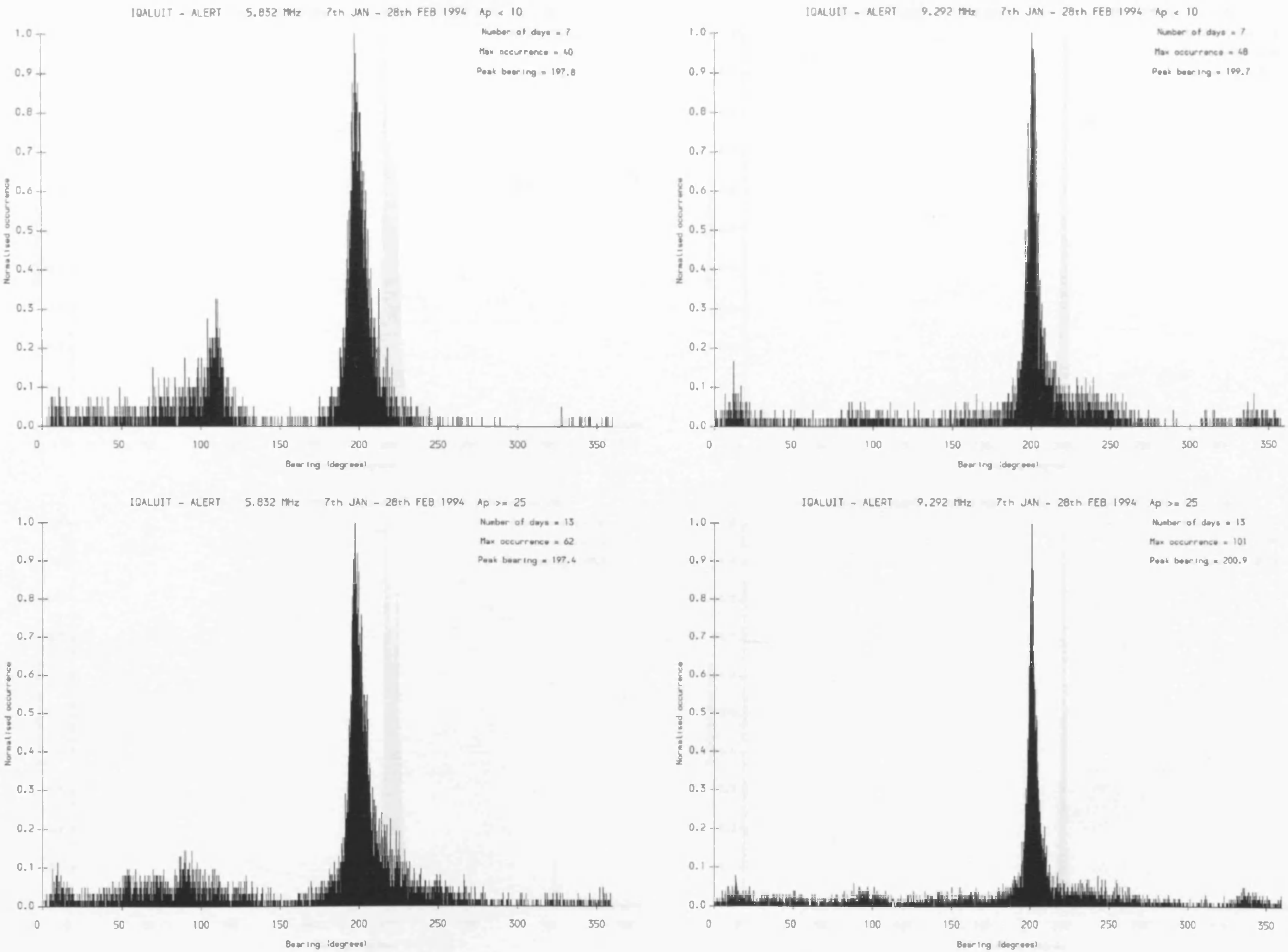

Figure 6.1: Histograms of the normalised occurrence of bearings measured on the Iqaluit-Alert path at 5.832 MHz (left) and 9.292MHz (right) during the period 7[th] Jan- 28[th] Feb 1994 for Ap < 10 (top) and Ap >= 25 (bottom).

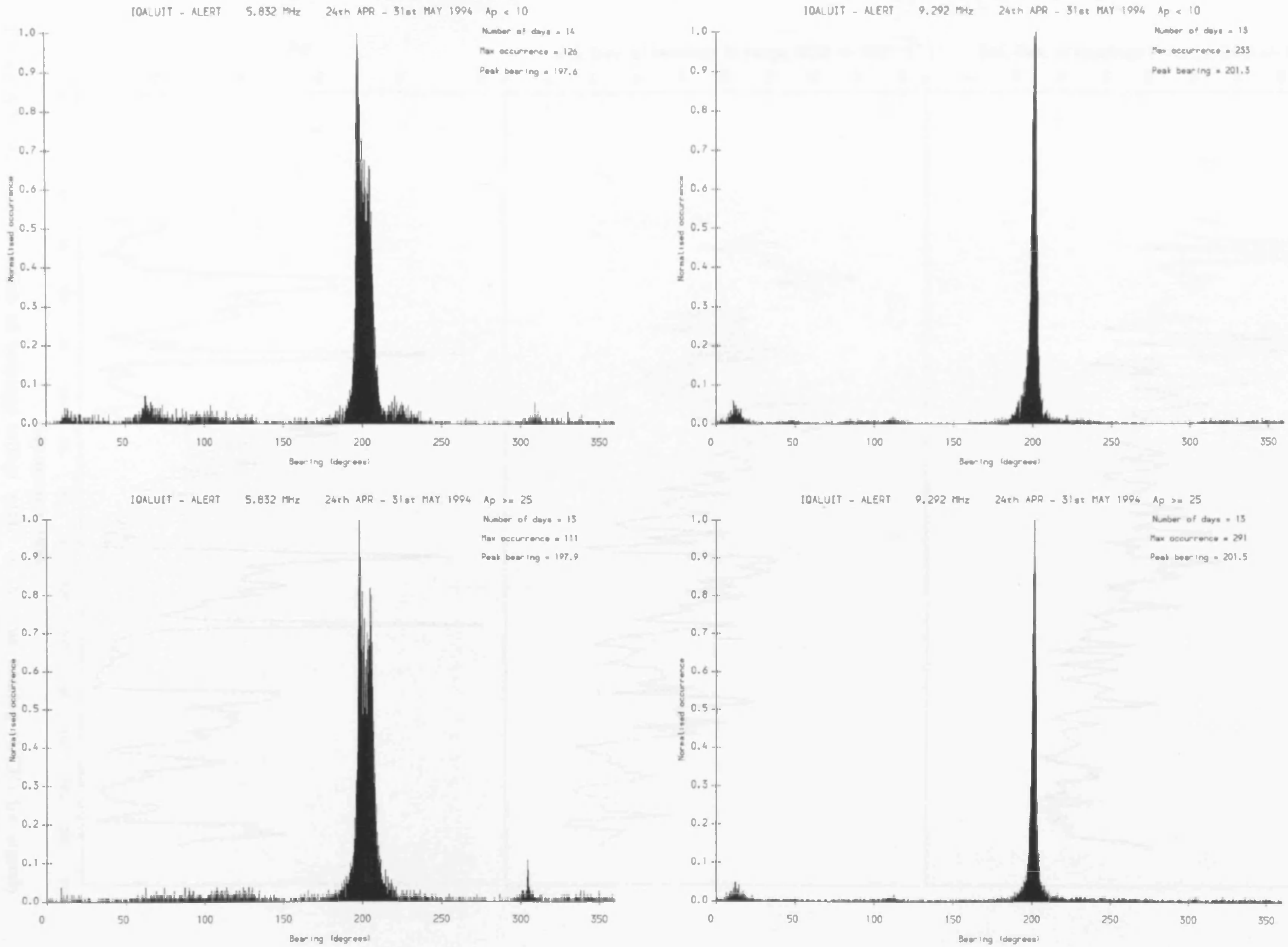

Figure 6.2: Histograms of the normalised occurrence of bearings measured on the Iqaluit-Alert path at 5.832 MHz (left) and 9.292MHz (right) during the period 24th April – 31st May, 1994 for Ap < 10 (top) and Ap >= 25 (bottom).

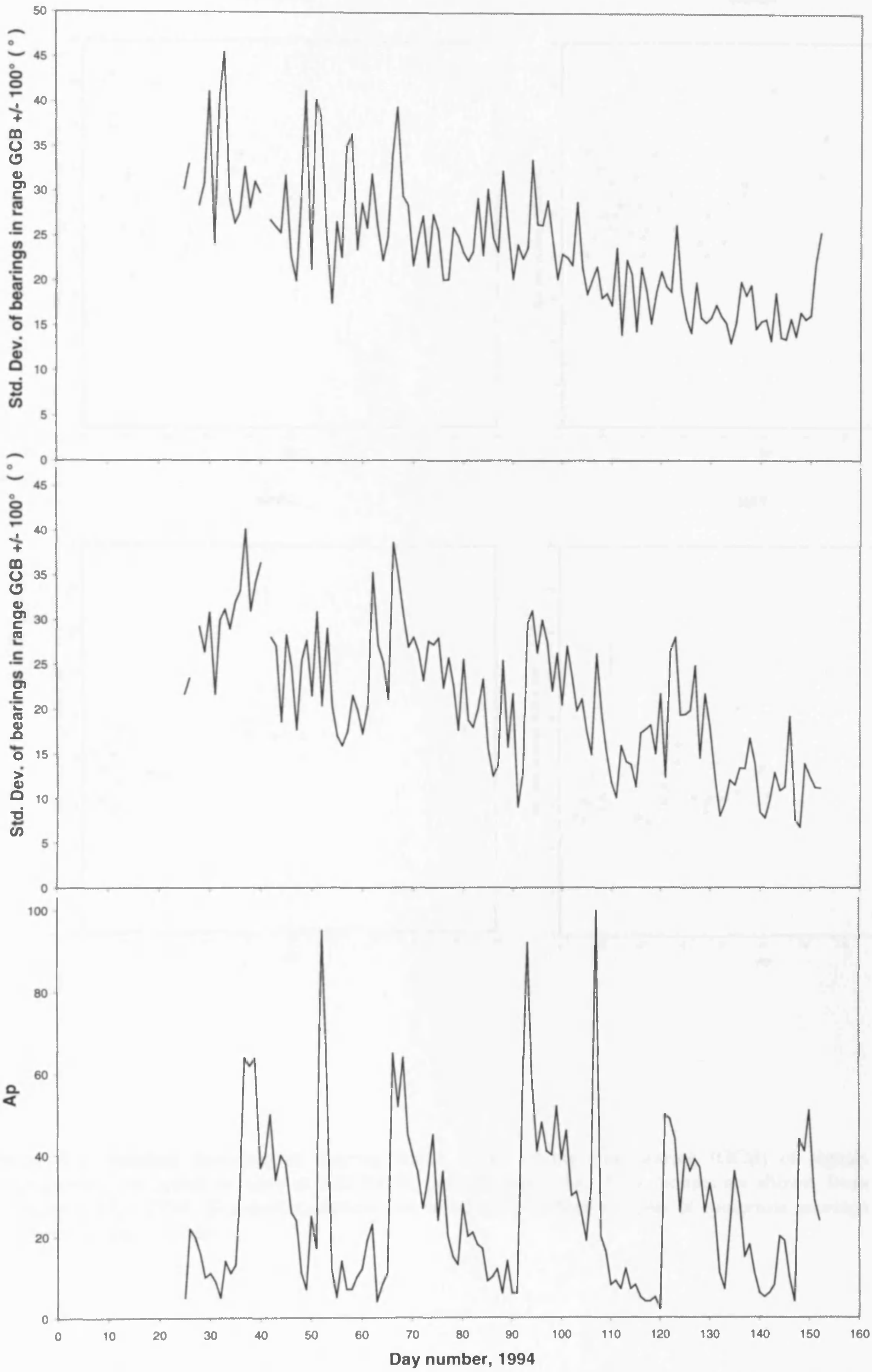

Figure 6.3: Standard deviation of bearings within ±100° of the true bearing (GCB) for signals propagating from Iqaluit to Alert at (a) 5.832MHz (top panel) and (b) 9.292MHz (middle panel) plotted against the day number in 1994. Standard deviations are based upon 24-hour samples of composite bearings measured for each UT day. The bottom panel (c) provides the Ap for each day for comparison.

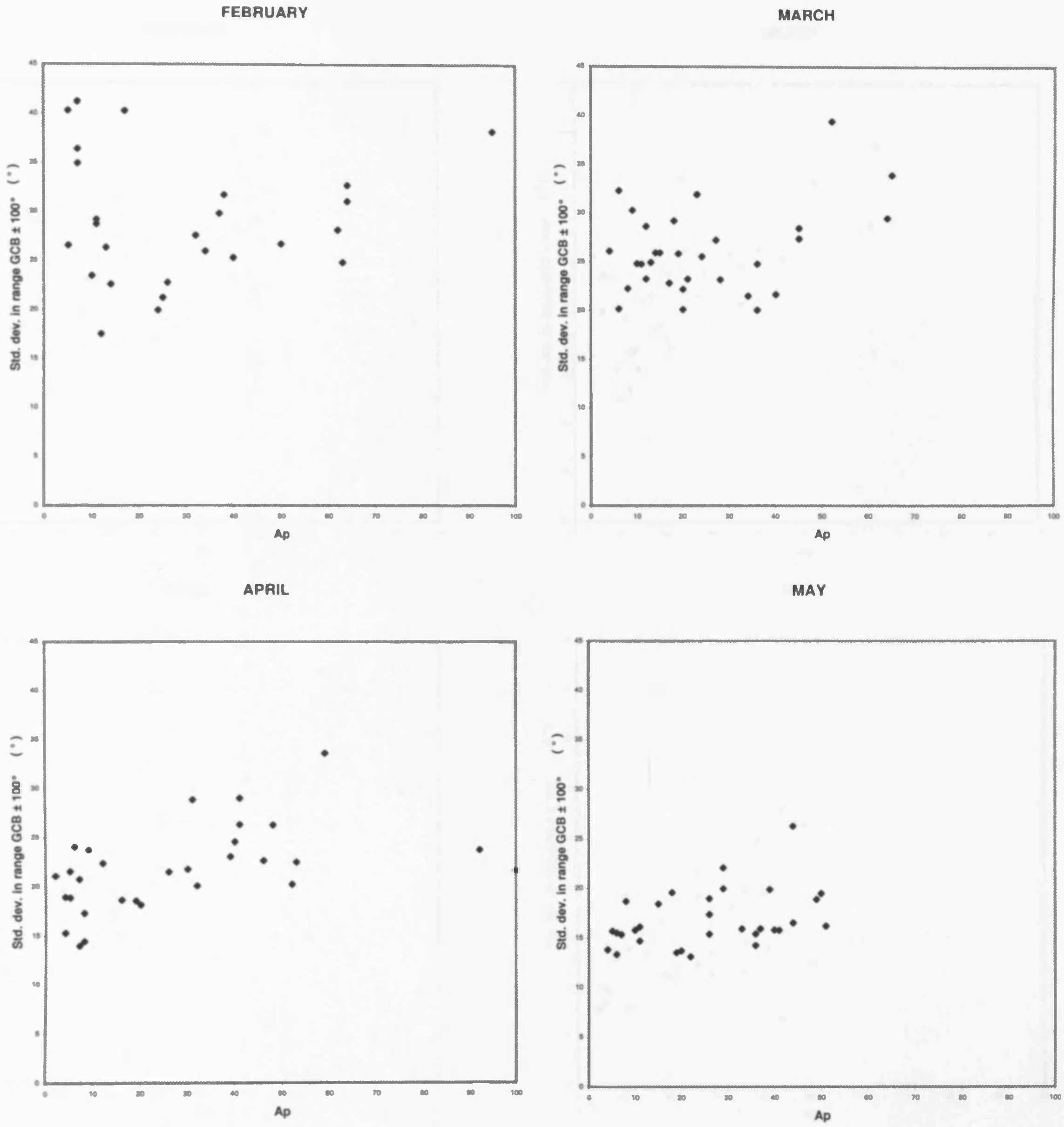

Figure 6.4: Standard deviation of bearing within ±100° of the true bearing (GCB) of signals propagating from Iqaluit to Alert at 5.832MHz, plotted against Ap. Four months are shown, from February to May 1994. Standard deviations are based upon 24-hour samples of composite bearings measured for each UT day.

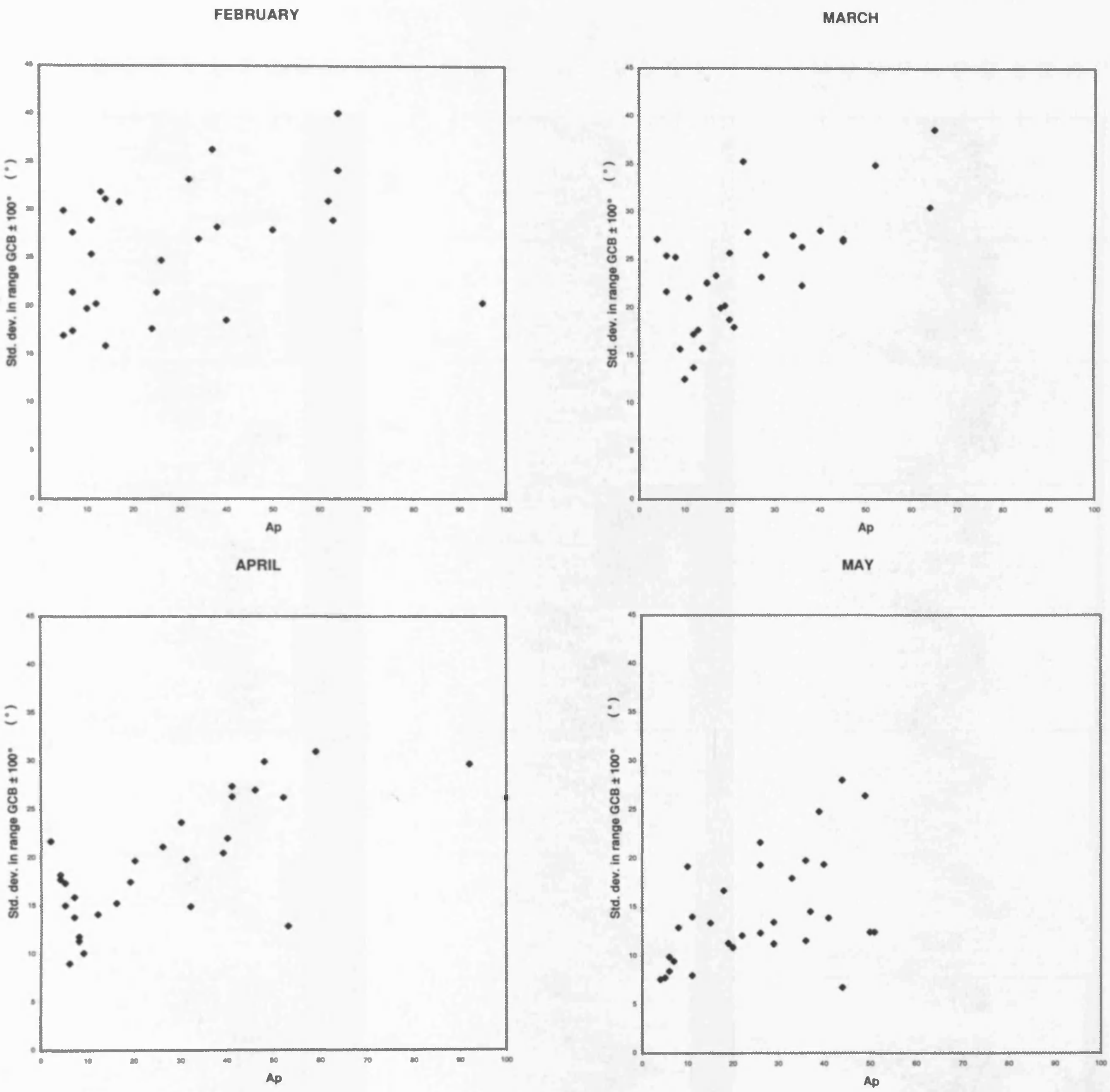

Figure 6.5: Standard deviation of bearing within ±100° of the true bearing (GCB) of signals propagating from Iqaluit to Alert at 9.232MHz, plotted against Ap. Four months are shown, from February to May 1994. Standard deviations are based upon 24-hour samples of composite bearings measured for each UT day.

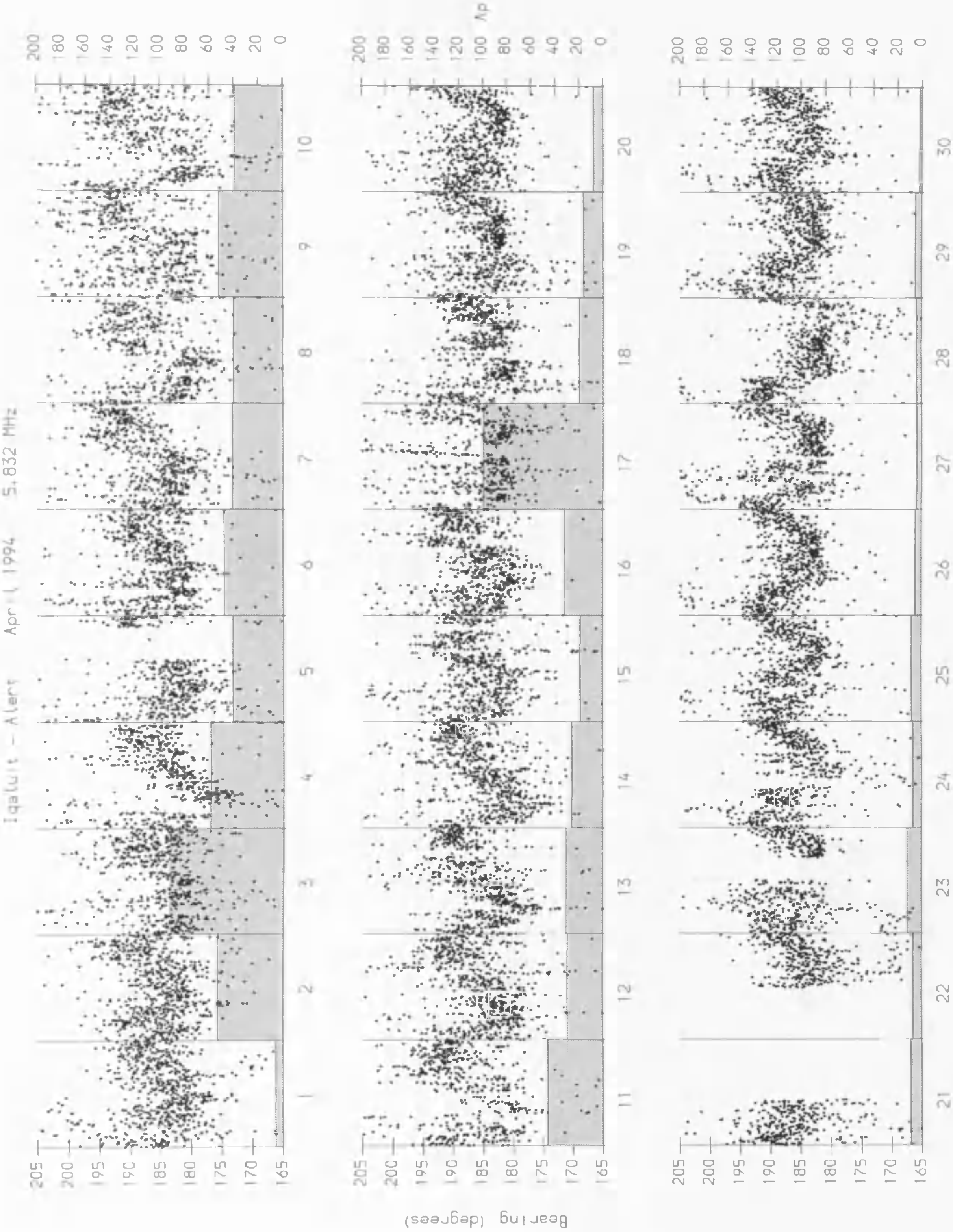

Figure 6.6: Bearings of 5.832 MHz signals on the Iqaluit-Alert path for April 1994. Vertical lines indicate 00:00 UT. The shaded bars indicate Ap index. The bearing scale is expanded to highlight the diurnal trend in the bearings.

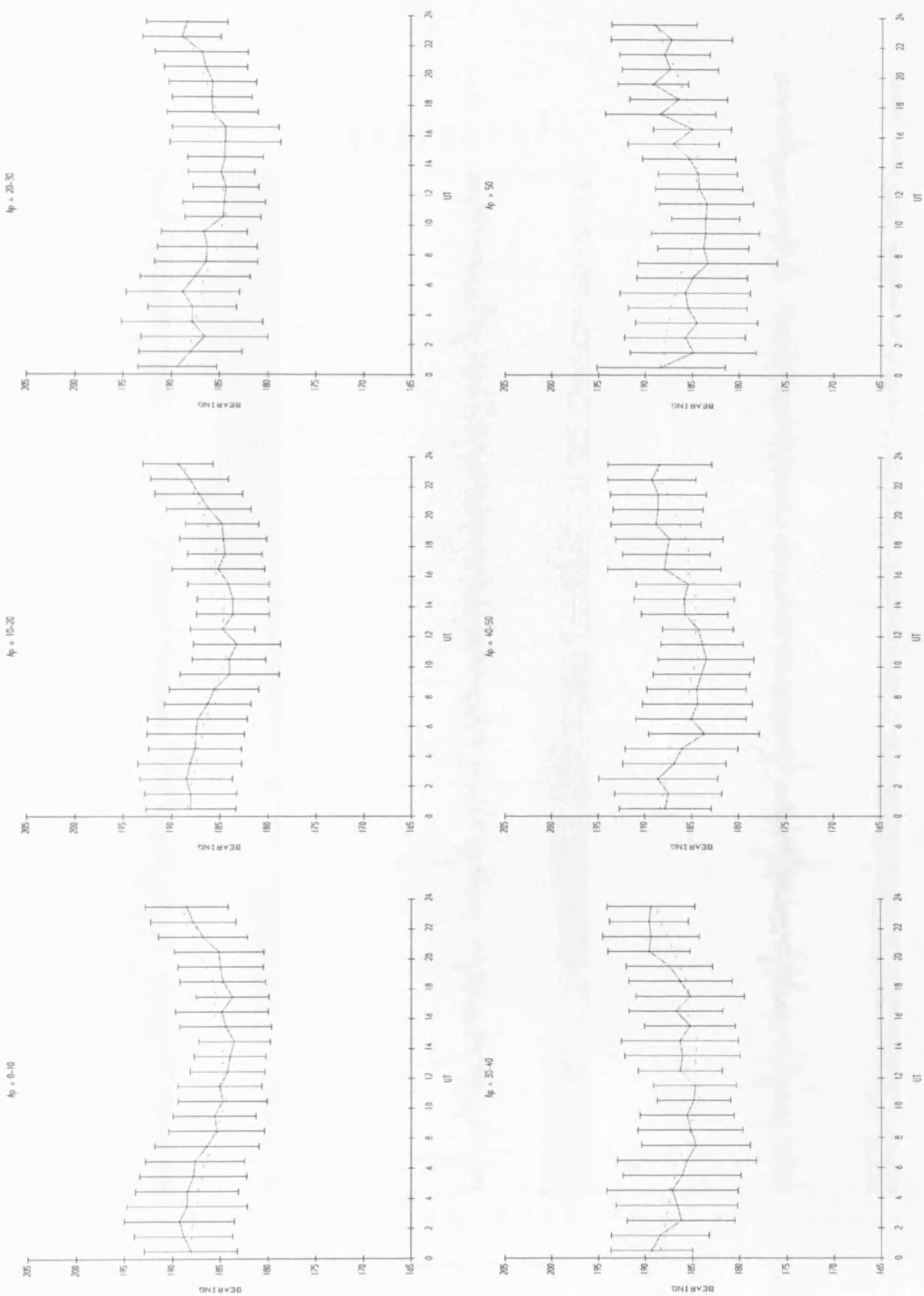

Figure 6.7: Mean bearings of 5.832MHz signals from Iqaluit at Alert, averaged for each UT hour for the period 1/4/94-31/5/94. Each panel represents a range of Ap values. Error bars indicate ±1 standard deviation. The dotted line represents the mean values calculated for all ranges of Ap.

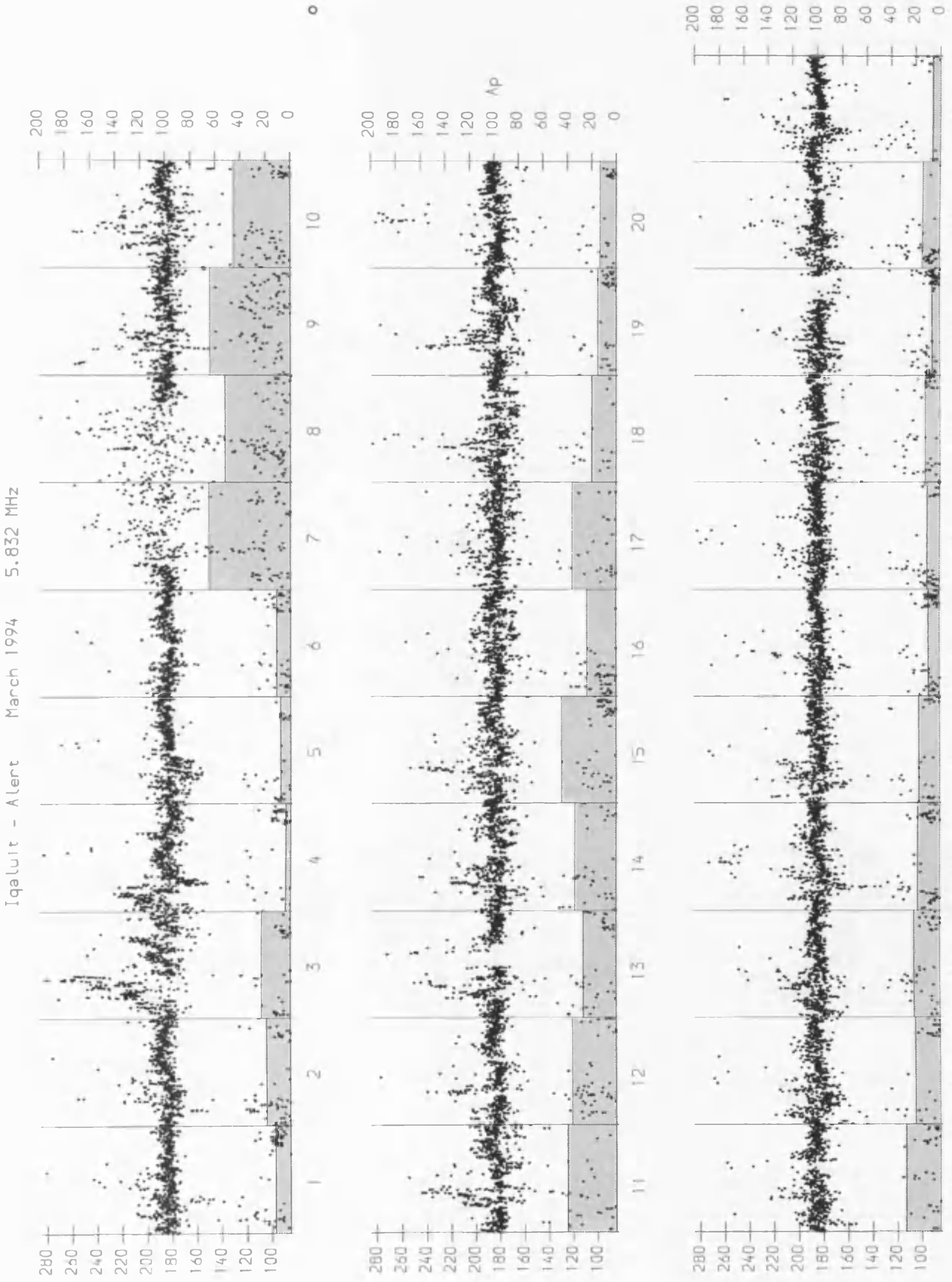

Figure 6.8: Bearings of 5.832MHz signals on the Iqaluit-Alert path for March 1994. Vertical lines indicate 00:00 UT. The shaded bars indicate Ap index.

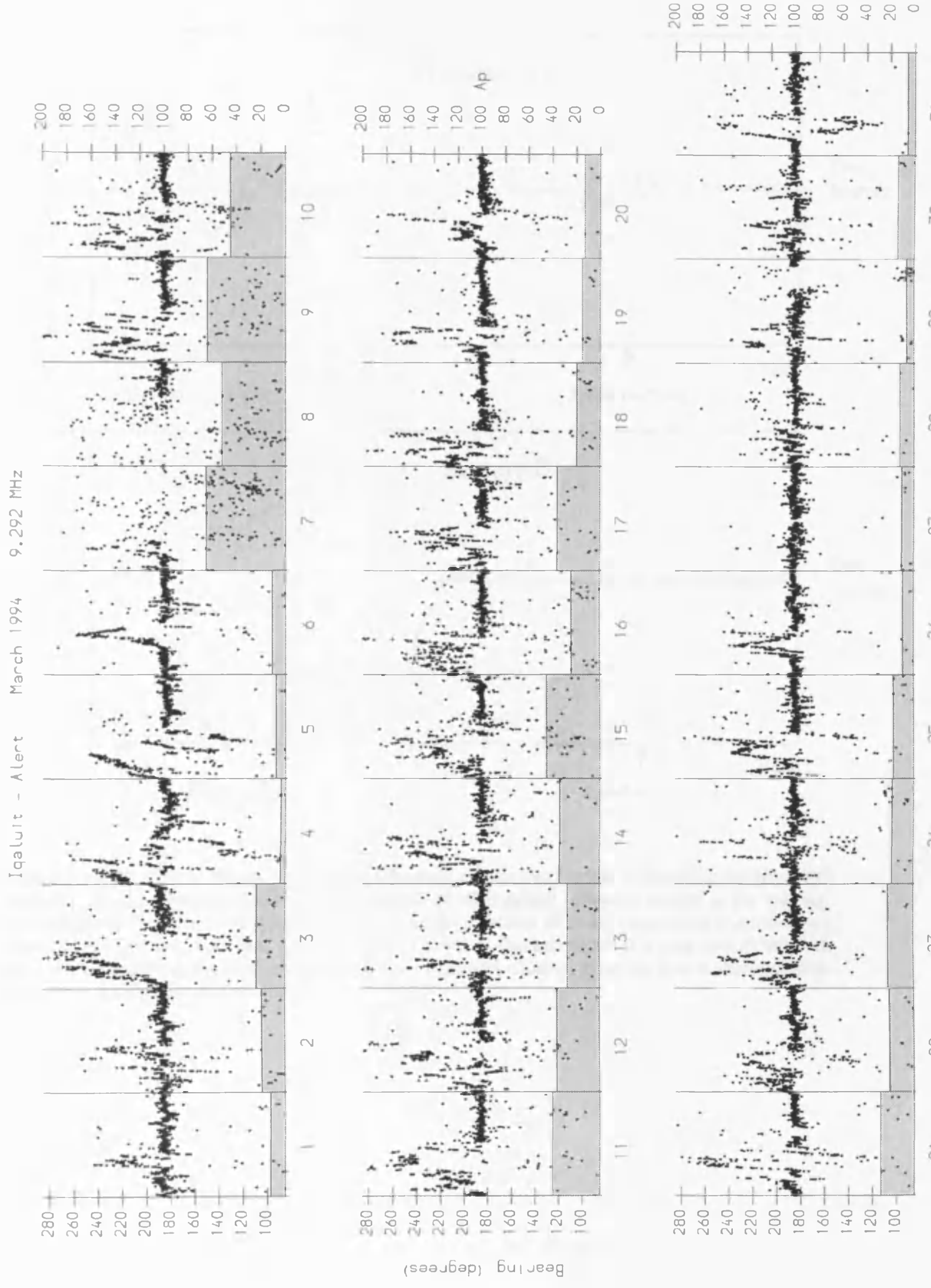

Figure 6.9: Bearings of 9.292MHz signals on the Iqaluit-Alert path for March 1994. Vertical lines indicate 00:00 UT. The shaded bars indicate Ap index.

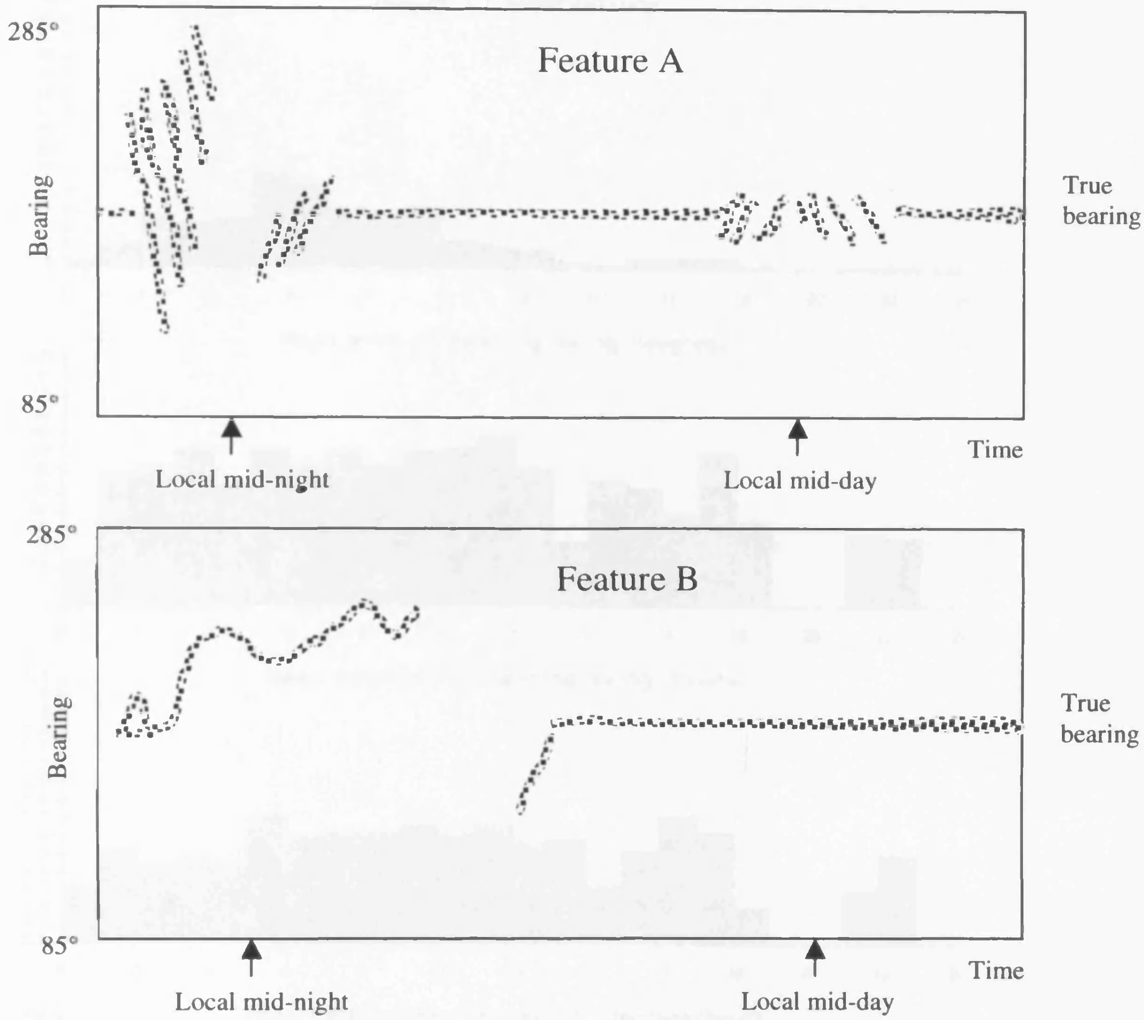

Figure 6.10: Schematic diagram of the classification of structures in the 9.292 MHz Iqaluit–Alert bearings. Feature A (top panel) consists of trains of short period (~30min) swings in the bearing. The amplitude is largest around local midnight and the direction of swing (increasing or decreasing) changes between local forenoon and afternoon. Feature B (bottom panel) is a long period 'drift' in the bearing, usually to the west, around local mid-night, and returning from the East at mid-morning. Often the two features are superposed.

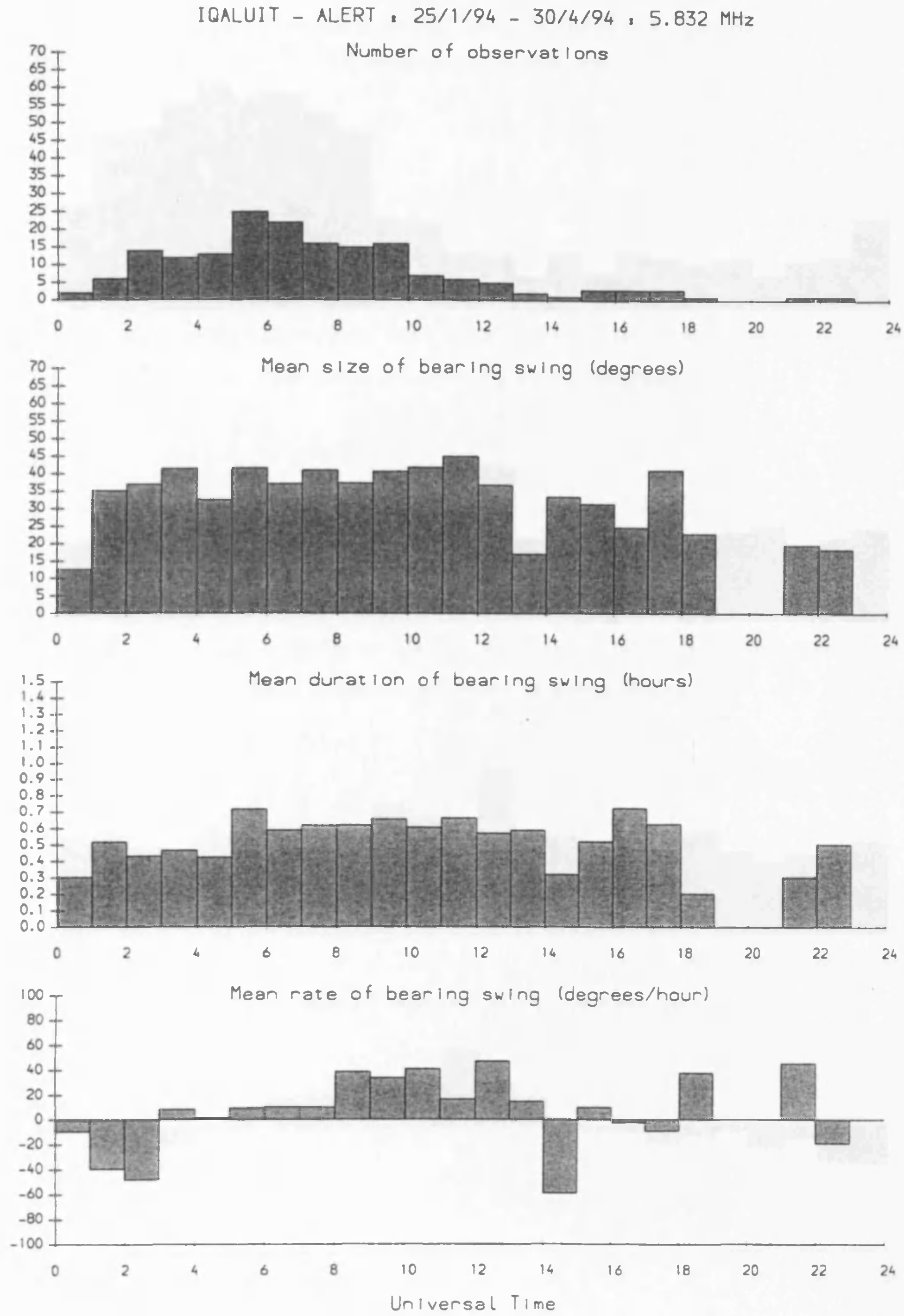

Figure 6.11: Mean magnitude, duration and bearing swing rate for each UT hour for all bearing swings on the 5.832MHz signals from Iqaluit-Alert, 25/1/94 - 30/4/94.

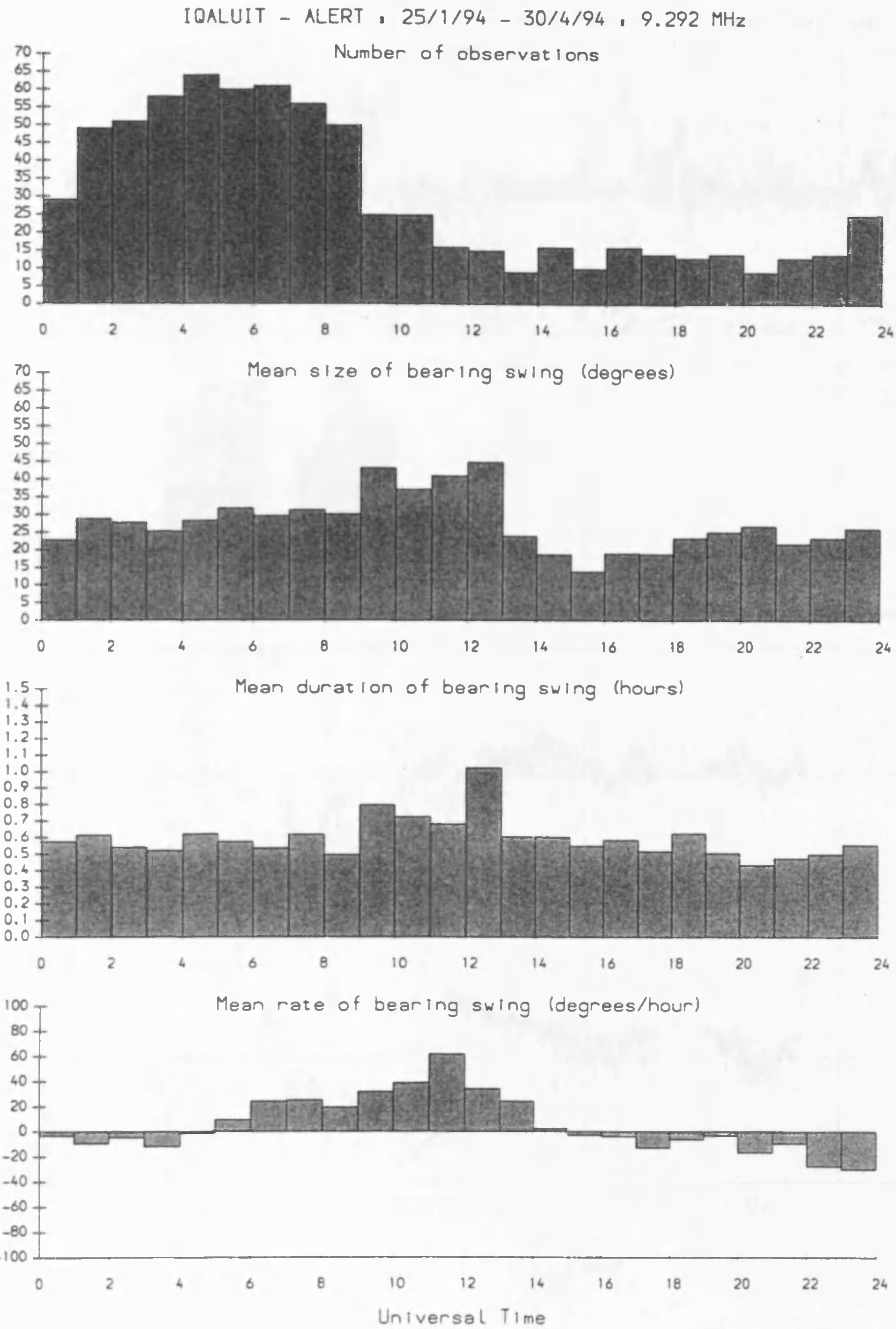

Figure 6.12: Mean magnitude, duration and bearing swing rate for each UT hour for all bearing swings on the 9.232MHz signals from Iqaluit-Alert, 25/1/94 - 30/4/94.

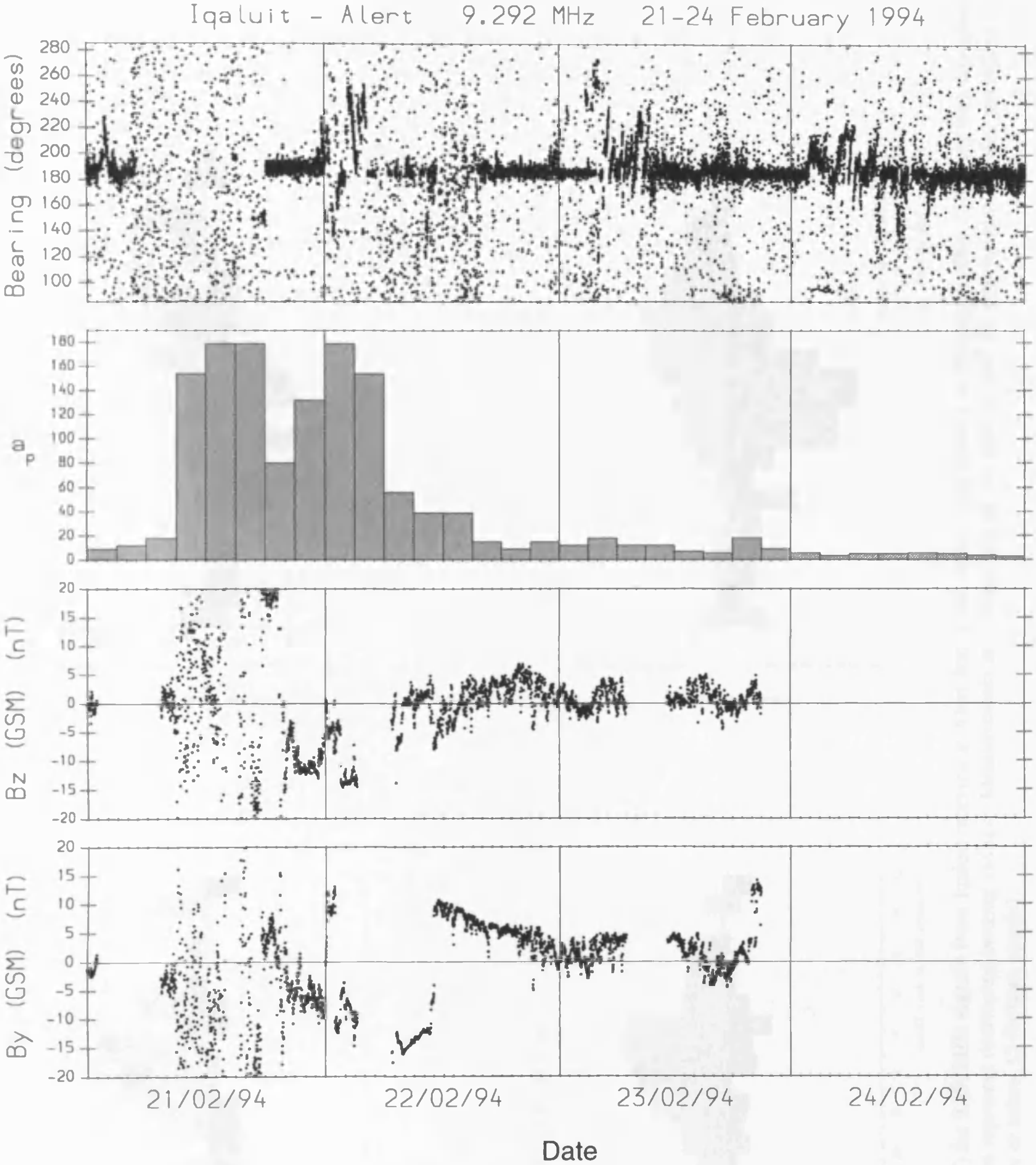

Figure 6.13: Bearings of 9.292MHz transmission from Iqaluit received at Alert for the period 21st-24th February 1994. Vertical lines indicate 00:00 UT. Three-hourly ap values (second from top) and IMF Bz and By values (lower panels) are also shown. Note that the bearings shown are snap bearings ('snaps') and not composite bearings since these provide a higher resolution image of the structure in the bearing swings.

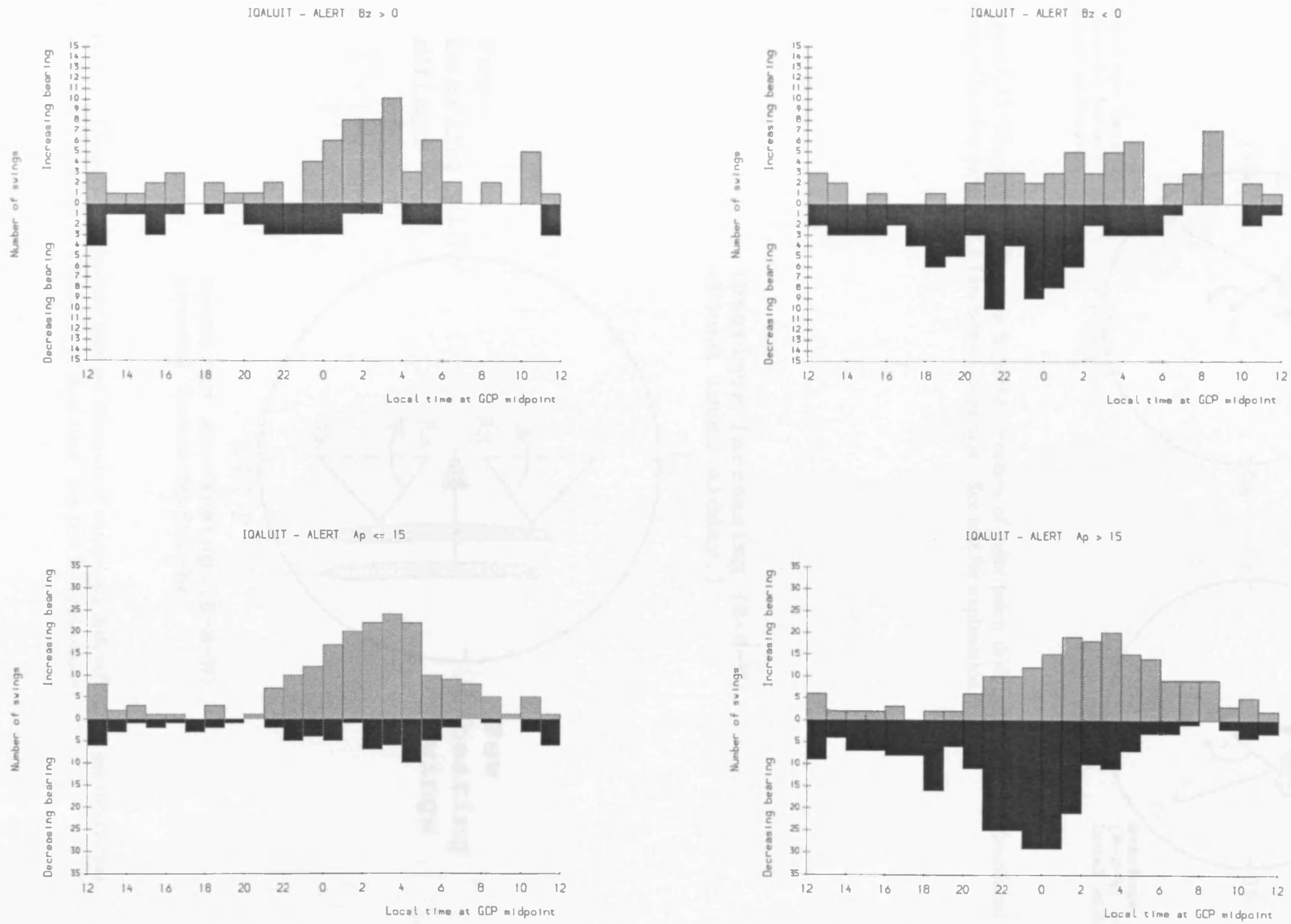

Figure 6.14: Number of swing per hour (LT) for 9.292MHz signals from Iqaluit received at Alert during the period 25th January to 30th April 1994. The grey bars represent increasing bearing swings and the black bars represent decreasing bearing swings. Measurements are categorised by the sign of IMF Bz (top panels) and also according to whether the three-hourly ap index was above or below 15 (bottom panels).

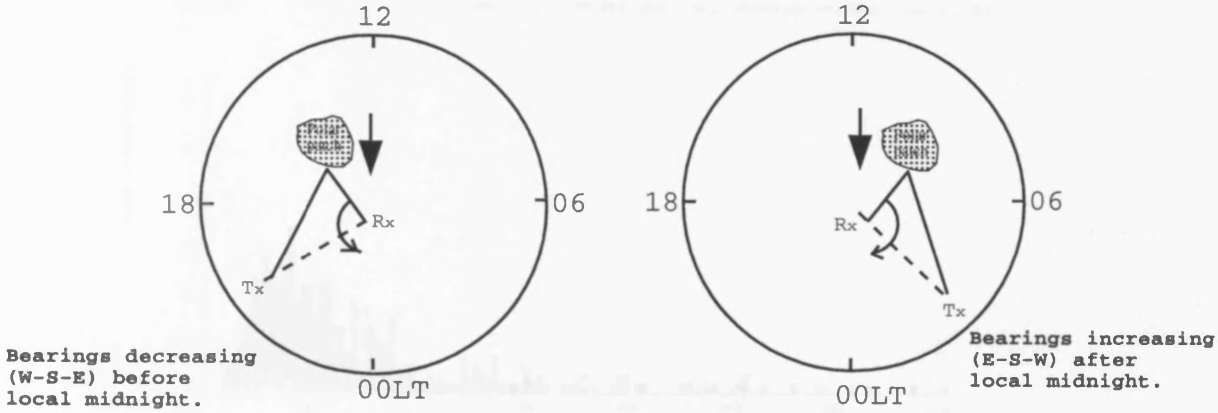

Figure 6.15: Diagrams to illustrate how the direction of polar patch drift influences the directional sense of bearing swings as a function of local time. See text for explanation.

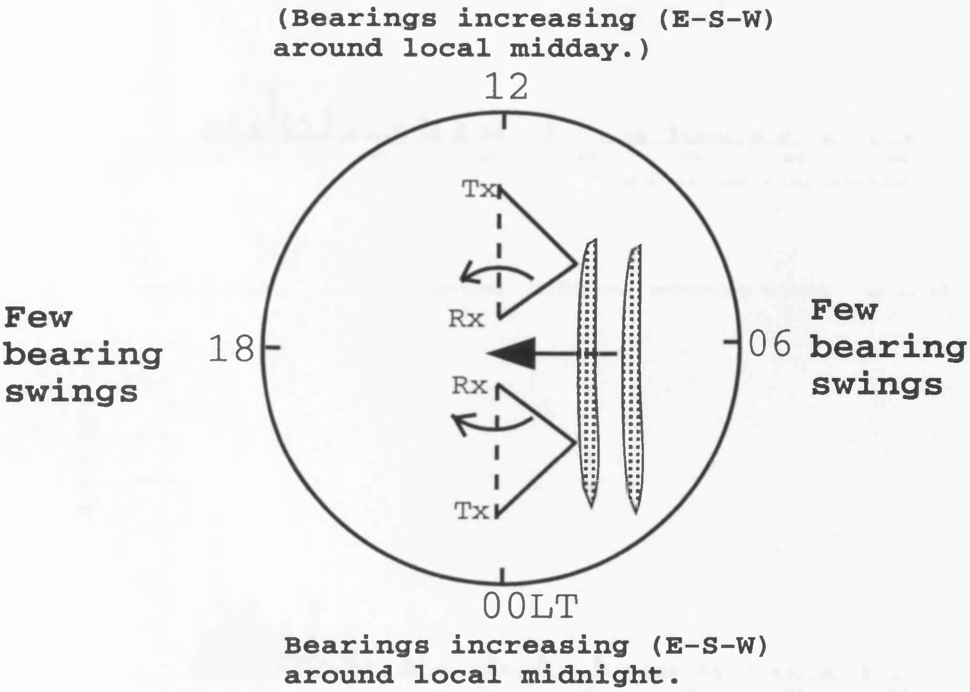

Figure 6.16: Diagrams to illustrate how the direction of auroral arc drift influences the directional sense of bearing swings as a function of local time. See text for explanation.

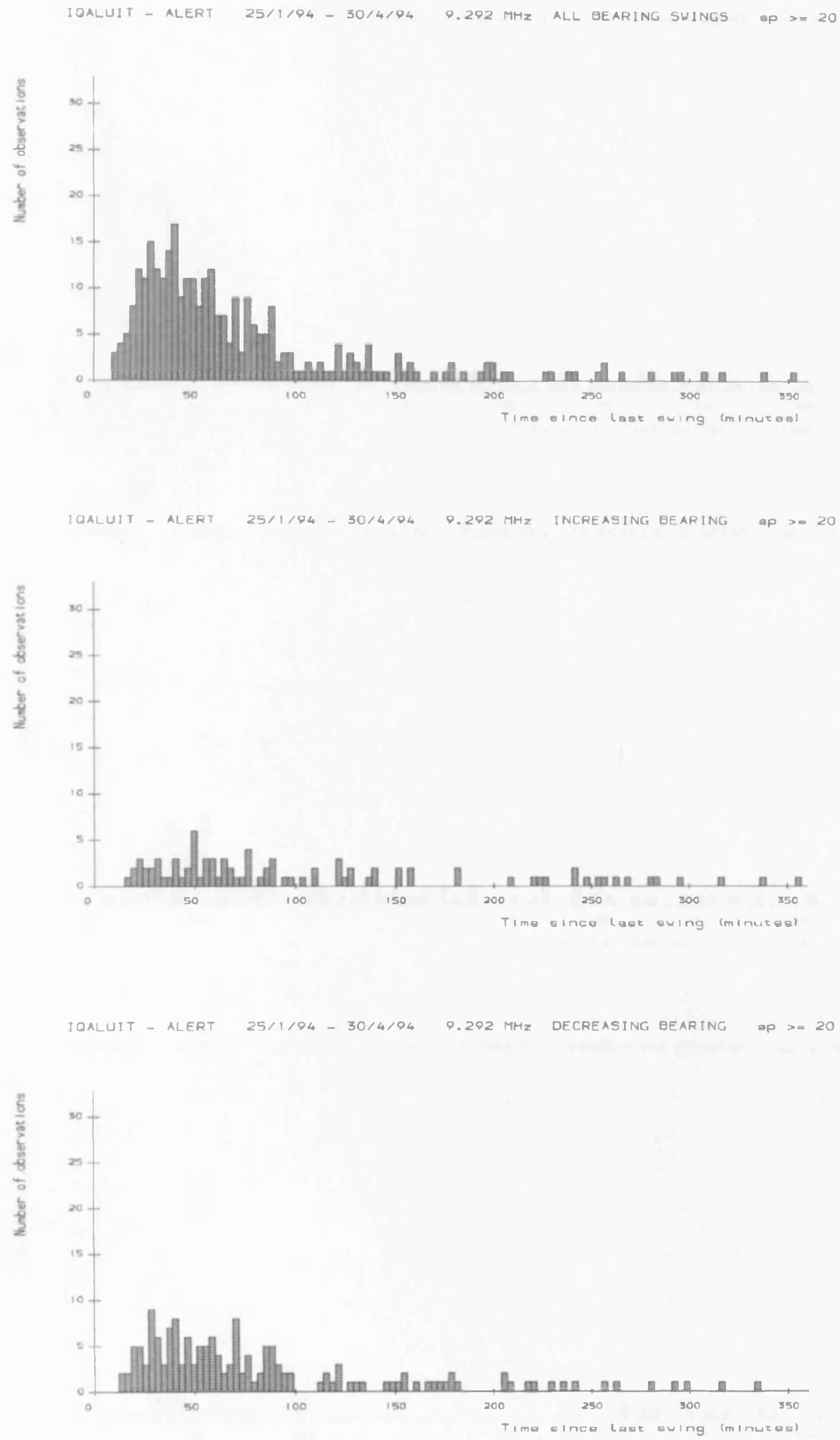

Figure 6.17a: Time intervals between successive bearing swings on 9.292MHz transmissions from Iqaluit to Alert over the period 25/1/94 - 30/4/94 for which $a_p >= 20$. The top panels represent all bearing swings, middle panels represent only the increasing bearing swings and lower panels represent decreasing bearing swings.

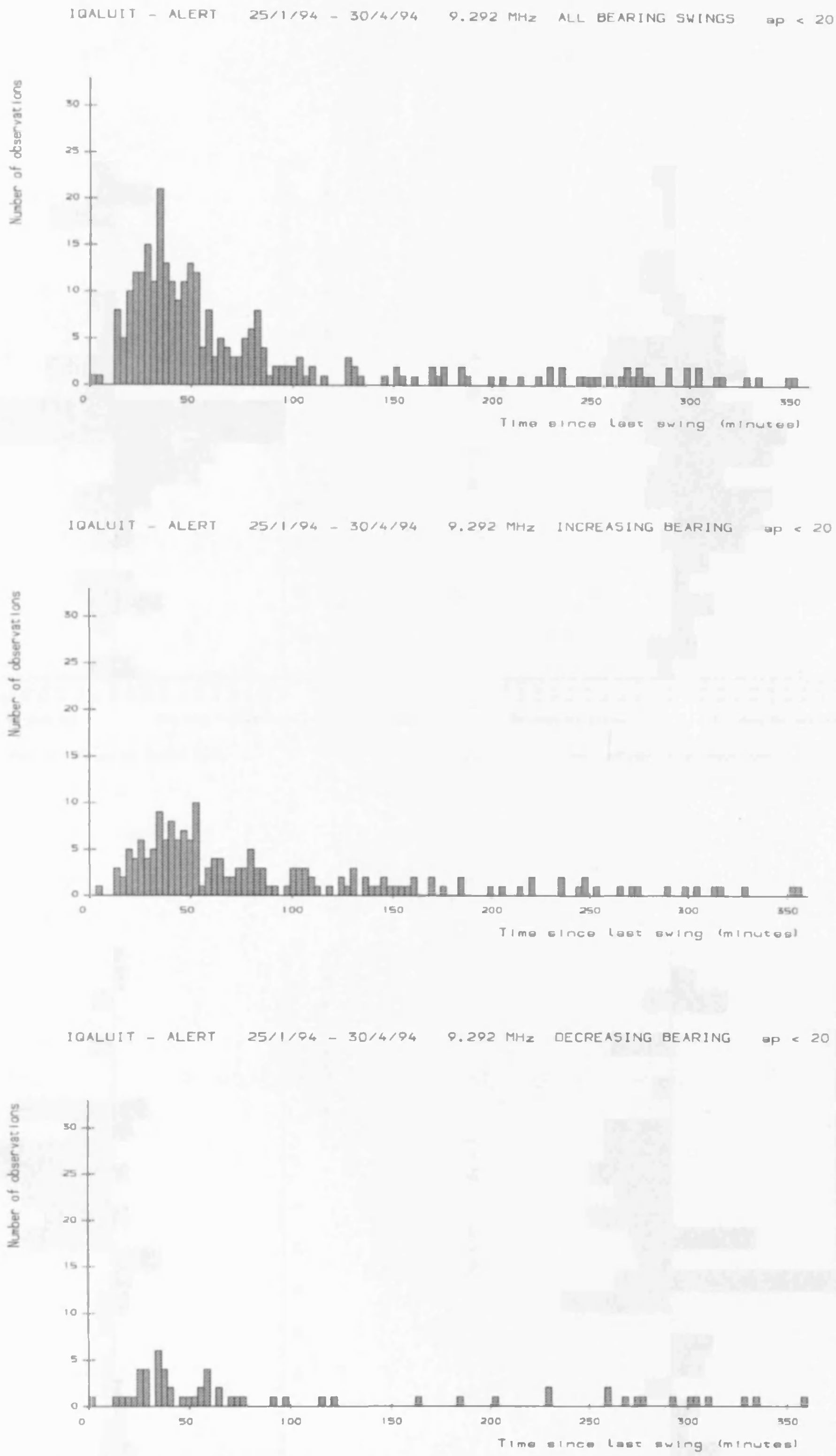

Figure 6.17b: Time intervals between successive bearing swings on 9.292MHz transmissions from Iqaluit to Alert over the period 25/1/94 - 30/4/94 for which $a_p < 20$. The top panels represent all bearing swings, middle panels represent only the increasing bearing swings and lower panels represent decreasing bearing swings.

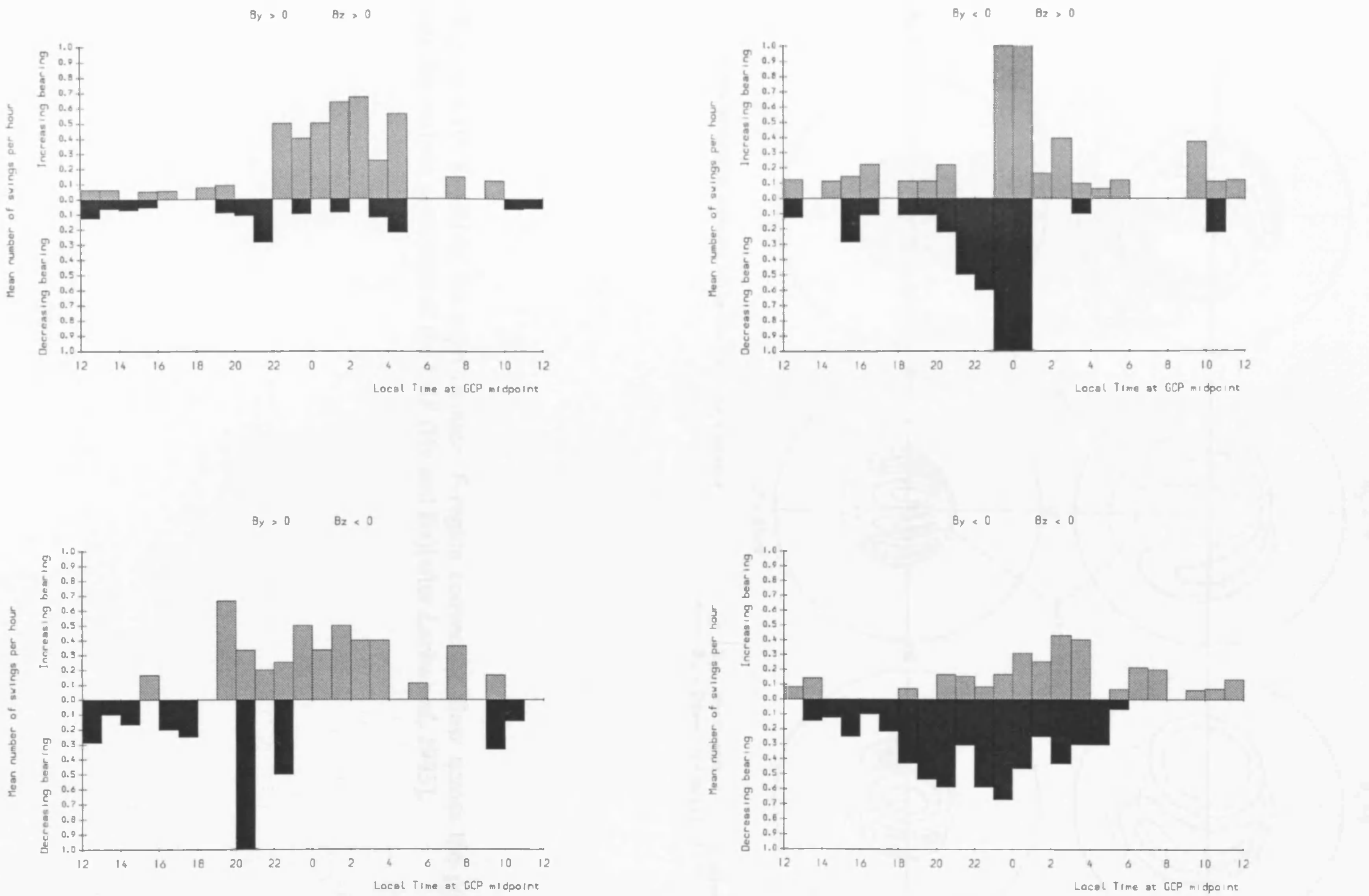

Figure 6.18: The average number of bearing swings recorded for each LT hour for 9.292MHz signals from Iqaluit received at Alert during the period 25 January 1994 to 30 April 1994. Increasing bearing angles are represented by light shading and decreasing bearing angles are represented by dark shading. Measurements are categorised by the B_y and B_z IMF directions.

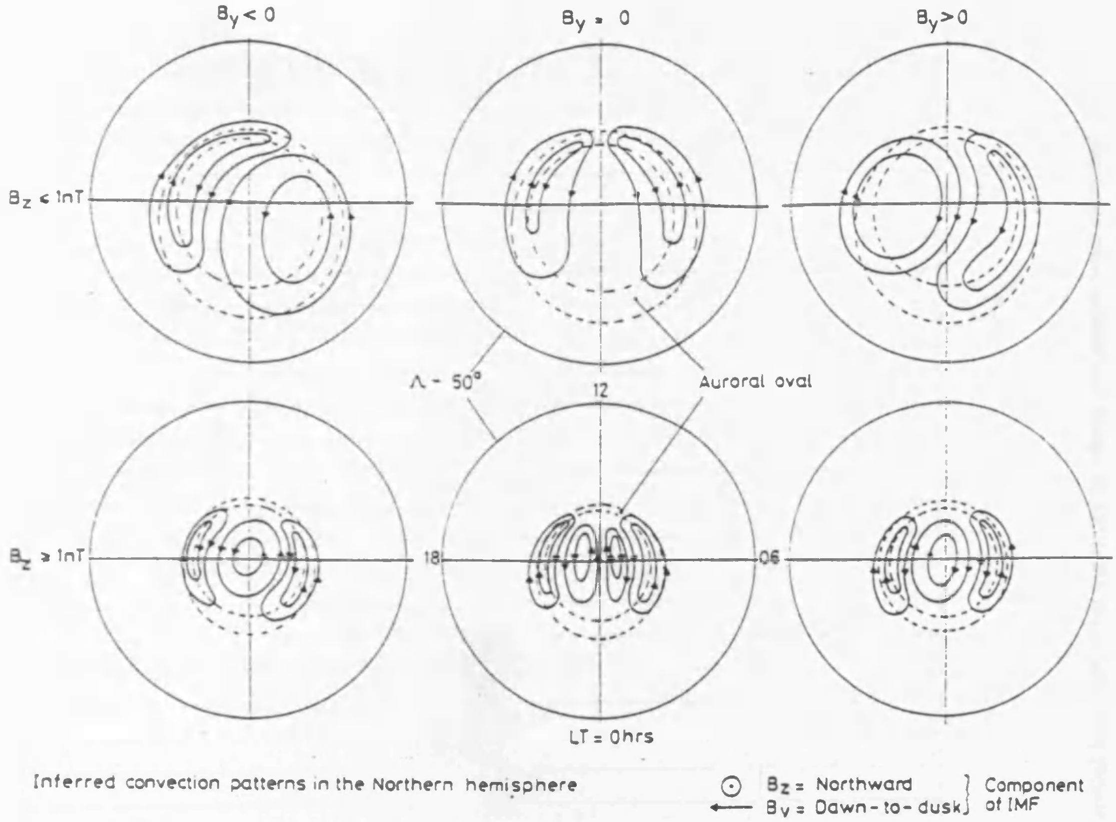

Figure 6.19: Model of the high latitude, F-region convection flow across the polar cap for various directions of the IMF (By and Bz)[after *Lockwood*, 1993].

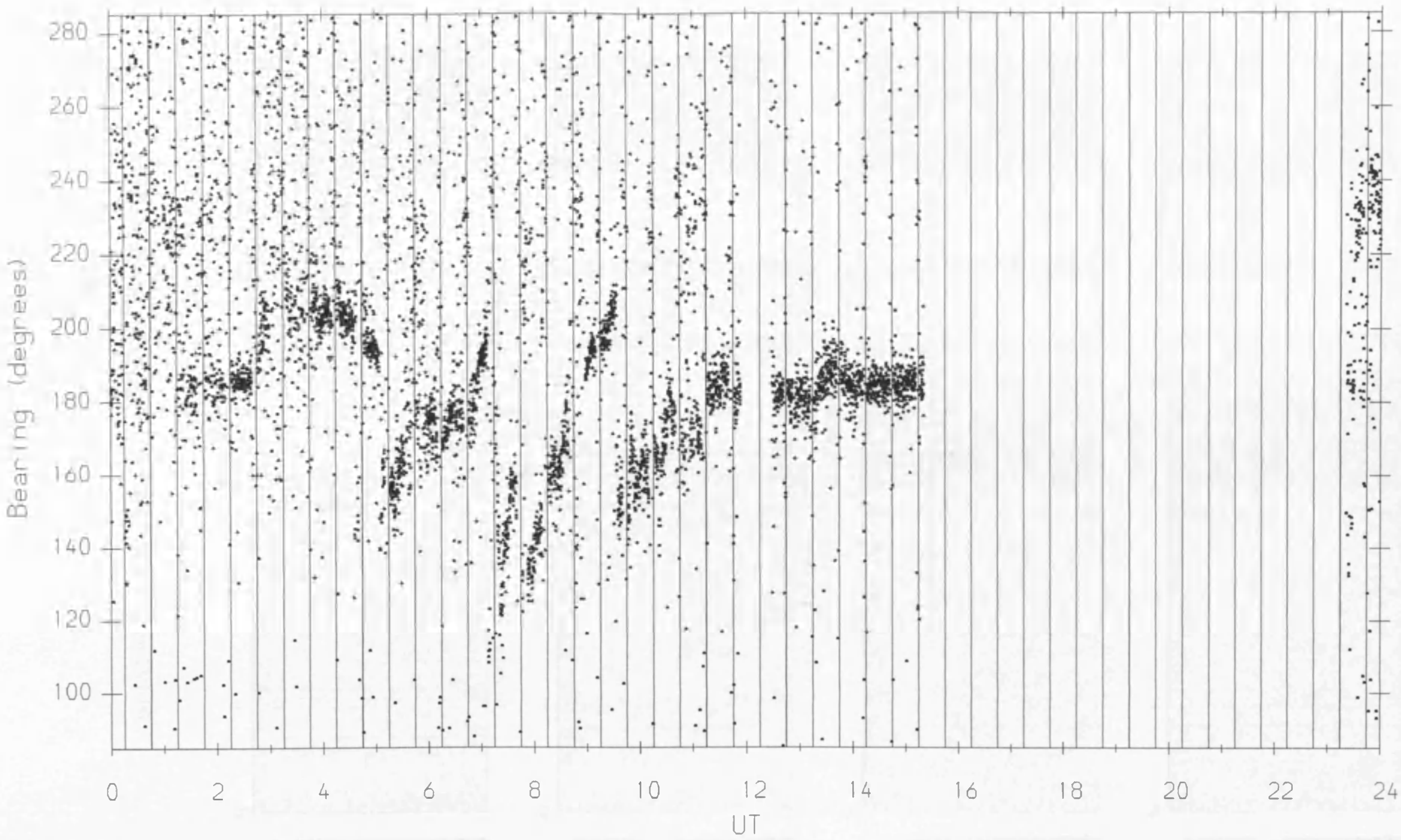

Figure 6.20: Bearings of 9.292MHz signals from Iqaluit to Alert on 23/1/96. Vertical lines represent the times at which ionograms were recorded.

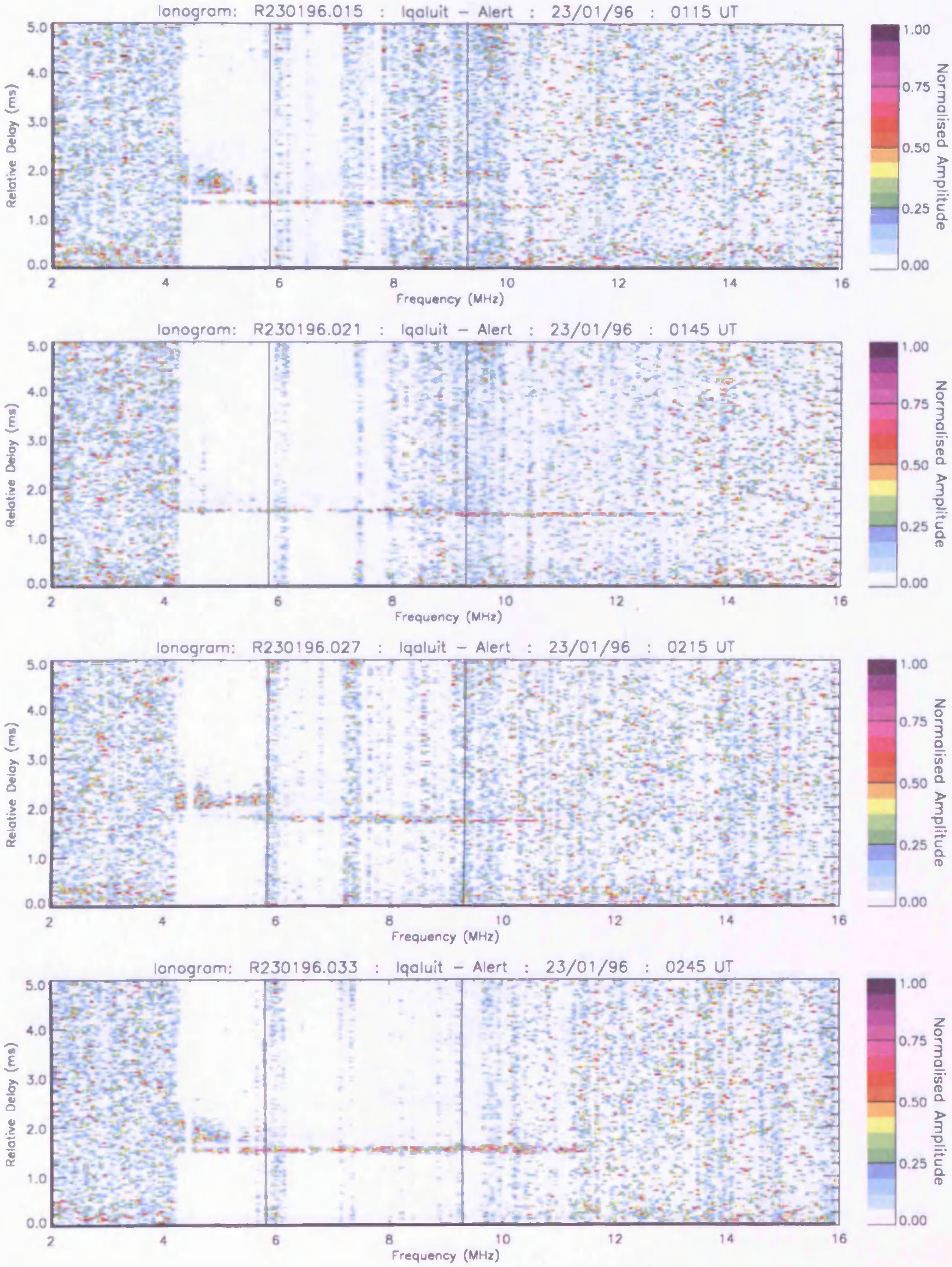

Figure 6.21: Ionogram sequence for the Iqaluit-Alert path on 23/1/96.

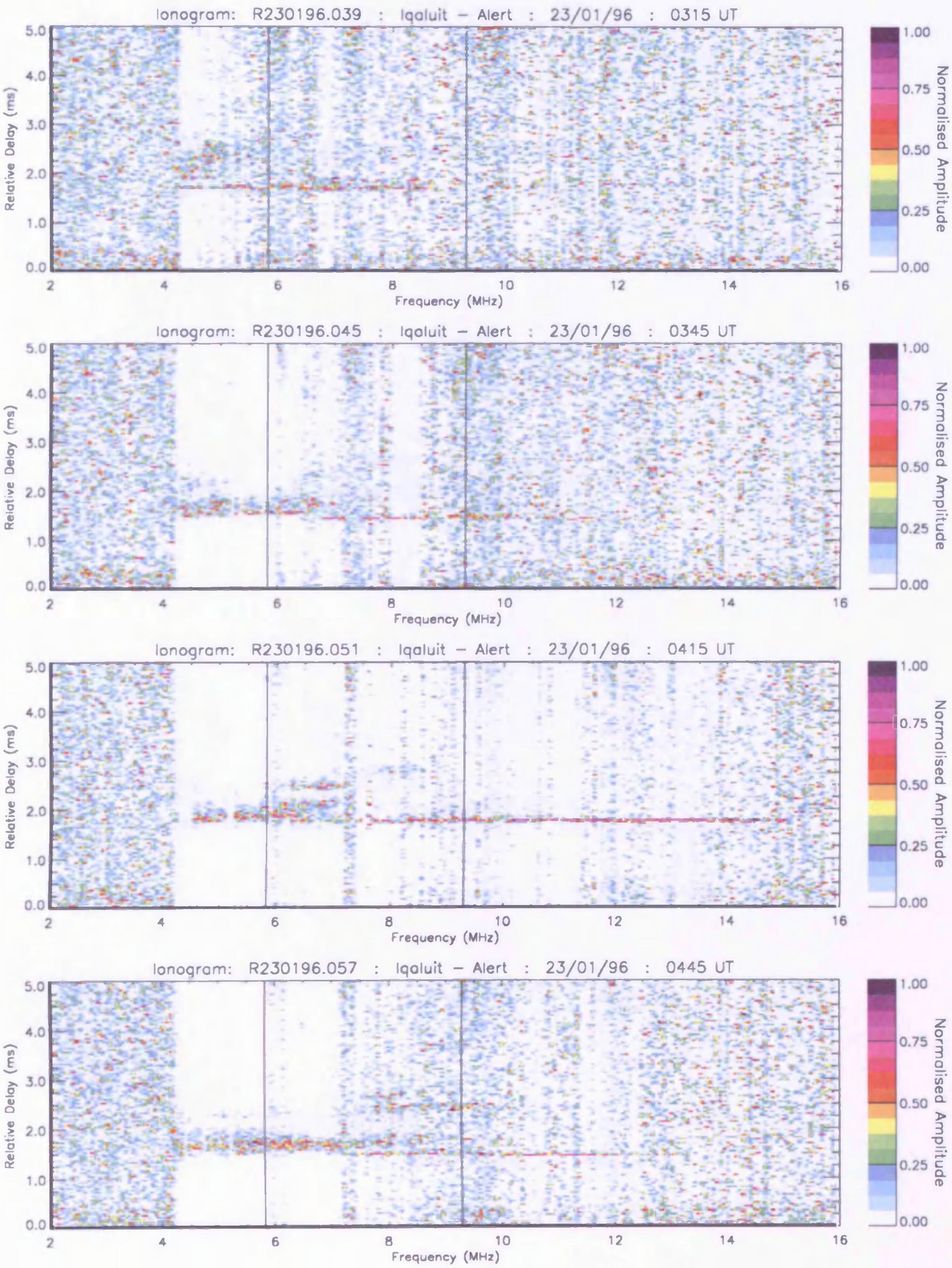

Figure 6.21(ctd): Ionogram sequence for the Iqaluit-Alert path on 23/1/96.

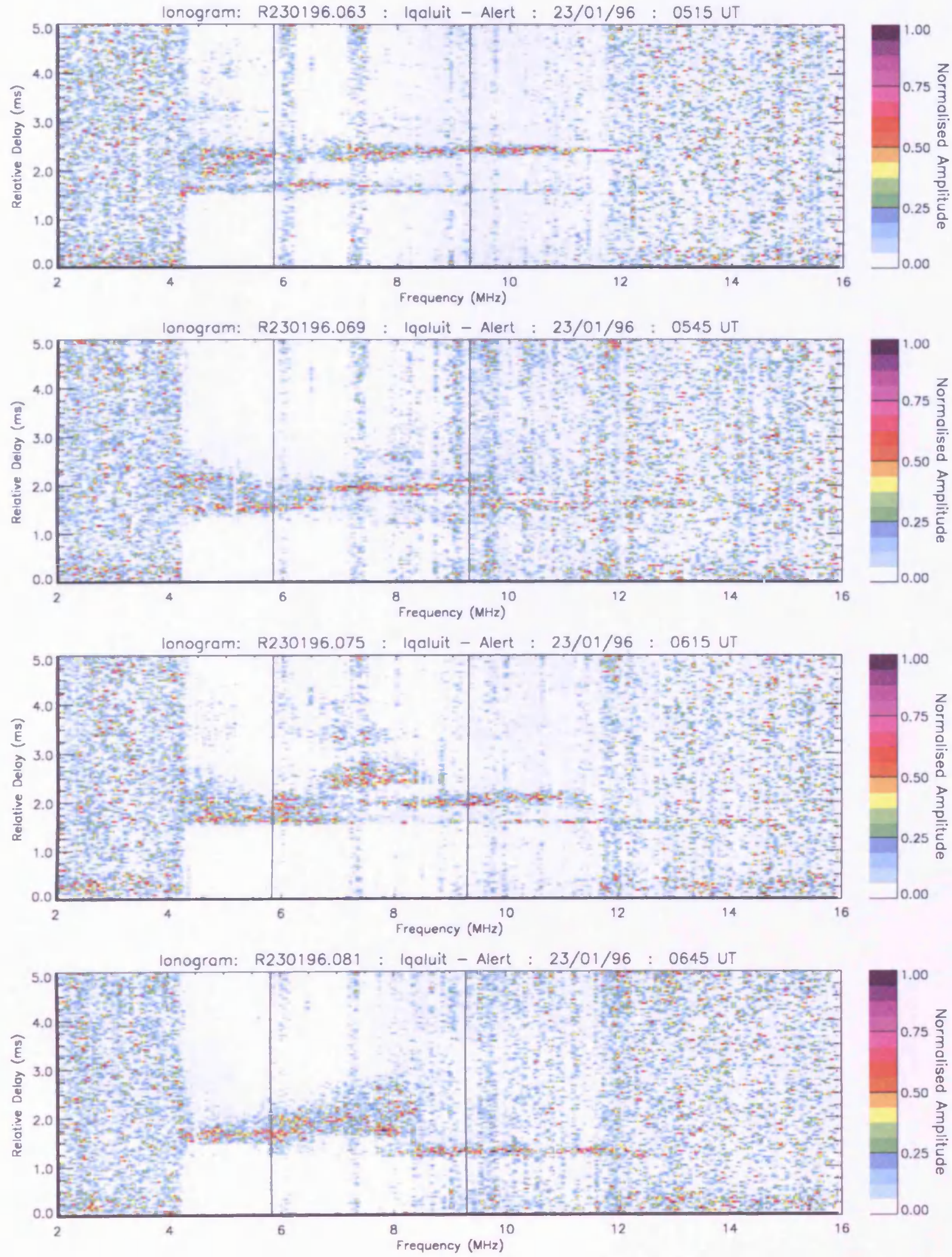

Figure 6.21(ctd): Ionogram sequence for the Iqaluit-Alert path on 23/1/96.

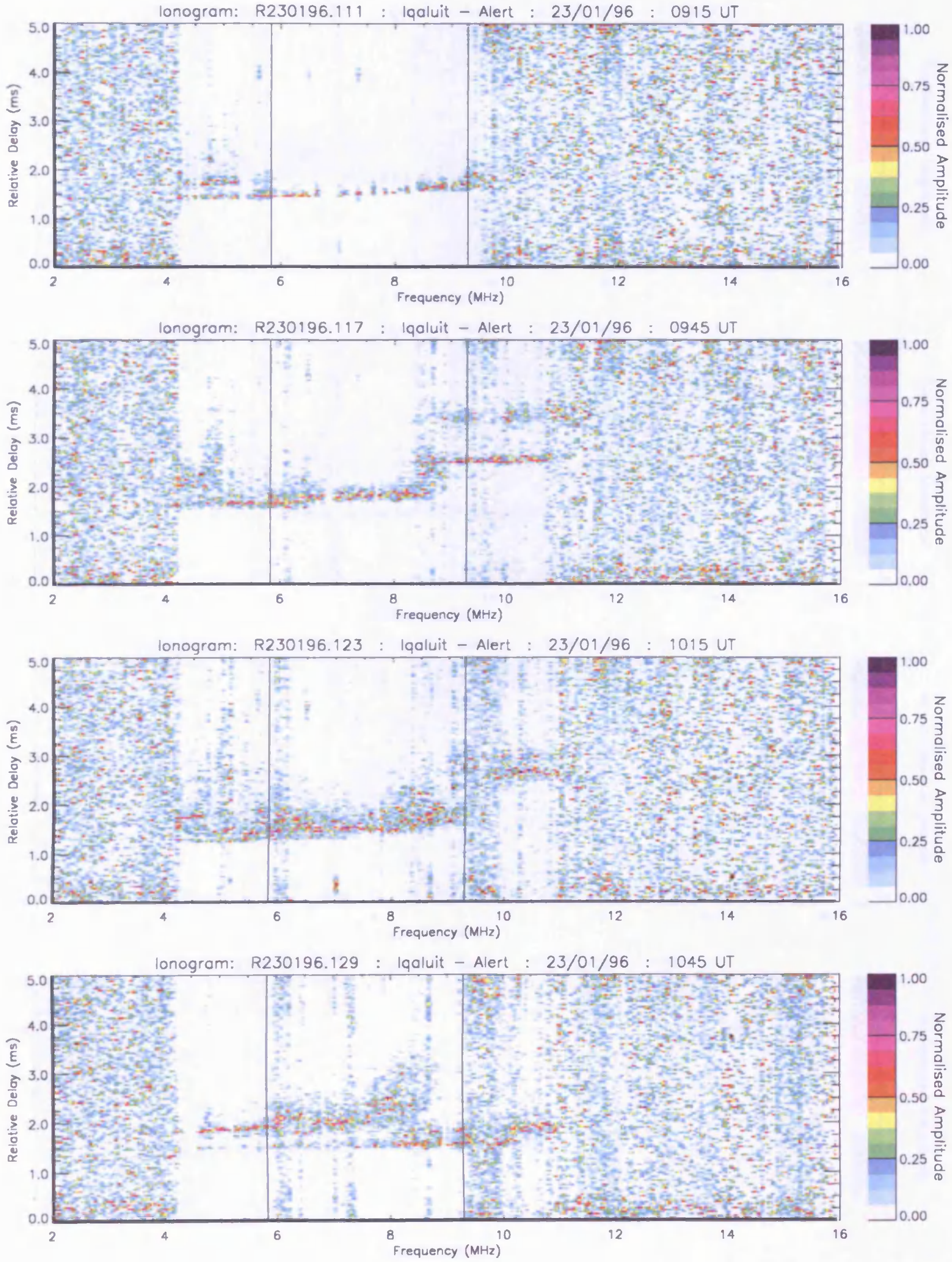

Figure 6.21(ctd): Ionogram sequence for the Iqaluit-Alert path on 23/1/96.

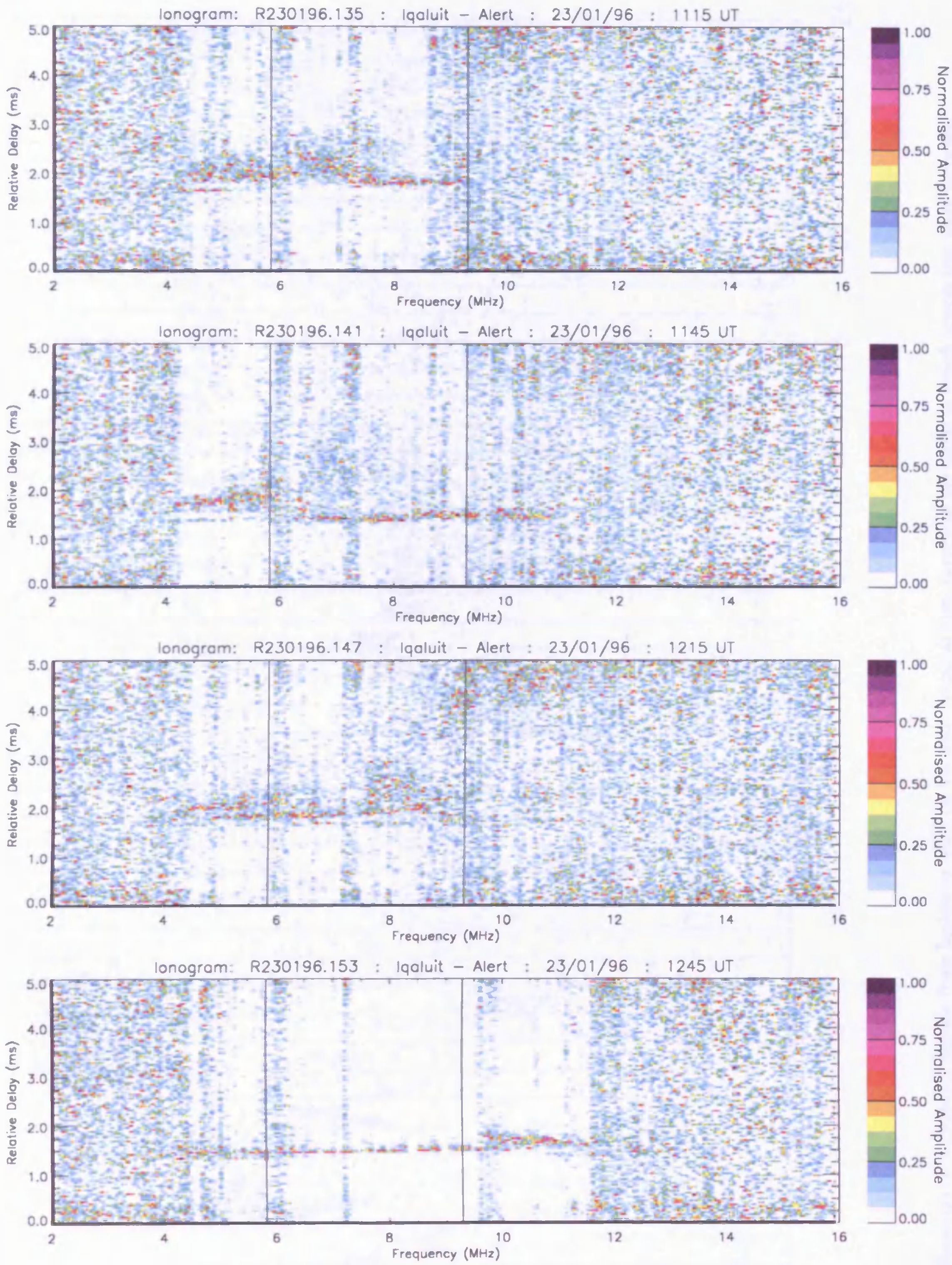

Figure 6.21(ctd): Ionogram sequence for the Iqaluit-Alert path on 23/1/96.

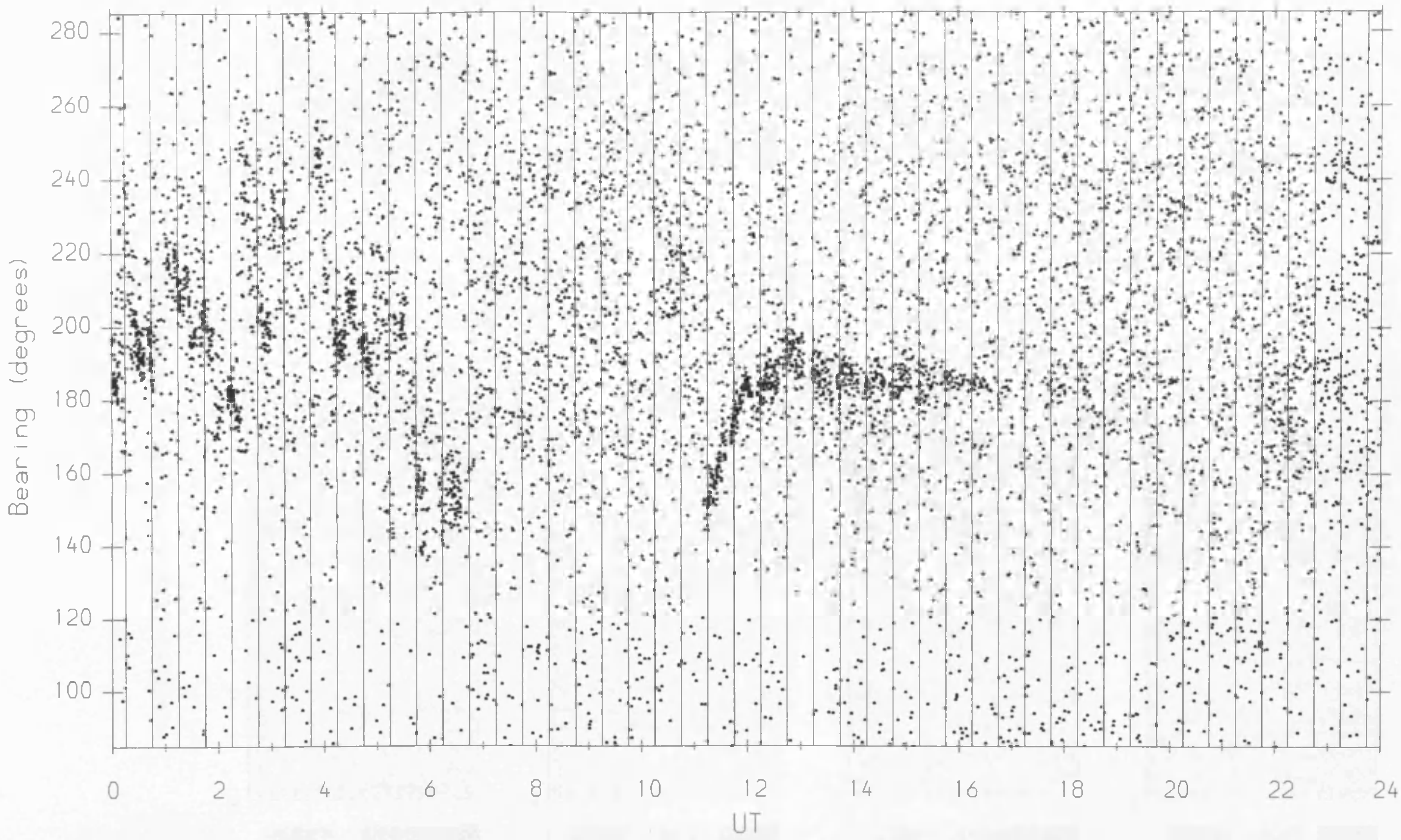

Figure 6.22: Bearings of 9.292MHz signals from Iqaluit to Alert on 24/2/96. Vertical lines represent the times at which ionograms were recorded.

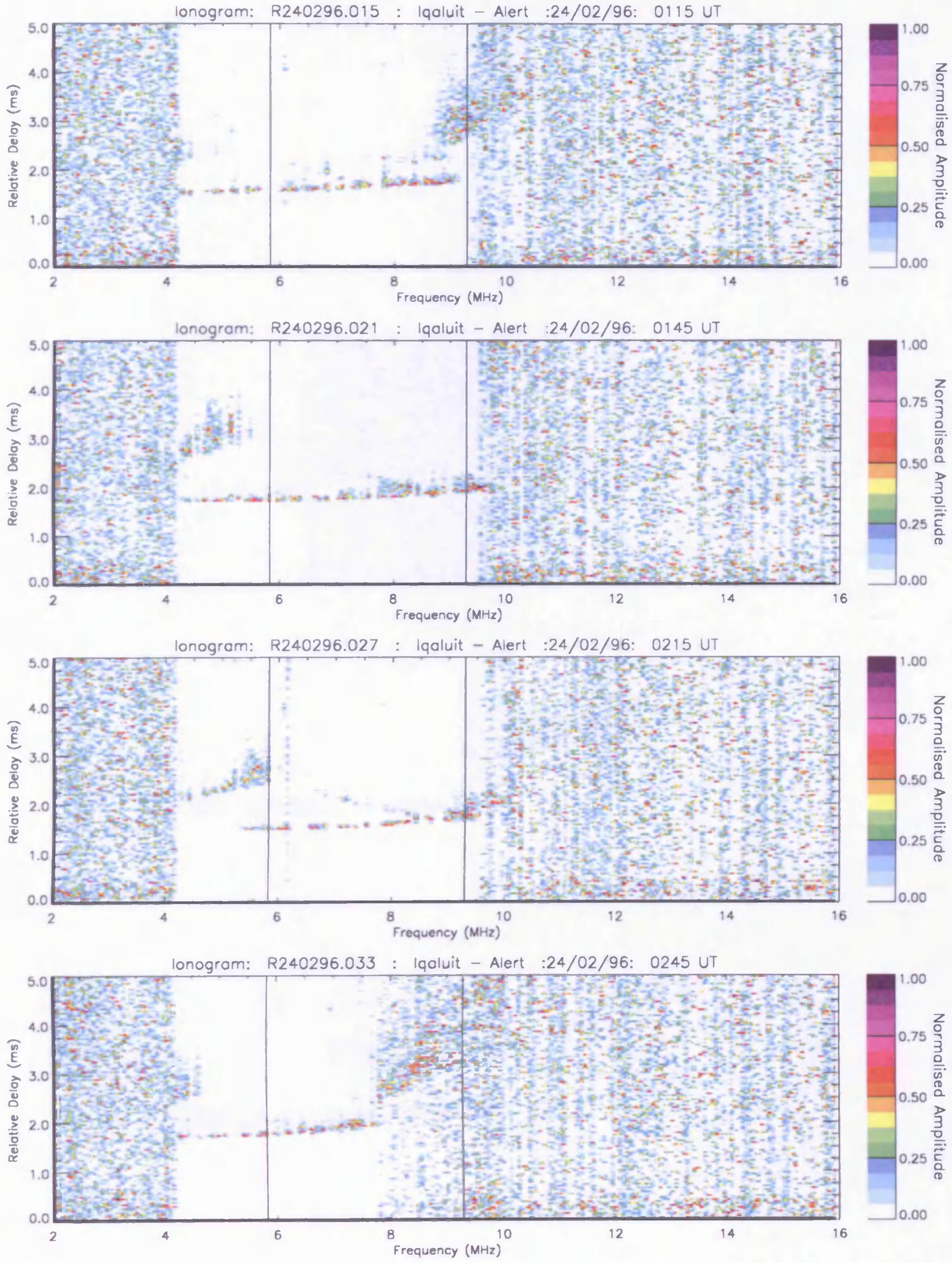

Figure 6.23: Ionogram sequence for the Iqaluit-Alert path on 24/02/96.

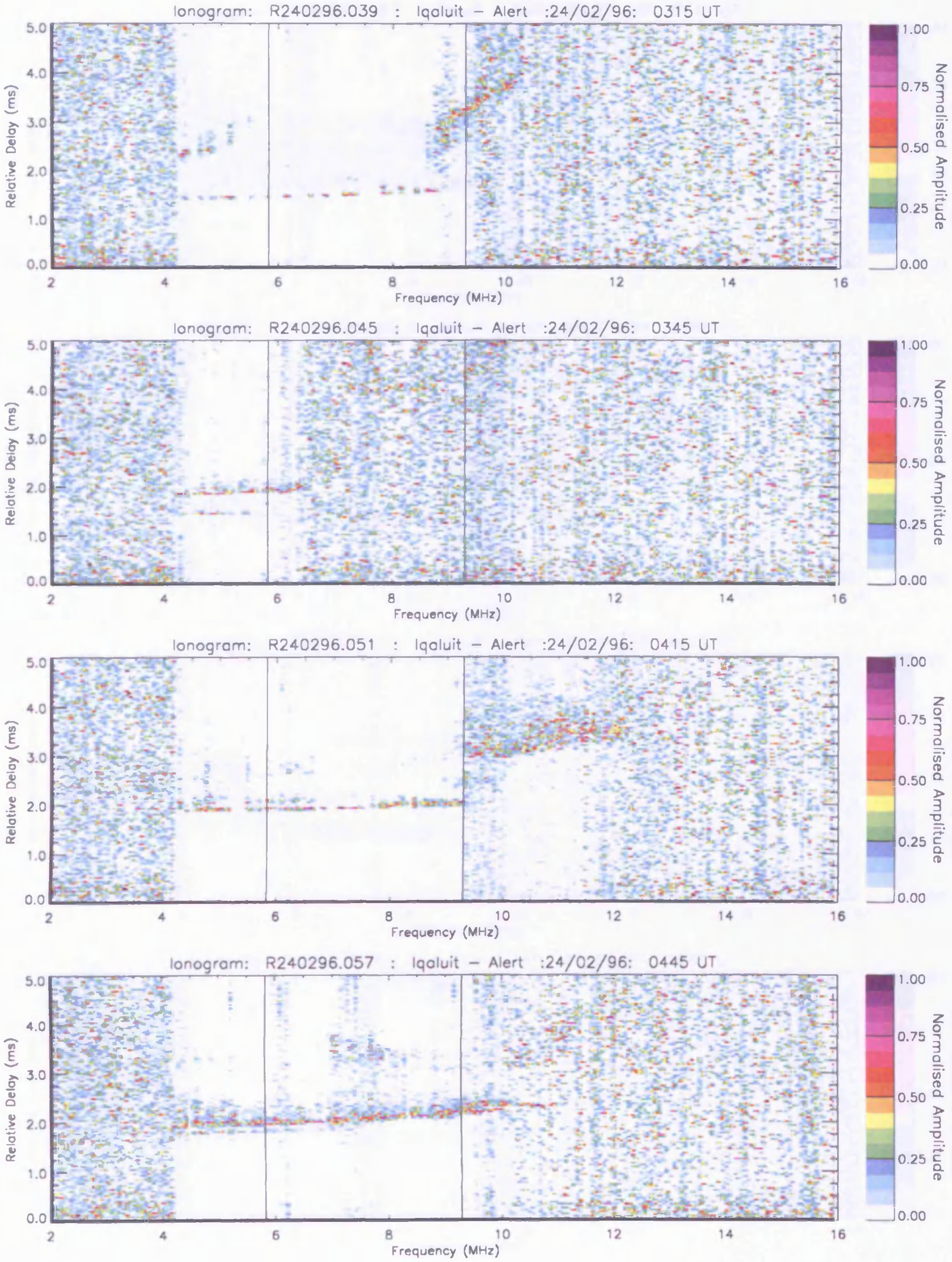

Figure 6.23 (ctd): Ionogram sequence for the Iqaluit-Alert path on 24/02/96.

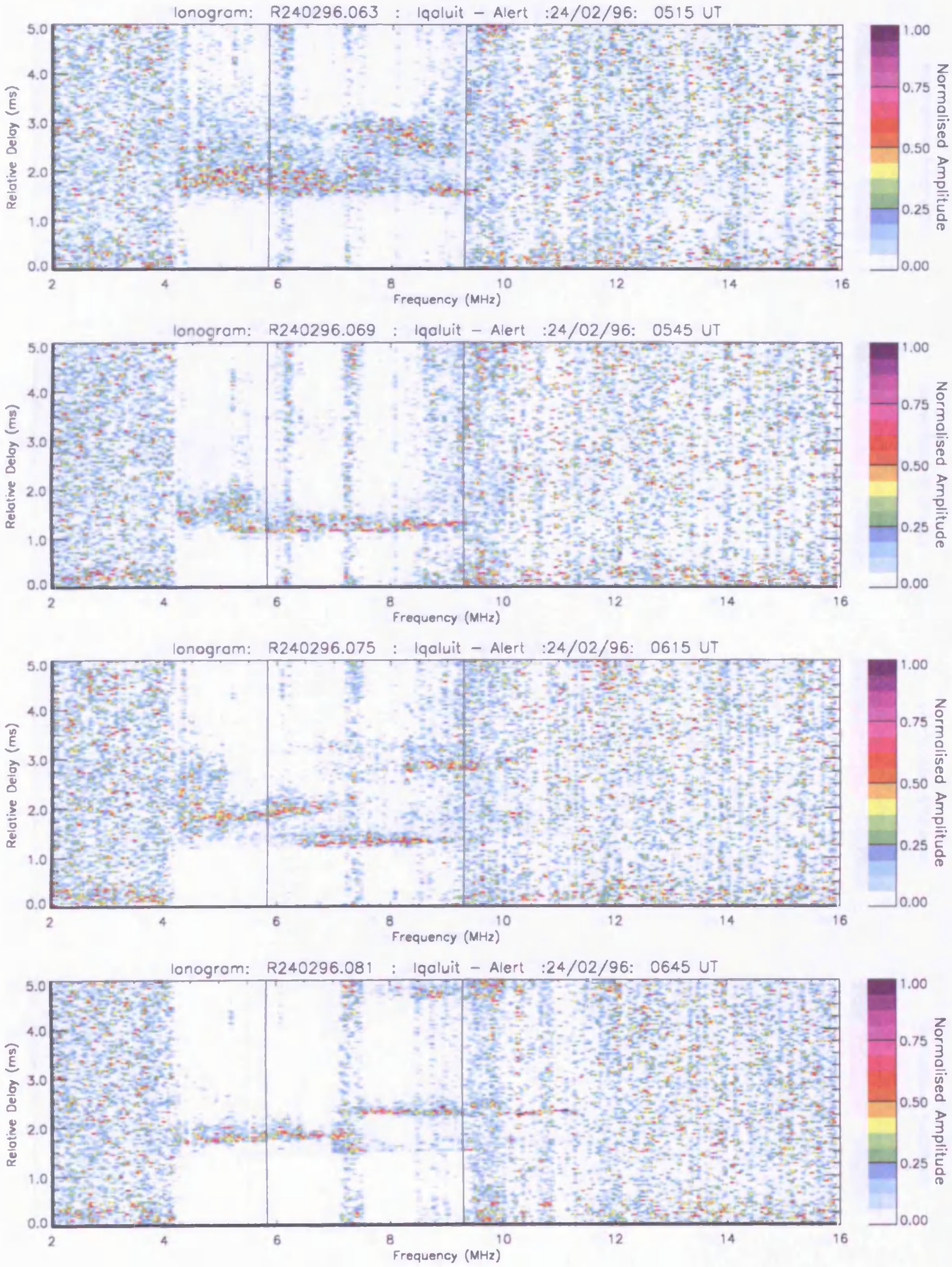

Figure 6.23 (ctd): Ionogram sequence for the Iqaluit-Alert path on 24/02/96.

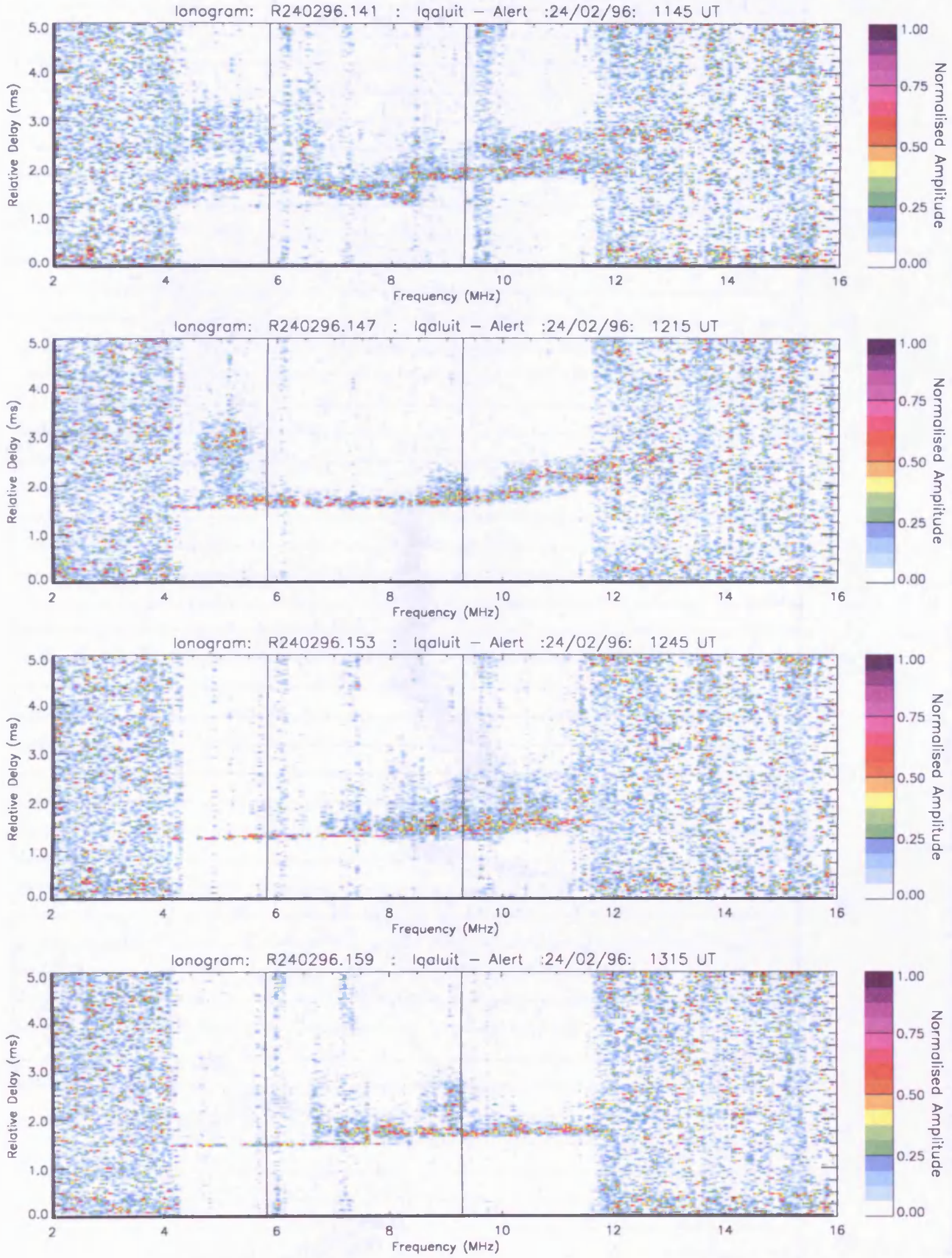

Figure 6.23 (ctd): Ionogram sequence for the Iqaluit-Alert path on 24/02/96.

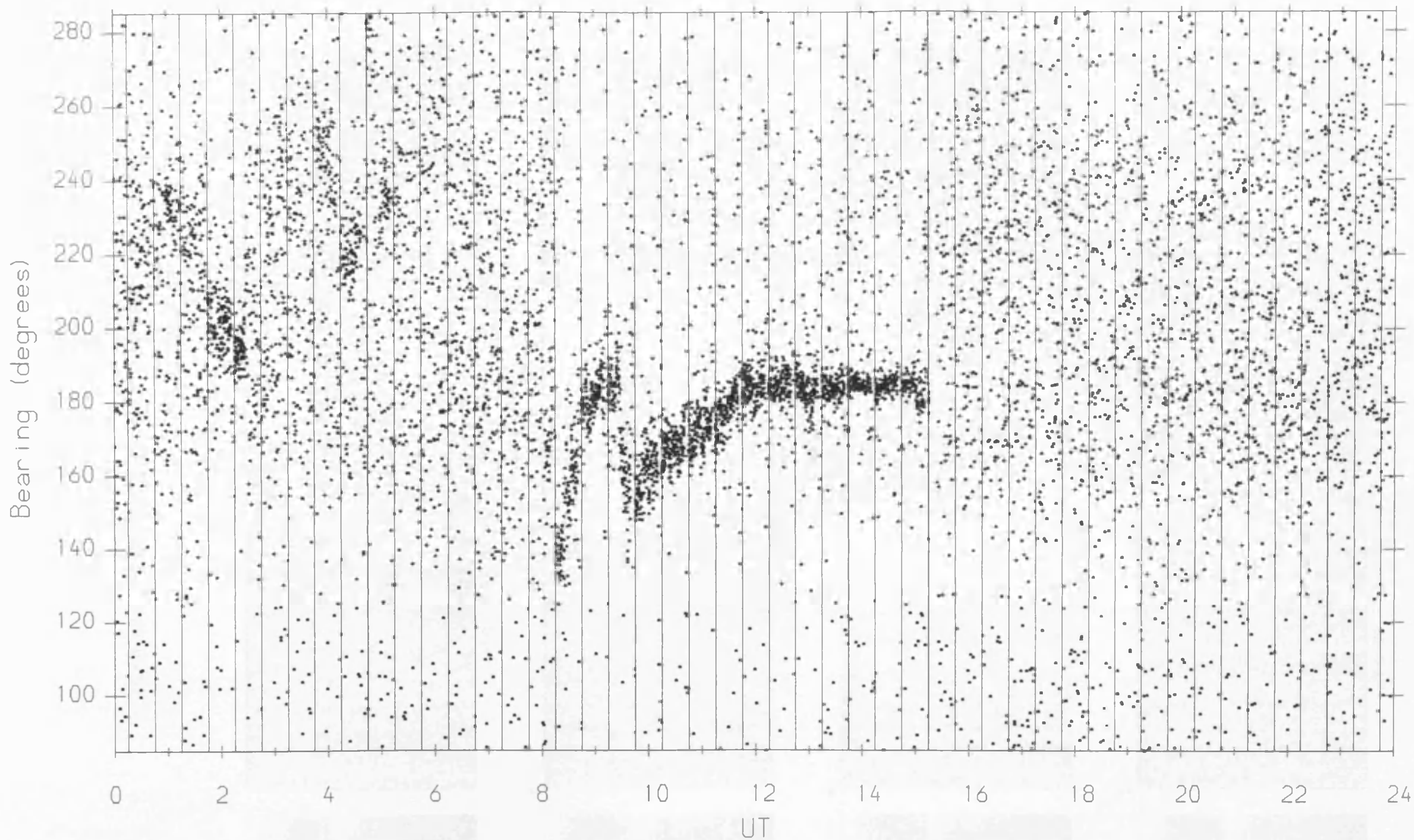

Figure 6.24: Bearings of 9.292MHz signals from Iqaluit to Alert on 4/3/96. Vertical lines represent the times at which ionograms were recorded.

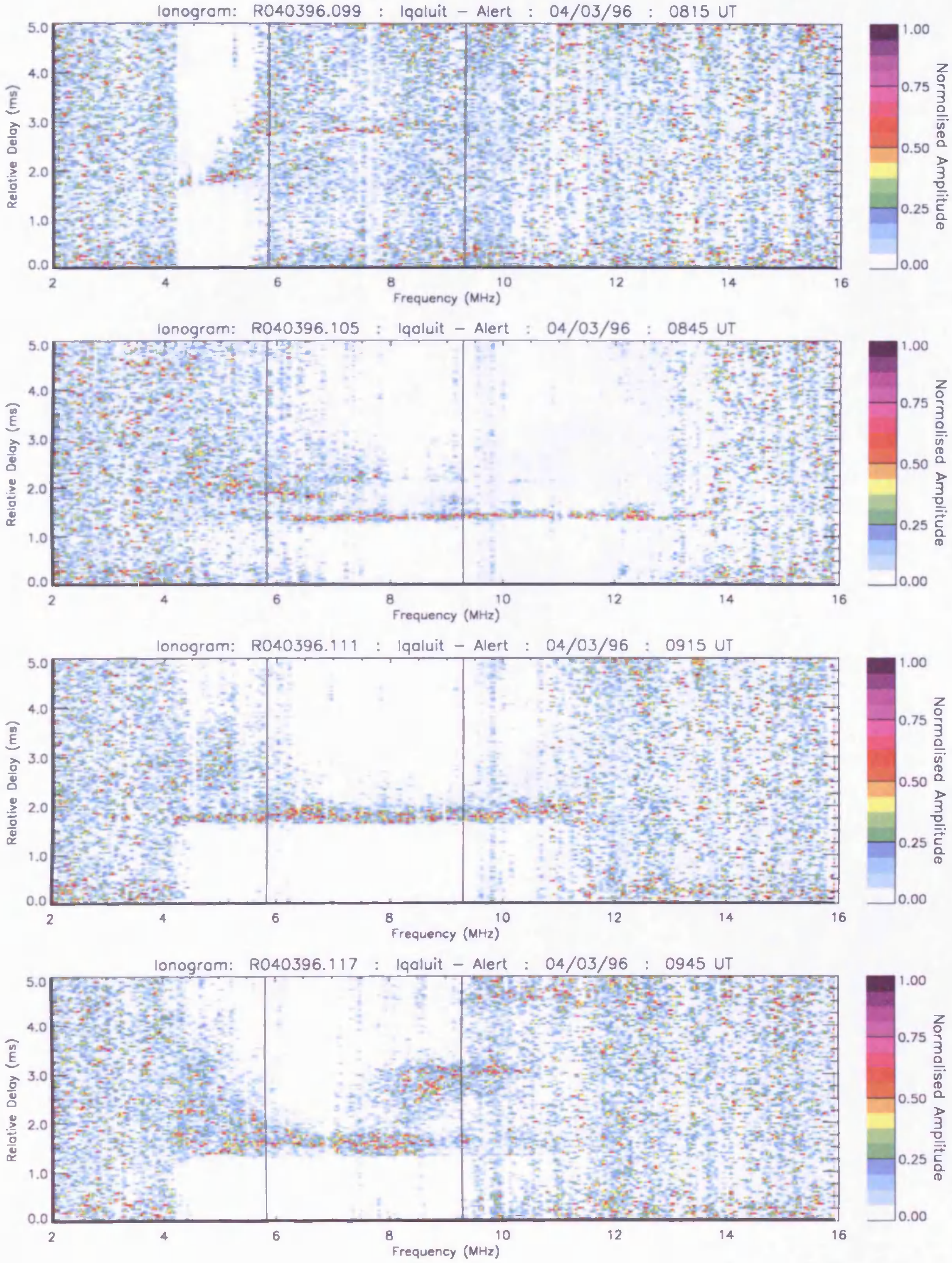

Figure 6.25: Ionogram sequence for the Iqaluit-Alert path on 4/3/96.

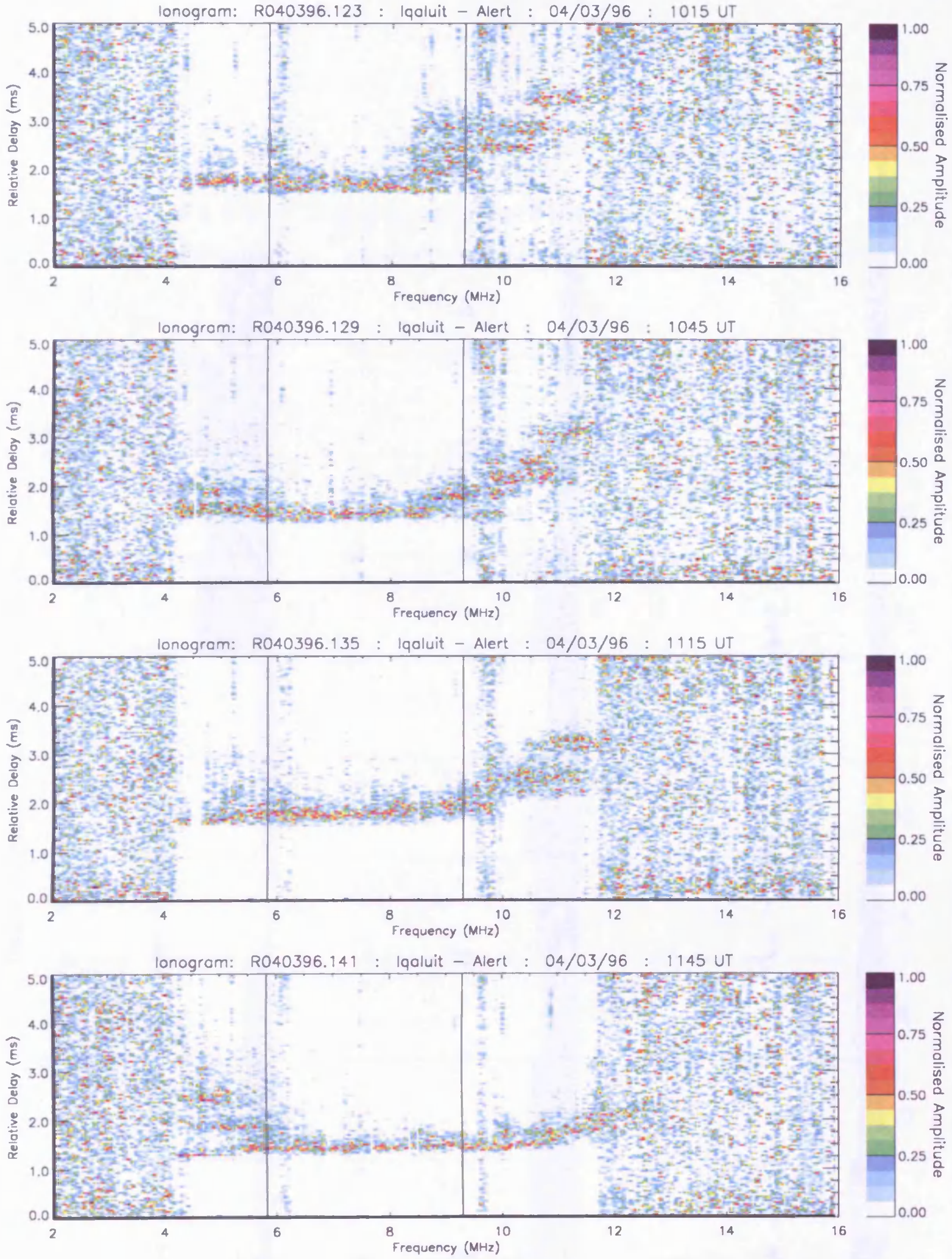

Figure 6.25 (ctd.): Ionogram sequence for the Iqaluit-Alert path on 4/3/96.

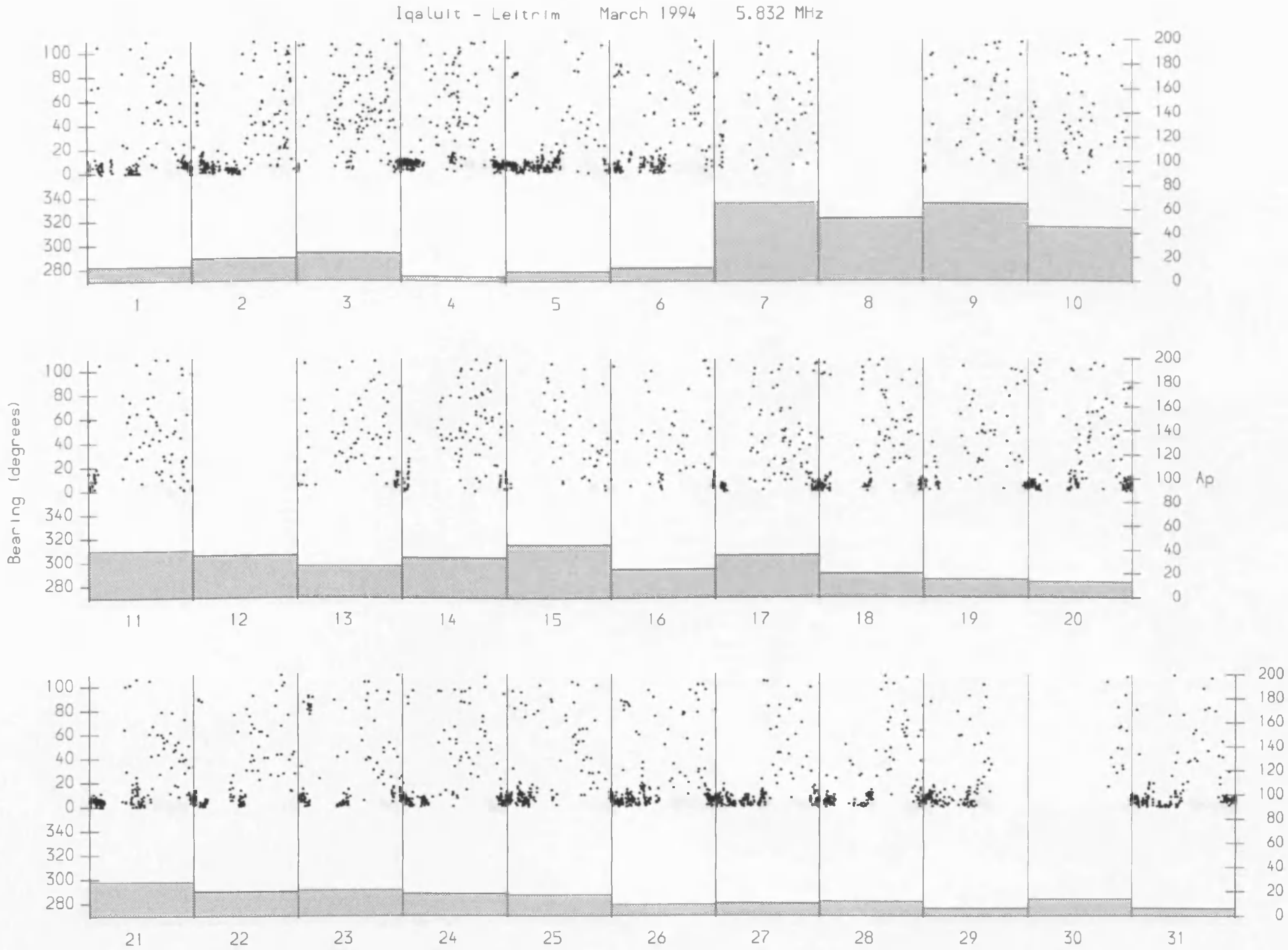

Figure 6.26: Bearings of 5.832 MHz signals on the Iqaluit-Leitrim path for March 1994. Vertical lines indicate 00:00 UT. The shaded bars indicate Ap index.

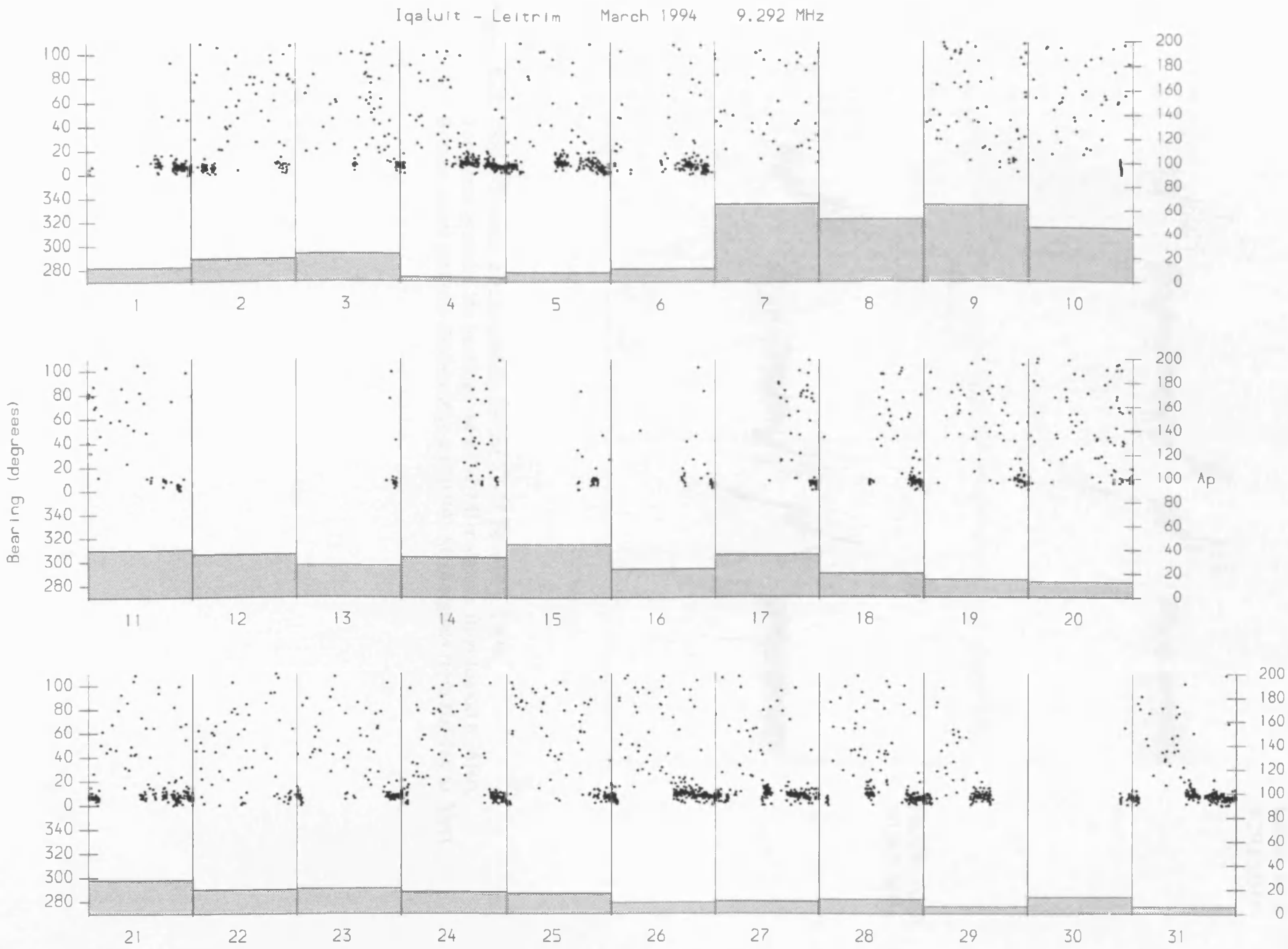

Figure 6.27: Bearings of 9.232 MHz signals on the Iqaluit-Leitrim path for March 1994. Vertical lines indicate 00:00 UT. The shaded bars indicate Ap index.

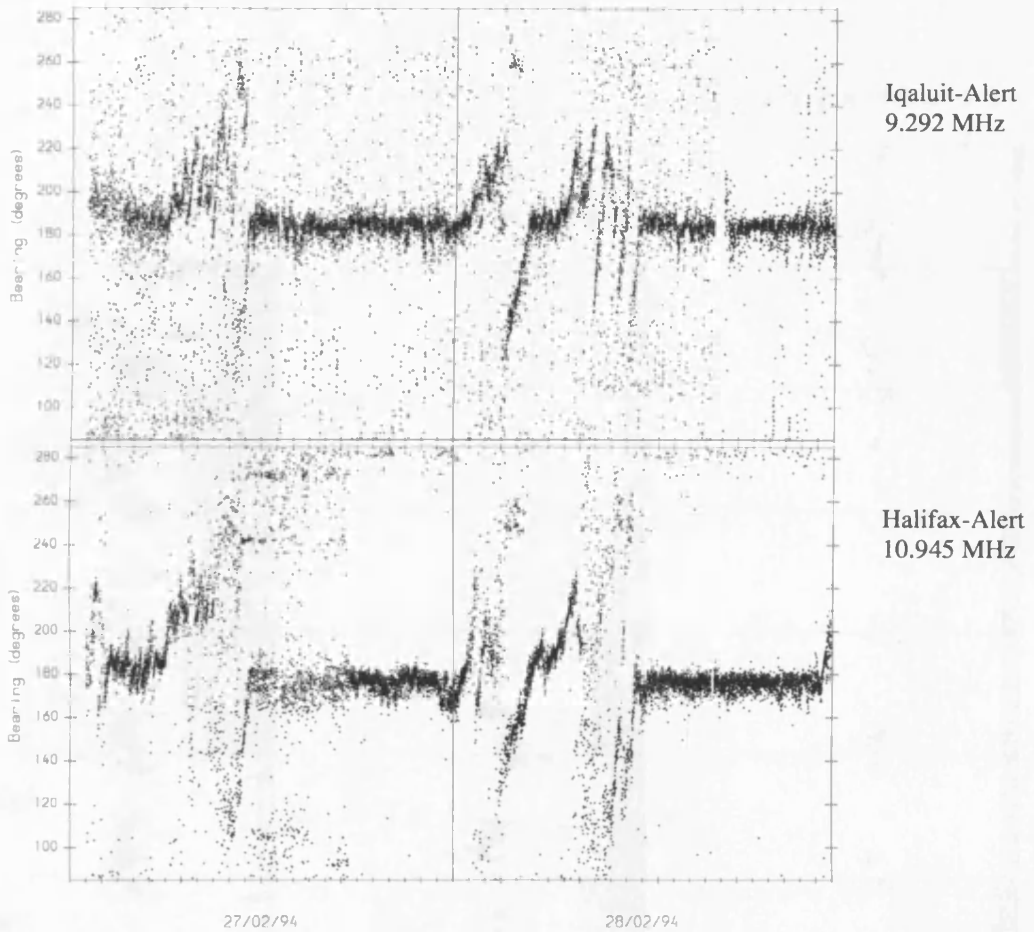

Figure 6.28: "Snap" bearing measurements for the 27-28 February, 1994.
Top panel presents the bearings on 9.292 MHz signals from Iqaluit to Alert,
Bottom panel presents the bearings on 10.945 MHz signals from Halifax to Alert.

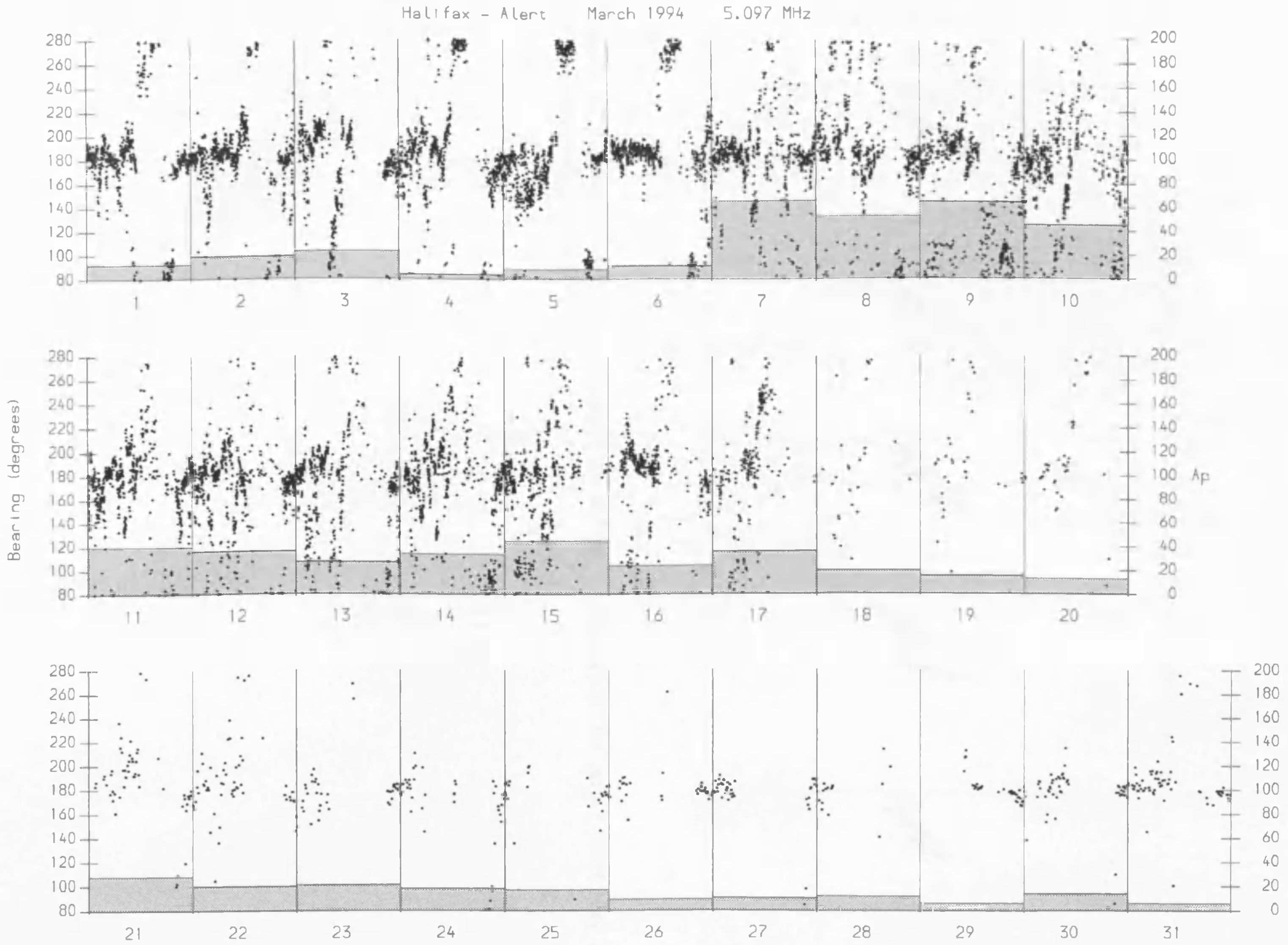

Figure 6.29: Bearings of 5.097 MHz signals on the Halifax-Alert path for March 1994. Vertical lines indicate 00:00 UT. The shaded bars indicate Ap index.

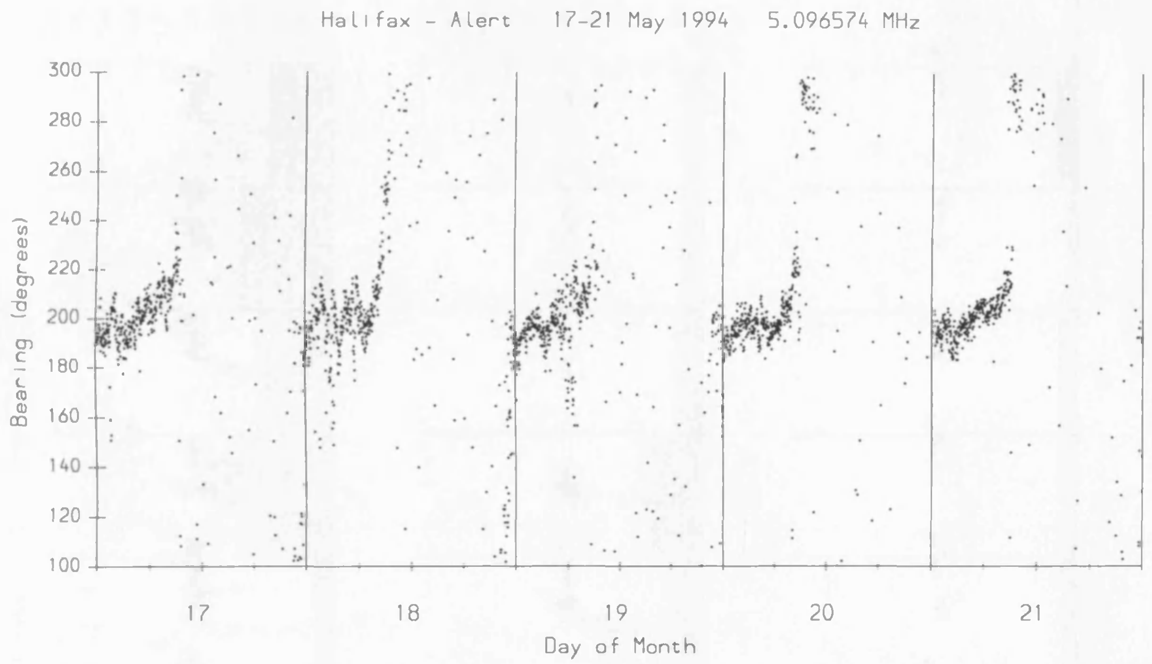

Figure 6.30: Bearings of 5.097 MHz signals on the Halifax – Alert path for the period 17-21 May 1994. Vertical lines indicate 00:00 UT.

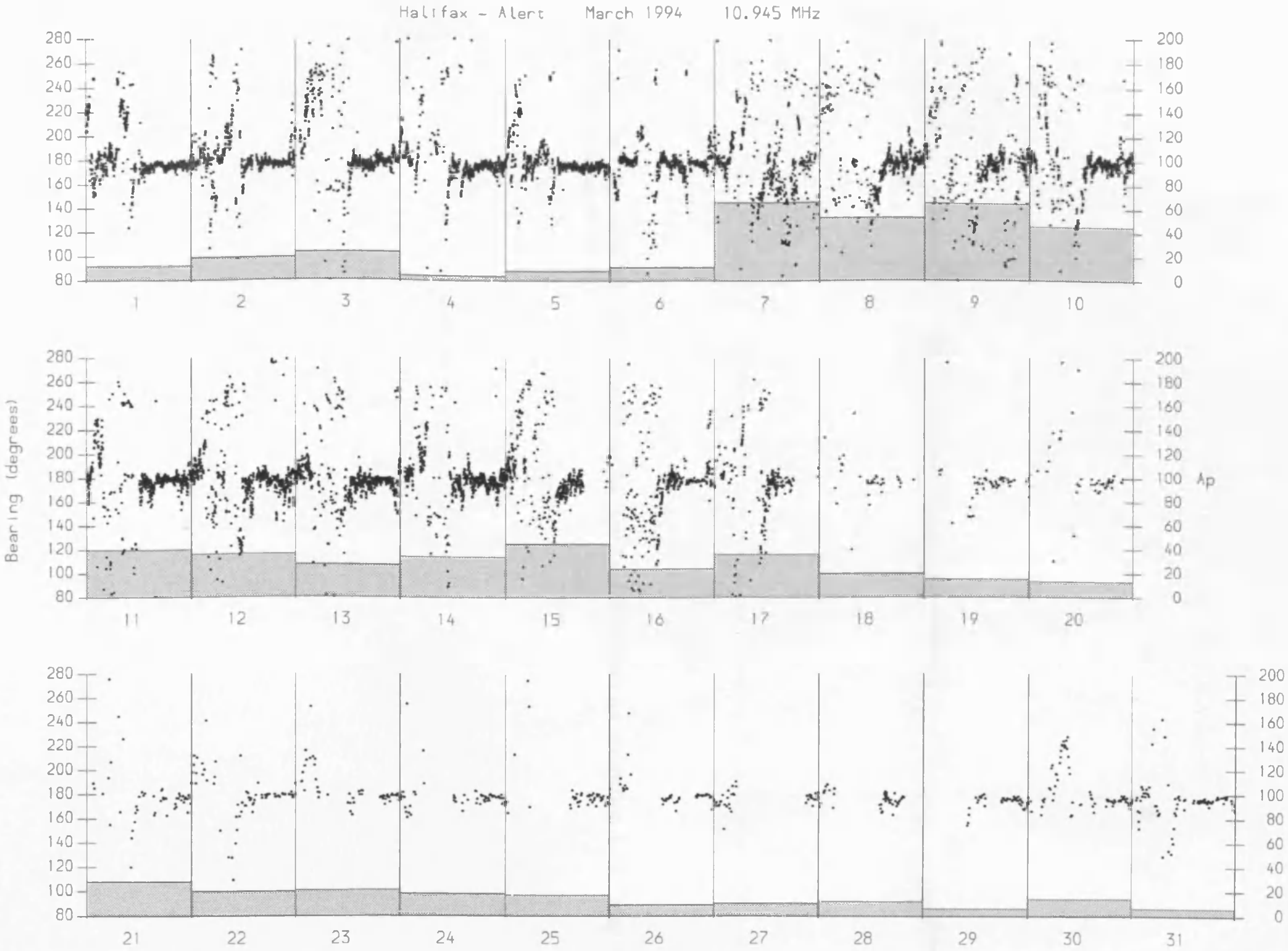

Figure 6.31: Bearings of 10.945 MHz signals on the Halifax-Alert path for March 1994. Vertical lines indicate 00:00 UT. The shaded bars indicate Ap index.

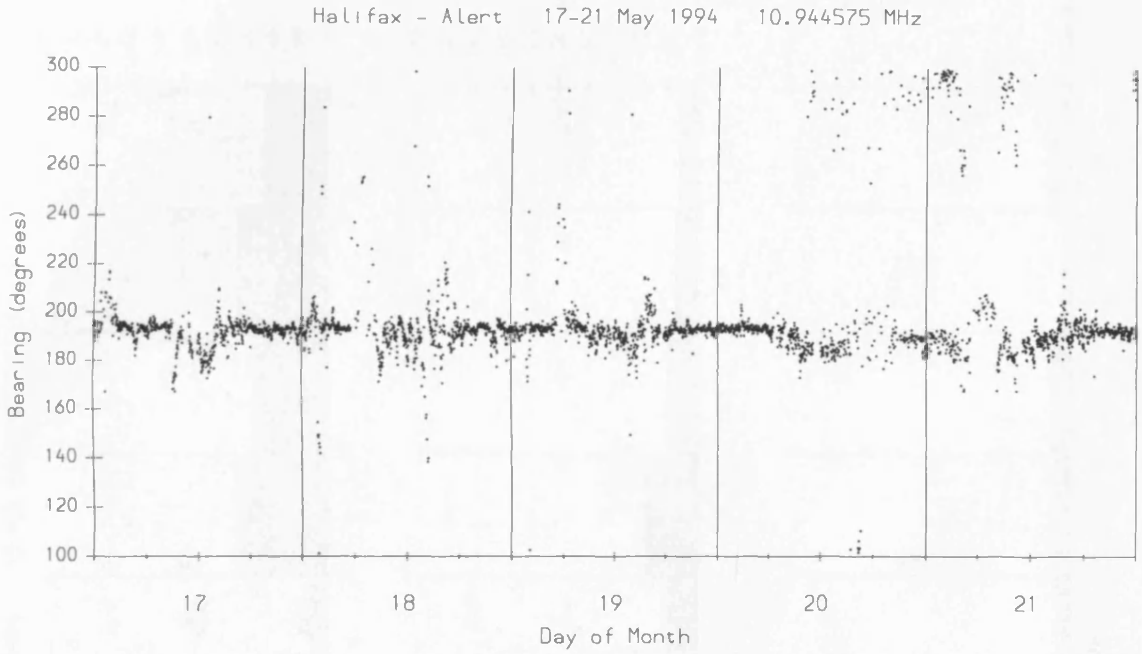

Figure 6.32: Bearings of 10.945 MHz signals on the Halifax – Alert path for the period 17-21 May 1994. Vertical lines indicate 00:00 UT.

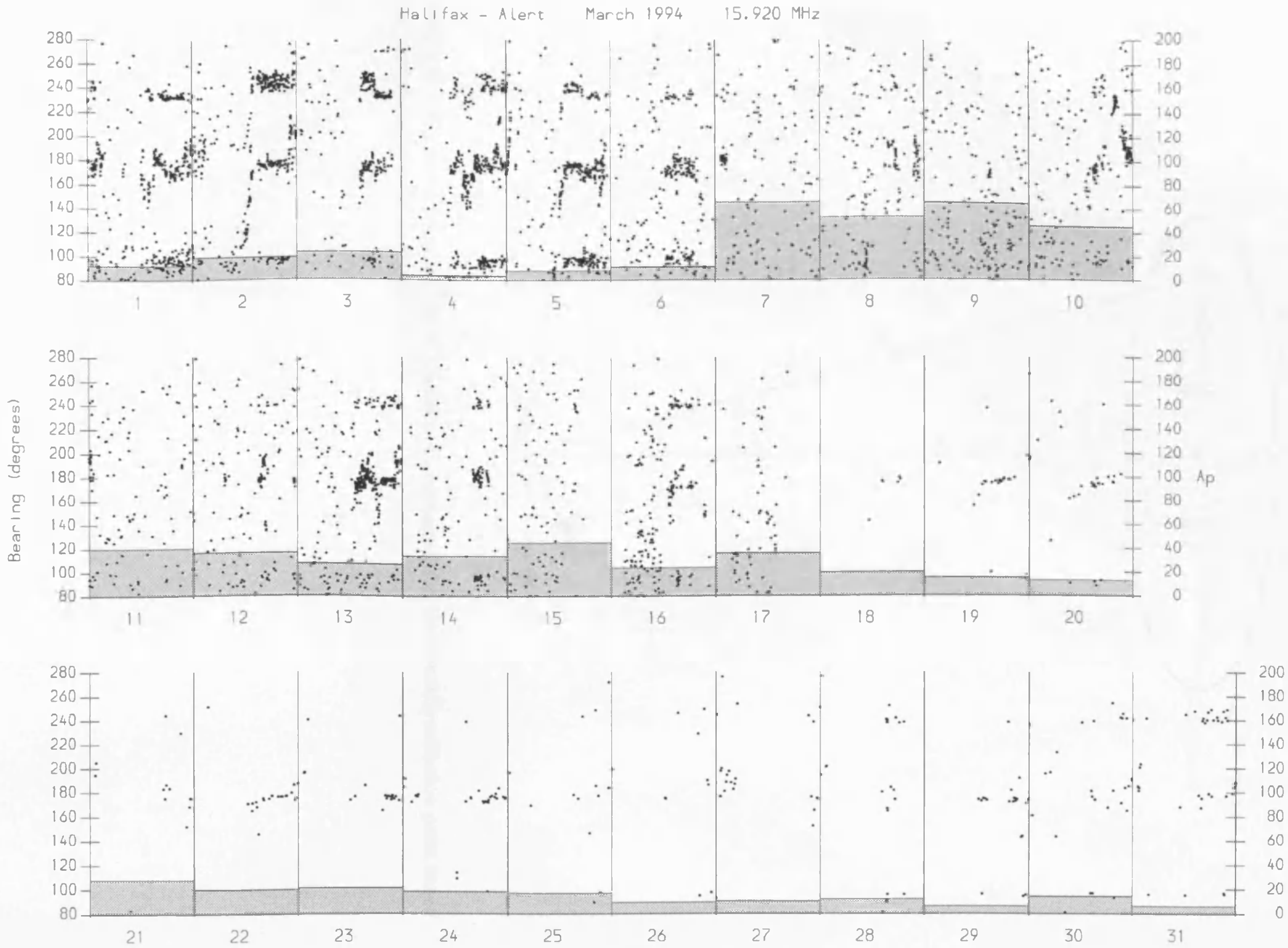

Figure 6.33: Bearings of 15.920 MHz signals on the Halifax-Alert path for March 1994. Vertical lines indicate 00:00 UT. The shaded bars indicate Ap index.

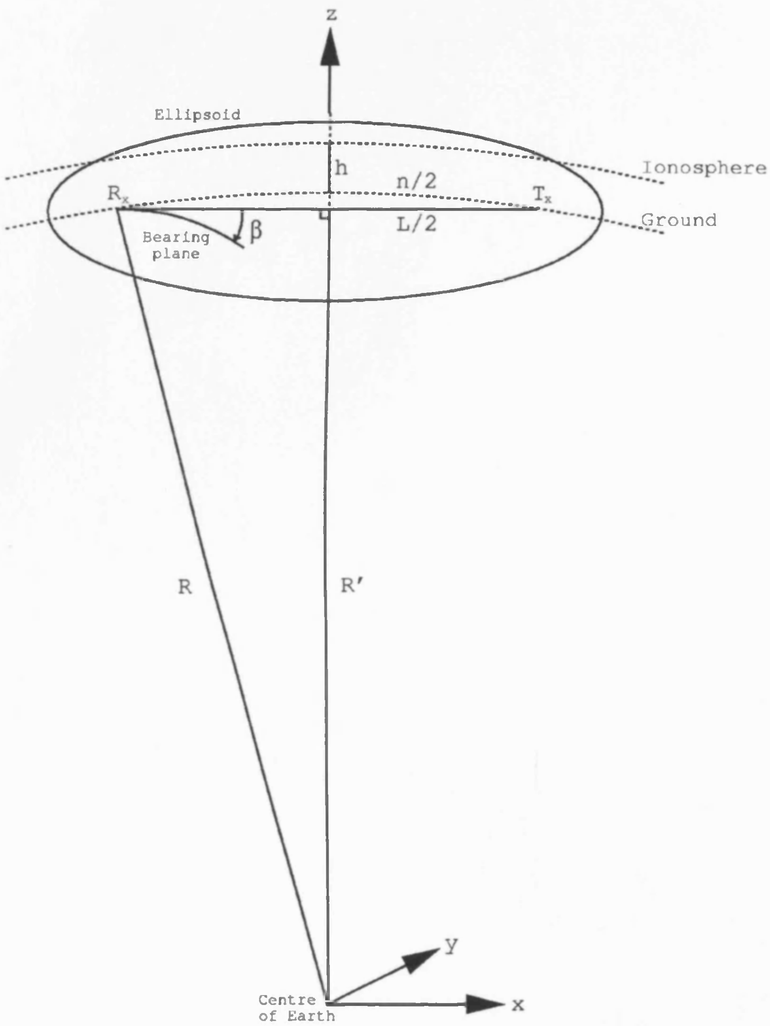

Figure D.1: Geometry of equations in Appendix D, estimating the position of a reflection point based on group path and bearing measurements.